Holographic Aspects of Quantum Gravity

Dissertation

zur Erlangung des Doktorgrades
der Naturwissenschaften (Dr. rer. nat.)
der Fakultät für Physik
der Universität Regensburg

vorgelegt von

Fabio Maria Mele

aus Neapel

im Jahr 2020

Promotionsgesuch eingereicht am: 09.06.2020
Diese Arbeit wurde angeleitet von: Dr. Norbert Bodendorfer

In loving memory of my mother

Author's Declaration

The content of this dissertation is based on research done during the author's doctoral studies at the University of Regensburg between October 2017 and September 2020. These are the result of the author's own work and of the scientific collaborations listed below, except where specifically indicated in the text and reference is made to the work of others. The material contained in this thesis has appeared on the electronic print archive `http://arXiv.org`, and has been published in the following papers:

- N. Bodendorfer, F. M. Mele and J. Münch, *Holographic Signatures of Resolved Cosmological Singularities II: Numerical Investigations*, Class. Quant. Grav. 36 (2019) no.24, 245013, DOI: 10.1088/1361-6382/ab4a92, `arXiv:1804.01387 [hep-th]`.

- N. Bodendorfer, F. M. Mele and J. Münch, *Effective Quantum Extended Spacetime of Polymer Schwarzschild Black Hole*, Class. Quant. Grav. 36 (2019) no. 19, 195015, DOI: 10.1088/1361-6382/ab3f16, `arXiv:1902.04542 [gr-qc]`.

- N. Bodendorfer, F. M. Mele and J. Münch, *(b,v)-type variables for black to white hole transitions in effective loop quantum gravity*, `arXiv:1911.12646 [gr-qc]`, (2019).

- N. Bodendorfer, F. M. Mele and J. Münch, *Mass and Horizon Dirac Observables in Effective Models of Quantum Black-to-White Hole Transition*, `arXiv:1912.00774 [gr-qc]`, (2019).

- N. Bodendorfer, F. M. Mele, J. Münch, and S. Pateloudis, *Quantum Corrected Polymer Black Hole Thermodynamics: Mass Relations and Logarithmic Entropy Corrections*, to appear

Other research papers produced by the author in the same period include

- F. M. Ciaglia, F. Di Cosmo, M. Laudato, G. Marmo, F. M. Mele, F. Ventriglia and P. Vitale, *A pedagogical intrinsic approach to relative entropies as potential functions of quantum*

metrics: The q-z family, Annals Phys. 395 (2018) 238-274, DOI: 10.1016/j.aop.2018.05.015, arXiv:1711.09769 [quant-ph].

- N. Bodendorfer, F. M. Mele and J. Münch, *Is limiting curvature mimetic gravity an effective polymer quantum gravity?*, Class.Quant.Grav. 35 (2018) no.22, 225001, DOI: 10.1088/1361-6382/aae74b, arXiv:1806.02052 [gr-qc].

- N. Bodendorfer, F. M. Mele and J. Münch, *A note on the Hamiltonian as a polymerisation parameter*, Class. Quant. Grav. 36 (2019) no.18, 187001, DOI: 10.1088/1361-6382/ab32ba, arXiv:1902.04032 [gr-qc].

- G. Chirco, M. Laudato and F. M. Mele, *Multi-symplectic Lie Group Thermodynamics for Covariant Field Theories*. In: Nielsen F., Barbaresco F. (eds) Geometric Science of Information. GSI 2019. Lecture Notes in Computer Science, vol 11712. Springer, Cham (2019) https://doi.org/10.1007/978-3-030-26980-7 7

- G. Chirco, M. Laudato and F. M. Mele, *Covariant Momentum Map Thermodynamics for Parametrized Field Theories*, arXiv:1911.06224 [math-ph], (2019).

They are however beyond the scope of this thesis and will not be discussed here.

Fabio Maria Mele

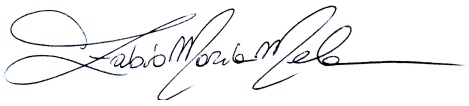

Regensburg, 2020

Preface

Thesis Aim and Structure of the Work

The unification of quantum principles with Einstein's General Relativity into a consistent theory of Quantum Gravity (QG) is one of the main challenges at the foundations of modern theoretical physics. On the one hand, the conceptual and foundational relevance of QG relies on reaching a deeper understanding of the two main pillars of our current description of the world as well as of the nature of space and time. On the other hand, it is expected to provide the key new insights to understand physical phenomena beyond the regime of applicability of the best theories currently at our disposal such as the early stages of the Universe and the properties of black holes. As such it has attracted considerable attention in the past half century and is now a wide and active field of research. Several approaches based on different motivations and techniques have been developed. Among them, the two main candidates are String Theory and Loop Quantum Gravity (LQG). Both are characterised by their own achievements and open issues so that the solution to the problem of QG remains still elusive and no definite answer has been reached so far. In particular, in lack of experimental guidance, to make progress it becomes of crucial importance to single out the essential features shared by different approaches which may then benefit from the mutual interchange of tools and ideas.

In this respect, one of the major recent development concerns the so-called holographic principle. This was originally motivated by black hole physics and in particular by the peculiar property of their entropy scaling with the horizon area rather than with their volume as one would instead expect from ordinary local quantum field theory arguments. The principle in a nutshell states that gravitational physics significantly reduces the number of physical degrees of freedom suggesting that a QG theory must be fundamentally non-local in the sense that all the information about its degrees of freedom is encoded on the boundary surfaces, the latter being finite or asymptotic. Although being strictly speaking still in the status of hypothesis as it has not been yet rigorously derived from first principles, various evidences in support of the holographic nature of gravity have been found in different QG approaches. As such the role of the holographic hypothesis as a guiding principle in our quest to unravel the quantum nature of gravity has now gained a widespread consensus and it is widely expected that any good candidate QG theory should exhibit holographic features, at least in certain regimes. Therefore,

the study of holographic aspects of QG comes to be a promising scenario for connecting different approaches as well as for understanding to which extent holography might be realised at a fundamental level.

On the String theory side, the best currently known realisation of the holographic principle is provided by the so-called Anti de-Sitter/Conformal Field Theory correspondence (AdS/CFT in short) also more generally referred to as Gauge/Gravity duality. This is a conjectured duality between a (quantum) theory of gravity in certain spacetimes and a non-gravitational gauge theory. More specifically, it states that the gravitational degrees of freedom in the bulk of a $(d+1)$-dimensional asymptotically AdS spacetime can be arranged in such a way that they can be equivalently described by a SU(N) gauge theory without gravity living on its d-dimensional boundary (a CFT for the case of a bulk String Theory). As such it is then the most promising arena in which we may look for a direct comparison between the non-perturbative techniques developed in the framework of LQG and String Theory non-perturbatively defined via its dual field theory. The ultimate goal would be to establish a connection between the relevant quantum corrections predicted by the two theories which can then benefit from tools and results of the other and try to gain new insights to solve some of their main open issues. Indeed, if on the one hand much progress has been made on the LQG side to incorporate QG corrections and study for instance cosmological and black hole singularities from a QG perspective, there are still some model building ambiguities left. Moreover, it is not yet clear in which sense holography might be realised in the LQG framework. From this point of view, a possible contact with a dual gauge theory description can provide useful insights to clarify both open issues as well as to look for indirect tests of LQG results via a candidate dual description. From a string perspective, instead, even though AdS/CFT provides an explicit example of holography, most of the evidences for such a duality have been provided in the low energy semi-classical gravity regime which corresponds to the planar $N \to \infty$ limit for the dual gauge theory. However, thinking for instance to well-established gauge theories such as quantum electrodynamics and quantum chromodynamics, the regime of interest for real world applications is that of finite number of colours. The study of the finite N regime, on the other hand, would require the inclusion of bulk QG effects and in turn of full quantum String theory which is currently out of reach. A systematic inclusion of non perturbative effects via LQG can then allow to go beyond the semi-classical approximation. Moreover, whether the gauge/gravity framework can be extended also to other kinds of spacetime not necessarily asymptotically AdS is one of the main open question and hence the application of background-independent techniques such as those on which LQG is mainly based can be in this sense of great help.

In the light of the above premises, the main question becomes then how to concretely bridge between such apparently different frameworks. To this aim, the point of view we take in this work is to focus on symmetry-reduced effective models incorporating LQG corrections and study their possible holographic consequences when compared with the AdS/CFT perspective. The reasons why we decided to center our work on symmetry-reduced models rather than full theory are multiple and can be summarised as follows. First of all, the application of QG theories in a symmetry-reduced setting is of great physical interest both from a conceptual and a phe-

nomenological point of view. Indeed on the one hand, due to the high amount of symmetries, symmetry-reduced spacetimes can be described by few degrees of freedom thus providing an ideal testbed where explicit calculations are possible keeping track also of the underlying assumptions and approximations made along the way. On the other hand, a systematic application of quantum gravity techniques to systems with increasing amount of complexity is crucial to identify possible observational signatures of quantum gravitational effects. Moreover, the application of quantisation techniques inspired by LQG to cosmological spacetimes has revealed successful leading to the development of the field of Loop Quantum Cosmology (LQC). In particular, within the LQC framework, the relevant LQG-type quantum corrections of spacetime geometry can be efficiently incorporated into an effective description in terms of a quantum corrected metric resolving the initial Big Bang singularity. Having then an explicit background spacetime taking into account QG effects puts us in a position to concretely study the role of quantum corrections in the high curvature regime where perturbative techniques fail and to ask whether they produce sensible results from a holographic perspective.

As we will discuss in the forthcoming chapters, some interesting results along this line of thoughts were obtained in the context of spatially flat homogeneous cosmology where it was shown that the holographic area-entropy bound apparently violated in presence of the classical singularity gets restored in the effective spacetime resulting from LQC where the singularity is smoothed out by QG effects. However, no explicit application or examples of quantum corrected asymptotically AdS spacetimes relevant for AdS/CFT have been proposed so far. Considering then the case of Kasner-AdS cosmological spacetimes, the first main result of this thesis consists in the construction of explicit proposals of LQG-inspired effective geometries and to use them to set up a prototype calculation to show how the inclusion of QG corrections leads to sensible improvements with respect to classical dual descriptions available in the AdS/CFT literature.

Leaving then the cosmological setting, next step is to consider other kinds of gravitational systems where quantum effects are expected to play a relevant role such as black hole spacetimes. Despite of the various developments of LQC, much less is known for the case of black holes. Most of the work in this case has focused on the study of the simplest spherically symmetric and static solution provided by Schwarzschild black holes. However, as we will discuss in the main part of the thesis, a fully satisfactory effective model of quantum corrected Schwarzschild spacetime has not been developed so far and some undesirable properties can arise depending on the details of the construction. The second main contribution of this work is then to develop a new consistent model surpassing previous limitations and to provide a detailed analysis of the properties of the resulting quantum corrected spacetime. The latter comes to be a necessary step before being able to consider asymptotically AdS black holes from a LQG perspective and compare and contrast with results currently available in the AdS/CFT framework.

More specifically, the thesis is divided into four parts. Part I consists of Chapter 1 and is meant to give a general introduction to clarify what is meant by holographic principle and its different forms. We first recall the main aspects that have motivated its original formulation as well as later generalisations focusing on their differences and underlying assumptions. We then give a non-technical overview on the current stage of the art of incorporating holographic

features in quantum gravity.

Part II is devoted to the presentation of the tools and concepts which are relevant for the main part of the thesis and is divided in two chapters. In Chapter 2, we try to give a pedagogical review of the main aspects of the AdS/CFT correspondence and in which sense it provides a concrete realisation of the holographic principle. To this aim, we try to focus on simple toy model examples without entering the details of string theory which are only mentioned for completeness as they provide the most studied realisation of the gauge/gravity duality. In Chapter 3, instead, we move on the LQG side. After discussing the main aspects of the quantisation procedure developed in the framework of homogeneous and isotropic LQC, we focus on the construction of the effective theory where the relevant quantum corrections are captured by a phase space regularisation called *polymerisation* according to which the canonical momenta are replaced by their exponentiated version in a similar spirit to the regularisation techniques for lattice gauge theory. This induce an upper bound on spacetime curvature which resolves the classical gravitational singularity when energy density reaches the Planck regime and QG effects become dominant.

Part III consists of Chapters 4,5 and 6 which provide the core of the thesis where the main results of the work are presented in detail. In Chapter 4, we focus on the study of possible holographic signatures of resolved singularities in cosmological quantum corrected asymptotically AdS spacetimes motivated by LQG. Specifically, we discuss various examples of effective quantum Kasner-AdS metrics progressively removing certain simplifying assumptions and use them to show that the resolution of the bulk cosmological singularity leads to a resolution of the finite distance pole in the equal time two-point correlator of the boundary field theory. As we will discuss, the latter was previously argued to be a holographic signature of the bulk singularity in the framework of AdS/CFT.

In Chapter 5, we move then to effective LQG-models of quantum black holes and the resolution of their interior singularities. After recalling the main strategy usually adopted in LQG-inspired investigations and the current status of previous proposals, we present two new effective polymer models for Schwarzschild black holes based on new canonical phase space variables inspired by physical considerations about the onset of quantum effects. In the resulting quantum corrected spacetime, the central singularity is replaced by a black-to-white hole transition, quantum effects become relevant at a unique mass independent curvature scale, while they become negligible in the low curvature region near the horizon. A key new feature of our work is the construction of two Dirac observables corresponding to the black and white hole masses, respectively. The study of these observables reveals that physically acceptable solutions in our first model require us to select a certain subset of initial conditions, corresponding to a specific relation between the masses after the bounce. In the second model, therefore, we construct new variables directly related to spacetime curvature allowing us to overcome the above limitations, keeping at the same time the simple structure of our first model.

In Chapter 6, instead, we discuss some work in progress about effective polymer black holes. This includes the analysis of the quantum corrections to thermodynamic quantities such has the temperature of the black hole and its horizon entropy. Second, moving beyond the effective

theory, we discuss the main steps of the construction of the quantum theory underlying the effective models of Schwarzschild black holes presented in Chapter 5. In particular, we show that the remarkably simple structure of our models might allow us to have full analytic control also in the quantum theory. Finally, coming back to our original motivations, we sketch a possible extension of our model to Schwarzschild-AdS black holes and discuss some subtleties that might arise in constructing the effective quantum theory.

Some concluding remarks and future research directions are reported in the last part of the thesis (Chapter 7). Moreover, in the attempt of being as much self-consistent as possible the thesis is supplemented by four appendices containing some further background material as well as numerical checks and explicit computations complementing the discussion and the results contained in the main body of the manuscript.

Notation and Conventions

The following list collects the main conventions and acronyms adopted in this work:

Spacetime $\mathcal{M}$, $\dim(\mathcal{M}) = d + 1$

Spatial hypersurface Σ, $\dim(\Sigma) = d$

Metric signature $(- + \cdots +)$

Greek spacetime indices $\mu, \nu = 0, \ldots, d$

Latin spatial indices $a, b = 1, \ldots, d$

Generic metric tensor $g_{\mu\nu}$

Flat Minkowski metric $\eta_{\mu\nu}$

Spatial metric q_{ab}

Cosmological constant Λ

Barbero-Immirzi parameter β

Newton's gravitational constant G

Vacuum speed of light c

Reduced Planck constant $\hbar = \frac{h}{2\pi}$

Vacuum speed of light c

Planck units $c, G, \hbar = 1$ (unless otherwise specified)

Planck length $\ell_P = \sqrt{\frac{\hbar G}{c^3}}$

Lie Group G

Lie algebra $\mathfrak{g}$

Lie algebra indices $i, j, k, \ldots$

(L)QG = (Loop) Quantum Gravity

LQC = Loop Quantum Cosmology

AdS = Anti de Sitter

SAdS = Schwarzschild-AdS

CFT = Conformal Field Theory

QFT = Quantum Field Theory

(S)YM theory= (Super) Yang-Mills theory

GR = General Relativity

FLRW = Fridman-Lemaître-Robertson-Walker

BH = Black Hole

WH = White Hole

l.h.s. = left hand side

r.h.s. = right hand side

w.r.t. = with respect to

d.o.f. = degrees of freedom

PDE = Partial Differential Equation

ODE = Ordinary Differential Equation

EOMs = Equations of Motion

Contents

Part I

INTRODUCTION AND MOTIVATIONS

Chapter 1

Quantum Gravity and the Holographic Principle

This introductory chapter is devoted to the presentation of the *holographic principle* and its role in quantum gravity. After briefly recalling the main aspects of black hole physics and the related upper bounds on matter entropy that motivated its original formulation and later generalisations, we focus on the underlying assumptions and the resulting different forms for the statement of the principle. The chapter closes with a summary of the current stage of the art of incorporating holography in some of the main approaches to quantum gravity. This gives us the opportunity to further clarify the framework in which the work contained in the main part of the dissertation can be inserted as well its main motivations.

1.1 Motivations from Black Hole Physics

Black holes provide us with physical systems in which gravity and quantum physics come to be deeply intertwined. Already at the semi-classical level, where the low-energy physics far from the singularity is captured by a description in terms of a local effective field theory on (curved) background[1], physical features at the horizon scale involve a subtle interplay of gravitational and quantum effects as signaled by the presence of both G and $\hbar$ in the relevant thermodynamic quantities [1][2]. Moreover, the classical description of spacetime geometry in terms of a smooth continuous manifold breaks down in the high curvature region near the singularity where quantum properties of the gravitational field itself are expected to become dominant so that a proper description of physical phenomena in such a regime would require a quantum theory of gravity. As such the study of black holes play a crucial role in quantum gravity research and have gained a considerable amount of attention from different approaches. In particular, Bekenstein's notion of black hole entropy [5–7], the related discovery of upper bounds on the entropy of matter systems

[1] Such assumption is based on the observation that local gravitational effects are extremely weak at the event horizon of large black holes as can be seen from the curvature invariants constructed from the Riemann tensor that depend on inverse powers of the black hole mass.

[2] For a review of black hole mechanics we refer to [2–4] and references within.

(see e.g. [2,8] for reviews), and the long-standing debate regarding the issue of information loss in the evaporation process, initiated by Hawking [9–11], played a key role in the development of the so-called *holographic principle* [8, 12–14]. In a nutshell, such a principle goes beyond black hole physics and establishes a limit to the amount of information contained in a space-time region. In its simplest form for spherical symmetry and weak gravity, originally formulated by t'Hooft [12] and Susskind [13], the principle establishes that the entropy of a region of space is limited by the area surrounding it. In its modern incarnations and generalisations, the holographic principle has guided the construction of some of the leading physical theories of spacetime in the last few years. Although a general proof is not yet available, many pieces of evidence have been provided over the years in support of the principle so that it has progressively gained the status of a fundamental principle and is now widely expected for any successful theory of quantum gravity to be able to derive it as a consequence of its framework. Before entering the details of the content of the holographic principle in its different forms, its underlying assumptions and its consequences, let us then start this chapter by briefly reviewing those aspects of black holes and the related entropy bounds that motivated its formulation.

1.1.1 Generalised Second Law and Spherical Entropy Bound

Due to its central role in what follows, let us start by focusing on the notion of black hole entropy. Following [15], there are different notions of black hole entropy and, as we will discuss in Sec. 1.2, their interpretations and relations will be relevant to understand the various formulations of the holographic principle together with their expected regimes of validity. The first one is the thermodynamical notion of Bekenstein-Hawking entropy introduced by Bekenstein [5–7] and Hawking [16] according to which a black hole carries an entropy S_{BH} given by a quarter of its horizon area A in Planck units, namely (for $c = \hbar = G = 1$):

$$S_{BH} = \frac{A}{4} \,. \tag{1.1}$$

Such a notion of black hole entropy was originally motivated by the analogy between black hole area and standard thermodynamic entropy suggested by Hawking's area theorem [17] according to which the horizon area never decreases with time. The later discovery of Hawking radiation [9,16] then confirmed the thermodynamic description of black holes to be based on physical properties rather than just an analogy. The thermodynamical notion of black hole entropy (1.1) is in fact the one entering the laws of black hole mechanics. In particular, a *generalised second law* (GSL) [5–7]

$$\delta S_{\text{tot}} \geq 0 \,, \tag{1.2}$$

holds for the total entropy S_{tot} of the system "black hole + matter" so that for an outside observer the decrease in the matter entropy when matter disappears behind the horizon is compensated by the increasing horizon area and hence of the black hole entropy[3].

[3] In four dimensions, for instance, the horizon area of a Schwarzschild black hole of mass M is given by $A = 4\pi R^2 = 16\pi M^2$, $R = 2M$ being the horizon radius. Thus, when matter falls behind the horizon, mass is added to the black hole, the horizon area grows, and the thermodynamical entropy increases accordingly.

Another important notion of black hole entropy which relies on a more statistical and information-theoretic interpretation is that of entropy as measure of information. In this respect, it is possible to distinguish two notions, the weak and strong black hole entropy, depending on the information to be referring to the exterior or the interior. More precisely [15], the so-called *weak black hole entropy* S_{BH}^{weak} is a measure of how much information on the interior can be gained by an external observer making measurements outside the horizon. The *strong black hole entropy* S_{BH}^{strong} instead measures the information contained in the interior region of a black hole. In other words, as we will discuss in more details later, these two statistical notions of entropy respectively give a measure of the number $N = e^S$ of degrees of freedom inside the black hole (S_{BH}^{strong}), or better of the number of distinct ways in which the black hole microstates can be assembled for certain given macroscopic parameters such as energy and volume, and the same quantity measured from a outside observer (S_{BH}^{weak}).

A natural question at this point is whether there is any relation between the different notions of black hole entropy. For what concerns the thermodynamical and weak entropy, the GSL implies the following inequality $S_{BH}^{\text{weak}} \leq S_{BH}$. Indeed, assuming the semi-classical approximation to be valid in the low curvature regime far from the singularity, the exchange of information between the interior and the exterior can only occur via Hawking radiation. On the other hand, as the semi-classical approximation breaks down deep in the interior region, no arguments based on the GSL can be used to infer any relation between the weak and strong notions of black hole entropy which in turn can only be postulated. As discussed in [15], one possibility is given by the so-called *strong entropy assumption* according to which $S_{BH}^{\text{strong}} = S_{BH}^{\text{weak}}$. Assuming its validity or not will play a key role in the arguments on which matter entropy bounds are based and ultimately in the different forms of the holographic principle.

The GSL has remarkable consequences on both gravitational and matter degrees of freedom. Indeed, the application of the thermodynamic properties of black hole physics leads to the so-called *spherical entropy bound* which poses an upper bound for the entropy of a matter system contained in a (spherical) region of space. This was first pointed out with an argument by Bekenstein [5–7], a modern *reductio ad absurdum* formulation of which can be found in [15, 18], and later by Susskind [13]. The derivation of such entropy bound can be summarised as follows. Let $\mathcal{M}$ be an asymptotically flat spacetime (i.e. such that the formation of black holes is allowed by the asymptotic structure), and let Γ be a space-like region in $\mathcal{M}$ whose boundary $\mathcal{B} = \partial\Gamma$ is specified by the imposition of certain boundary conditions. Let us further assume $\mathcal{B}$ to be of spherical topology and gravity to be sufficiently weak so that the radius is well defined. Let then consider a thermodynamic system completely contained into the region Γ. The latter can then be thought of as the smallest sphere that fits around the system. The matter system is assumed to be in thermal equilibrium and gravitationally stable so that the size of the region Γ can be considered to be approximately constant in time. Now, the total mass of the system cannot be larger than the mass of a black hole of horizon area $A(\mathcal{B})$ just fitting inside Γ, whose entropy is given by $S_{\mathcal{B}} = A(\mathcal{B})/4$. Otherwise from the outside point of view the system would already be a black hole, and could not be stable. Let then consider the process in which the system is converted into a black hole. This can be done by collapsing a spherically symmetric

shell of matter such that 1) its energy together with the original mass of the system will form in the end a black hole which just fills Γ, and 2) the shell can be adiabatically brought to within Γ without radiating or ejecting mass so that the entropy of its exterior is not raised. The total entropy at the beginning of the process is thus given by $S^{(\mathrm{i})}_{\mathrm{tot}} = S_{\mathrm{matter}} + S_{\mathrm{shell}}$, with $S_{\mathrm{shell}} \geq 0$ and $S_{\mathrm{matter}} = S^{\mathrm{weak}}_{\Gamma}$ as measured from the outside of Γ. The final entropy is $S^{(\mathrm{f})}_{\mathrm{tot}} = S_{\mathcal{B}} = A(\mathcal{B})/4$. Therefore, applying the GSL to the process

$$0 \leq S^{(\mathrm{f})}_{\mathrm{tot}} - S^{(\mathrm{i})}_{\mathrm{tot}} = S_{\mathcal{B}} - (S_{\mathrm{matter}} + S_{\mathrm{shell}}) \leq S_{\mathcal{B}} - S_{\mathrm{matter}} \ , \tag{1.3}$$

we get the following upper bound for the entropy of the original matter system:

Spherical entropy bound

The entropy of a weakly gravitating system contained in a spherical region of space Γ in an asymptotically flat spacetime cannot be larger than a quarter of the area $A(\mathcal{B})$ of the boundary surface $\mathcal{B} = \partial\Gamma$ of that region (in Planck units), i.e.

$$S^{\mathrm{weak}}_{\Gamma} \leq \frac{A(\mathcal{B})}{4} \qquad \text{(weak form)} \ , \tag{1.4}$$

or, including the strong entropy assumption as additional independent requirement

$$S^{\mathrm{strong}}_{\Gamma} \leq \frac{A(\mathcal{B})}{4} \qquad \text{(strong form)} \ . \tag{1.5}$$

1.1.2 Counting Degrees of Freedom: Locality vs Non-locality

The spherical entropy bound imposes a remarkable restriction on the number of degrees of freedom of weakly gravitating systems contained in a (spherical) region of space Γ which deviates from the behaviour expected by standard local quantum field theory considerations.

To see this, let us regard the region Γ with its matter content as a quantum mechanical system and denote by $\mathcal{H}_{\mathcal{B}}$ and $\mathcal{H}_{\Gamma}$ the boundary and bulk Hilbert spaces, respectively[4]. According to the interpretation of the weak and strong entropy discussed before, the dimensions of such Hilbert spaces are given by $\dim \mathcal{H}_{\mathcal{B}} = e^{S^{\mathrm{weak}}_{\Gamma}}$ and $\dim \mathcal{H}_{\Gamma} = e^{S^{\mathrm{strong}}_{\Gamma}}$. The spherical entropy bound (1.4) then requires that

$$\dim \mathcal{H}_{\mathcal{B}} \leq e^{\frac{A(\mathcal{B})}{4}} \ . \tag{1.6}$$

Combining (1.6) with the *strong entropy assumption* ($S^{\mathrm{weak}}_{\Gamma} = S^{\mathrm{strong}}_{\Gamma}$), we conclude that

$$\dim \mathcal{H}_{\Gamma} \leq e^{\frac{A(\mathcal{B})}{4}} \ , \tag{1.7}$$

according to which the number $N = \log(\dim \mathcal{H}_{\Gamma})$ of degrees of freedom contained in the region Γ, given by the logarithm of the number of independent quantum states describing the physics in

[4] We can think of $\mathcal{H}_{\mathcal{B}}$ and $\mathcal{H}_{\Gamma}$ respectively as the carrier space of the smallest (faithful) representation of the algebras $\mathcal{A}_{\mathcal{B}}$ and $\mathcal{A}_{\Gamma}$ of observables measurable on the boundary $\mathcal{B}$ and in the interior of Γ.

Γ, cannot exceed a quarter of the area (in Planck units) of the boundary surface of that region.

Let us then compare this result with the expectations from quantum field theory (QFT) according to which the number of degrees of freedom contained in Γ would scale with the volume of the region rather than with the area of its boundary. To see this, let us assume the physics inside Γ to be described by a local QFT on a classical background spacetime. Let further consider the space to be discretised into a cubical lattice with lattice spacing a and assume the volume $V(\Gamma)$ of Γ to be large compared to a^3. Naively, being the minimal length that can be resolved given by the Planck length, we can think of this lattice as a Planck grid with one quantum harmonic oscillator per each Planck sized lattice site. The total number of oscillators inside the region Γ will be thus given by $V(\Gamma)/a^3$. Denoting by $n < \infty$ the number of states of each oscillator[5], the total number of independent quantum states in Γ is given by $n^{(V(\Gamma)/a^3)}$ so that the number of degrees of freedom in the region $N = \frac{V(\Gamma)}{a^3} \log n$ is proportional to the volume.

The above discrepancy in counting the number of degrees of freedom that can be stored into a spherical region of space is due to a not proper inclusion of gravitational back reaction in the QFT argument. Indeed, we demanded that each Planck volume must not contain more than one Planck mass so that the mass contained in a sphere of radius R would be of order $M \sim R^3$. But a spherical surface cannot contain more mass than a black hole of the same area, say $M \sim R$ in the static case. Therefore, the introduced UV cut-off does not prevent the formation of black holes on larger scales. In other words, the QFT argument overestimates the number of degrees of freedom as most of the states of the system would be too massive to be gravitationally stable and a black hole will form before such energies can be reached. Finally, if such a black hole has to be contained within the specified region, its entropy saturates the spherical bound thus resolving the apparent contradiction. Moreover, the non-extensive scaling of the number of degrees of freedom with the area rather then the volume would be compatible with the requirement of unitarity for the black hole formation process. Indeed, if a region initially described by a Hilbert space of dimension e^V would be converted into a black hole with a final Hilbert space of dimension $e^{A/4}$, the number of states would have decreased. It would then be impossible to recover the initial state from the final state and unitarity of the dynamical evolution would be violated. On the contrary, this would not be the case if the dimension of the Hilbert space is taken to be $e^{A/4}$ from the beginning as suggested from the spherical entropy bound[6]. The insistence on unitarity in presence of black holes provided one of the main motivations for the formulation of the holographic principle. In particular, the so-called *black hole complementarity* proposal [28, 29], according to which there are two self-consistent but complementary descriptions of black holes respectively corresponding to an infalling and an outside observer, suggested that unitarity can be retained at the expense of locality thus providing the conceptual core that led 't Hooft [12] and Susskind [13] to the original formulation of the holographic principle.

[5] As discussed in [8], the number of states can be considered to be finite as the discrete energy spectrum of each harmonic oscillator is bounded from below by finite volume effects and from above by a Planck scale cutoff.

[6] This of course only concerns the formation of black holes and not whether unitarity has to be preserved once the black hole has been created and ultimately evaporates. Such a question goes back to the information loss paradox originally advocated by Hawking in the semi-classical framework [9–11] and whose possible resolution in a theory of quantum gravity is still under active debate within different approaches (see e.g. [19–27]).

1.1.3 Beyond Spherical Bound

The spherical entropy bound is "universal", in the sense that it is independent of the specific characteristics and composition of matter systems [30]. However, its validity is not truly universal as its application relies on specific assumptions. These include a suitable asymptotic structure of the underlying spacetime, a spherical boundary surface, and gravitational stability of the enclosed region of space so that it can be converted into a black hole. It is therefore natural to ask whether it is possible to overcome such apparent limitations and consider more general kinds of entropy upper bounds. A maybe intuitive extension of the spherical entropy bound can be argued by simply relaxing some of (possibly all) the assumptions on which it is based. As a first attempt one may drop the assumption of spherical symmetry and consider a generic spatial region with no specific boundary conditions[7]. This leads to conjecture the so-called *space-like entropy bound* according to which the entropy contained in *any* region of space cannot exceed the area of the boundary surface of that region. More precisely, we have the following weak and strong version [15]:

Space-like entropy bound (weak form)

Let $\mathcal{B}$ be a generic closed co-dimension 2 surface, which bounds a region Γ contained in a spatial slice of a given spacetime, and let $\mathcal{H}_{\mathcal{B}}$ be the representation space of the algebra of observables measurable on $\mathcal{B}$ (when no boundary conditions have been imposed), then

$$S_{\Gamma}^{\text{weak}} = \log\left(\dim \mathcal{H}_{\mathcal{B}}\right) \leq const. \cdot A(\mathcal{B}) \, . \tag{1.8}$$

or combining it with the strong entropy assumption

Space-like entropy bound (strong form)

Let Γ be a generic region of space in a given spacetime and let $\mathcal{B}$ its boundary surface. Then, denoting by $\mathcal{H}_{\Gamma}$ the representation space of the algebra of observables measurable in the interior of Γ, we have

$$S_{\Gamma}^{\text{strong}} = \log\left(\dim \mathcal{H}_{\Gamma}\right) \leq const. \cdot A(\mathcal{B}) \, . \tag{1.9}$$

Despite of its apparent naturalness, the strong version of the space-like entropy bound turns out to be violated in known physical examples. Some counterexamples can be already found in simple cosmological situations and can be summarised as follows (we refer to [8,15] and references within for details as well as further objections in non-cosmological setups).

Spatially flat FLRW universe: Let Γ be a spherical region of proper radius R in three-dimensional, flat, homogeneous and isotropic space of a FLRW universe. The volume and surface area of this region are then given by $V = \frac{4}{3}\pi R^3$ and $A = 4\pi R^2$, respectively. The matter entropy contained in Γ can be written as $S_{\Gamma} = \sigma V$, where σ is the non-zero average entropy density[8].

[7] The underlying spacetime manifold does not need to be asymptotically flat so that in principle also cosmological spacetimes are taken into account.

[8] We may assume for instance the universe to be filled with a homogeneous and isotropic radiation.

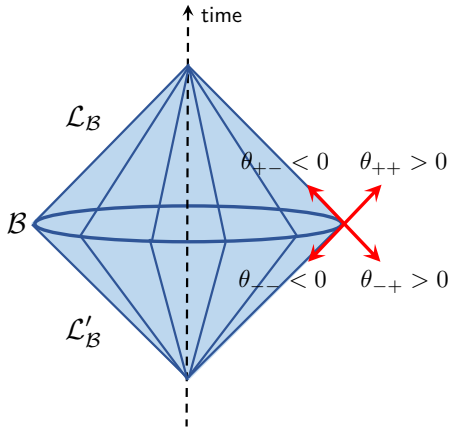

Figure 1.1: Construction of light-sheets for a spherical region $\mathcal{B}$ in flat space. The four null directions orthogonal to the surface are marked by red arrows as schematically shown for a single point in $\mathcal{B}$. Future and past directed outgoing light rays have positive expansion, while future and past directed ingoing light rays have negative expansion. Ingoing light rays intersect into a single point, respectively in the past and the future, so that there are two light sheets $\mathcal{L}_\mathcal{B}$ and $\mathcal{L}'_\mathcal{B}$ given by the blue cones bounded by $\mathcal{B}$.

Denoting by C the constant factor entering the space-like entropy bound, we see that the bound can be violated for a sufficiently large radius $R \geq \frac{3C}{4\sigma}$ [31].

Closed FLRW space: Consider a FLRW cosmological spacetime with positive spatial curvature, whose equal time spatial slices have a 3-sphere geometry, and a matter system of entropy $S_\Gamma > 0$ contained in a large region Γ centered for instance around the north pole which fills the spatial hypersurface up to a small compact region. The space-like entropy bound is thus violated in the limit in which Γ approaches the south pole and its boundary surface area shrinks to zero.

Therefore, the space-like entropy bound turns out to be too naive and is only valid in very restrictive assumptions which do not allow to include known physical situations. As discussed in [15], the great deal of evidence in support of a true physical role for the laws of black hole thermodynamics suggests that the only assumption without independent support comes to be the strong entropy assumption. Nevertheless, the space-like entropy bound provides us with a useful step towards a more general entropy bound known as *null entropy bound*. This was proposed by Bousso [32, 33] and can be regarded as a generalisation and refinement of a previous proposal by Fischler and Susskind [31] according to which a light-like rather than space-like formulation is needed in cosmological situations. Bousso's entropy bound relies on the following geometric construction. Unlike the space-like entropy bound, the starting point is not a co-dimension 1 spatial region but rather a co-dimension 2 surface $\mathcal{B}$. Independently of the shape and location of the given surface, there exist four null hypersurfaces bordering on $\mathcal{B}$ which are uniquely generated by the four orthogonal null directions locally identified by the past and future directed light rays emanating from $\mathcal{B}$ (see Fig. 1.1). The expansion θ of a family of light rays orthogonal to a smooth surface in a given spacetime is negative (positive) if the rays are converging (diverging) as one moves along them away from the surface. Indeed, the expansion of a family of infinitesimally neighboring light rays spanning a surface area A is given by the ratio $\frac{\mathrm{d}A/\mathrm{d}\lambda}{A}$, where λ denotes the affine parameter along the light ray, so that the area of the hypersurface spanned by null directions with negative expansion decreases moving away from $\mathcal{B}$. The null directions which

satisfy the conditions $\theta(\lambda) \leq 0$ are called *light-sheet directions* and are thought of as "inside" directions[9]. For any surface $\mathcal{B}$, the null hypersurface $\mathcal{L}_\mathcal{B}$ generated by the families of inside light rays orthogonal to $\mathcal{B}$ is called a *light-sheet* of $\mathcal{B}$ and is characterised by a non-positive expansion $\theta(\lambda) \leq 0$ everywhere on it. The expansion decreases moving away from $\mathcal{B}$ along the light-sheet surface so that light-sheets must terminate at caustics where light rays locally intersect and θ becomes positive. For a spherical surface in Minkowski spacetime, for instance, $\mathcal{B}$ is a normal surface, future and past directed ingoing light rays have negative expansion, and light-sheets are cones bounded by $\mathcal{B}$ as schematically reported in Fig. 1.1[10].

The null entropy bound then still compares the area of the surface $\mathcal{B}$ with entropy, the latter however is now the entropy of matter on light-sheets of $\mathcal{B}$. What changes compared to the space-like bound is then where to look for the entropy. Specifically, denoting by $\tilde{s}^a$ the entropy current density of matter so that the entropy crossing the light-sheet is given by $S(\mathcal{L}_\mathcal{B}) = \int_{\mathcal{L}_\mathcal{B}} \mathrm{d}^{D-1}x_a \tilde{s}^a$, Bousso's conjecture for the null entropy bound can be stated as follows:

Null entropy bound

Let $A(\mathcal{B})$ be the area of an arbitrary (possibly open) codimension 2 spatial surface $\mathcal{B}$. The entropy $S(\mathcal{L}_\mathcal{B})$ on any light-sheet $\mathcal{L}_\mathcal{B}$ of $\mathcal{B}$ will not exceed a quarter of the area of the surface $\mathcal{B}$ in Planck units, i.e.

$$S(\mathcal{L}_\mathcal{B}) \leq \frac{A(\mathcal{B})}{4} \,. \tag{1.10}$$

Although it has not been proven to hold in general, such an upper bound is supported by plenty of examples thus suggesting it to be universally applicable (for a review we refer to [8] and reference within). The bound has been proven in the context of general relativity with the assumption that entropy can be described by a continuum fluid and under certain conditions relating entropy and energy densities [34]. However, at a fundamental level entropy is not expected to be a fluid and the assumed conditions for entropy and energy are not necessarily satisfied. Moreover, the formulation of the null entropy bound relies on geometric concepts defined in a fixed spacetime equipped with a classical (or semi-classical) metric on which matter fields live. Therefore, the null entropy bound has not been derived from first principles, but is rather a feature of matter and gravity at the (semi-)classical level that should be explained by a more fundamental theory. In specific situations, the null entropy bound reduces to the space-like bound [32] but is valid much more generally [8, 33, 35]. This can be easily understood in the case depicted in Fig. 1.1 where one considers a closed, weakly gravitating, smooth surface $\mathcal{B}$ admitting at least one future-directed complete light sheet ($\mathcal{L}_\mathcal{B}$) whose only boundary is $\mathcal{B}$. Independently of the choice of the spatial slicing, all matter present in the spatial region $\Gamma_\mathcal{B}$ enclosed by $\mathcal{B}$ on the same side as $\mathcal{L}_\mathcal{B}$ will pass through $\mathcal{L}_\mathcal{B}$. The second law of thermodynamics then implies $S_{\Gamma_\mathcal{B}} \leq S(\mathcal{L}_\mathcal{B})$, from which it follows that in this case the null entropy bound implies the space-like bound.

[9] There will always be at least two light-sheet directions. Indeed, at least one of each opposite pairs of null directions would be an inside direction as the generating light rays are continuations of each other. In degenerate cases in which the light rays are locally neither contracting nor expanding ($\theta = 0$), both directions of the pair are inside directions. A surface $\mathcal{B}$ with two light-sheet directions on the same spatial side is called *normal surface*.

[10] In this simple example, light-sheet directions have the same caustic point at the tip of the cone. In more general situations, each light ray in a light-sheet will have a different caustic point thus yielding a caustic surface.

Let us then close this section by briefly discussing how the null entropy bound deals with the objections to the space-like bound considered before.

Spatially flat FLRW universe: The past directed light sheet of the surface enclosing the very large region of space under consideration will terminate at the initial singularity and has therefore less entropy on it than is contained in the original spatial volume. It is actually possible to show [31] that the entropy passing through the light-sheet is less than a quarter of the surface area of the region under consideration and the null entropy bound is thus satisfied.

Closed FLRW space: Light rays starting at the boundary surface of Γ and traversing it directed towards the north pole have positive expansion. Therefore, they do not generate a light sheet and the null entropy bound does not apply. Light sheets are instead directed towards the south pole and the null entropy bound is valid for the complement of Γ in this case.

1.2 Statement of the Holographic Principle(s)

The different kinds of entropy bounds discussed in the previous sections impose remarkable limitations on the d.o.f. attributed to codimension 2 surfaces, or to space-like or null hypersurfaces bounded by them. These are kinematical restrictions as no reference to any form of the dynamics of such degrees of freedom is involved. A *holographic principle* is then a statement about dynamics. It extends an entropy bound at a dynamical level by postulating a form of the dynamics for matter fields and spacetime which can be entirely described in terms of the d.o.f. and observables measurable on the surface[11]. Depending on which kind of entropy bound is taken as starting point, the principle admits different formulations which as such are based on different assumptions and have different expected range of applicability.

The *strong holographic principle* takes as starting point the strong space-like entropy bound stating that all the dynamical information about the d.o.f. in a region of space is completely stored on its boundary. More precisely, it can be summarised as follows [15]:

Holographic principle (strong version)

Let $\mathcal{M}$ be a spacetime with boundary $\partial\mathcal{M} = \mathbb{R} \times \mathcal{B}$, where $\mathbb{R}$ corresponds to the time-like direction and $\mathcal{B} = \partial\Sigma$ denotes the boundary of the spatial manifold Σ. Denoting by $\mathcal{H}_{\text{bulk}}$ and $\mathcal{H}_{\mathcal{B}}$ the bulk and boundary Hilbert spaces, respectively, and by H_{bulk} and $H_{\mathcal{B}}$ the corresponding Hamiltonians, the principle states that there exists an isomorphism between such Hilbert spaces

$$I_{\text{hol}} : \mathcal{H}_{\text{bulk}} \longrightarrow \mathcal{H}_{\mathcal{B}} \,, \tag{1.11}$$

such that bulk and boundary dynamics are related by

$$H_{\mathcal{B}} = I_{\text{hol}} \circ H_{\text{bulk}} \,. \tag{1.12}$$

According to the discussion of the previous sections and the limitations of the strong entropy

[11] The metaphorical name of the principle first used by 't Hooft [12] refers to a conceptual analogy with optical holograms in which the information about a three-dimensional image is stored on a two-dimensional surface.

bound (and of the underlying strong entropy assumption), the above version of the holographic principle cannot however be expected to be of universal applicability. At best, the strong form of the principle may only be valid for non-compact spacetimes with boundary thus excluding for instance, already at the classical level, generic cosmological situations. Moreover, even in the case of spacetimes of the kind compatible with the underlying assumptions of the principle, troubles might arise once situations beyond the weak gravitational regime are considered and fluctuations of gravitational d.o.f. are included. As we will discuss in Ch. 2, the strong holographic principle admits an explicit realisation in the case of Anti de Sitter spacetime and its most known implementation is the so called Anti-de Sitter/Conformal Field Theory (AdS/CFT) correspondence which relates a bulk gravitational theory in AdS background (supergravity or string theory) with a conformal field theory (super Yang-Mills) thought of as living on its conformal boundary [36–41]. In such a framework, however, much evidence for the construction of the holographic isomorphism is provided in the semiclassical and weak gravity approximation for the bulk gravitational theory and its extension beyond such a regime to include all possible states for the bulk spacetime comes to be the core of a more general (still conjectured) holographic gauge/gravity duality.

The next step towards a more general formulation of the holographic principle would then be based on the null entropy bound. The corresponding version of the holographic principle involves a collection of light sheets covering spacetime so that the dynamics of matter fields is described in terms of the d.o.f. measured on them. More precisely, the *null holographic principle* can be then stated as follows [8, 15]:

Holographic principle (null version)

A spacetime $\mathcal{M}$ is said to have a (*single*) *null holographic structure* if there exists a one parameter family $\mathcal{B}(t)$ of *screens*, i.e. codimension 2 space-like surfaces where measurements are performed thus encoding information on the causal past of the surface, such that there is a one parameter family $\mathcal{H}(t)$ of Hilbert spaces associated to the corresponding family $\mathcal{L}(t)$ of light sheets of $\mathcal{B}(t)$ satisfying the bound

$$\dim \mathcal{H}(t) \leq e^{A(\mathcal{B}(t))/4} \qquad \forall\, t\,, \tag{1.13}$$

and, for any two times t_1 and t_2, there is a unitary operator $U(t_2, t_1)$ such that

$$\mathcal{H}(t_2) = U(t_2, t_1) \circ \mathcal{H}(t_1) \qquad \forall\, t_1, t_2\,, \tag{1.14}$$

i.e., for any t, the number of independent quantum states describing the light sheet $\mathcal{L}(t)$ of $\mathcal{B}(t)$ is bounded by a quarter of the surface area (in Planck units) and, for any t_1 and t_2, the state of matter fields on $\mathcal{L}(t_2)$ is completely determined by that on $\mathcal{L}(t_1)$.

Such a version of the holographic principle would still be tied by some potential limitations. First of all, the constructions underlying the null entropy bound are based on the regime of QFT on a fixed (approximately) classical background spacetime whose metric and causal structure

are necessary for instance to determine congruences of light rays orthogonal to the screen. But, already at the level of classical general relativity, spacetime itself becomes a dynamical entity so that a background-independent version of the principle would require for instance a phase space formulation to include dynamical fluctuations of gravitational d.o.f. One might also take the point of view that the holographic structure is an emergent property of spacetime in the semiclassical limit of a more fundamental quantum theory. Even in this respect, however, the above version of the holographic principle could not be expected to apply in generic situations. Indeed, the screens are all assumed to have the same area in (1.13) so that the Hilbert spaces can be unitarily equivalent (cfr. Eq. (1.14)). In general, this would not be the case as light sheets in generic spacetimes might be of limited extension and not be complete so that they do not cover the complete future or past of any Cauchy surface[12]. As discussed in [15, 18], this requirement can be weakened by considering a description of the system in terms of more than one screen encoding the (partial) information available to local observers in spacetime. One is thus lead to ask whether there is a more general version of the holographic principle possibly surviving in a background-independent quantum theory of gravity. Such a formulation of the principle would involve a weak form of entropy bound, the only logical possibility left in the light of the above discussions. By considering a discrete abstract notion of quantum spacetime based on the concept of *causal histories*, i.e. partially ordered sets of events under their causal relations, Markopoulou and Smolin [15, 42] proposed a *weak holographic principle* containing the possible criteria for a discrete holographic theory. Without entering the technical details which are not relevant for the purposes of this work where we focus on effective models rather than full quantum gravity, such a weak form of holography reverses the relation between geometry and information content suggesting a more radical perspective according to which all observables of the quantum theory are associated with screens and the properties of the former can be used to define the geometrical properties of the latter. This is not in contradiction with the previous semiclassical perspectives which might eventually be recovered in a suitable limit of a more fundamental quantum theory incorporating weak holographic features.

1.3 Implementing Holography in Quantum Gravity

The implementation of a suitable form of the holographic principle in full quantum gravity is still an open issue in various approaches. This is due first of all to the fact that a complete consistent theory of quantum gravity is still missing and hence whether and how holography can be incorporated as a fundamental feature of the theory strongly depends on the details of the specific approach. Although based on different notions of holography, some progress has been achieved over the last years both in string theory and loop quantum gravity.

From the string theory side, as we will discuss in Ch. 2, most of the progress in understanding the possible holographic nature of gravity comes from AdS/CFT where the null (and eventually the strong) holographic principle can be explicitly realised. This however strongly depends on the

[12] This instead turns out to be the case for asymptotically AdS spacetimes considered in AdS/CFT. Remarkably, complete light sheets can also be found for other kinds of spacetime of interest such as de Sitter or Minkowski (see e.g. [8, 33, 35] and references within).

presence of a asymptotically AdS background spacetime and on the properties of its conformal boundary. Moreover, most of the results in such a framework are based on the low energy semi-classical bulk approximation so that whether quantum string theory is holographic or whether the known results can be generalised to other kinds of spacetimes remain some of the main open questions of the field. The main difficulties in this respect come from the fact that string theory in its current formulation mostly relies on perturbative techniques and non-perturbative quantum string theory is still poorly understood even on a fixed background spacetime (see however [43–46] for reviews in this direction). In particular, a background-independent formulation of the theory is out of reach. This has motivated the attempt of applying background-independent techniques developed in loop quantum gravity to string theory. These include for instance the attempt of a direct LQG-quantisation of classical string theory on flat background [47] or proposals for more abstract extensions of the LQG formalism to higher dimensional objects such as strings and membranes [48–50]. More recently, a loop quantisation of supergravity theories has also been initiated [51–53] aiming at the identification of a possible LQG-type subsector of string theory which in turn has motivated some preliminary proposal to go beyond the semi-classical approximation in AdS/CFT [54, 55]. However, the considerably high amount of complexity of the full theory setting makes the attempt to set up explicit calculations a very hard task and no definite relation between string theory and LQG has been established so far.

Independently of a possible contact with string theory, from the LQG side and related formalisms, two main parallel directions have been pursued to study holographic aspects. The first one concerns the kinematical structure of the theory and proposes a relation between the quantum states of LQG (spin networks) and tensor networks [56–59]. The latter describes the quantum correlations of the boundary d.o.f. resulting from a coarse-graining of the more fundamental LQG states thus realising a bulk/boundary holographic mapping. This has been used to study possible relations between entanglement and spacetime geometry[13]. The second line concerns instead the establishment of a so-called *quasi-local* dynamical holographic duality for non-perturbative quantum gravity. The main point is that the inbuilt diffeomorphism invariance of gravity prevents already at the classical level a local definition of the basic dynamical quantities such as energy, momentum and angular momentum. For arbitrary regions in spacetime, these can only be defined in terms of so-called quasi-local observables [64, 65], that is as integrals over the two dimensional boundary surfaces. This implies that if some notion of holography can be defined in a diffeomorphism invariant context this must be quasi-local for finite boundaries and eventually reproduce the other notions only when asymptotic boundaries are present. Most of the work in this direction has been done in three dimensions where, exploiting the topological nature of 3d gravity, explicit dual theories have been recently constructed for covariant path integral models of non-perturbative QG [66–68]. Much less is known in four dimensions (see however [69, 70] for some recent results).

Given the above situation and the technical difficulties that arise in different approaches when

[13] In this respect, it is worth to mention that tensor networks have gained considerable attention also in the AdS/CFT literature where they have been proposed as a tool to construct holographic dualities opening the way to fruitful interdisciplinary overlaps with other fields ranging from quantum information to condensed matter physics (see e.g. [60–63] and references therein).

considering the respective full theory settings, the work presented in this manuscript is based a more "pragmatic" perspective and can be though of as the starting point of a parallel research program which focuses on effective models for symmetry-reduced spacetimes such as cosmology or black holes. Indeed, as anticipated in the preface of the thesis, the main reason motivating us to study such kind of systems relies on the fact that they provide us with relatively simple examples where explicit quantum corrected geometries can be constructed and open questions can be addresses with reasonable effort either analytically or numerically. As such they become the ideal arena to try to learn useful lessons for the full theory and eventually make contact between various approaches and the different notions of holography associated with them. Moreover, symmetry-reduced models may open a window on observational tests of QG predictions.

Before entering the details of our work, however, some background material needs to be introduced. In particular, since our long term goal is the application of LQG techniques in AdS/CFT, the second part of the thesis is then devoted to discussing the main aspects of both.

Part II

BACKGROUND MATERIAL

Chapter 2

The AdS/CFT Correspondence

Gauge/gravity duality is one of the major developments in modern theoretical physics over the last two decades. It is a conjectured duality between an ordinary (non-gravitational) quantum field theory and a gravity theory itself. As such it can offer new perspectives and tools for addressing open issues on both sides. In fact, being a strong/weak coupling duality, hard tasks on the one side – regarding for instance the quantum nature of gravity (at least in certain spacetimes) or strongly coupled field theories – can be translated into the other side where they hugely simplify. Originally motivated from string theory, it has now become a very active and rich research field by its own at the crossroad of different scientific fields ranging from quantum information and condensed matter to gravitational and particle physics. In this chapter we review the main aspects of gauge/gravity duality and its most studied example: the so-called AdS/CFT correspondence proposed by Maldacena in his seminal paper [36]. There, the QG theory is a string theory in asymptotically Anti-de Sitter (AdS) spacetimes and the gauge theory is a conformal field theory (CFT). For the sake of clarity, we will try to avoid specific technicalities of string theory, rather focusing on toy-model examples to emphasize those aspects which will be relevant for the forthcoming chapters. Standard references on the topic are the textbooks [71–73] as well as review articles [41, 74–76] on which the main content of the chapter is based.

2.1 Hints from Both Sides

In order to understand the details of the AdS/CFT correspondence and its motivations, let us start by introducing some key features of the two sides involved in such a duality. On the field theory side, this includes the fact that that the quantum field theory is a conformal field theory and the large N behaviour of gauge theories. On the gravity side, properties of AdS spacetime and its conformal structure will play a crucial role.

2.1.1 Basics of Conformal Field Theories

A d-dimensional conformal field theory (CFT_d in short) is a field theory over a d-dimensional spacetime whose fields transform covariantly under conformal coordinate transformations. In

other words, the field content of a CFT_d is organised in terms of (irreducible) representations of the algebra of the conformal group in d dimensions[1].

Let then $(\mathcal{M}, g)$ be a d-dimensional spacetime equipped with a metric g of signature (p, q), i.e., such that $p + q = d$. Intuitively speaking, a conformal transformation is a transformation which preserves the angle $g_{\mu\nu}u^\mu v^\nu/\sqrt{u^2 v^2}$ between two vectors u and v. More precisely, the conformal group is the subgroup of coordinate transformations $\varphi : \mathcal{M} \to \mathcal{M}$ which leave the metric invariant up to a (spacetime dependent) scale factor, i.e., such that $\varphi : g \mapsto g' = \varphi^* g := \Omega g$ or in components

$$g_{\mu\nu}(x) \longmapsto g'_{\mu\nu}(x') = \Omega(x) g_{\mu\nu}(x) \ . \tag{2.1}$$

The case of interest for the discussion of the forthcoming sections is that of a flat metric $g_{\mu\nu} = \eta_{\mu\nu}$, i.e. $\mathcal{M} = \mathbb{R}^{p,q}$. In this case, as can be checked by direct computation for an infinitesimal transformation $x^\mu \mapsto x'^\mu = x^\mu + \xi^\mu(x)$, the transformation behaviour of the metric under generic coordinate transformations together with the definition (2.1) of conformal transformations yield the conformal Killing equation[2]

$$\partial_\mu \xi_\nu + \partial_\nu \xi_\mu = \mathcal{K}(x)\eta_{\mu\nu} \qquad , \qquad \mathcal{K}(x) = \Omega(x) - 1 = \frac{2}{d}(\partial \cdot \xi) \ , \tag{2.2}$$

where ξ satisfies the constraint

$$(d-1)\Box(\partial \cdot \xi) = 0 \ . \tag{2.3}$$

In $d = 2$ dimensions, Eq. (2.2) reduces to the Cauchy-Riemann equations, which are solved by any holomorphic function. Therefore, in the two dimensional case, the conformal algebra is infinite dimensional and we have an infinite number of conserved quantities. For $d > 2$, however, conformal symmetry is finite dimensional and (2.3) tells us that $\xi^\mu(x)$ can be at least quadratic in x. The generic solution to the conformal Killing equation (2.2) reads as

$$\xi^\mu(x) = a^\mu + m^\mu_\nu x^\nu + \lambda x^\mu + b^\mu x^2 - 2(b \cdot x)x^\mu \quad \text{with} \quad m_{\mu\nu} = -m_{\nu\mu} \ , \ \mathcal{K}(x) = \lambda - 2b \cdot x \tag{2.4}$$

so that the conformal group in $d > 2$ dimensions comprises the following transformations: translations (zeroth order in x), Lorentz rotations and dilatations (linear in x), and special conformal transformations (quadratic in x). Counting then the number of independent parameters $(a^\mu, m^{\mu\nu}, \lambda, b^\mu)$, we see that the total number of generators is given by

$$\#\text{ generators} = d + \frac{d(d-1)}{2} + 1 + d = \frac{(d+1)(d+2)}{2} = \frac{(p+q+1)(p+q+2)}{2} \ , \tag{2.5}$$

which is exactly the same as for the $\mathfrak{so}(p+1, q+1)$ algebra[3]. In particular, conformal invariance

[1] In what follows we will just briefly review those aspects of CFT which are relevant for the present chapter. We refer to standard textbooks [77–79] for an extensive exposition.

[2] In the general non flat case, the conformal Killing vector is defined as a vector field ξ on $\mathcal{M}$ such that when the metric is dragged along the curves generated by ξ its Lie derivative is proportional to itself, i.e. $\mathcal{L}_\xi g = \mathcal{K} g$, for some scalar field $\mathcal{K} = \mathcal{K}(x)$, $x \in \mathcal{M}$.

[3] Strictly speaking, the special orthogonal group only contains elements continuously connected to the identity. The conformal group is an extension that contains also the inversion $x^\mu \mapsto x^\mu/x^2$. Indeed, all conformal transformations can be generated by combining the inversion with rotations and translations. For details on the

in flat $(1, d-1)$ dimensions ($d > 2$) corresponds to the symmetry group $\mathsf{SO}(2, d)$ ($\mathsf{SO}(1, d+1)$ in the Euclidean case) which, as we will discuss in the next section, is the isometry group of $(d+1)$-dimensional AdS space. This is the first hint of a relation between CFT on d-dimensional Minkowski space and a gravity theory in AdS_{d+1} spacetime.

Conformal symmetry imposes restrictions also on the stress-energy tensor. Indeed, under an infinitesimal scaling transformation $x^\mu \mapsto (1 + \delta\lambda)x^\mu$, the change in the metric is given by $\delta g_{\mu\nu} = 2\delta\lambda g_{\mu\nu}$ so that the corresponding change in the action reads as

$$\delta S = \int \mathrm{d}^d x \, \sqrt{-g}\, T^{\mu\nu}\, \delta g_{\mu\nu} = 2 \int \mathrm{d}^d x \, \sqrt{-g}\, T^\mu_\mu \, \delta\lambda \, . \tag{2.6}$$

A (sufficient) condition to have scale invariance of the action ($\delta S = 0$ for any $\delta\lambda$) is then the stress-energy tensor to be traceless

$$T^\mu_\mu = 0 \, . \tag{2.7}$$

At the classical level, the traceless property of the stress-energy tensor tells us that the theory is also invariant under active changes of the manifold called Weyl transformations $g_{\mu\nu} \mapsto e^{\omega(x)} g_{\mu\nu}$, for arbitrary $\omega(x)$. In the quantum theory this symmetry exhibits a calculable anomaly [78].

The generators of the conformal group can be constructed from the stress tensor via the standard procedure for Noether currents, namely

$$J^{(\mathrm{conformal})}_\mu = T_{\mu\nu}\delta x^\nu \qquad , \qquad Q^{(\mathrm{conformal})} = \int \mathrm{d}^{d-1} x \, J^{(\mathrm{conformal})}_0 \, . \tag{2.8}$$

Denoting by P_μ the momentum operator generator of translations, by $J_{\mu\nu}$ the generators of Lorentz transformations, and by D, K_μ respectively the generators of dilatations and special conformal transformations, the conformal algebra in $d > 2$ dimensions is identified by the Poincaré algebra supplemented by the following commutation relations

$$\begin{aligned} &[J_{\mu\nu}, K_\rho] = i(\eta_{\mu\rho} K_\nu - \eta_{\nu\rho} K_\mu) \, , \\ &[D, P_\mu] = iP_\mu \quad , \quad [D, K_\mu] = -iK_\mu \quad , \quad [D, J_{\mu\nu}] = 0 \, , \\ &[K_\mu, K_\nu] = 0 \quad , \quad [K_\mu, P_\nu] = -2i(\eta_{\mu\nu} D - J_{\mu\nu}) \, . \end{aligned} \tag{2.9}$$

Fields in a CFT transform in irreducible representations of the conformal algebra. The latter can be constructed via the so-called *method of induced representations* as follows. From the commutation relations (2.9) we see that the generators $J_{\mu\nu}$ and D provide a maximal subalgebra of compatible operators. Irreducible representations are thus labeled by the eigenvalues of these operators, i.e., they are defined in terms of eigenfunctions of the dilatation operator D with eigenvalue $-i\Delta$, where Δ is the so-called *scaling dimension*, namely[4]

$$[D, \phi(0)] = -i\Delta\phi(0) \, , \tag{2.10}$$

construction of the isomorphism relating the generators of these groups see for instance Sec. 3.2 in [71].

[4]Note that it is sufficient to analyse the transformation properties of the fields at $x = 0$ and the general transformation rules can be then obtained by shifting the argument of the field to an arbitrary point x by means of the momentum operator, say $\phi(x) = \mathcal{T}(x)\phi(0)\mathcal{T}^{-1}(x)$ with $\mathcal{T}(x) = \exp(-ix^\mu P_\mu)$.

in addition to which we have the commutation relations with the Lorentz generators $[J_{\mu\nu}, \phi(0)] = -\mathcal{J}_{\mu\nu}\phi(0)$, where $\mathcal{J}_{\mu\nu}$ denotes a finite-dimensional representation of the Lorentz group determining the spin for the field $\phi(0)$. Moreover, as can be easily checked by applying the commutation relations of D with P_μ and K_μ to the eigenstates of D, the operator P_μ increases the scaling dimension while K_μ decreases it. To organise the representation spaces, it is then sufficient to consider the so-called *quasi-primary fields* defined by the commutation relations

$$[K_\mu, \phi(0)] = 0 \,, \tag{2.11}$$

i.e., which are annihilated by K_μ at $x = 0$ (*highest weight states*). In a given irreducible multiplet of the conformal algebra, quasi-primary fields are the fields of lowest scaling dimension. All other fields spanning the representation space can be obtained by acting successively with P_μ on the quasi-primary fields ϕ and are called the *conformal descendants* of ϕ.

The relation (2.10) implies that under dilatations $x \mapsto x' = \lambda x$ the field ϕ transforms as

$$\phi(x) \longmapsto \phi'(x') = \lambda^{-\Delta}\phi(\lambda x) \,. \tag{2.12}$$

which at the infinitesimal level yields

$$\delta_D\phi(x) = [D, \phi(x)] = -i\Delta\phi(x) - ix^\mu\partial_\mu\phi(x) \,. \tag{2.13}$$

For a generic infinitesimal conformal transformation with Killing vector ξ given in (2.4), the infinitesimal transformation rules can be summarised in the form

$$\delta_\xi\phi(x) = -\mathcal{L}_\xi\phi(x) \quad , \quad \mathcal{L}_\xi = \xi^\mu(x)\partial_\mu + \frac{\Delta}{d}\partial_\mu\xi^\mu(x) - \frac{i}{2}\partial^{[\mu}\xi^{\nu]}(x)J_{\mu\nu} \,. \tag{2.14}$$

Covariance under conformal transformations imposes remarkable restrictions on the correlation functions of quasi-primary fields. To see this, let us consider for instance the 2-point function of two scalar quasi-primary fields ϕ_1, ϕ_2 for which we have

$$\langle\phi_1(x_1)\phi_2(x_2)\rangle = \left|\frac{\partial x'}{\partial x}\right|^{\Delta_1/d}_{x=x_1}\left|\frac{\partial x'}{\partial x}\right|^{\Delta_2/d}_{x=x_2}\langle\phi_1(x_1')\phi_2(x_2')\rangle \,. \tag{2.15}$$

Now, translations and rotations have unit Jacobian while for dilatations and special conformal transformations we have

$$\left|\frac{\partial x'}{\partial x}\right| = \lambda^d \quad , \quad \left|\frac{\partial x'}{\partial x}\right| = \frac{1}{(1 + 2b\cdot x + b^2x^2)^d} \,, \tag{2.16}$$

respectively. Invariance under translations and rotations forces the l.h.s. of Eq. (2.15) to depend only on $r_{12} \equiv |x_1 - x_2|$. Invariance under dilatations $x \mapsto \lambda x$ then implies that

$$\langle\phi_1(x_1)\phi_2(x_2)\rangle = \frac{C_{12}}{r_{12}^{\Delta_1+\Delta_2}} \,, \tag{2.17}$$

where C_{12} is a constant due to the normalization of the fields. Finally, by applying a special

conformal transformation to r_{12} and using (2.16), the condition (2.15) requires that $\Delta_1 = \Delta_2$ if $C_{12} \neq 0$, and hence

$$\langle \phi_1(x_1)\phi_2(x_2)\rangle = \begin{cases} \frac{C_{12}}{r_{12}^{2\Delta}} & \Delta_1 = \Delta_2 = \Delta \\ 0 & \Delta_1 \neq \Delta_2 \end{cases} . \tag{2.18}$$

Similar restrictions hold for higher correlation functions. 3-point functions are also completely determined (up to constant factors) by conformal symmetry, while n-point functions with $n \geq 4$ are not in general but can only depend of the $n(n-3)/2$ independent cross-ratios $r_{ij}r_{kl}/r_{ik}r_{jl}$.

2.1.2 Anti-de Sitter Spacetime and its Conformal Structure

Anti-de Sitter (AdS) spaces play an important role in the AdS/CFT correspondence. This is due to the fact that: First of all, the isometries of $(d+1)$-dimensional AdS space (AdS_{d+1} in short) form the group $\mathsf{SO}(d,2)$, which corresponds to the conformal group of a CFT in d dimensions. Moreover, AdS space has a constant negative curvature and a time-like boundary which can be intuitively thought of as the background spacetime on which this CFT lives.

In order to understand this, let us discuss in a bit more detail the geometry of AdS space and its causal structure. AdS_{d+1} spacetime is a maximally symmetric Lorentzian manifold with constant negative scalar curvature. It is a $(d+1)$-dimensional solution of Einstein field equations with negative cosmological constant ($\Lambda < 0$) given by

$$\mathcal{R} = -\frac{d(d+1)}{L_{AdS}^2} = \frac{2(d+1)}{d-1}\Lambda \quad , \quad \Lambda = -\frac{d(d-1)}{2L_{AdS}^2} \tag{2.19}$$

where $\mathcal{R}$ is the Ricci scalar and L_{AdS} is the so-called AdS *radius*. As a metric space, AdS_{d+1} can be actually described as an hyperboloid embedded in $\mathbb{R}^{2,d}$, i.e.

$$\text{AdS}_{d+1} := \left\{ X \in \mathbb{R}^{2,d} \;\middle|\; -X_{-1}^2 - X_0^2 + \sum_{k=1}^{d} X_k^2 = -L_{AdS}^2 \right\} , \tag{2.20}$$

with $X_{-1}, X_0, \ldots, X_d$ denoting the coordinates of the ambient space. The boundary of AdS_{d+1} is defined by the limit of all X coordinates being asymptotically large for which the hyperboloid identified by (2.20) approaches the light-cone in $\mathbb{R}^{2,d}$

$$-X_{-1}^2 - X_0^2 + \sum_{k=1}^{d} X_k^2 = 0 . \tag{2.21}$$

In other words, the asymptotic boundary corresponds to the set of all lines on the light-cone which originate from the origin of $\mathbb{R}^{2,d}$. As we will discuss soon, such a space corresponds to the conformal compactification of Minkowski spacetime $\mathbb{R}^{1,d-1}$. Moreover, note that the action of the $\mathsf{SO}(2,d)$ symmetry group on $\mathbb{R}^{2,d}$ descends also to AdS_{d+1} where it also acts as isometry group since the embedding equation (2.20) respects this symmetry[5].

[5] In the case of Euclidean signature, which can be obtained by Wick rotating X_{-1}, the isometry group is $\mathsf{SO}(1,d+1)$ and compatibly it corresponds to the conformal group of a Euclidean CFT_d.

The metric on AdS_{d+1} is given by the induced metric onto the hyperboloid from the natural metric on $\mathbb{R}^{2,d}$ whose line element reads as

$$\mathrm{d}s^2 = -\mathrm{d}X_{-1}^2 - \mathrm{d}X_0^2 + \sum_{k=1}^{d} \mathrm{d}X_k^2 \,. \tag{2.22}$$

The solutions of (2.20) can be parametrised by the following set of coordinates

$$\begin{cases} X_{-1} = L_{AdS} \cosh\rho \cos\tau \\ X_0 = L_{AdS} \cosh\rho \sin\tau \\ X_k = L_{AdS}\, \hat{\Omega}_k \sinh\rho \qquad k = 1, \dots, d \end{cases} \tag{2.23}$$

where $\hat{\Omega}_k$ are unit vectors parametrising a $\mathbb{S}^{d-1}$ sphere with $\sum_{k=1}^{d} \hat{\Omega}_k^2 = 1$, $\rho \in \mathbb{R}^+$, and we have unfolded $\tau \in \mathbb{S}^1$ into the universal covering space $\mathbb{R}$ to avoid closed time-like curves. $(\rho, \tau, \hat{\Omega}_k)$ are called *global coordinates*. In such coordinates, the induced metric on AdS_{d+1} reads as

$$\mathrm{d}s^2 = L_{AdS}^2 \left(-\cosh^2\rho\, \mathrm{d}\tau^2 + \mathrm{d}\rho^2 + \sinh^2\rho\, \mathrm{d}\Omega_{d-1}^2 \right) \,, \tag{2.24}$$

where $\mathrm{d}\Omega_{d-1}^2$ denotes the metric on $\mathbb{S}^{d-1}$. Thus, although the ambient space $\mathbb{R}^{2,d}$ had two "time directions", the embedded AdS_{d+1} is a standard Lorentzian spacetime. To draw the Penrose diagram we perform the coordinate redefinition $\sinh\rho = \tan\theta$ with $\theta \in [0, \pi/2)$ so that the metric (2.24) becomes

$$\mathrm{d}s^2 = \frac{L_{AdS}^2}{\cos^2\theta} \left(-\mathrm{d}\tau^2 + \mathrm{d}\theta^2 + \sin^2\theta\, \mathrm{d}\Omega_{d-1}^2 \right) \,, \tag{2.25}$$

which, after removing the prefactor via a Weyl rescaling, yields the metric on $\mathbb{B}^d \times \mathbb{R}$ with $\mathbb{B}^d$ the d-dimensional ball. The asymptotic boundary located at $\rho \to +\infty$ comes to be at finite coordinate distance $\theta = \pi/2$ and it is isometric to $\mathbb{R} \times \mathbb{S}^{d-1}$ (more precisely the metric covers the hemisphere times $\mathbb{R}$ as $0 \leq \theta < \pi/2$). The boundary of conformally compactified AdS_{d+1} is thus equal to the conformal compactification of $\mathbb{R}^{1,d-1}$. Unwrapping the boundary, AdS spacetime can be thought of as a solid cylinder whose interior represent the bulk of AdS_{d+1}, while the boundary is the cylinder itself as schematically reported in Fig. 2.1. Moreover, since the boundary of AdS_{d+1} is time-like, AdS spacetime is not globally hyperbolic. Evolution in the bulk requires the specification of data on the time-like asymptotic boundary. The Cauchy problem is thus ill-posed without prescribed boundary conditions and as a result the boundary degrees of freedom are part of a complete specification of the dynamics of the bulk theory. As we will discuss in the remaining of the chapter, this is a key feature from the AdS/CFT perspective.

Finally, another useful parametrisation of AdS spacetime is given in terms of the the so-called *Poincaré coordinates* defined by

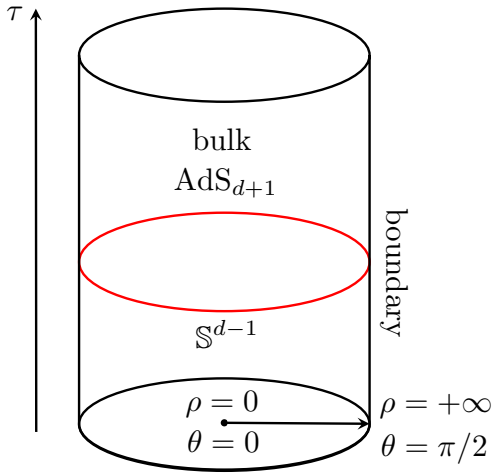

Figure 2.1: Solid cylinder representation of the Penrose diagram for AdS$_{d+1}$ spacetime. The boundary $\mathbb{R} \times \mathbb{S}^{d-1}$ in global coordinates contains the time direction (vertical) and a $(d-1)$-sphere represented here as a circle.

$$\begin{cases} X_{-1} = \frac{r\,t}{L_{AdS}} \quad , \quad X_i = \frac{r\,x_i}{L_{AdS}} \qquad i = 1, \dots, d-1 \\ X_0 = \frac{L_{AdS}^2}{2r}\left(1 + \frac{r^2}{L_{AdS}^4}\left(L_{AdS}^2 + \vec{x}^2 - t^2\right)\right) \\ X_d = \frac{L_{AdS}^2}{2\,r}\left(1 - \frac{r^2}{L_{AdS}^4}\left(L_{AdS}^2 - \vec{x}^2 + t^2\right)\right) \end{cases} \tag{2.26}$$

so that the induced metric on AdS$_{d+1}$ reads as

$$\mathrm{d}s^2 = \frac{L_{AdS}^2}{r^2}\mathrm{d}r^2 + \frac{r^2}{L_{AdS}^2}\left(-\mathrm{d}t^2 + \mathrm{d}\vec{x}^2\right) = \frac{L_{AdS}^2}{z^2}\left(\mathrm{d}z^2 - \mathrm{d}t^2 + \mathrm{d}\vec{x}^2\right) \ , \tag{2.27}$$

where in the second equality we introduced the coordinate $z = L_{AdS}^2/r$. Unlike global coordinates, Poincaré coordinates do not cover the entire spacetime but only a causal patch and there is a horizon at $z = \infty$ where the Killing vector ∂_t has zero norm. However, this is just a coordinate singularity as in fact the patch can be embedded into the global coordinates where there is no horizon and spacetime curvature remains finite (cfr. Eq. (2.19)). The boundary of AdS_{d+1} in Poincaré coordinates is located at $z \to 0$ ($r \to \infty$) and is a copy of Minkowski space $\mathbb{R}^{1,d-1}$ as can be easily inferred from the metric (2.27). But $\mathbb{R}^{1,d-1}$ and $\mathbb{R} \times \mathbb{S}^{d-1}$ are conformal to each other, so the passage from global to Poincaré coordinates in the bulk just corresponds to a conformal transformation in the boundary. From the AdS/CFT perspective, the dual CFT$_d$ only cares about the conformal structure of the underlying background spacetime and we can think of it as living on the asymptotic boundary of AdS$_{d+1}$ parametrised in different coordinate charts[6]. Note that the $\mathsf{SO}(2,d)$-isometry of Lorentzian AdS$_{d+1}$ is not manifest in such coordinate descriptions. Poincaré coordinates keep manifest a $\mathsf{SO}(1,d-1) \times \mathsf{SO(1,1)}$ symmetry where $\mathsf{SO}(1,d-1)$ is the Lorentz subgroup of the AdS isometry group and $\mathsf{SO(1,1)}$ corresponds to dilatations $(z,t,\vec{x}) \to \lambda(z,t,\vec{x})$. In global coordinates, a $\mathsf{SO}(d) \times \mathbb{R}_\tau$ symmetry is manifest.

[6]For a CFT, which as we have discussed before is invariant under Weyl transformations, the Penrose diagram provides a faithful representation of spacetime.

2.1.3 The Large N Limit of Gauge Theories

Another aspect which plays an important role in AdS/CFT concerns the behaviour of field theories with large number of colour degrees of freedom. As originally pointed out by 't Hooft [80] studying the theory of strong interactions in the limit of large number of colours, the crucial point is that $\mathsf{SU}(N)$ (or $\mathsf{U}(N)$) gauge theories with large N admit a significant simplification. This has to do with the following two facts:

1) in the so-called 't Hooft limit, the theory admits a simpler $1/N$ perturbation expansion, bearing much similarity to the string perturbation theory, leading to a long-held belief that strongly coupled gauge theories are secretly string theories;

2) the large N limit is essentially a classical limit for the theory.

To visualise the above statements let us consider a prototype example given by a simple matrix field theory described by the Lagrangian density[7]

$$\mathscr{L} = \frac{1}{g^2}\,\mathrm{Tr}\,\left[(\partial M)^2 + M^2 + M^3 + \dots\right]\,, \tag{2.28}$$

where M denotes a field transforming in the adjoint representation of the $\mathsf{U}(N)$ gauge group (the action is invariant under the transformation $M \mapsto UMU^\dagger$, $U \in \mathsf{U}(N)$), and g is the gauge coupling. We can then represent M as a $N \times N$ matrix

$$M^i_j = M^a(\tau_a)^i_j \qquad i,j = 1,\dots,N \tag{2.29}$$

where τ_a are the generators of $\mathsf{U}(N)$ which satisfy the completeness relations[8]

$$\sum_{a=1}^{N^2}(\tau_a)^i_j(\tau_a)^k_l = \delta^i_l\delta^k_j\,. \tag{2.30}$$

To keep track of the powers of N in the perturbative expansion it is convenient to rewrite the Lagrangian (2.28) as

$$\mathscr{L} = \frac{N}{\lambda}\,\mathrm{Tr}\,\left[(\partial M)^2 + M^2 + M^3 + \dots\right]\,, \tag{2.31}$$

where we have multiplied and divided by N and introduced the so-called *'t Hooft coupling*

$$\lambda = g^2N\,. \tag{2.32}$$

Moreover, in order to draw Feynman diagrams 't Hooft introduced a double-line notation for

[7] We refer to the chapter "1/N" in Coleman's book [81] for a detailed exposition of the subject as well as for other relevant examples.

[8] For the $\mathsf{SU}(N)$ case, we have

$$\sum_{a=1}^{N^2-1}(\tau_a)^i_j(\tau_a)^k_l = \delta^i_l\delta^k_j - \frac{1}{N}\delta^i_j\delta^k_l\,,$$

where the additional term comes from the trace constraint and it is negligible in the $N \to \infty$ limit. Therefore, for large N, there is essentially no difference at leading order between $\mathsf{U}(N)$ and $\mathsf{SU}(N)$ theories.

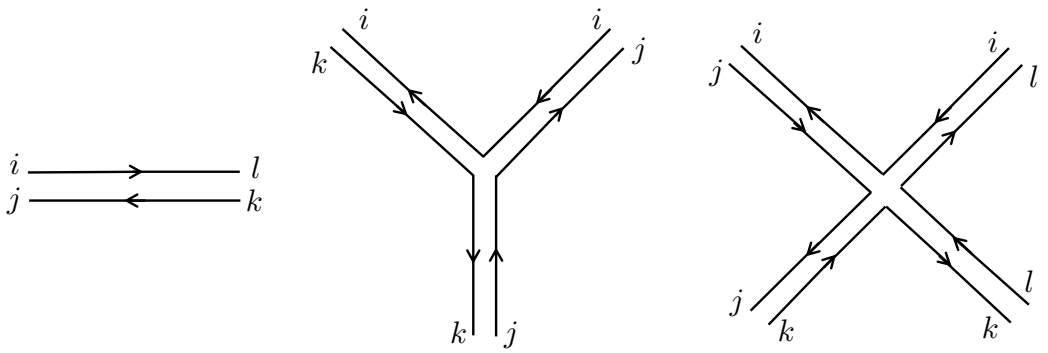

Figure 2.2: Double-line representation of elementary Feynman diagrams for the matrix theory (2.31).

matrix index contractions according to which the elementary diagrams for the theory can be graphically represented as in Fig. 2.2.

Looking at (2.31), it is straightforward to see that in a given diagram each propagator contributes with a factor λ/N, each vertex with a factor N/λ and, since each closed line represents a sum over matrix indices, each loop contributes with a factor N. In such a double-line notation, Feynman diagrams can be translated into a discretisation of a two-dimensional surface in which propagators, vertices, and loops of the diagrams respectively correspond to the edges (E), the vertices (V), and the faces (F) of the triangulation. For connected vacuum diagrams, the resulting surface is compact, closed and oriented. A given diagram $\mathcal{F}$ will then contribute as

$$\mathcal{F} \sim \left(\frac{N}{\lambda}\right)^V \left(\frac{\lambda}{N}\right)^E N^F = \lambda^{E-V} N^\chi \,, \tag{2.33}$$

where $\chi = V - E + F$ is the Euler characteristic of the surface which, for a compact surface without a boundary, is related to its genus G via the relation $\chi = 2 - 2G$. Therefore, Feynman diagrams come to be organised into topological classes classifying the powers of N. In particular, in the limit $N \to \infty$ with $\lambda = g^2 N$ fixed (*'t Hooft limit*), the leading contribution comes from the genus $G = 0$ which corresponds to planar diagrams with sphere topology while non-planar diagrams are $1/N^2$ suppressed. Moreover, in the large N limit the theory is essentially classical as can be naively argued from the path integral $\int [\mathcal{D}M] e^{-\frac{i}{\hbar}\int \mathscr{L}}$ which localises at the saddle point for $\hbar_{\text{eff}} = \frac{\hbar}{N} \to 0$. More precisely, a closer inspection of correlation functions for gauge invariant operators, obtained by taking functional derivatives of the generating functional, and simple counting arguments show that the dominant contribution to two-point functions comes from disconnected diagrams and higher-point functions are suppressed by powers of $1/N$. Cross-correlation functions due to quantum effects are thus suppressed in the large N limit.

The above description of Feynman diagrams has a formal similarity with string-theory diagrams with g_s and α' playing the role of $1/N$ and λ, respectively. This can be taken as a hint that large N field theories are related to string theories. However, despite of the fact that the above discussion is valid for any matrix theory, it does not tell us which kind of string theory is given by the collection of field-theory Feynman diagrams. As briefly discussed in the next section, the AdS/CFT correspondence in turn provides an explicit example of such a relation.

2.2 Statement of the Correspondence

The term *duality* generically refers to a dynamical equivalence between two theories which describe the same physical system. In other words, the two theories – which might have a priori different Lagrangian (or Hamiltonian) formulations – represent different ways to encode the same kind of degrees of freedom thus describing the same physics. *Gauge/gravity duality*, as the name itself suggests, is a duality which relates a quantum field theory without gravity (gauge theory) with a gravity theory. Although many examples in support of its existence have been studied, it has not been derived from first principle and hence it is still a conjecture so far. The most studied examples in which such a duality can be tested (at least in certain regimes of approximation) involve on the one side gravity in asymptotically AdS spacetimes, and conformal field theories on the other side. The latter can be thought of as living on the time-like asymptotic boundary of AdS. This is the framework of the so-called AdS/CFT correspondence originally proposed by Maldacena in 1997 [36], which in its strongest form can be summarised as follows:

$\mathrm{AdS}_{d+1}/\mathrm{CFT}_d$ correspondence (general statement)

Quantum gravity in asymptotically $\mathrm{AdS}_{d+1} \times \mathcal{X}$ spacetimes, with $\mathcal{X}$ a compact space, is dynamically equivalent to a CFT_d on a d-dimensional spacetime $\mathcal{B}_d$. The latter can be thought of as the AdS asymptotic boundary $\mathcal{B}_d = \partial(AdS_{d+1})$ in the sense that boundary conditions for the dynamics of the "bulk" gravitational theory are provided by CFT data.

The original motivation for the above correspondence comes from string theory[9]. Indeed, the bulk quantum theory of gravity in Maldacena's focal example is Type IIB superstring theory on asymptotically $\mathrm{AdS}_5 \times \mathbb{S}^5$ spacetimes, while the dual CFT is $\mathcal{N} = 4$ Super Yang-Mills (SYM) theory in four dimensions. The so-called *strongest form* of such a $\mathrm{AdS}_5/\mathrm{CFT}_4$ duality reads as [36,71]

AdS/CFT correspondence (Maldacena's conjecture)

Four dimensional $\mathcal{N} = 4$ SYM with gauge group $\mathsf{SU}(N)$ and coupling constant g_{YM} is dynamically equivalent to a Type IIB superstring theory in asymptotically $\mathrm{AdS}_5 \times \mathbb{S}^5$ spacetimes whose free parameters, the string constant α' and the string coupling g_s, are related to the free parameters N, g_{YM} of the gauge theory by

$$L^4_{AdS}/\alpha'^2 = 2\, g^2_{\mathrm{YM}} N = 2\lambda \qquad , \qquad 2\pi g_s = g^2_{\mathrm{YM}} \,. \tag{2.34}$$

Without entering the details of the argument which are not relevant for the purposes of the present work, let us just briefly recall the strategy for completeness and then comment on the main aspects involved. Maldacena's argument focuses on the analysis of the decoupling limit of the open + closed strings dynamics associated with a stack of N coincident D3-branes in type IIB string theory. The key point is that in the low-energy limit where only massless degrees

[9] Further motivations from a more modern perspective which are independent of string theory can be found for instance in [82–85].

of freedom contribute, open strings give rise to gauge theories while closed strings give rise to gravity theories. Indeed on the one hand, at weak coupling $g_sN \ll 1$, D-branes can be thought of as charged hypersurfaces on which open strings may end (the "D" actually stands for Dirichlet boundary condition). The total action for the system is then $S_{\rm tot} = S_{\rm open} + S_{\rm closed} + S_{\rm int}$, where $S_{\rm open}$ describes the dynamics of open strings ending on the D-branes, $S_{\rm closed}$ describes the closed string excitations in flat $\mathbb{R}^{1,9}$ spacetime, and $S_{\rm int}$ the interactions between open and closed string modes. In the low-energy limit in which the string length $\ell_s = \sqrt{\alpha'} \to 0$, the open strings decouple from the closed strings and $S_{\rm int}$ goes to zero. In such a limit, the closed strings are described by type IIB supergravity in flat Minkowski spacetime $\mathbb{R}^{1,9}$, while the open string sector yields a (3+1)-dimensional $\mathsf{SU}(N)$ SYM theory with effective coupling $g^2_{\rm YM} = 2\pi g_s$.

At strong coupling $g_sN \gg 1$, on the other hand, the branes can be viewed as massive objects so that they backreact and curve the spacetime sourcing an extremal black brane geometry given by the solution of type IIB supergravity [86]

$$\mathrm{d}s^2 = f(r)^{-\frac{1}{2}}\eta_{\mu\nu}\mathrm{d}x^\mu \mathrm{d}x^\nu + f(r)^{\frac{1}{2}}\left(\mathrm{d}r^2 + r^2\mathrm{d}\Omega_5^2\right) \quad , \quad f(r) = 1 + \frac{4\pi g_s N\alpha'^2}{r^4} \tag{2.35}$$

where x^μ are the coordinates along the (3+1)-dimensional world-volume of the D3-branes, and the second term in (2.35) describes the six transverse directions with $\mathrm{d}\Omega_5^2$ the metric of a $\mathbb{S}^5$ sphere. One is thus left with a theory of closed stings propagating in this background. In the low-energy limit, there are two kinds of closed strings. Indeed, asymptotically for large r, $f(r) \to 1$ and we recover a flat (9+1)-dimensional spacetime. Modes propagating in the asymptotic region decouple from the near-horizon region ($r \sim 0$)[10] since its cross section vanishes in this limit [87]. Moreover, from the asymptotic viewpoint, any finite-energy excitation E_r near the horizon will be strongly redshifted as $E_\infty = f(r)^{-1/4}E_r \sim \frac{r}{\alpha'}(\ell_s E_r)$ approaches zero as $\ell_s = \sqrt{\alpha'} \to 0$ (keeping r/α' fixed so that E_∞ remains finite). In such a limit, defining $z = L^2/r$ with $L = (4\pi g_s N\alpha'^2)^{1/4}$, the near-horizon geometry of (2.35) reads as

$$\mathrm{d}s^2 = \frac{L^2}{z^2}\left(\mathrm{d}z^2 + \eta_{\mu\nu}\mathrm{d}x^\mu\mathrm{d}x^\nu\right) + L^2\mathrm{d}\Omega_5^2 \,, \tag{2.36}$$

which is nothing but the metric of $AdS_5 \times \mathbb{S}^5$ with curvature scales L_{AdS} and $L_{\mathbb{S}^5}$ given by $L = (4\pi g_s N\alpha'^2)^{1/4} = (4\pi g_s N)^{1/4}\ell_s$ (cfr. Eq. (2.27)).

The AdS/CFT correspondence can be then argued by combining the above open and closed string low-energy descriptions of our D3-brane system. In both pictures there are massless modes corresponding to free gravity in $\mathbb{R}^{1,9}$. For the other massless modes, we have type IIB supergravity on $AdS_5 \times \mathbb{S}^5$ in the near-horizon region of the closed string picture with $g_sN \gg 1$, while in the open string picture we have a $(3+1)$-dimensional $\mathcal{N} = 4$ SYM theory when $g_sN \ll 1$. This observation led Maldacena to conjecture a duality between these two theories providing that their free parameters are related as in (2.34). Strictly speaking, the above argument concerns the so-called *weak form* of the correspondence [71] which involves classical supergravity and SYM in the regime $N \gg \lambda \gg 1$. Indeed, the condition $L_{AdS} \gg \ell_s$ is necessary in order to trust the

[10] As it will become clear in a while, such an horizon does not enclose any spacetime singularity and just corresponds to the AdS apparent horizon in Poincaré coordinates.

(super)gravity approximation, i.e. to suppress stringy α' corrections to the geometry. On the gauge theory side, we have $L_{AdS}/\ell_s = (4\pi g_s N)^{1/4} \sim \lambda^{1/4}$ so that this translates into large 't Hooft coupling $\lambda \gg 1$. Moreover, to neglect quantum Planck corrections and trust perturbative string theory, g_s needs to be small which in turn corresponds to the large $N \gg \lambda$ planar limit on the field theory side ($2\pi g_s = \lambda/N$). Nevertheless, since the gauge theory is well-defined at any coupling, the duality is conjectured to extend for any value of λ. This yields the so-called *strong form* of the duality [71] between large N SYM with fixed but arbitrary λ and classical string theory ($g_s \to 0, \alpha' \neq 0$). Pushing further the range of parameters, one is led to the *strongest form* mentioned at the beginning of this section according to which quantum string theory ($g_s, \alpha' \neq 0$) on $AdS_5 \times \mathbb{S}^5$ is equivalent to $\mathcal{N} = 4$ SYM for any value of N and λ. Since non-perturbative quantum string theory is not yet fully understood, most of the tests of the duality are provided in the classical or semi-classical regime as schematically summarised in the following diagram

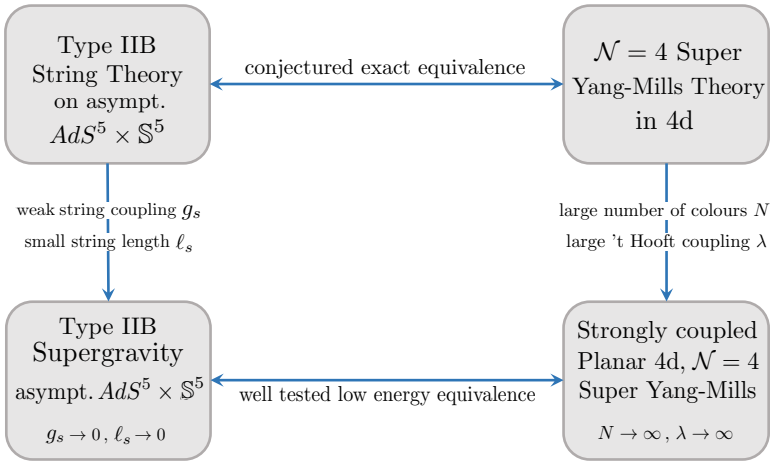

Before moving to discuss some of these tests which concern the dynamical aspects of the correspondence[11], few remarks on some general features are in order. First of all, in the l.h.s of the diagram the bulk theory has dynamical gravity and only asymptotic boundary conditions are fixed. By gravity (or string theory) on $AdS_5 \times \mathbb{S}^5$ we mean on a spacetime which is asymptotically $AdS_5 \times \mathbb{S}^5$ so that in principle all gravitational processes/geometries with that asymptotic structure are included. The dual field theory is instead defined on a fixed four dimensional background[12]. Second, as we have discussed before, the relation between the parameters on the two sides tells us that AdS/CFT is a *strong/weak coupling duality*. This is one of the most interesting aspects of AdS/CFT both from a practical and conceptual point of view. In fact, when

[11] A first immediate check at the kinematical level is that the symmetries on the two sides agree. $\mathcal{N} = 4$ SYM is a maximally supersymmetric theory in 4 dimensions. It has 32 supersymmetries (16 supersymmetries and 16 superconformal symmetries). The black-brane geometry, on the other hand, preserves all the 32 supercharges of Type IIB supergravity. The bosonic symmetries are $\mathsf{SO}(2,4) \times \mathsf{SO}(6)$. On the gravity side, they correspond to the isometries of $AdS_5 \times \mathbb{S}^5$. On the CFT side, they are global symmetries: $\mathsf{SO}(2,4)$ is the conformal group in 4 dimensions and $\mathsf{SO}(6)$ corresponds to the R-symmetry relating the supercharges.

[12] Although one might naively think the boundary of 10-dimensional $AdS_5 \times \mathbb{S}^5$ to be 9-dimensional, it is four dimensional. This can be easily seen from the metric (2.36). Indeed, by Weyl rescaling it by a factor L^2_{AdS}/z^2 so that the rescaled metric at the boundary ($z = 0$) is finite, we have

$$\mathrm{d}s^2 = \mathrm{d}z^2 + \eta_{\mu\nu}\mathrm{d}x^\mu \mathrm{d}x^\nu + z^2 \mathrm{d}\Omega_5^2 \,,$$

so that approaching the boundary the sphere shrinks to zero and we get a 3+1 dimensional geometry.

the gauge theory is strongly-coupled (and perturbative techniques fail), we can study it using the weakly-coupled gravity dual. Vice versa, long-standing questions in (quantum) gravitational physics can be studied by recasting them in a non-gravitational language.

2.3 Dynamical Aspects of the Correspondence

In the previous sections we discussed some of the kinematical evidences for the correspondence (matching of parameters and global symmetries). But as already stressed before, duality is a dynamical equivalence between two theories. In this section we will then focus on the dynamical aspects of AdS/CFT. The main point we want to show is that there is a 1-to-1 correspondence between fields in the bulk spacetime and gauge invariant operators of the field theory. This will then suggest a relation between the partition functions of the two theories thus allowing to put the equivalence between the two sides in more precise terms. To this aim, it is sufficient to keep the discussion generic and consider fields propagating in the bulk of AdS_{d+1} spacetime[13]. We will use Poincaré coordinates so that the field theory can be thought of as living on $\mathbb{R}^{1,d-1}$.

2.3.1 A Glimpse of the Bulk/Boundary Dictionary: Field-Operator Map

Let us start by considering the following toy-model action for a massive scalar field in AdS_{d+1} minimally coupled to gravity

$$S = \frac{1}{2}\int \mathrm{d}^{d+1}x\,\sqrt{-g}\left(\partial_A\phi\,\partial^A\phi + m^2\phi\right)\,, \tag{2.37}$$

where we used capital letters as a collective shorthand notation for all directions in AdS spacetime (including the radial z-direction). The scalar field ϕ then satisfies the Klein-Gordon equation

$$(\Box_g - m^2)\phi = 0\,, \tag{2.38}$$

with

$$\Box_g = \frac{1}{\sqrt{-g}}\partial_A\left(\sqrt{-g}\,g^{AB}\partial_B\right) = \frac{1}{L^2_{AdS}}\Big(z^2\partial_z^2 - (d-1)z\partial_z + z^2\eta^{\mu\nu}\partial_\mu\partial_\nu\Big)\,, \tag{2.39}$$

for the AdS_{d+1} metric (2.27) in Poincaré coordinates. Exploiting the $\mathsf{SO}(1,d-1)$ symmetry manifest in such a coordinate description, the field ϕ can be decomposed in Fourier modes as

$$\phi(z,x) = F(z)\,e^{ik_\mu x^\mu}\,, \tag{2.40}$$

and Eq. (2.38) gives the following second order PDE for $F(z)$

$$\left(z^2\frac{\mathrm{d}^2}{\mathrm{d}z^2} - (d-1)z\frac{\mathrm{d}}{\mathrm{d}z} - (k_\mu k^\mu)z^2 - m^2L^2_{AdS}\right)F(z) = 0\,. \tag{2.41}$$

[13]From the viewpoint of the setting considered in the previous section, there is no loss of generality. Indeed, as discussed before, the 5-sphere shrinks to zero approaching the boundary. Therefore, as discussed in [88], fields in the bulk of $\mathrm{AdS}_5\times\mathbb{S}^5$ can be thought of as fields propagating in AdS_5 after Kaluza-Klein compactification.

The solutions of such equation can be written exactly in terms of Bessel functions. However, for the purposes of the present discussion we are only interested in the asymptotic behaviour as $z \to 0$ for which Eq. (2.41) has two independent solutions

$$F(z) \underset{z\to 0}{\sim} z^{\Delta_\pm} \qquad , \qquad \Delta_\pm = \frac{d}{2} \pm \sqrt{\frac{d^2}{4} + m^2 L^2_{AdS}} \, . \tag{2.42}$$

The asymptotic behaviour of the general solution of Eq. (2.38) can be thus written as

$$\phi(z,x) \underset{z\to 0}{\sim} \phi_0(x) z^{\Delta_-} + \phi_1(x) z^{\Delta_+} + O(z^2) \, . \tag{2.43}$$

By definition we have $\Delta_+ \geq \Delta_-$ and $\Delta_- = d - \Delta_+$ (cfr. Eq. (2.42)) so the modes with fall-off z^{Δ_-} dominate as $z \to 0$ and one usually imposes the boundary condition on the dominant solution, namely[14]

$$\phi_0(x) := \lim_{z\to 0} \phi(z,x) z^{-\Delta_-} = \lim_{z\to 0} \phi(z,x) z^{\Delta_+ - d} \, . \tag{2.44}$$

Now, considering correlation functions for a scalar operator $\mathcal{O}$ with conformal dimension Δ in the boundary CFT_d, the generating functional would involve a term of the kind $\int \mathrm{d}^d x \, \mathcal{J}_0(x) \mathcal{O}(x)$, with $\mathcal{J}_0(x)$ denoting the source. Thus, recalling the scaling behaviour (2.12) for a primary conformal field, we see that to ensure this term to be dimensionless, $\mathcal{J}_0(x)$ has scaling dimesion $d - \Delta$. On the other hand, by definition $\Delta_- = d - \Delta_+$ (cfr. Eq. (2.42)) so that by looking at the behaviour of the near-boundary expansion (2.43) under rescaling $(z, x^\mu) \mapsto \lambda(z, x^\mu)$ (for which the AdS metric (2.27) is invariant), we see that for the bulk scalar field to remain invariant, the coefficients $\phi_0(x)$ and $\phi_1(x)$ have the correct scaling dimensions to be respectively the source $\mathcal{J}_0(x)$ and the vacuum expectation value for a CFT operator with dimension $\Delta = \Delta_+$. Therefore, there is a 1-to-1 correspondence between bulk fields and boundary operators: each bulk field provides the source for a boundary CFT operator, the conformal dimension of the latter being related to the mass of the dual gravity field via (2.42). To be precise, the identification of which mode is associated with the boundary source depends on the mass of the bulk field. First of all, from (2.42), one needs $m^2 L^2_{AdS} \geq -d^2/4$ to have a real square root[15]. For $0 > m^2 L^2_{AdS} \geq -d^2/4$ the dual field theory operators have conformal dimension $d/2 \leq \Delta = \Delta_+ < d$. Moreover, for $-d^2/4 \leq m^2 L^2_{AdS} \leq -d^2/4 + 1$, both fall-off modes $z^{\Delta_\pm}$ can be used to assign boundary conditions. Indeed, on the one hand, the on-shell action evaluated for a scalar field $\phi \sim z^\Delta$ converges for $\Delta \geq d/2$. On the other hand, integrating by parts and neglecting the boundary term, it converges for $\Delta \geq d/2 - 1$. In such a mass range, the identification of the source and the vacuum expectation value of the field theory operator can be interchanged.

Finally, here we considered the simple example of a scalar field but a field-operator correspondence can be established also for tensorial fields. This can be argued via symmetry considerations. Indeed, as discussed in Sec. 2.1.2, isometries of AdS_{d+1} correspond to the conformal group on the d-dimensional asymptotic boundary. Moreover, as discussed in Sec. 2.1.1, the field content

[14] Actually, since the boundary of AdS lies at infinity, one usually introduces a cut-off at $z = \epsilon$, impose "renormalised" boundary conditions there, and than send $\epsilon \to 0$ so that the solution in the bulk has finite limit.

[15] This is known as Brietenlohner-Freedman lower bound and was originally derived by demanding positive energy theorem in AdS [89,90]. Scalar fields in AdS are thus allowed to have negative mass squared and be stable, as long as it is not too negative.

of a CFT is entirely characterized in terms of irreducible representations of the conformal group labeled by their conformal dimension. Therefore, it is somehow natural to expect a relation between bulk fields and boundary CFT operators which belong to the same representations of the isometry or symmetry group, respectively[16]. In the case of a Maxwell field A_C in the bulk, for instance, the dual operator must be a vector J^μ coupled to the source as

$$\int \mathrm{d}x^d \, A_\mu(x) \, J^\mu(x) \, . \tag{2.45}$$

Gauge invariance of the bulk theory (in absence of anomalies, i.e. for gauge transformations vanishing at infinity) then implies that the boundary coupling must be invariant as well

$$\nabla_\mu J^\mu = 0 \, , \tag{2.46}$$

i.e., the boundary dual is a conserved current. This is the simplest example of bulk gauge symmetries manifesting themselves as global boundary symmetries. It can also be extended to higher p-form fields [38].

Similarly, the bulk metric is dual to the field theory energy-momentum tensor. Indeed, the boundary value of the bulk metric is the boundary metric, which is the background source for the energy-momentum tensor in the field theory. Moreover, being the energy-momentum tensor a dynamical quantity of the field theory, this is consistent with the bulk gravity to be dynamical. Different states in the field theory correspond to different configurations of the bulk spacetime geometry compatible with the (fixed) asymptotic structure. For instance, pure AdS corresponds to the vacuum of the field theory, the only state in the gauge theory which respects all the symmetries. Sufficiently excited states for which the symmetries are broken would correspond to deformed bulk geometries. Indeed, low energy excitations will not backreact on the geometry and can be described by fields propagating on AdS [38]. High energy excitations instead deform the bulk geometry. Such excited states have a non-zero expectation value of the boundary stress-energy tensor, which can be thought of as arising from the bulk metric being deformed from pure AdS. The precise identification between field theory states and bulk geometries is in general very difficult. Progress has been made in some special situation such as gravitational shock waves in the bulk [91] or Schwarzschild-AdS black holes [92]. More systematic approaches aiming at determining the bulk metric from the stess-energy tensor by means of the so-called *holographic renormalisation* have also been pursued (see e.g. [93, 94] and references within). This however goes beyond the purposes of this work and we will not enter the details here.

The above excursus was just meant to give a glimpse of the relation between bulk and boundary quantities. These are some of the early checks of the AdS/CFT correspondence and provide some of the entries of the *bulk/boundary dictionary*. This is a work in progress under active investigation and new entries have been added over the years [40, 41, 71–73, 83] benefiting also from tools from other research fields[17]. In the next section we will focus on correlation

[16] In the case of a bulk $\mathrm{AdS}_{d+1} \times \mathcal{X}$ spacetime, the symmetry group is of the kind $\mathsf{SO}(2,d) \times \mathsf{G}$, with G the symmetry of the compact space $\mathcal{X}$. The latter symmetries correspond to additional bosonic symmetries in the field theory. For instance, in $d = 4$ $\mathcal{N} = 4$ SYM case considered in Sec. 2.2, $\mathcal{X} = \mathbb{S}^5$ and $\mathsf{G} = \mathsf{SO}(6) \cong \mathsf{SU}(4)$.

[17] Recent results relating bulk geometric quantities such as the area of minimal surfaces and quantum entan-

functions of local operators which are important observables in a CFT and will turn useful in Ch. 4.

2.3.2 Generating Functionals and Correlation Functions

The field-operator map discussed above suggests a relation between the generating functionals on both sides of the correspondence. Indeed, the identification (2.44) of boundary values of bulk fields with sources for operators in the dual field theory suggests an equivalence between the bulk partition function, functional of the asymptotic boundary conditions, and the generating functional of CFT correlators, functional of the sources. More precisely, this provides us with the following mathematical statement of the correspondence:

AdS/CFT correspondence (mathematical statement)

Let $\mathcal{O}$ be an operator of conformal dimension Δ and let ϕ be its dual bulk field with leading asymptotic behaviour $\phi(z,x) \sim \phi_0(x) z^{d-\Delta}$ near the conformal boundary at $z=0$. The strongest form of the AdS/CFT correspondence states the following equivalence between the bulk quantum gravity partition function $\mathcal{Z}_{\text{QG}}[\phi]$ and the generating functional of CFT correlation functions

$$\mathcal{Z}_{\text{QG}}[\phi]\Big|_{\lim_{z\to 0}\phi(z,x)z^{\Delta-d}=\phi_0(x)} = \left\langle e^{i\int \mathrm{d}^d x\, \phi_0(x)\mathcal{O}(x)} \right\rangle_{\text{CFT}} , \tag{2.47}$$

where we suppressed any index so that the field ϕ can be a scalar, vector, tensor, etc., and integration over all possible field configurations is meant in $\mathcal{Z}_{\text{QG}}$. In the regime in which gravity in the bulk is weakly coupled, the QG partition function is dominated by the saddle points, i.e. the classical solutions to the EOMs. It can be thus approximated by the exponential of the classical on-shell gravitational action. The weak form of the AdS/CFT correspondence then amounts to the following equivalence

$$e^{iI_{\text{on-shell}}[\phi]}\Big|_{\lim_{z\to 0}\phi(z,x)z^{\Delta-d}=\phi_0(x)} = \left\langle e^{i\int \mathrm{d}^d x\, \phi_0(x)\mathcal{O}(x)} \right\rangle_{\text{CFT}} , \tag{2.48}$$

according to which the on-shell bulk gravitational action $I_{\text{on-shell}}$ is identified with the generating functional $\mathcal{W}[\phi_0]$ for CFT connected correlation functions

$$I_{\text{on-shell}}[\phi]\Big|_{\lim_{z\to 0}\phi(z,x)z^{\Delta-d}=\phi_0(x)} = \mathcal{W}[\phi_0] = -i\log \mathcal{Z}_{\text{CFT}}[\phi_0] \tag{2.49}$$

where $\mathcal{Z}_{\text{CFT}}[\phi_0]$ denotes the field theory partition function for the action $S + i\int \mathrm{d}^d x\, \phi_0(x)\mathcal{O}(x)$ deformed with a source term.

This is a non-trivial statement from both a conceptual and practical point of view. In fact, on the one hand, the full quantum gravity partition function is in general a very complicated object.

glement in the dual field theory [95–98] seem to suggest an intriguing relation between quantum information and the architecture of spacetime [99–102].

The partition function of full quantum string theory for instance is not known explicitly. The relation (2.47) can then be thought of as providing a non-perturbative definition for it via the dual quantum field theory. On the other hand, taking full advantage of the weak/strong coupling duality, the above relation between generating functionals can be used to compute correlation functions of composite operators in the strongly coupled gauge theory by translating it into a weakly coupled gravitational computation. Specifically, for a set of operators $\mathcal{O}_k$, $k = 1, \dots, n$ in the field theory, the connected correlation functions are obtained by taking derivatives of the generating functional $\mathcal{W}[\phi_0^k]$ w.r.t. the corresponding sources ϕ_0^k:

$$\langle \mathcal{O}_1(x_1) \dots \mathcal{O}_n(x_n) \rangle = (-i)^{n-1} \frac{\delta^n \mathcal{W}}{\delta\phi_0^1(x_1) \dots \delta\phi_0^n(x_n)} \bigg|_{\phi_0^k=0} . \tag{2.50}$$

According then to (2.49), the AdS/CFT prescription for computing correlation functions of local gauge invariant operators on the gravity side is the following:

1. Determine the bulk fields ϕ^k dual to the operators $\mathcal{O}_k$ of dimension Δ_k;

2. Solve the classical EOMs in the bulk theory with boundary conditions $\phi^k(z, x) \sim \phi_0^k(x) z^{d-\Delta_k}$ for $z \to 0$;

3. Evaluate the bulk action on such solutions;

4. Take variational derivatives of the resulting on-shell action w.r.t. the sources ϕ_0^k.

Such a recipe to compute correlation functions is known as GKPW prescription and has been worked out in the seminal papers by Gubser-Klebanov-Polyakov [40] and Witten [38], where it was shown that bulk computations reproduce the expected behaviour for CFT correlation functions thus providing important checks of the AdS/CFT correspondence.

As an example let us consider the two-point function for a scalar operator $\mathcal{O}$ with conformal dimension Δ in the CFT$_d$ side, which is dual to a scalar field ϕ in the $(d+1)$-dimensional gravity theory. Neglecting the backreaction of the field to the geometry, the bulk propagation is governed by the action (2.37) where the mass of of the scalar field satisfies $m^2 L_{AdS}^2 = \Delta(\Delta - d)$. The on-shell action can be computed integrating by parts the action (2.37) so that one term yields the bulk EOMs which vanish on-shell and we are left with a pure boundary term

$$I_{\text{on-shell}}[\phi] = -\frac{1}{2} \int_{z=\epsilon} \mathrm{d}^d x \, \sqrt{-g}\, g^{zz}\, \phi(z, x) \partial_z \phi(z, x) \, , \tag{2.51}$$

where the divergent contribution $\sqrt{-g} g^{zz} = (L_{AdS}/z)^{d-1}$ at $z = 0$ in the integrand needs to be regularised by introducing a small cut-off $\epsilon \ll 1$ for the radial coordinate $0 < z \leq \epsilon$ near the boundary, imposing boundary conditions at $z = \epsilon$, and then taking the limit $\epsilon \to 0$. Since the scalar field ϕ behaves as $z^{d-\Delta}$ at the boundary (cfr. Eq. (2.43)), we set

$$\phi(z, x) = \int \frac{\mathrm{d}^d p}{(2\pi)^d} \, e^{ip\cdot x} \Phi(z, p) \qquad \text{with} \qquad \Phi(z, p) = \frac{\phi_1(z, p)}{\phi_1(\epsilon, p)} \phi_0(p) \epsilon^{d-\Delta} \tag{2.52}$$

so that the field induced on the $z = \epsilon$ shell is ϕ_0. Inserting (2.52) and the explicit form of g^{zz} and $\sqrt{-g}$ for the metric (2.27) into the on-shell action (2.51), we get

$$\begin{aligned} I_{\text{on-shell}} &= -\frac{L_{AdS}^{d-1}}{2\epsilon^{d-1}} \int \frac{\mathrm{d}^d p}{(2\pi)^d} \frac{\mathrm{d}^d q}{(2\pi)^d} (2\pi)^d \delta^d(p+q) \Phi(z,q) \partial_z \Phi(z,p) \Big|_{z=\epsilon} \\ &= -\frac{L_{AdS}^{d-1}}{2\epsilon^{2\Delta-(d+1)}} \int \frac{\mathrm{d}^d p \mathrm{d}^d q}{(2\pi)^d} \delta^d(p+q) \phi_0(q) \partial_z \frac{\phi_1(z,p)}{\phi_1(\epsilon,p)} \phi_0(p) \Big|_{z=\epsilon} . \end{aligned} \tag{2.53}$$

On the $z = \epsilon$ shell, the two-point function for the dual operator $\mathcal{O}$ in momentum space is thus given by[18]

$$\langle \mathcal{O}(p)\mathcal{O}(q) \rangle_\epsilon = (2\pi)^d \frac{\delta^2 I_{\text{on-shell}}}{\delta\phi_0(-p)\delta\phi_0(-q)} = -\frac{(2\pi)^d L_{AdS}^{d-1}}{\epsilon^{2\Delta-(d+1)}} \delta^d(p+q) \partial_z \frac{\phi_1(z,p)}{\phi_1(\epsilon,p)} \Big|_{z=\epsilon} , \tag{2.54}$$

where the $\epsilon \to 0$ limit still needs to be taken to get the two-point function. To this aim one needs to consider the expansion of the general solution ϕ_1 of the EOMs, which as already mentioned in Sec. 2.3.1 can be written in terms of Bessel functions. The resulting expression is in general divergent and contains contact terms, which have to be removed. After ignoring scheme dependent terms, the remaining logarithmic divergences can be dealt with via counter terms to the action, which allow to finally take the $\epsilon \to 0$ limit. This yields the following result for the two-point function transformed back to position space [38, 40, 71]

$$\langle \mathcal{O}(x_1)\mathcal{O}(x_2) \rangle = \frac{L_{AdS}^{d-1}\, \Gamma(\Delta)}{\pi^{d/2}\, \Gamma(\Delta - d/2)} \frac{1}{|x_1 - x_2|^{2\Delta}} , \tag{2.55}$$

in agreement with the spatial dependence expected from conformal invariance (cfr. Eq. (2.18)).

One can then think of correlation functions in the gauge theory between operators $\mathcal{O}$ inserted at certain points on the boundary as propagation of corresponding fields in the bulk between these points [103, 104]. In particular, and this will be useful for later discussions in Ch. 4, equal time two-point functions for a scalar operator $\mathcal{O}$ with large conformal dimension Δ in the dual CFT can be written in terms of the bulk propagator for a scalar field of mass $m \sim \Delta$ (cfr. Eq. (2.42)) which in the worldline representation is given by a path integral over particle trajectories connecting the two points

$$\langle \mathcal{O}(x_1)\mathcal{O}(x_2) \rangle = \int \mathcal{D}\mathcal{P}\, e^{i\Delta L(\mathcal{P})} \qquad \text{with} \qquad L(\mathcal{P}) = \int_{\mathcal{P}} \mathrm{d}s \sqrt{-g_{\mu\nu} \dot{X}^\mu \dot{X}^\nu} , \tag{2.56}$$

where $L(\mathcal{P})$ is the proper length of the path and it is imaginary for spacelike trajectories. For large Δ, using WKB approximation, the path integral localises at its saddle points so that the leading order contribution to the bulk propagator can be written as a sum over all spacelike geodesics connecting the boundary endpoints

[18] In momentum space, we have $\int \mathrm{d}^d x\, \phi(x)\mathcal{O}(x) = \int \frac{\mathrm{d}^d p}{(2\pi)^d} \phi_0(-p)\mathcal{O}(p)$ so that in computing correlation functions we have take derivatives w.r.t. $\phi_0(-p)/(2\pi)^d$ thus yielding the $(2\pi)^d$ factor in the numerator of (2.54).

$$\langle \mathcal{O}(x_1)\mathcal{O}(x_2)\rangle \sim \sum_{\text{geodesics}} e^{-\Delta L_{\text{ren}}(x_1,x_2)} \,, \tag{2.57}$$

where $L_{\text{ren}}(x_1, x_2)$ denotes the (renormalised) geodesic length[19]. This is known as *geodesic approximation* and it was originally proposed in [105], where it was shown that it correctly reproduces the CFT leading order contribution in the large N semiclassical limit.

This will turn useful in Ch. 4, where we study the holographic consequences of bulk singularities in Kasner-AdS spacetimes. In particular, as we will discuss there, in such a cosmological spacetime space-like bulk geodesics are bent toward the singularity and can be thus used to probe the high curvature region.

2.4 Holographic Principle in AdS/CFT

Let us close this chapter with some final remarks on the holographic features of the AdS/CFT correspondence. Naively, the picture of the dual CFT living on the conformal boundary of AdS and encoding all physics in the bulk is already suggestive of the realisation of the holographic principle in AdS/CFT. However, to make this more precise, the following two points need to be studied. First of all, a quantitative check of the holographic bound would required to compute the number of degrees of freedom in the dual CFT. Second, as discussed in Ch. 1, different statements of the holographic principle can be formulated (cfr. Sec. 1.2). Thus, it is somehow natural to ask in which sense the holographic principle can be implemented within the AdS/CFT framework. In particular, as we will try to explain in this section, depending on which form of the AdS/CFT correspondence is considered, one might expect different realisation of the principle. Let us discuss these points a bit more explicitly.

To check the holographic bound we need to compare the area of the boundary surface with the number of degrees of freedom in the CFT. As discussed in Sec. 2.1.2, the AdS boundary in global coordinates is given by $\mathbb{R} \times \mathbb{S}^{d-1}$. The proper area of any finite coordinate patch is divergent as the boundary of AdS is approached. This is in principle compatible with the expectation of having an infinite number of degrees of freedom in continuum QFT. To make a more sensible comparison, this divergence is usually regularised by introducing an infrared cut-off $\delta \ll 1$ in the radial direction of the bulk spacetime near the boundary [106]. Thus, in the case of asymptotically $\text{AdS}_5 \times \mathbb{S}^5$ spacetime, the area of the regularised $\mathbb{S}^3 \times \mathbb{S}^5$ boundary surface is given by (cfr. Eqs. (2.24) and (2.36))

$$A \propto \frac{L^3_{AdS}}{\delta^3} \cdot L^5_{AdS} = \frac{L^8_{AdS}}{\delta^3} \,, \tag{2.58}$$

where we omitted constant numerical factors which are not relevant for the present discussion. Next step is then to understand what is the effect of this bulk infrared cut-off in the boundary theory. This involves the so-called *UV/IR relation* which is a peculiar aspect of AdS/CFT

[19] Since the boundary of AdS lies at infinity, the geodesic length needs to be renormalised by introducing a cut-off near the boundary and subtracting the divergent contribution. We will come back on this point in Ch. 4.

according to which infrared effects in the bulk correspond to ultraviolet effects on the boundary. Detailed arguments for it can be found in [107, 108]. Here it is just sufficient to notice that, due to the invariance under rescaling transformations of the AdS metric ($(z,t,x) \mapsto \lambda(z,t,x)$ for the AdS metric in Poincaré coordinates), small spatial distances on the boundary correspond to small distances in the bulk inverse radial coordinate z. The asymptotic bulk infrared cutoff δ then translates into a short distance cut-off in the dual gauge theory defined on a $\mathbb{R} \times \mathbb{S}^3$ background spacetime. Consequently, the spatial unit 3-sphere will be partitioned into $1/\delta^3$ cells of size δ. Within each such cell the fields are constant so that the number of degrees of freedom contained in each cell is of order N^2 corresponding to the $N \times N$ components of the $\mathsf{U}(N)$ adjoint representation. The total number of degrees of freedom is thus given by

$$\#\,\text{d.o.f} = \frac{N^2}{\delta^3} \propto \frac{L_{AdS}^8}{\delta^3}\ , \tag{2.59}$$

where we used the relation (2.34) between L_{AdS} and N. Therefore, comparing (2.58) and (2.59), we see that the number of CFT degrees of freedom agrees with the holographic bound of not exceeding A bits of information. The (asymptotic) distant $\mathbb{S}^3 \times \mathbb{S}^5$ hypersurface provides a holographic screen on which data encoding the description of the interior can be stored. Indeed, such a spatial hypersurface admits two (past and future) ingoing light-sheets, i.e. it is a normal surface [33]. In absence of singularities for the asymptotically $\mathrm{AdS}_5 \times \mathbb{S}^5$ bulk spacetime, these light-sheets are complete. At a fixed instant of time, the state in the dual CFT thus contain holographic data for a complete slice of the bulk spacetime. Including also the time-like direction of the asymptotic AdS boundary, we have a one-parameter family of $\mathbb{S}^3 \times \mathbb{S}^5$ screens, each of which admit a complete future directed light-sheet. In agreement with the null form of the holographic principle discussed in Sec. 1.2, the AdS/CFT correspondence would then provide a slice-by-slice holographic duality between bulk physics and dual CFT data. The bulk state on each slice is fully described by data whose number is bounded by the area of the boundary of the slice. The unitary evolution of such boundary data is generated by the CFT dynamics.

Finally, let us notice that the above discussion refers to the weak form of the AdS/CFT correspondence. As such, the corresponding realisation of the null holographic principle concerns those states in the dual field theory which describe continuum semiclassical bulk geometries. This is the regime of approximation in which most of the tests for the correspondence has been performed. If one believes then in the strongest form of AdS/CFT, the correspondence conjectures a complete duality between the full Hilbert spaces of the two theories. In this sense, the equivalence (2.47) for the generating functionals of the full quantum theory would provide a realisation of the strong holographic principle. A derivation of all the entries in the bulk/boundary dictionary – which amounts to prove the conjecture – would provide us with an explicit construction for the holographic isomorphism between the two theories.

Chapter 3

Loop Quantum Cosmology

Before moving to the main part of the thesis, one last ingredient is needed: the inclusion of quantum corrections motivated by Loop Quantum Gravity (LQG) in effective symmetry-reduced models. To this aim, in this chapter we introduce the main aspects of Loop Quantum Cosmology (LQC), which is the result of the application to cosmological spacetimes of the quantisation techniques developed in LQG. We will focus on the simplest cosmological setting, that is a homogeneous and isotropic spacetime in the presence of a massless and minimally coupled scalar field, the latter playing the role of a relational matter clock. After recalling the classical phase space formulation of this simple cosmological model, we will discuss the main steps in the construction of the quantum theory and its main physical implications. In particular, as we will discuss, quantum effects become dominant in the high-curvature regime and induce a upper bound on matter energy density thus resolving the initial Big Bang singularity. The latter is replaced by a quantum bounce smoothly connecting a contracting and an expanding branch whose geometry is well approximated by classical general relativity far from the Planck regime. We move then to the study of the effective level, where the relevant quantum corrections of LQC are captured at the semiclassical level via a phase space regularisation known as *polymerisation* according to which the canonical momenta are replaced by combinations of their exponentiated versions (point holonomies). From a spacetime point of view, such an effective level provides us with a continuum metric description in which quantum gravity effects induce relevant corrections to the geometry at high curvatures. As discussed at the end of the chapter, the availability of an effective metric allows to investigate holographic bounds for the resulting quantum corrected spacetime. Seminal papers on LQC include [109–115]. We refer to them as well as useful reviews [116–119] for a more detailed exposition of the subject.

3.1 Classical Theory: Hamiltonian Formulation

To prepare the stage for the quantum theory let us start by recalling the classical Hamiltonian description of the system. We will focus on the simplest cosmological spacetime that is a spatially flat, homogeneous and isotropic Friedmann-Lemaitre-Robertson-Walker (FLRW) model

with zero cosmological constant ($\Lambda = 0$) coupled with a massless scalar field. After briefly recalling the phase space formulation based on metric variables, we will recast the theory in terms of the canonical variables adopted in LQG. As we will discuss in the next section, this allows then to mimic the LQG construction in this symmetry-reduced setting to get a well-defined quantum theory for the FLRW model. Unlike the previous chapters where generic $(d+1)$-dimensional spacetimes were mainly considered, in this chapter we will focus on 3+1 dimensions for which most of the work in LQG (and LQC) has been done[1].

3.1.1 Homogeneous and Isotropic Geometrodynamics

In the case of a homogeneous and isotropic spacetime, the line element associated to the metric can be written as

$$\mathrm{d}s^2 = g_{\mu\nu}\mathrm{d}x^\mu \mathrm{d}x^\nu = -N(t)^2\mathrm{d}t^2 + q_{ab}\mathrm{d}x^a\mathrm{d}x^b = -N(t)^2\mathrm{d}t^2 + a(t)^2\left(\mathrm{d}x_1^2 + \mathrm{d}x_2^2 + \mathrm{d}x_3^2\right) \ , \quad (3.1)$$

where q_{ab} is the physical spatial metric, $a(t)$ is the scale factor which due to homogeneity and isotropy is the same in all spatial directions and depends only on time, and N is the lapse function encoding the gauge freedom in choosing the time coordinate. Fixing $N = 1$ corresponds to identify the coordinate t with the proper time along the world lines of observers moving orthogonal to the homogeneous spatial slices. As we will discuss in the next section, the most convenient choice for quantisation is $N \propto a^3$ for which the theory turns out to be exactly solvable.

Plugging the metric ansatz (3.1) into the Einstein-Hilbert action (with $\Lambda = 0$, $c = 1$), we get

$$S_{\mathrm{EH}} = \frac{1}{2\kappa}\int_{\mathcal{M}} d^4x\,\sqrt{-g}\,\mathcal{R} = \frac{3}{\kappa}V_o\int \mathrm{d}t\,\frac{a}{N^2}\left(a\ddot{a}N + \dot{a}^2N - \dot{N}a\dot{a}\right) \ , \quad (3.2)$$

where $\kappa = 8\pi G$, dots denote derivatives w.r.t. the time coordinate, and we used the expressions

$$\sqrt{-g} = Na^3 \qquad , \qquad \mathcal{R} = \frac{6}{N^3a^2}\left(a\ddot{a}N + \dot{a}^2N - \dot{N}a\dot{a}\right) \ . \quad (3.3)$$

for the metric determinant and the Ricci scalar, respectively. Here V_o denotes the coordinate volume of the spatial slice, so that we assume either spacetime to be spatially compact (e.g. with a 3-torus topology) or a fiducial cell is introduced in the case of non-compact manifolds ($\mathbb{R}^3$ topology in our case). Indeed, in the non-compact case, volume integrals like those occurring in the expressions of the action, the Hamiltonian and the symplectic structure diverge. Therefore, we need to introduce a fiducial cell $\mathcal{C}$, which due to the symmetries of the model can be assumed to be cubical, and restrict all integrals to it [118, 125]. The introduction of a fiducial cell plays the role of an infrared regulator and it has to be removed in the end to extract physical results by taking the limit $\mathcal{C} \to \mathbb{R}^3$. Physical observable quantities must be independent of the choice of the fiducial cell. In the following, we will then distinguish between the physical spatial metric q_{ab} and the non-dynamical fiducial metric $^\circ q_{ab}$ defined w.r.t. Cartesian coordinates adapted to

[1] Higher dimensional LQG has been developed in [120–123]. The underlying canonical formulation of general relativity with higher dimensional connection variables has been later used as starting point towards extending LQC to generic spacetime dimensions in [124].

the edges of the cell $\mathcal{C}$. The former is related to the latter via $q_{ab} = a^2 {}^\circ q_{ab}$ so that the physical volume of $\mathcal{C}$ is given by $V = a^3 V_o$.

Coming back to the action (3.2) and integrating by parts the first term to get rid of the second order derivatives, we get the following expression for the first-order gravitational action (up to boundary terms)

$$S_{\text{grav}} = -\frac{3}{\kappa} V_o \int dt \, \frac{a\dot{a}^2}{N} \, . \tag{3.4}$$

Moreover, as we will discuss at various points in the following, in general relativistic systems coordinates have no physical meaning so that in order to describe dynamical evolution in a coordinate-independent way one is usually lead to use a relational time associated with physical fields. To this aim, it is convenient to couple the gravitational action with a massless, real scalar field ϕ and use the values of the scalar field as an internal clock. Considering then the matter action for such a scalar field given by

$$S_{\text{matter}} = -\frac{1}{2} \int \mathrm{d}^4x \, \sqrt{-g} \, g^{\mu\nu} \nabla_\mu \phi \, \nabla_\mu \phi = V_o \int \mathrm{d}t \, \frac{a^3}{2N} \dot{\phi}^2 \, , \tag{3.5}$$

the total action of the system reads as

$$S = S_{\text{grav}} + S_{\text{matter}} = V_o \int \mathrm{d}t \, \left(-\frac{3}{\kappa} \frac{a\dot{a}^2}{N} + \frac{a^3}{2N} \dot{\phi}^2 \right) \, , \tag{3.6}$$

where we note that all differential geometric densities are multiplied by V_o, whereas scalars such as ϕ depend only on t due to homogeneity. The canonical momenta p_a and p_ϕ conjugate to a and ϕ are given by

$$p_a = \frac{\delta S}{\delta \dot{a}} = -\frac{6 V_o}{\kappa N} a\dot{a} \qquad , \qquad p_\phi = \frac{\delta S}{\delta \dot{\phi}} = \frac{a^3 V_o}{N} \dot{\phi} \tag{3.7}$$

while the action (3.6) not depending on $\dot{N}$ yields the primary constraint $p_N \approx 0$[2]. Here $\approx$ denotes *weak equality*, that is equality on the submanifold in phase space where the constraints are satisfied (constraint surface) so that it can be set to zero only after all Poisson brackets have been evaluated. According to Dirac's theory of constrained systems [126–128], the total Hamiltonian then reads as

$$H_T = p_a \dot{a} + p_\phi \dot{\phi} - L + \lambda p_N = N \left(-\frac{\kappa p_a^2}{12 V_o a} + \frac{p_\phi^2}{2 V_o a^3} \right) + \lambda p_N \, , \tag{3.8}$$

where λ is a Lagrange multiplier, and we expressed the velocities $\dot{a}$, $\dot{\phi}$ in terms of the momenta p_a, p_ϕ by means of Eqs. (3.7). Stability $\dot{p}_N \approx 0$ of the primary constraint gives the secondary constraint

$$\mathcal{H} = -\frac{\kappa p_a^2}{12 a V_o} + \frac{p_\phi^2}{2 a^3 V_o} \approx 0 \, . \tag{3.9}$$

Therefore, N plays the role of a Lagrange multiplier and the last term in (3.8) can be dropped.

[2] A brief review of the Hamiltonian description of systems with constraints and their classification is reported in Appendix A.

To sum up, the phase space of this simple cosmological model is spanned by (a, p_a, ϕ, p_ϕ) with non-vanishing Poisson brackets

$$\{a, p_a\} = 1 \qquad , \qquad \{\phi, p_\phi\} = 1 \, , \tag{3.10}$$

and the Hamiltonian of the system is constrained to vanish

$$H = N\mathcal{H} \qquad , \qquad \mathcal{H} = -\frac{\kappa p_a^2}{12 a V_o} + \frac{p_\phi^2}{2a^3 V_o} \approx 0 \, . \tag{3.11}$$

This is a peculiar feature of reparametrisation invariant systems such as general relativity[3]. The constraint (3.11) generates gauge transformations which in this case amount to the freedom of choosing a time coordinate. This means that asking for the value of some quantities at a certain coordinate time t is not a gauge invariant statement. Rather, one should ask for their value when some other event takes place, e.g. when the scalar field ϕ takes a certain value. We will come back to this soon. Before discussing it, let us first rephrase the classical theory in terms of canonical variables that are more suited for a canonical quantisation *à la* LQG.

3.1.2 Connection Dynamics and (b,v) Variables

Loop quantum gravity can be thought of as a diffeomorphism invariant extension of lattice gauge theory where the dynamical lattice itself encodes the quantum properties of spacetime geometry [129–131]. The main strategy is to reformulate classical general relativity in terms of canonical variables resembling those of Yang-Mills theories so that non-perturbative quantisation techniques can be applied to gravity as well[4]. The basic phase-space variables are represented by an $\mathsf{SU(2)}$ gauge connection A_a^i on the spatial Cauchy surface and its Lie-algebra valued conjugate momentum given by the densitised triad E_i^a. The latter is related to the metric on the spatial slice via $qq^{ab} = E_i^a E_j^b \delta^{ij}$, where q is the determinant of the spatial metric q_{ab} and we use initial letters of the Latin alphabet to denote spatial indices and middle letters for Lie algebra indices. Unlike standard gauge theories, the $\mathsf{SU(2)}$ gauge group does not refer to any internal symmetry but rather to rotations of the local orthonormal frames defined by the triads. In the FLRW case under consideration, the underlying spacetime symmetries imply the canonical variables on each gauge orbit to be given by [110, 116]

$$A_a = \tilde{c}\, {}^\circ\omega_a^i \, \tau_i \qquad , \qquad E^a = \tilde{p}\, \sqrt{{}^\circ q}\, {}^\circ e_i^a \, \tau^i \tag{3.12}$$

where ${}^\circ q$ is the determinant of the fiducial metric, ${}^\circ e_i^a$, ${}^\circ\omega_a^i$ respectively denote the orthonormal frames and co-frames associated with Cartesian coordinates x^a along the edges of the cubic fiducial cell, and the τ's are the generators of the $\mathfrak{su}(2)$ algebra

[3] We refer to the Appendices A and B for examples and further details.

[4] A brief overview of the canonical formulation of general relativity in connection variables and the main steps of the quantisation underlying LQG are reported in Appendix B to which we refer as a complement to the material presented in this chapter.

$$[\tau_i, \tau_j] = \epsilon_{ijk}\tau^k \qquad , \qquad \tau_k = -\frac{i}{2}\sigma_k \tag{3.13}$$

σ_k being the Pauli matrices. In the parametrisation (3.12), all the information about the gravitational field configuration is then encoded in the two functions of time $(\tilde{c}, \tilde{p})$. These are related to the scale factor a via

$$\tilde{c} = \frac{\beta \dot{a}}{N} \qquad , \qquad \tilde{p} = a^2 \tag{3.14}$$

where β is the so-called Barbero-Immirzi parameter. Using then the expression (3.7) for the momentum p_a conjugate to a and the canonical Poisson brackets (3.10), we have

$$\{\tilde{c}, \tilde{p}\} = \frac{\kappa\beta}{3V_o} = \frac{8\pi G\beta}{3V_o} \, , \tag{3.15}$$

where we recall that V_o denotes the volume of the fiducial cell w.r.t. the metric ${}^\circ q_{ab}$. The dependence on fiducial structures in the above Poisson brackets can be reabsorbed by simply redefining the canonical variables as

$$c = V_o^{1/3}\, \tilde{c} \qquad , \qquad p = V_o^{2/3}\, \tilde{p} \tag{3.16}$$

so that the LQC phase space is spanned by the canonical pairs (c, p), (ϕ, p_ϕ) with non-vanishing Poisson brackets

$$\{c, p\} = \frac{\kappa\beta}{3} \qquad , \qquad \{\phi, p_\phi\} = 1 \, . \tag{3.17}$$

Before moving to the quantum theory, it is convenient to perform one last change of variables for the gravitational sector of the system which, as we will discuss in the next section, significantly simplifies the quantum dynamics. Let us then introduce the new canonically conjugate variables (b, v) defined by

$$b := -\frac{3c}{\beta |p|^{1/2}} \qquad , \qquad v := |p|^{3/2}\mathrm{sgn}(p) \tag{3.18}$$

where $\mathrm{sgn}(p)$ is the sign of p chosen to be ± 1 depending on the physical triad e^a_i to have the same or opposite orientation as the fiducial one ${}^\circ e^a_i$. In what follows, we assume the orientation to be the same. Using then the expressions (3.14) and (3.16), we have

$$b = -\frac{3\dot{a}}{Na} \qquad , \qquad v = V_o a^3 \tag{3.19}$$

from which we see that b is related to the Hubble rate $\frac{\dot{a}}{a}$, while v measures the physical volume of the universe (restricted to the fiducial cell). Furthermore, using the Poisson brackets (3.17), it is straightforward to check that

$$\{v, b\} = \frac{3\kappa}{2} \, , \tag{3.20}$$

so that the canonical Poisson brackets $\{v, b\} = 1$ are obtanined by setting $\kappa = 2/3$ (i.e. $12\pi G = 1$). In the new variables, the Hamiltonian (3.11) reads as

$$H = H_{\text{grav}} + H_{\text{matter}} = N\left(-\frac{b^2 v}{2} + \frac{p_\phi^2}{2v}\right) \approx 0 \tag{3.21}$$

and the corresponding EOMs are given by

$$\begin{aligned} \dot{v} = \{v, H\} = -Nbv \qquad &, \qquad \dot{\phi} = \{\phi, H\} = \frac{N p_\phi}{v} \,, \\ \dot{b} = \{b, H\} = \frac{Nb^2}{2} - \frac{N p_\phi^2}{2v^2} \qquad &, \qquad \dot{p}_\phi = \{p_\phi, H\} = 0 \,. \end{aligned} \tag{3.22}$$

Let us solve the above EOMs for $N = 1$ in which case t measures the proper time. First, the equation for $\dot{p}_\phi$ tells us that p_ϕ is a constant of motion related to the geometry via the Hamiltonian constraint as

$$p_\phi^2 = b^2 v^2 = const. \tag{3.23}$$

Inserting (3.23) into the equation for $\dot{b}$ we get

$$\dot{b} = b^2 \qquad \Rightarrow \qquad b(t) = -\frac{1}{t - t_0} \,, \tag{3.24}$$

and consequently solving the equation for $\dot{v}$ or simply using directly the Hamiltonian constraint yields

$$v(t) = \pm |p_\phi| (t - t_0) \,, \tag{3.25}$$

where the sing of v corresponds to the choice of orientation of the manifold and we set the initial conditions such that $v = 0$ at $t = t_0$. Such a finite proper time can be identified with the Big Bang (or Big Crunch in the time reversed picture) where, as can be easily seen from the on-shell values of the Ricci scalar (3.3) and the energy density of the scalar field[5]

$$\mathcal{R} = -\frac{6\dot{a}^2}{a^2} = -\frac{2\dot{v}^2}{3v^2} = -\frac{2b^2}{3} \qquad , \qquad \rho = \frac{\dot{\phi}^2}{2} = \frac{p_\phi^2}{2v^2} = \frac{b^2}{2} \,, \tag{3.26}$$

a curvature singularity occurs and matter energy density diverges.

Finally, let us solve the EOM for the scalar field. Inserting the result (3.25) into the equation for $\dot{\phi}$ in (3.22), we find

$$\dot{\phi} = \pm \frac{\text{sgn}(p_\phi)}{t - t_0} \qquad \text{i.e.} \qquad \phi - \phi_0 = \pm \text{sgn}(p_\phi) \log(t - t_0) \,. \tag{3.27}$$

so that (3.25) can be expressed as a function of ϕ as

$$v(\phi) = \pm \exp\big(\pm \text{sgn}(p_\phi)(\phi - \phi_0)\big) \,. \tag{3.28}$$

This suggests a second Dirac observable given by the value of the volume at a scalar field time $\tilde{\phi}$

$$v\big|_{\phi=\tilde{\phi}} = \pm \exp\big(\pm \text{sgn}(p_\phi)(\tilde{\phi} - \phi_0)\big) = v \exp\big(\mp \text{sgn}(p_\phi)(\phi - \tilde{\phi})\big) \,, \tag{3.29}$$

[5] We recall that $\rho N^2 = T_{00}$ with $T^{\alpha\beta} = g^{\alpha\mu} g^{\beta\nu} \partial_\mu \phi \partial_\nu \phi - \frac{1}{2} g^{\alpha\beta} g^{\mu\nu} \partial_\mu \phi \partial_\nu \phi$ for a scalar field.

which, as can be checked by direct computation, Poisson commutes with the constraint (3.21) and hence, as already anticipated, is a gauge-invariant quantity. Therefore, in agreement with the general discussion of first class constraints in Appendix A, the constraint (3.21) removes 2 of the 2+2 phase space d.o.f. and we are left with a (1+1)-dimensional reduced phase space parametrised by the two independent Dirac observables p_ϕ and $v\big|_{\phi=\tilde{\phi}}$, whose values at some scalar field time $\tilde{\phi}$ set the Cauchy data for the dynamics. Moreover, as expected for reparametrisation invariant systems, the Hamiltonian is constrained to vanish and the time parameter has no physical meaning. Gauge-invariant quantities (Dirac observables) describe correlations between physical fields. In particular, the introduction of a relational clock (here our real scalar field ϕ) allows us to deparametrise the theory. Indeed, by considering ϕ as time variable, the generator of ϕ-time translations is p_ϕ which in turn can be written as $p_\phi = \pm\sqrt{b^2v^2}$ via the Hamiltonian constraint. This suggests us to consider

$$H_{\text{true}} = \pm bv \ , \tag{3.30}$$

as a true Hamiltonian generating the evolution w.r.t. ϕ, which in fact reproduces the EOMs

$$\frac{\mathrm{d}v}{\mathrm{d}\phi} = \{v, H_{\text{true}}\} = \pm v \qquad , \qquad \frac{\mathrm{d}b}{\mathrm{d}\phi} = \{b, H_{\text{true}}\} = \mp b \tag{3.31}$$

whose solutions $v(\phi) \propto \exp(\pm\phi)$, $b(\phi) \propto \exp(\mp\phi)$ are compatible with the above results (cfr. Eq. (3.28)), and correspondingly bv is a conserved quantity.

3.2 Quantum Theory

The quantisation of our symmetry-reduced cosmological system can be performed by mimicking the steps of the construction of the quantum theory in full LQG[6]. According to the discussion of Appendix B, the main steps of the construction can be summarised as follows:

- The starting point of the LQG program is to consider holonomies of the gravitational connection and fluxes of the conjugate electric field. Therefore, we need to define the analogue of the holonomy-flux algebra on the phase space of our cosmological model;
- Promote them to elementary operators on a kinematical Hilbert space whose elements and scalar product are defined by means of group techniques as planned for the full theory;
- Regularise the classical Hamiltonian in terms of holonomies and fluxes so that it can be implemented as an operator at the quantum level;
- The physical Hilbert space is identified with the solutions of the quantum constraint $\hat{H} = 0$.

[6]It is important to stress that LQC is a LQG-inspired quantisation of cosmological spacetimes and it is not derived from full LQG. A systematic identification of a quantum reduction procedure and consequently of a cosmological sector within the LQG Hilbert space is one of the main open challenges in the field. Some progress in bridging between LQG and LQC has been made over the last years. Different approaches have been pursued based for instance on a slightly different formulation of the full theory and implementing gauge fixing conditions for a quantum reduction [132, 133], or via a cubic lattice truncation of LQG spin networks [134–137], or via coherent states in both a canonical and path integral framework [138–140].

The first two of the above steps define the kinematical framework of LQC, the other two instead concern the quantum dynamics. Let us discuss them in a bit more detail.

3.2.1 LQC Kinematics

Let us recall from Sec. 3.1.2 that the classical phase space of minimally coupled FLRW cosmology is spanned by the canonically conjugate variables (v, b, ϕ, p_ϕ) with non-vanishing Poisson brackets

$$\{v, b\} = 1 \qquad , \qquad \{\phi, p_\phi\} = 1 \ . \tag{3.32}$$

Following the LQG logic, let us focus on the gravitational sector described by the variables (v, b). According to the definition (3.18), the information about the gravitational connection is entirely encoded in the variable b. Holonomy-like objects for our cosmological system are thus given by the quantity

$$h^\varrho(b) = e^{-i\varrho b} \qquad , \qquad \varrho \in \mathbb{Z} \tag{3.33}$$

which can be thought of as a point holonomy (b is a 0-form and as such it has zero smearing dimension). Comparing with the general definition of holonomies $h^{(j)}(A)$ given in (B.20), we have that here the underlying group structure is that of $\mathsf{U}(1)$ with b effectively taking values in the interval $[0, 2\pi)$, the integers ϱ playing the role of labels of the $\mathsf{U}(1)$-irreducible representations, and $-i\varrho$ that of the anti-hermitian generators of the representation labeled by ϱ. Correspondingly, flux-like objects have 3+0=3 smearing dimension so that they are given by the integrated volume v over a 3-dimensional hypersurface. The analogue of the holonomy-flux algebra in our variables is thus given by the following Poisson brackets

$$\{v, h^\varrho(b)\} = -i\varrho h^\varrho(b)\{v, b\} = -i\varrho h^\varrho(b) \ . \tag{3.34}$$

Working in b-polarisation, the kinematical Hilbert space can easily be constructed as follows. The basis states $|\varrho\rangle$ labeled by ϱ are defined as

$$\langle b|\varrho\rangle = e^{-i\varrho b} \qquad , \qquad \varrho \in \mathbb{Z} \tag{3.35}$$

with scalar product

$$\langle \varrho|\varrho'\rangle := \int_{\mathsf{U}(1)} \mathrm{d}\mu_{\mathrm{Haar}}(b)\, \overline{e^{-i\varrho b}}\, e^{-i\varrho' b} = \frac{1}{2\pi}\int_0^{2\pi} \mathrm{d}b\, e^{i(\varrho-\varrho')b} = \delta_{\varrho,\varrho'} \ . \tag{3.36}$$

This is the analogue of the orthogonality relation for $\mathsf{SU}(2)$ Wigner matrices involved in the Peter-Weyl decomposition of spin network states (cfr. Eqs. (B.27) and (B.28)). Indeed, similarly to the construction of the scalar product for cylindrical functions, the scalar product (3.36) now is defined via integration against the Haar measure on $\mathsf{U}(1)$. The kinematical Hilbert space is thus given by the (countable) complex linear span of $\langle b|\varrho\rangle = e^{-i\varrho b}$, $\varrho \in \mathbb{Z}$, and a generic state $|\chi\rangle$ can be written in the b-representation as

$$|\chi\rangle = \sum_{\varrho\in\mathbb{Z}} \chi(\varrho)\,|\varrho\rangle \qquad \text{with} \qquad \sum_{\varrho\in\mathbb{Z}} \overline{\chi(\varrho)}\chi(\varrho) < \infty\,, \tag{3.37}$$

so that

$$\chi(b) = \langle b|\chi\rangle = \sum_{\varrho\in\mathbb{Z}} \chi(\varrho) e^{-i\varrho b} \qquad , \qquad \chi(\varrho)\in\mathbb{C} \tag{3.38}$$

satisfying the normalisability condition

$$\begin{aligned}\langle\chi|\chi\rangle &= \frac{1}{2\pi}\int_0^{2\pi} \mathrm{d}b\ \langle\chi|b\rangle\,\langle b|\chi\rangle \\ &= \frac{1}{2\pi}\int_0^{2\pi} \mathrm{d}b \sum_{\varrho,\varrho'} \overline{\chi(\varrho)}\,\chi(\varrho') e^{i(\varrho-\varrho')b} \\ &= \sum_{\varrho} \overline{\chi(\varrho)}\,\chi(\varrho) < \infty\,.\end{aligned} \tag{3.39}$$

Note that a priori, in the definition (3.33), one would require ϱ to be real instead of integer to get back b with arbitrary precision as expected for a properly chosen subalgebra of point-separating phase space functions. As it is usually done in the LQC literature, it is also possible to take $\varrho\in\mathbb{R}$, which corresponds to using square integrable functions on the Bohr compactification $\mathbb{R}_{\text{Bohr}}$ of the real line as wave functions [110, 118, 141] (see also Appendix 28 in [129]). $\mathbb{R}_{\text{Bohr}}$ is a compact Abelian group, which roughly speaking corresponds to the real line equipped with discrete topology (cfr. (3.36)). In particular, a translation-invariant normalised Haar measure exists so that the above definitions can be generalised straightforwardly. This can be thought of as the generalisation of $\mathsf{U}(1)$ to include real representation labels. However, we will avoid these technicalities here as they are not needed when using our current variables.

In analogy with the definition of the elementary operators corresponding to holonomies and fluxes (cfr. Appendix B), we define the operators ($\hbar = 1$)

$$\widehat{e^{-i\varrho b}} \qquad , \qquad \hat{v} = i\frac{\partial}{\partial b} \tag{3.40}$$

respectively acting as multiplicative and derivative operators for the wave functions in the b-representation. The corresponding action on the basis states (3.35) reads as

$$\widehat{e^{-i\varrho b}}\,|\varrho'\rangle = |\varrho+\varrho'\rangle \qquad , \qquad \hat{v}\,|\varrho\rangle = \varrho\,|\varrho\rangle\ , \tag{3.41}$$

from which we see that the ϱ's are the eigenvalues of the volume operator. Finally, the operators (3.41) satisfy the commutation relations

$$\Big[\hat{v}, \widehat{e^{-i\varrho b}}\Big]\,|\varrho'\rangle = \big(\varrho+\varrho'-\varrho'\big)\,|\varrho+\varrho'\rangle = \varrho\widehat{e^{-i\varrho b}}\,|\varrho'\rangle = i\{\widehat{v, e^{-i\varrho b}}\}\,|\varrho'\rangle\ , \tag{3.42}$$

while the commutator of $\hat{v}$ (resp. $\widehat{e^{-i\varrho b}}$) with itself vanishes. This is the commutator algebra

expected from the quantisation of the classical Poisson brackets (3.34) by means of the usual choice for the quantization map $\{\cdot,\cdot\} \to -i\,[\cdot,\cdot]$. The resulting quantum representation is however not equivalent to the standard Schrödinger representation adopted for instance in the Wheeler-de Witt approach to quantum cosmology [113, 118]. In fact, similarly to the case of holonomy operators in LQG, the presence of a Kronecker delta (instead of a Dirac delta) in the definition (3.36) of the scalar product implies the above b-representation to be not weakly continuous. Specifically, considering a one-parameter unitary group $\hat{U}(\lambda) = \widehat{e^{-i\lambda b}}$, $\lambda \in \mathbb{R}$, acting on the basis states $f_\lambda(b) = e^{-i\lambda b}$ as in (3.41), i.e.

$$\hat{U}(\lambda)\,|f_{\lambda'}\rangle = |f_{\lambda+\lambda'}\rangle \ , \tag{3.43}$$

we have

$$\langle f_\lambda | f_\lambda\rangle = 1 \neq 0 = \lim_{\lambda'\to 0} \langle f_\lambda | \hat{U}(\lambda') f_\lambda\rangle \ . \tag{3.44}$$

This means that the differential quotient $\frac{\mathrm{d}}{\mathrm{d}\lambda}\big|_{\lambda=0}\widehat{e^{-i\lambda b}} = \lim_{\lambda\to 0}\frac{\hat{U}(\lambda)-\hat{U}(0)}{\lambda}$ diverges when taking expectation values w.r.t. $|f_{\lambda'}\rangle$. Thus, a bare operator $\hat{b} := \frac{\mathrm{d}}{\mathrm{d}\lambda}\big|_{\lambda=0}\widehat{e^{-i\lambda b}} = \lim_{\lambda\to 0}\frac{\hat{U}(\lambda)-\hat{U}(0)}{\lambda}$ does not exist and only linear combinations of its exponentiated form (point holonomies) are well-defined operators on the kinematical Hilbert space. From a mathematical point of view, weak discontinuity allows to bypass the assumptions of Stone-von Neumann theorem so that the above representation, known as the *polymer representation* [142, 143], is not unitarily equivalent to the Schrödinger one[7]. As we will discuss in the next subsection, such a LQG-inspired representation is intimately related to a dynamical discreteness of the volume. The latter can be thought of as being inspired by the Planckian discreetness of the geometric operators in LQG, which in this case would correspond to the integers labelling the irreducible representations of $\mathsf{U}(1)$.

3.2.2 LQC Dynamics

In order to implement the quantum dynamics we need to quantise the Hamiltonian constraint (3.21) and solve the resulting quantum operator constraint to determine the physical states. Following up on the discussion at the end of Sec. 3.1.2 for the classical theory, the strategy is then to use the scalar field ϕ as a time variable and compute the evolution w.r.t. to this "time" which is generated by the true Hamiltonian $H_{\text{true}} := p_\phi = \sqrt{b^2 v^2}$. To this aim, the following two problems need to be addressed:

1) As we have discussed in the previous section, b as an operator does not exist on the kinematical polymer Hilbert space. Therefore, in order to be promoted to a well-defined operator at the quantum level, any phase space function depending on b has to be regularised by expressing it in terms of combinations of its exponentiated form. This regularisation procedure is usually referred to as *polymerisation*.

[7] Remarkably, similar results for the uniqueness of the quantum representation of the holonomy-flux algebra in LQG under the assumptions of spatial diffeomorphism invariance and irreducibility [144, 145] can be found also for the LQC representation [146, 147].

2) A factor ordering choice needs to be specified in implementing the polymerised classical quantity as an operator acting on the kinematical Hilbert space.

The simplest choice for the polymerisation of b often adopted in the LQC literature [110, 118] is given by the following replacement

$$b \longmapsto \frac{\sin(\lambda b)}{\lambda} = \frac{1}{2i\lambda}\left(e^{i\lambda b} - e^{-i\lambda b}\right) , \tag{3.45}$$

where λ is called *polymerisation scale* and controls the onset of quantum effects. In fact, for $b\lambda \ll 1$, we can approximate $\sin(\lambda b)/\lambda \sim b$ and the classical behaviour is recovered. Moreover, according to the classical on-shell interpretation (3.26) for the variable b, the above polymerisation is expected to produce sensible corrections when curvature and matter energy density approaches the Planck scale. This corresponds to the regime in which $\lambda b \sim 1$ so that we can think of λ as being of order of the Planck length ℓ_P. As we will discuss in the following, the fundamental discreteness of the LQC quantum representation will produce an upper bound on matter energy density and in turn a Planck scale cut-off for the Ricci curvature scalar, thus resolving the classical Big Bang singularity.

The above polymerisation can be motivated by arguments borrowed from lattice gauge theory suitably adapted to take into account the features suggested by LQG. Specifically, as discussed in [110, 111, 118], the replacement (3.45) can be thought of as the result of approximating the field strength of the gravitational connection in terms of holonomies, namely

$$F^k_{ab} \simeq 2 \lim_{\mathcal{A}_\square \to \Delta_{\mathrm{LQG}}} \mathrm{Tr}\left(\frac{h_{\square_{ij}} - \mathbb{1}}{\mathcal{A}_\square}\tau^k\right) {}^\circ\omega^i_a \, {}^\circ\omega^j_b , \tag{3.46}$$

where $\square$ denotes a plaquette in the a-b plane, which due to homogeneity and isotropy can be taken to be cubic with edges parallel to those of the fiducial cell, $\mathcal{A}_\square$ is the area of the plaquette allowed to shrink only up to the minimal value $\Delta_{\mathrm{LQG}} = 4\sqrt{3}\,\pi\beta\ell_P^2$ of the LQG area spectrum (cfr. discussion below Eq. (B.32)) rather than to a point, and $h_{\square_{ij}}$ is the holonomy around the plaquette given by

$$h_{\square_{ij}} = h^{(\bar\mu)\,-1}_j h^{(\bar\mu)\,-1}_i h^{(\bar\mu)}_j h^{(\bar\mu)}_i \qquad , \qquad h(A) = \exp(\bar\mu c \tau_k) = \cos\left(\frac{\bar\mu c}{2}\right)\mathbb{1} + 2\sin\left(\frac{\bar\mu c}{2}\right)\tau_k \tag{3.47}$$

for the connection (3.12), $\bar\mu$ being the ratio of the edge-length of the plaquette with the edge-length of the fiducial cell. The value of $\bar\mu$ can be determined by specifying the plaquette as follows [111, 118]. The argument is based on heuristic considerations about the kinematical LQG states (spin networks) possibly describing the quantum geometry of the cosmological system under consideration. Specifically, since with our starting FLRW ansatz (3.1) we singled out three axes w.r.t. which the spatial metric q_{ab} is diagonal and to which the cubical cell $\mathcal{C}$ is adapted, the underlying spin network state should consist of a graph whose edges are parallel to the three spatial axes. Moreover, as schematically depicted in Fig. 3.1, since the geometry must be homogeneous at the macroscopic level, the edges of the spin network graph should be packed as tightly as possible so that, even if the microscopic configuration is not exactly homogeneous, the

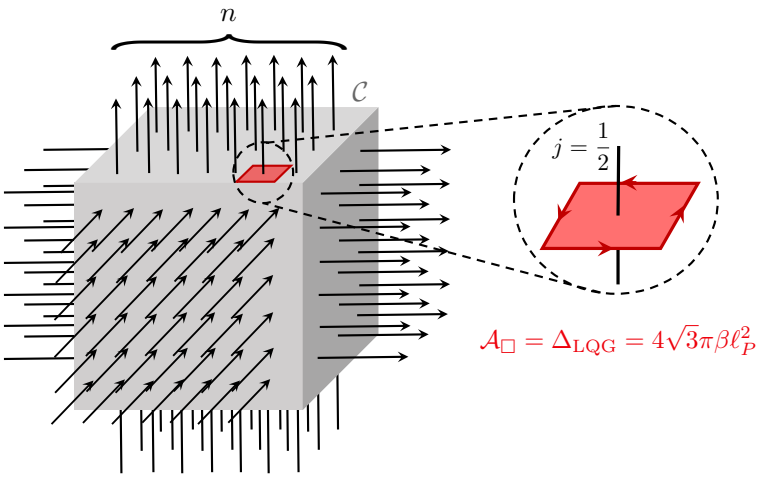

Figure 3.1: Schematic representation of the spin network states describing the macroscopic spatially homogeneous geometry of the cubical cell $\mathcal{C}$ with edges adapted to the axes. The edges of the spin network graph are parallel to the edges of the cell. The faces of the cell are punctured by n edges carrying the smallest quantum number $j = 1/2$ so that the faces of the cell are divided into n square patches which in turn identify the elementary plaquettes enclosing the minimal area $\Delta_{\rm LQG} = 4\sqrt{3}\pi\beta\ell_P^2$.

corresponding quantum state is highly coarse-grained. In other words, all the edges are labeled by the smallest non-zero quantum number $j = 1/2$ so that each edge puncturing the faces of the cell identifies a patch of minimal area $\Delta_{\rm LQG}$. Assuming then the faces to be punctured by n edges, the total area $V_o^{2/3}a^2 = |p|$ of a face of the cell $\mathcal{C}$ is given by

$$|p| = n\Delta_{\rm LQG} \ , \tag{3.48}$$

i.e., the faces of the cell are divided into n identical squares of area $\Delta_{\rm LQG}$ each of which is punctured by only one edge of the spin network. Such minimal area patches provide the elementary square plaquettes considered in Eq. (3.46). Recalling now from Eq. (3.47) that $\bar{\mu}$ is the dimensionless ratio between the edge-length of the plaquette and the edge-length of the cell, the edge-length of the plaquette w.r.t. the fiducial metric ${}^\circ q_{ab}$ is $\bar{\mu}V_o^{1/3}$ and the area $V_o^{2/3}$ of a face of the cell (w.r.t. ${}^\circ q_{ab}$) can be written in terms of the n patches as

$$V_o^{2/3} = n(\bar{\mu}V_o^{1/3})^2 \ . \tag{3.49}$$

Therefore, combining Eqs. (3.48) and (3.49), we get

$$\bar{\mu}^2 = \frac{\Delta_{\rm LQG}}{|p|} = \frac{4\sqrt{3}\pi\beta\ell_P^2}{|p|} \ . \tag{3.50}$$

In terms of the (b, v)-variables, the polymerisation scale λ is related to $\bar{\mu}$ as $\lambda b = \bar{\mu}c$ which, according to the definitions (3.18) of b, yields $\bar{\mu} = 3\lambda/\beta\sqrt{|p|}$ with $\sqrt{|p|}$ the physical edge-length of the cell. Indeed, in the FLRW case (3.12), the gravitational Hamiltonian (B.18) reads as (with $N = v$ and $\kappa = 2/3$)

$$H_{\rm grav} = -\frac{3}{2\beta^2}V_o^{\frac{2}{3}}\epsilon_k^{ij}\,{}^\circ e_i^a\,{}^\circ e_j^b\,p^2F_{ab}^k = -\frac{9p^2}{\beta^2}\frac{\sin^2(\bar{\mu}c)}{\bar{\mu}^2} = -\frac{\sin^2(\lambda b)}{\lambda^2}v^2 \ . \tag{3.51}$$

This is one of the main advantages of using the variables (b, v) instead of the more traditional connection variables. In fact, according to the relation between λ and $\bar{\mu}$ and the expression (3.50), λ is purely constant and is related to the Planck length (and hence $\hbar$) via the area gap $\Delta_{\rm LQG}$ as $\lambda^2 = \beta^2\Delta_{\rm LQG}/9 \propto \ell_P^2$. In particular, a constant polymerisation scale allows to avoid technical problems of having a phase space dependent scale $\bar{\mu}$ in the quantum theory[8].

Note however that the above arguments involving the area gap are only heuristic as they refer to full LQG in the low spin regime, i.e. where the quanta of area are close to the area gap. It is unclear whether the effective LQC dynamics, which is successful for large volumes, is accurate here. Moreover, it just transfers the ambiguity of choosing a regularisation to the full theory, but does not solve it. Without additional insights, one can better understand such schemes as demanding boundedness of curvature invariants as they cut off the integrated gravitational connection at order 1 over distances of order 1 in natural units.

Once the choice of a polymerisation has been made, the Hamiltonian regularised via (3.45) can be promoted to an operator on the kinematical Hilbert space upon specification of a suitable factor ordering. To this aim, recalling that $p_\phi = H_{\rm true}$ and using the Hamiltonian constraint (3.21) to express p_ϕ^2 in terms of b and v, we choose the following symmetric ordering for the (squared) true Hamiltonian [153, 154]

$$H^2_{\rm true} = \frac{1}{\lambda^2}\sqrt{|v|}\sin(\lambda b)|v|\sin(\lambda b)\sqrt{|v|}\,, \tag{3.52}$$

where we dropped operator hats $\hat{\cdot}$ to simplify the notation. The same result can also be obtained by choosing the lapse $N = v$ and quantising the full Hamiltonian constraint as in [113]. The operator (3.52) annihilates the zero volume eigenstate $|0\rangle := |\varrho = 0\rangle$ (cfr. Eq. (3.41)). Moreover, using the expression (3.45) for $\sin(\lambda b)$ in terms of exponentials and their action (3.41) on a state $|\varrho\rangle$, we find the following finite difference equation

$$\begin{aligned} H^2_{\rm true}\,|\varrho\rangle &= \frac{1}{\lambda^2}\left(\sqrt{|v|}\sin(\lambda b)|v|\sin(\lambda b)\sqrt{|v|}\right)|\varrho\rangle \\ &= -\frac{\sqrt{|\varrho|}}{4\lambda^4}\Big(|\varrho+\lambda|\sqrt{|\varrho+2\lambda|}\,|\varrho+2\lambda\rangle - \sqrt{|\varrho|}\,(|\varrho+\lambda| + |\varrho-\lambda|)\,|\varrho\rangle + |\varrho-\lambda|\sqrt{|\varrho-2\lambda|}\,|\varrho-2\lambda\rangle\Big) \end{aligned} \tag{3.53}$$

from which we see that the operator (3.52) preserves the lattice with support on

$$\varrho_n = C + 2\lambda n \quad , \quad C \in \mathbb{R} \quad , \quad n \in \mathbb{Z}\,. \tag{3.54}$$

In particular, for $C = 0$ or $C = \lambda$, positive (resp. negative) volume states are mapped into

[8] In the LQC literature, the case of constant polymerisation scale is often referred to as μ_o-*scheme* to distinguish it from the non-constant $\bar{\mu}$-*scheme*. Moreover, it should be stressed that other choices for the polymerisation (3.45) are possible. Different models which might have a different phenomenology have been proposed. These are based for instance on choosing different functions, or polymerising only parts of the phase space, or different choices for the polymerisation scales [138, 148–152]. These are motivated by physical inputs or full theory based results and arguments like general covariance and anomaly-free realisations of the constraint algebra at the quantum level. However, for simplicity here we do not consider such alternative choices and focus on (3.45). This will be the kind of polymerisation adopted also in the quantum corrected models developed in the next chapters.

positive (resp. negative) volume states, and the zero volume state is annihilated. Thus, the operator (3.52) preserves the subset of states with positive or negative volumes. Moreover, its action on positive and negative volume states is the same (i.e. $v \mapsto -v$ commutes with the Hamiltonian) so that we have two copies of the same system respectively for positive and negative volumes, while the zero volume state is dynamically isolated.

Now, in order to study the solutions of the Hamiltonian constraint operator, we need to translate the difference equation (3.53) into an analytically tractable equation. To this aim, we first rescale the wave function as

$$\chi(\varrho) = \sqrt{|\varrho|}\,\psi(\varrho) \qquad (\varrho \neq 0)\ . \tag{3.55}$$

Restricting then to $C = 0$ and performing a Fourier transform on the lattice $2\lambda n$, $n \in \mathbb{Z}$, the wave function in the b-representation reads as[9]

$$\tilde{\psi}(b) = \sum_{\varrho \in 2\lambda\mathbb{Z}} \psi(\varrho) e^{-i\varrho b} \qquad , \qquad \psi(\varrho) = \frac{\lambda}{\pi}\int_0^{\pi/\lambda} \mathrm{d}b\, e^{i\varrho b}\tilde{\psi}(b)\ . \tag{3.56}$$

Due to the preservation of the positive and negative volume subsectors discussed above or to be precise now semi-positive and semi-negative subsectors due to the rescaling (3.55) (the zero ψ-volume state being however annihilated once rescaling back to χ), $|v|$ can be simply written as v. The true Hamiltonian operator in b-representation then becomes (cfr. Eq. (3.40))

$$\hat{H}^2_{\text{true}} = -\frac{1}{\lambda^2}\sin(\lambda b)\frac{\partial}{\partial b}\sin(\lambda b)\frac{\partial}{\partial b}\ , \tag{3.57}$$

from which, mapping the interval $[0, \pi/\lambda]$ to $(-\infty, \infty)$ via the variable transformation

$$x = \log\left(\tan(\lambda b/2)\right) \qquad \Leftrightarrow \qquad b = \frac{2}{\lambda}\tan^{-1}(e^x)\ , \tag{3.58}$$

it follows that

$$\frac{\partial}{\partial x} = \frac{\sin(\lambda b)}{\lambda}\frac{\partial}{\partial b} \quad , \quad \frac{\partial}{\partial b} = \lambda\cosh(x)\frac{\partial}{\partial x} \quad , \quad \mathrm{d}x = \frac{\lambda}{\sin(\lambda b)}\mathrm{d}b \quad , \quad \mathrm{d}b = \frac{1}{\lambda\cosh(x)}\mathrm{d}x \tag{3.59}$$

and the true Hamiltonian simplifies to $\hat{H} = \sqrt{-\partial_x^2}$. The Hamiltonian constraint thus takes the form of a (1+1)-dimensional Klein-Gordon equation

$$\left(\partial_\phi^2 - \partial_x^2\right)\Psi(x,\phi) = 0\ , \tag{3.60}$$

with positive energy condition $-i\partial_\phi > 0$, the momentum conjugate to the scalar field ϕ being represented as a derivative operator $-i\partial_\phi$ on the Hilbert space of the matter sector[10]. The

[9] The use of the $\sin(\lambda b)$-polymerisation implies b to be $(2\pi/\lambda)$-periodic. On top of it, the superselection of the $2\lambda n$ lattice (3.54) demands $b \sim b + \pi/\lambda$. Choosing $b \in [0, \pi/\lambda)$ in the Fourier transform (3.56) is then equivalent to choosing $b \in [-\pi/2\lambda, \pi/2\lambda)$, and hence a sign change of b is allowed in the formalism. Invariance under parity leads us to consider only symmetric wave functions and we choose to work with the interval $[0, \pi/\lambda)$.

[10] In the light of the discussion of Sec. 3.2.1, the total kinematical Hilbert space of our cosmological system coupled to a scalar field is $\mathcal{H}^{\text{grav}}_{\text{kin}} \otimes \mathcal{H}^{\text{matter}}_{\text{kin}}$, with $\mathcal{H}^{\text{grav}}_{\text{kin}} \cong L^2(\mathsf{U}(1) \text{ or } \mathbb{R}_{\text{Bohr}}, \mathrm{d}\mu_{\text{Haar}})$ and $\mathcal{H}^{\text{matter}}_{\text{kin}} \cong L^2(\mathbb{R}, \mathrm{d}\mu_{\text{Lebesque}})$.

solutions of the Klein-Gordon operator are spanned by

$$\psi_k(x) = e^{-ikx+i|k|(\phi-\phi_0)} \,, \tag{3.61}$$

where k^2 denotes the eigenvalue of $-\partial_x^2$ and, for each k^2, the solution space is 2-dimensional since ψ_k and ψ_{-k} have the same eigenvalue. Physical states for positive frequency solutions can be then written via Fourier transform as[11]

$$\begin{aligned}\Psi_{\text{phys}}(x,\phi) &= \int_{-\infty}^{\infty} \mathrm{d}k\, \tilde{\Psi}_{\text{phys}}(k) e^{-ikx+i|k|(\phi-\phi_0)} \\ &= \int_{-\infty}^{0} \mathrm{d}k\, \tilde{\Psi}_{\text{phys}}(k) e^{-ik(\phi+x)} e^{ik\phi_0} + \int_0^{\infty} \mathrm{d}k\, \tilde{\Psi}_{\text{phys}}(k) e^{ik(\phi-x)} e^{-ik\phi_0} =: \Psi_L(\phi+x) + \Psi_R(\phi-x).\end{aligned} \tag{3.62}$$

Finally, in the x-representation (3.59), the volume operator $\hat{v} = i\partial_b$ becomes $\hat{v} = i\lambda\cosh(x)\partial_x$ and the scalar product (3.39) reads as

$$\begin{aligned}\langle\chi|\chi'\rangle &= \sum_{n\in 2\lambda\mathbb{Z}\setminus 0} \overline{\chi(n)}\, \chi'(n) \\ &= \sum_{n\in 2\lambda\mathbb{Z}\setminus 0} \overline{\psi(n)}\, |n| \psi'(n) \\ &= \frac{\lambda}{\pi}\int_0^{\pi/\lambda} \mathrm{d}b\, \overline{\tilde{\psi}(b)}\, |i\partial_b|\, \tilde{\psi}'(b) \\ &= \frac{\lambda}{\pi}\int_{-\infty}^{\infty} \frac{\mathrm{d}x}{\cosh(x)}\, \overline{\psi(x)}\, |i\cosh(x)\partial_x|\, \psi'(x) \,,\end{aligned} \tag{3.63}$$

where we excluded the zero volume state as it decouples. Hence, by considering the expectation value of the absolute value of the volume operator on left-moving states, we get for large k

$$\begin{aligned}\big\langle \Psi_L(\phi)\big|\, |\hat{v}|\, \big|\Psi_L(\phi)\big\rangle &= \frac{\lambda^2}{\pi}\int_{-\infty}^{\infty} \frac{\mathrm{d}x}{\cosh(x)}\, \overline{\Psi_L(x+\phi)}\, |i\cosh(x)\partial_x|\, |i\cosh(x)\partial_x|\, \Psi_L(x+\phi) \\ &= -\frac{\lambda^2}{\pi}\int_{-\infty}^{\infty} \mathrm{d}x\, \overline{\Psi_L(x+\phi)}\, \partial_x \cosh(x)\partial_x \Psi_L(x+\phi) \\ &= \frac{\lambda^2}{\pi}\int_{-\infty}^{\infty} \mathrm{d}x'\, \overline{\partial_{x'}\Psi_L(x')}\, \frac{e^{x'}e^{-\phi} + e^{-x'}e^{\phi}}{2} \partial_{x'}\Psi_L(x') \quad \text{with } x' = x+\phi \\ &=: V_+ e^{\phi} + V_- e^{-\phi} \\ &=: V_{\min}\, \langle\Psi_L|\Psi_L\rangle \cosh(\phi - \phi_{\text{bounce}}) \,,\end{aligned} \tag{3.64}$$

where

$$V_\pm = \frac{\lambda^2}{\pi}\int_{-\infty}^{\infty} \mathrm{d}x\, |\partial_x\Psi_L(x)|^2 e^{\mp x} \quad , \quad V_{\min} = \frac{2\sqrt{V_+V_-}}{\langle\Psi_L|\Psi_L\rangle} \quad , \quad \phi_{\text{bounce}} = \frac{1}{2}\log\left(\frac{V_-}{V_+}\right) \tag{3.65}$$

and similar results hold for right-moving states. The large k approximation is needed to de-

[11] Such a Fourier transform exists in the sense of tempered distributions.

couple left- and right-moving states so that contributions from negative frequency states can be neglected. Eq. (3.64) shows that the expectation value of the spatial volume has a lower bound $V_{\min}$ and the evolution is symmetric around it. In the LQC quantum theory, the classical Big-Bang singularity is thus resolved by a bounce induced by quantum gravity effects. Numerical investigations, supported by analytic results using coherent states peaked on large volumes, show that also for generic states the evolution remains free of singularity [113, 118, 155].

Compatibly, comparing the expectation value of $|\hat{p}_\phi|$ in the x-representation

$$\left\langle \Psi \right| |\hat{p}_\phi| \left| \Psi \right\rangle = \frac{\lambda}{\pi} \int_{-\infty}^{\infty} \mathrm{d}x \, \overline{\Psi(x)} \, |i\partial_x| |i\partial_x| \Psi(x) = \frac{\lambda}{\pi} \int_{-\infty}^{\infty} \mathrm{d}x \, |\partial_x \Psi(x)|^2 \tag{3.66}$$

with that of $|\hat{v}|$ (cfr. Eq. (3.64))

$$\left\langle \Psi \right| |\hat{v}| \left| \Psi \right\rangle = \frac{\lambda^2}{\pi} \int_{-\infty}^{\infty} \mathrm{d}x \, |\partial_x \Psi(x)|^2 \cosh(x) \geq \lambda \left\langle \Psi \right| |\hat{p}_\phi| \left| \Psi \right\rangle , \tag{3.67}$$

we have the following upper bound on the matter energy density

$$\rho = \frac{\langle |\hat{p}_\phi| \rangle^2}{2 \langle |\hat{v}| \rangle^2} \leq \frac{1}{2\lambda^2} . \tag{3.68}$$

3.3 Effective Quantum Corrected Dynamics

The considerations of the previous section suggest that the quantum corrections due to the polymerisation (3.45) can be described at a phase space level by means of the following effective Hamiltonian

$$H_{\text{eff}} = N \left(\frac{p_\phi^2}{2v} - \frac{v}{2} \frac{\sin^2(\lambda b)}{\lambda^2} \right) \approx 0 , \tag{3.69}$$

which reduces to the Hamiltonian (3.21) of the classical theory for $\lambda b \ll 1$. To convince ourselves let us study the effective dynamics generated by (3.69)[12]. As we are interested in using the scalar field ϕ as a clock to express the evolution of phase space quantities in a gauge-independent way, we can fix the lapse to be $N = v$. The effective Hamiltonian then reads as

$$H_{\text{eff}} = \frac{p_\phi^2}{2} - \frac{v^2}{2} \frac{\sin^2(\lambda b)}{\lambda^2} . \tag{3.70}$$

and we have

$$\dot{v} = \{v, H_{\text{eff}}\} = -v^2 \frac{\sin(\lambda b)}{\lambda} \cos(\lambda b) \qquad , \qquad \dot{\phi} = \{\phi, H_{\text{eff}}\} = p_\phi \tag{3.71}$$

with p_ϕ a conserved quantity ($\dot{p}_\phi = \{p_\phi, H_{\text{eff}}\} = 0$) and we note that the condition $\dot{\phi} > 0$ for ϕ

[12] More precisely, the form of the effective Hamiltonian can be motivated by looking at coherent states and their quantum fluctuations. Remarkably, it was shown that the effective dynamics generated by the polymerised Hamiltonian (3.69) agrees with the full quantum dynamics projected on a finite-dimensional submanifold spanned by properly constructed semiclassical states [155–157]. The effective polymerised theory is thus capturing quantum geometry corrections descending from the loop quantised cosmological theory.

to be a good clock implies $p_\phi = const. > 0$. Using now the constraint $H_{\text{eff}} = 0$, we have

$$\frac{\sin^2(\lambda b)}{\lambda^2} = \frac{p_\phi^2}{2} = 2\rho \,, \tag{3.72}$$

from which it follows that

$$\dot{v} = -p_\phi \, v \sqrt{1 - \frac{\lambda^2 p_\phi^2}{v^2}} = -p_\phi \sqrt{v^2 - \lambda^2 p_\phi^2} \qquad \text{i.e.} \qquad \frac{\mathrm{d}v}{\sqrt{v^2 - \lambda^2 p_\phi^2}} = -p_\phi \mathrm{d}t = -\mathrm{d}\phi \,. \tag{3.73}$$

Integrating the above equation yields

$$\log\left(\sqrt{\frac{v^2}{\lambda^2 p_\phi^2} - 1} + \frac{v}{\lambda |p_\phi|}\right) = \phi_0 - \phi \,, \tag{3.74}$$

from which, using the identity $\operatorname{arccosh}(x) = \log(\sqrt{x^2 - 1} + x)$, we get

$$v(\phi) = \lambda |p_\phi| \cosh(\phi - \phi_0) \,, \tag{3.75}$$

in agreement with the behaviour for the expectation value of the volume operator discussed in the previous section. Note that, in the above calculation, we set the initial conditions so that

$$\rho = \frac{p_\phi^2}{2v^2} = \frac{1}{2\lambda^2} \frac{1}{\cosh^2(\phi - \phi_0)} \leq \frac{1}{2\lambda^2} \tag{3.76}$$

compatibly with the upper bound on matter energy density (3.68). Alternatively, we can see this from the first equality in (3.73) which gives

$$\left(\frac{\dot{v}}{v}\right)^2 = p_\phi^2 \left(1 - \frac{\lambda^2 p_\phi^2}{v^2}\right) \,, \tag{3.77}$$

from which, taking out the density weight from $\dot{v}$ due to our choice of the lapse, we get

$$\left(\frac{\dot{v}}{v}\right)^2 = \left(\frac{3\dot{a}}{a}\right)^2 = 2\rho \left(1 - \frac{\rho}{\rho_{\text{crit}}}\right) \qquad , \qquad \rho_{\text{crit}} = \frac{1}{2\lambda^2} \,. \tag{3.78}$$

These are the effective quantum corrected Friedmann equations and we see that $\frac{\dot{v}}{v} = 0$ when ρ reaches the critical density $\rho_{\text{crit}} = \frac{1}{2\lambda^2}$, i.e. the volume reaches its minimum and the bounce replacing the classical singularity occurs. Moreover, far from the Planck regime ($\rho \ll \rho_{\text{crit}}$ i.e. $\lambda b \ll 1$) the classical behaviour is recovered. For later purposes (see Ch. 4), it is convenient to work out the quantum corrected solution for the volume and hence the scale factor also in the proper time parametrisation. This can be done by solving the effective dynamics governed by the Hamiltonian (3.69) with $N = 1$, or equivalently by looking at the modified effective Friedmann equations (3.78), yielding

$$\frac{\mathrm{d}v}{\sqrt{1-\frac{\lambda^2 p_\phi^2}{v^2}}} = -|p_\phi|\mathrm{d}t \qquad \Rightarrow \qquad \sqrt{v^2-\lambda^2 p_\phi^2} = -|p_\phi|(t-t_0)\,, \tag{3.79}$$

i.e.

$$v(t) = \pm|p_\phi|\sqrt{(t-t_0)^2+\lambda^2} = \frac{v_{\mathrm{ext}}}{\lambda}\sqrt{(t-t_0)^2+\lambda^2}\,, \tag{3.80}$$

where v_{ext} denotes the extremal value of the volume at the bounce $t = t_0$ for which the square root in (3.79) vanishes. The classical solution (3.25) is reproduced at large t in the past and in the future as well as in the small λ limit. Recalling then the relation (3.19) between v and a, we get

$$a(t)^2 = \frac{a_{\mathrm{ext}}^2}{\lambda^{2/3}}\Big((t-t_0)^2+\lambda^2\Big)^{1/3}\,, \tag{3.81}$$

where $a_{\mathrm{ext}} = (\frac{v_{\mathrm{ext}}}{V_o})^{1/3}$ is the extremal value of the scale factor at the bounce.

To sum up, the heart of the construction of the effective quantum theory and the source of the resulting bounce mechanism solving the classical singularity rely on the following phase space regularisation (polymerisation):

Construction of the effective theory

Starting from the canonically conjugate phase space variables, say (Q, P), describing the geometry of the minisuperspace model under consideration (e.g., the volume v and its conjugate momentum b for FLRW cosmology), the passage to the effective quantum theory is achieved by regularising the momenta P in terms of their exponentiated versions. The simplest choice consists of the replacement

$$P \longmapsto \frac{\sin(\lambda P)}{\lambda}\,, \tag{3.82}$$

where λ is a parameter (called *polymerisation scale*) controlling the onset of quantum effects. The structure of such modifications is inspired by similar ones in LQG that are closely related to lattice gauge theory supplemented with quantum geometry considerations, which suggest to take λ at the Planck scale instead of taking the limit $\lambda \to 0$. For $\lambda P \ll 1$, we have $\sin(\lambda P)/\lambda \sim P$ and the classical behaviour is recovered.

3.4 Holographic Entropy Bound in LQC

As discussed in Ch. 1, despite of its wide validity in comparison with other entropy bounds, Bousso's null entropy bound [8, 32, 33] strongly relies on the semi-classical approximation of having a smooth metric geometry at our disposal far from the Planck scale. It is in general unclear whether or not such a holographic entropy bound would survive in a fully fledged quantum theory of gravity, the very concept of space-like surfaces and their light-sheets not being well-defined

once quantum fluctuations of spacetime geometry are involved. To have effective descriptions in which a smooth quantum corrected metric incorporating quantum gravity effects becomes available might be then important to check the validity of the bound beyond the classical regime. In this respect, the LQC effective description discussed in the previous section provides an ideal scenario to concretely address such kind of questions. In [158] it was actually shown that, within the classical description of FLRW spacetime, the null entropy bound can be violated in the Planck regime. Remarkably, the modified effective spacetime geometry suggested by LQC allows to restore the validity of the bound. Since this provides us with a simple explicit example sharing similar motivations with the line of thoughts underlying the forthcoming chapters, let us close this chapter by briefly recalling the main steps of the analysis of [158].

Let us consider a flat FLRW spacetime filled with a radiation fluid. Classically, the system is described by the Friedmann equations ($c = 1$, $12\pi G = 1$)

$$\left(\frac{3\dot{a}}{a}\right)^2 = 2\rho \,, \tag{3.83}$$

supplemented by the continuity equations

$$\dot{\rho} + 3\frac{\dot{a}}{a}(\rho + P) = 0 \,, \tag{3.84}$$

as derived from the conservation of the energy-momentum tensor for a perfect fluid $T^{\mu\nu} = (\rho + P)u^\mu u^\nu + g^{\mu\nu}P$, with P the fluid pressure and u^μ the unit vector field orthogonal to the $t = const$ slices [159]. In the case of radiation-dominated universe, $P = \rho/3$ and we get the solution

$$\rho = \frac{C}{a(t)^4} \qquad , \qquad a(t) = \left(\frac{8C}{9}t^2\right)^{1/4} \tag{3.85}$$

where C is an integration constant. Assuming that the universe is instantaneously in equilibrium, the time dependence of the temperature can be obtained via the Stefan-Boltzmann law ($\hbar = 1$)

$$T(t) = \left(\frac{135}{8\pi^2 t^2}\right)^{1/4} \,. \tag{3.86}$$

Let then $\mathcal{B}$ be a metric 2-sphere in a homogeneous $t = const$ slice, say $t = t_f$. Since the FLRW spacetime does not admit a trapped surface, $\mathcal{B}$ must admit a past light-sheet. Moreover, being the spacetime conformally flat, the congruence of ingoing null geodesics would either terminate on the Big Bang singularity or be the future null cone of a point. In the latter case, the light-sheet $\mathcal{L}_\mathcal{B}$ of $\mathcal{B}$ is the future light-cone of such a caustic point (cfr. Fig. 1.1 in Sec. 1.1.3 and the surrounding discussion). Denoting by $t_i > 0$ the time defined by the point, the area $A(\mathcal{B})$ of $\mathcal{B}$ is given by

$$A(\mathcal{B}) = 4\pi a(t_f)^2 r_f^2 \qquad , \qquad r_f = \int_{t_i}^{t_f} \frac{\mathrm{d}t'}{a(t')} \,. \tag{3.87}$$

Computing then the entropy flux $S(\mathcal{L}_\mathcal{B}) = \int_{\mathcal{L}_\mathcal{B}} s^a \epsilon_{abcd}$ through $\mathcal{L}_\mathcal{B}$, with $s^a = su^a$, $s = (\rho+P)/T$, and ϵ_{abcd} the volume form, it turns out that the ration between S and the area of $\mathcal{B}$ in Planck

units is given by (up to numerical factors that are not relevant for the purposes of the present discussion) [158]

$$\frac{S(\mathcal{L}_{\mathcal{B}})}{A(\mathcal{B})/4} \propto \frac{1}{\sqrt{t_f}} \left(1 - \sqrt{\frac{t_i}{t_f}}\right) , \tag{3.88}$$

from which we see that the r.h.s. grows as t_f approaches the singularity at $t = 0$ (note that $t_i/t_f < 1$) and the null entropy bound is violated.

On the contrary, in the case of a LQC effective quantum corrected spacetime described by the modified Friedmann equations (3.78) (with the same continuity equations (3.84) as demanded by the conservation law $\nabla^a T_{ab} = 0$), one gets

$$\rho = \frac{C}{a(t)^4} \qquad , \qquad a(t) = \left(\frac{8C}{9}t^2 + \frac{C}{\rho_{\text{crit}}}\right)^{1/4} \tag{3.89}$$

and repeating the same analysis as before

$$\frac{S(\mathcal{L}_{\mathcal{B}})}{A(\mathcal{B})/4} \propto r_f \left(\frac{8t_f^2}{9} + \frac{1}{\rho_{\text{crit}}}\right)^{-1/2} , \tag{3.90}$$

where r_f can be expressed in terms of hypergeometric functions (see [158] for details). Therefore, since the temperature $T \sim \rho^{1/4}$ now reaches a finite upper bound at the bounce $t = 0$, the entropy current also does and the r.h.s. of (3.90) remains finite as $t_f \to 0$. Moreover, as discussed in [158] for the values of the critical density and the Barbero-Immirzi parameter usually adopted in LQC, it turns out that the above entropy-area ratio is smaller than 1 for all round surfaces $\mathcal{B}$. The null entropy bound is thus restored by quantum gravity effects which become dominant in the high curvature regime and resolve the classical singularity.

This shows that, independently of the fate of holography in a full QG theory, holographic features might emerge at the effective level and are shared by other QG approaches, not only in a string theory or AdS/CFT framework. Moreover, as it was the case for the entropy bound in the cosmological example discussed above, the general idea of incorporating QG effects via effective quantum corrected spacetime geometries might provide significant improvements smoothing out those divergencies which would occur at high curvature in the classical description. In the next chapter we will discuss another example of improved holographic description, within the AdS/CFT framework, for which the application of quantum corrections inspired by LQG turns out to be successful.

Part III

LQG EFFECTIVE MODELS, RESOLVED SINGULARITIES AND HOLOGRAPHIC ASPECTS

Chapter 4

Holographic Signatures of Resolved Cosmological Singularities

Drawbacks and inconsistencies may arise when the classical description is pushed forward to the Planck regime where quantum gravitational effects are expected to be dominant. In the previous chapter we discussed a simple cosmological example in which the otherwise violated holographic entropy bound is restored by including QG corrections which provide sensible improvements by smoothing out divergences occurring at the classical level. In a similar spirit, in this chapter we focus on another cosmological situation and study the consequences of the resolution of gravitational singularities within the holographic framework of the AdS/CFT correspondence. As discussed in Ch. 2, a common strategy in such a framework is to translate hard tasks on one side to the dual theory where they may simplify. However, the generic presence of singularities in classical gravity limits the applicability of AdS/CFT to regimes where the singularities are avoided by bulk probes and the classical description can be trusted. Due to recent progress in singularity resolution via non-perturbative QG, it is natural to turn the question around and to ask about field theory signatures of resolved singularities. A first prototype calculation was provided in [160], where an effective quantum corrected Kasner-AdS metric inspired by results from LQG has been used to compute the CFT 2-point correlator in the geodesic approximation. The correlator derived in the classical gravity approximation has previously been shown to contain a pole at finite distance as a signature of the singularity [161, 162]. After briefly recalling the classical setting of the latter investigations, we discuss various examples of quantum corrected metrics for which the bulk gravitational singularity is resolved and use them to compute the boundary correlator. The resulting analysis shows that the finite-distance pole gets resolved by smoothing out the bulk singularity. In order to perform analytic computations, in [160] two key simplifications in the quantum corrected metric were necessary. In the second part of the chapter, based on our paper [163], we lift such simplifications by tackling the problem numerically and show that similar results for the 2-point correlator hold true. The chapter closes with some comments and remarks on the possible implications from the holographic viewpoint.

4.1 Classical Preparation: Setup and Strategy

Let us start by recalling the setup of [161, 162], where the AdS/CFT correspondence was used to study holographic signatures of cosmological bulk singularities in the classical gravity approximation. The bulk spacetime is described by a 5-dimensional Kasner-AdS geometry whose line element reads as [164]

$$\mathrm{d}s_5^2 = \frac{1}{z^2}\Big(\mathrm{d}z^2 + \mathrm{d}s_4^2(t)\Big) \qquad , \qquad \mathrm{d}s_4^2(t) = -\mathrm{d}t^2 + \sum_{a=1}^{3} t^{2p_a}\mathrm{d}x_a^2 \tag{4.1}$$

where we recall from Ch. 2 that $z = L_{AdS}^2/r$ denotes the inverse radial direction in Poincaré coordinates for which the asymptotic boundary is located at $z = 0$, and we have set the AdS radius L_{AdS} to 1. The exponents p_a are called *Kasner exponents* and as long as they satisfy the vacuum Kasner conditions $\sum_a p_a = 1 = \sum_a p_a^2$, the metric $\mathrm{d}s_4^2$ is a solution of the 4d vacuum Einstein equations without cosmological constant, while the full metric $\mathrm{d}s_5^2$ is a solution of 5d vacuum Einstein equations with negative cosmological constant. In less than five spacetime dimensions, the only possible values for p_a are $0, 1$ and the metric is equivalent to pure AdS. For a p_a neither vanishing nor 1, the spacetime described by the metric (4.1) has a curvature singularity at $t = 0$ as can be seen from the Kretschmann scalar given by [162]

$$\mathcal{K}^{(5)} = R^{(5)}_{\mu\nu\rho\sigma}R^{(5)\,\mu\nu\rho\sigma} = 40 - 16(p-1)p^2\frac{z^4}{t^4} \,, \tag{4.2}$$

where p denotes any of the Kasner exponents p_a. In addition to the translational symmetries in the x^a-directions, the metric (4.1) is also invariant under the following scaling transformation

$$z \longmapsto \alpha z \qquad , \qquad t \longmapsto \alpha t \qquad , \qquad x_a \longmapsto \alpha^{1-p_a}x_a \qquad (\alpha \in \mathbb{R}) \,. \tag{4.3}$$

As discussed in Ch. 2, following the AdS/CFT dictionary, the dual description of asymptotically AdS spacetimes involves $\mathcal{N} = 4$ Super Yang-Mills theory thought of as living on the asymptotic boundary of the bulk spacetime. For the system under consideration, this consists of a 4-dimensional Kasner background as can be seen from the metric (4.1) in the limit $z \to 0$ and rescaling away the conformal factor $1/z^2$ in front of it. Alternatively, by pulling out a factor t^2 and changing the time coordinate by setting $t = e^\tau$, the metric (4.1) can be rewritten as

$$\mathrm{d}s_5^2 = \frac{t^2}{z^2}\Big(e^{-2\tau}\mathrm{d}z^2 - \mathrm{d}\tau^2 + \sum_{a=1}^{3} e^{-2(1-p_a)\tau}\mathrm{d}x_a^2\Big) \,, \tag{4.4}$$

so that the boundary metric is non-singular and it describes an anisotropic deformation of de Sitter space with (4.3) leaving the conformal factor invariant, thus acting as an isometry of the boundary metric.

Now, as discussed in Sec. 2.3.2 (cfr. Eq. (2.57)), in the large N semiclassical bulk limit, the leading contribution to the equal time two-point correlator of a high conformal dimension (heavy) scalar operator $\mathcal{O}$ is determined in the so-called geodesic approximation [105] by the

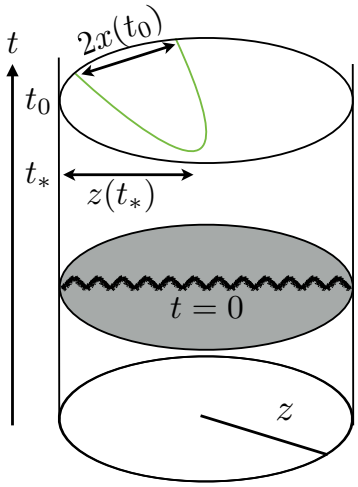

Figure 4.1: Setup to probe bulk singularities by studying the equal-time correlator in the dual field theory: in the geodesics approximation the two-point function of a heavy scalar operator $\mathcal{O}$ is specified by the length of space-like bulk geodesics anchored at two points on some boundary time slice, say at $t = t_0$.

length of space-like bulk geodesics connecting two points on some boundary time slice at $t = t_0$, i.e.

$$\langle \mathcal{O}(x)\mathcal{O}(-x)\rangle \sim \sum_{\text{geodesics}} e^{-\Delta L_{\text{ren}}} \,, \tag{4.5}$$

where Δ is the conformal dimension of the boundary operator $\mathcal{O}$, which is related to the mass m of the bulk field sourcing $\mathcal{O}$ and the dimension d of the boundary spacetime via (cfr. Eq. (2.42))

$$\Delta = \frac{d}{2} + \sqrt{\frac{d^2}{4} + m^2} \underset{m\gg 1}{\simeq} m \,, \tag{4.6}$$

and, as as sketched in Fig. 4.1, we consider geodesics anchored on the same boundary time slice whose endpoints are separated in only one spatial direction, hereafter denoted simply by x (and the corresponding Kasner exponent by p). This is due to the translation symmetry in the x^a-directions which allows us to think of that geodesics as traveling in a $(2+1)$-dimensional effective spacetime coordinatised by (t, x, z). L_{ren} in (4.5) denotes the renormalised length of a space-like bulk geodesics connecting the boundary points $(t_0, -x, 0)$ and $(t_0, x, 0)$. Indeed, since the boundary lies at infinity, the length of such geodesics would generically be infinite. As anticipated in Ch. 2, such a divergence can be cured by truncating the geodesics at some boundary regulator $z = \epsilon$, which corresponds to a UV cutoff at energy scale $1/\epsilon$ in the dual field theory, and subtracting the divergent contribution in the $\epsilon \to 0$ limit. We will come back on the explicit form of such a counterterm later with the expression of the two-point correlation at our hand. Moreover, as explicitly meant with the sum in Eq. (4.5), multiple contributions can occur coming from geodesics satisfying the same boundary data and a sum over the individual contributions must be included in evaluating the two-point correlator[1].

[1] As discussed in [161, 162], complex solutions have also to be taken into account as they contribute to the long distance fall-off behaviour $\sim (L_{\text{bdy}})^{\frac{2\Delta}{1-p}}$ of the two-point correlator for geodesics with proper boundary separation L_{bdy} and not crossing the singularity. Reality of the correlator implies these solutions to contribute in complex conjugate pairs.

AdS cosmologies and their duals have been extensively studied in the gauge/gravity literature, see e.g. [164–173]. The interesting feature of the above setup lies however in the fact that, unlike other isotropic AdS cosmologies, in the anisotropic spacetime described by the metric (4.1) geodesics that propagate in a direction with negative Kasner exponent ($p < 0$) are bent towards the singularity and can be used then to probe the high curvature region near the singularity. This can be seen by looking at the geodesic equations obtained from the metric (4.1). In x-parametrisation, the equation for $t(x)$ is given by [162]

$$t''(x) + p\,\frac{t(x)^{2p} - 2t'(x)^2}{t(x)} = 0\,, \tag{4.7}$$

where primes denote derivatives w.r.t. x. Since the endpoints of the geodesics under consideration are anchored at an equal time boundary slice, there must be a turning point x_* at which $t'(x_*) = 0$ (cfr. Fig. 4.1). Near this point, Eq. (4.7) reduces to

$$t(x)t''(x) = -p\,t(x)^{2p}\,, \tag{4.8}$$

from which we see that, considering positive t so that the singularity at $t = 0$ is in the past of the $t = t_0$ slice, $t''(x_*)$ is positive (resp. negative) for negative (resp. positive) values of p. Therefore, geodesics that propagate in a direction with positive Kasner exponent ($p > 0$) are curved away from the singularity, while if we consider the x-separation in a negative p direction, geodesics are bent towards the singularity and are thus characterised by a turning time $t_* < t_0$ for real solutions and $t_0 > 0$. Moreover, evaluating the Kretschmann scalar (4.2) at the turning point, we see that it diverges as z_*^4/t_*^4 when t_* approaches the $t = 0$ singularity. Bulk geodesics propagating in a negative p direction can be thus used to probe the high curvature region in the vicinity of the singularity.

In order to compute the (renormalised) geodesic length it is convenient to look at geodesic equations in the affine parametrisation, which can be easily derived from the length functional

$$S = \int \mathrm{d}s\,\sqrt{g_{\mu\nu}\frac{\mathrm{d}x^\mu}{\mathrm{d}s}\frac{\mathrm{d}x^\nu}{\mathrm{d}s}} = \int \mathrm{d}s\,\sqrt{\frac{\dot{z}^2}{z^2} - \frac{\dot{t}^2}{z^2} + t^{2p}\frac{\dot{x}^2}{z^2}}\,, \tag{4.9}$$

where dots denote derivatives w.r.t. the affine parameter s and we chose the sign under the square root appropriate for space-like geodesics. In this case, in fact, the equations decouples and it is possible to derive the expression from the geodesic length s directly from the solution of the equation for $z(s)$ as follows. The equation for $z(s)$ reads

$$\ddot{z} - \frac{\dot{t}^2}{z} + \frac{t^{2p}\dot{x}^2}{z} - \frac{\dot{z}^2}{z} = 0\,, \tag{4.10}$$

which, using the space-like condition $1 = g_{\mu\nu}\dot{x}^\mu\dot{x}^\nu = \frac{\dot{z}^2}{z^2} - \frac{\dot{t}^2}{z^2} + \frac{t^{2p}\dot{x}^2}{z^2}$, simplifies to

$$\ddot{z} - 2\frac{\dot{z}^2}{z} + z = 0\,, \tag{4.11}$$

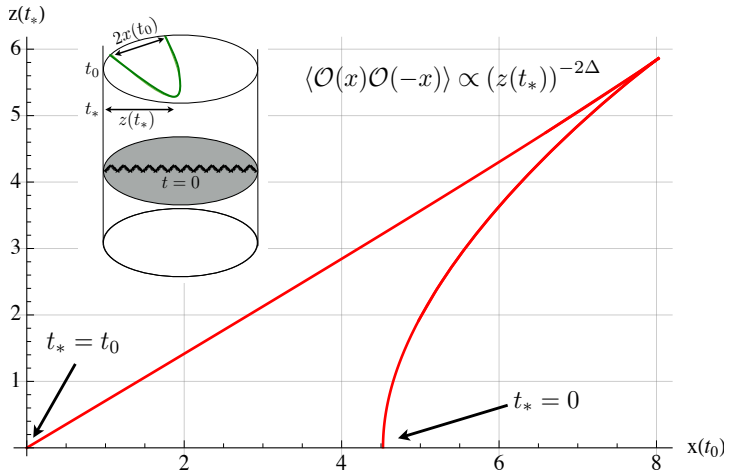

Figure 4.2: Plot of $z(t_*)$ vs. $x(t_0)$ for $p = -1/4$ and $t_* = t_0 = 4$ at (0,0). For comparison with the notation, the set up for computing the equal time 2-point correlator in the geodesic approximation is recalled in the top left corner of the plot, while the $z(t_*)$-dependence of the correlator (4.14) is reported on the top right.

whose solution is given by

$$z(s) = \frac{z(t_*)}{\cosh(s - s_0)} \,. \tag{4.12}$$

With no loss of generality we can set $s_0 = 0$ to start counting the proper distance from the turning point of the geodesics. The solution (4.12) shows that the geodesic length diverges as $z \to 0$. As already anticipated, the geodesic length needs then to be renormalised by introducing a finite but small cutoff $z = \epsilon$ and subtracting the divergence occurring in the $\epsilon \to 0$ limit. Specifically, in the limit $\epsilon \to 0$, Eq. (4.12) yields

$$\pm\, s(\epsilon) = \log\left(2z(t_*)\right) - \log(\epsilon) \,, \tag{4.13}$$

from which, subtracting the divergent term $-\log(\epsilon)$, we get[2]

$$L_{\rm ren} = 2\log\left(2z(t_*)\right) \qquad \Rightarrow \qquad \langle \mathcal{O}(-x)\mathcal{O}(x)\rangle = \exp(-\Delta L_{\rm ren}) = \left(2z(t_*)\right)^{-2\Delta} \,. \tag{4.14}$$

The study of the two-point correlator (4.14) requires the analysis of the geodesic equations in t-parametrisation. The general solutions are however quite involved and can be found in [162] for generic dimensions and Kasner exponent p (the case $p = -1/4$ with a (4+1)-dimensional bulk spacetime is discussed in [161], while a (5+1)-dimensional example with $p = -1/2$ can be found in [162]). Here we report in Fig. 4.2 the plot of the value $z(t_*)$ of z at the turning point in terms of the boundary separation $x(t_0)$ for $p = -1/4$. As we can see from the plot, the correlator diverges at the origin $(z(t_*), x(t_0)) = (0, 0)$ which corresponds to the usual behaviour in the coincidence

[2]This can be understood as the effect of the conformal rescaling of the metric induced by $\mathrm{d}s_5^2$ in (4.1) on a fixed z slice to remove the otherwise divergent conformal factor $1/z^2$ from the boundary metric $\mathrm{d}s_4^2$. Indeed, recalling the transformation behaviour (2.12) of primary conformal fields, we have $\langle \mathcal{O}\mathcal{O}\rangle_{\rm CFT} = z^{-2\Delta}\,\langle \phi\phi\rangle_{\rm bulk}$ according to the bulk/boundary dictionary. In the geodesic approximation $\langle \phi\phi\rangle_{\rm bulk} = \exp(-\Delta L)$ so that, in the $z = \epsilon \to 0$ limit, the divergent logarithmic term in the geodesic length $L \overset{\epsilon\to 0}{=} 2\log(2z(t_*)) - 2\log(\epsilon)$ removes the $\epsilon^{-2\Delta}$ divergence in the boundary two-point correlator, thus yielding the result (4.14).

limit of zero boundary separation. Note that the same $x(t_0)$-value can correspond to multiple $z(t_*)$ values so that multiple contributions from geodesics with the same boundary separation must be added in the two-point correlator. Moreover, $z(t_*)$ vanishes also at a finite value of $x(t_0)$ thus yielding a finite-distance pole in the two-point correlator. This is due to a null geodesics lying entirely on the boundary ($z = 0$). As discussed in [162] by studying the near boundary expansion of the full solutions of the geodesics equations, in the limit $t_* \to 0$, space-like bulk geodesics approach such a null boundary geodesic for $p < 0$ and their tip approaches the bulk singularity. Correspondingly, the two-point correlator exhibits a pole at the cosmological horizon scale which is interpreted as a dual signature of the classical bulk singularity. The presence of such a pole indicates that the state in the dual field theory description of the Kasner-AdS metric is not normalisable [162].

4.2 Improved Correlator from Quantum-Corrected Bulk Geometry

The possibility that the pole occurring at non-vanishing spatial separation might be smoothed out by quantum gravity effects thus making the equal time two-point correlator finite has been discussed in [162]. However, no explicit example was proposed. Following up on this line of thoughts, a prototype calculation to check the above statement has been set up in [160] where a first simplified example of quantum corrected bulk metric inspired by the effective spacetimes emerging from LQG was used to compute the improved CFT correlator. Specifically, the effective bulk geometry considered in [160] is described by the following 1-parameter family of quantum corrected Kasner-AdS metrics

$$\mathrm{d}s_5^2 = \frac{1}{z^2}\left(\mathrm{d}z^2 + \mathrm{d}s_4^2(t)\right) \qquad , \qquad \mathrm{d}s_4^2(t) = -\mathrm{d}t^2 + \frac{a_{\mathrm{ext}}^2}{\lambda^{2p}}\left(t^2+\lambda^2\right)^p \mathrm{d}x^2 + \dots \tag{4.15}$$

where λ is a parameter controlling the onset of quantum effects, dots refer to the other spatial directions which might have different Kasner exponents, and a_{ext} is the extremal value of the scale factor, i.e., its value at the bounce resolving the $t = 0$ classical singularity. For $\lambda > 0$, the metric (4.15) is in fact free of any curvature singularity, while the classical Kasner metric (4.1) with scale factor $a(t) = t^{2p}$ is recovered in the double scaling limit $\lambda \to 0$ and $a_{\mathrm{ext}}/\lambda^p \to 1$. Note that we set the time of bounce to be $t = 0$, but it can be equivalently chosen to be any time t_0 by simply shifting $t \mapsto t - t_0$ in the above expression of the metric.

The form of the quantum corrected metric (4.15) can be motivated from LQG, or more precisely from effective symmetry-reduced spacetimes stemming from Loop Quantum Cosmology (LQC). Specifically, since the 5d classical metric (4.1) is singular only in its 4d part and the 5d Einstein's equations with negative cosmological constant imply $\mathrm{d}s_4^2$ to be Ricci-flat, the idea is to keep the components of the metric in z-direction classical as no Planck regime curvatures are associated with them[3] and quantise only the components orthogonal to the z-direction using

[3]The cosmological constant is taken to be small enough for this to be true. From the point of view of the 10-dimensional asymptotically $\mathrm{AdS}_5 \times \mathbb{S}^5$ spacetimes used in AdS/CFT, this amounts to consider the value of N^2 given by the ratio of L^8_{AdS} and the 10d Newton constant to be very large, as otherwise quantum corrections for the z-direction should be expected.

4d (loop) quantum gravity with vanishing cosmological constant. The most studied scenario in the LQG framework is that of a spatially flat homogeneous and isotropic FLRW cosmological spacetime coupled with a massless scalar field for which analytic results are available. As discussed in Ch. 3, the relevant quantum corrections can be incorporated at the phase space level via the polymerisation procedure thus leading to the quantum corrected geometry described by the effective metric (3.81). The latter can be though of as a particular case of (4.15) with all Kasner exponents given by $p = 1/3$[4]. No analytic solution is known in the general non-isotropic case. Numerical investigations have been undertaken in [177] to study the quantum dynamics described by effective equations derived from expectation values of the minisuperspace Hamiltonian constraint operator. It turns out that the singularity gets resolved and is replaced by a smooth transition between Kasner universes at late times. The detailed behaviour of the solutions is more complicated than that of (4.15). In particular, unlike the case of (4.15) where each p_a remains the same before and after the bounce, in the general case Kasner exponents may smoothly change during the bounce [177–179]. Positive Kasner exponents may transition into other positive Kasner exponents, while negative exponents always change into positive ones. We will come back on this point and a further key simplification concerning the scale at which quantum effects become relevant implicitly assumed in the above choice of the metric in the next sections. The choice of the bulk metric (4.15) used in [160] was justified by the fact that it provides a relatively simple example of quantum corrected metric for which the analysis of the previous section can be still performed analytically. Indeed, for such kind of bulk metric, the geodesic equations can be solved completely in the t-parametrisation (see [160] for details). As in the classical case, however, the affine parametrisation turns out to be more convenient for computing the renormalised geodesic length. The equation for $z(s)$ now reads

$$\ddot{z} - \frac{\dot{t}^2}{z} + \frac{a_{\text{ext}}^2}{\lambda^{2p}}(t^2+\lambda^2)^p\frac{\dot{x}^2}{z} - \frac{\dot{z}^2}{z} = 0\,, \tag{4.16}$$

which, using the condition $g_{\mu\nu}\dot{x}^\mu\dot{x}^\nu = 1$ with the 5d metric $g_{\mu\nu}$ given in (4.15), yields the same equation (4.11) as in the classical case. The functional form of the solution (4.12) as well as the renormalisation procedure and the resulting expression (4.14) for the two-point correlator remain the same as in the classical case. What changes now is the behaviour of $z(t_*)$ as the solutions of the geodesic equations are now modified by the quantum corrections descending from the metric (4.15) and parametrised by λ. The explicit form of the solutions in the t-parametrisation can be found in [160]. In Fig. 4.3 below, we report the value $z(t_*)$ of z at the turning point as a function of the boundary separation. As we can see from the plot, the correlator still diverges at the origin $(0,0)$ which corresponds to the standard divergence occurring in the coincidence limit. However, unlike the classical case corresponding to the red curve with $\lambda = 0$, $z(t_*)$ does not vanish at finite boundary separation for $\lambda = 1$ corresponding to the quantum corrected case (blue curve). The pole in the two-point correlator occurring at finite boundary separation in the

[4]Similar results for the quantum corrected metric have been derived also in other approaches such as group field theory condensate cosmology [174], improved regularisation schemes in the canonical framework of quantum reduced loop gravity [175], as well as non-singular modifications of general relativity incorporating a limiting curvature [176].

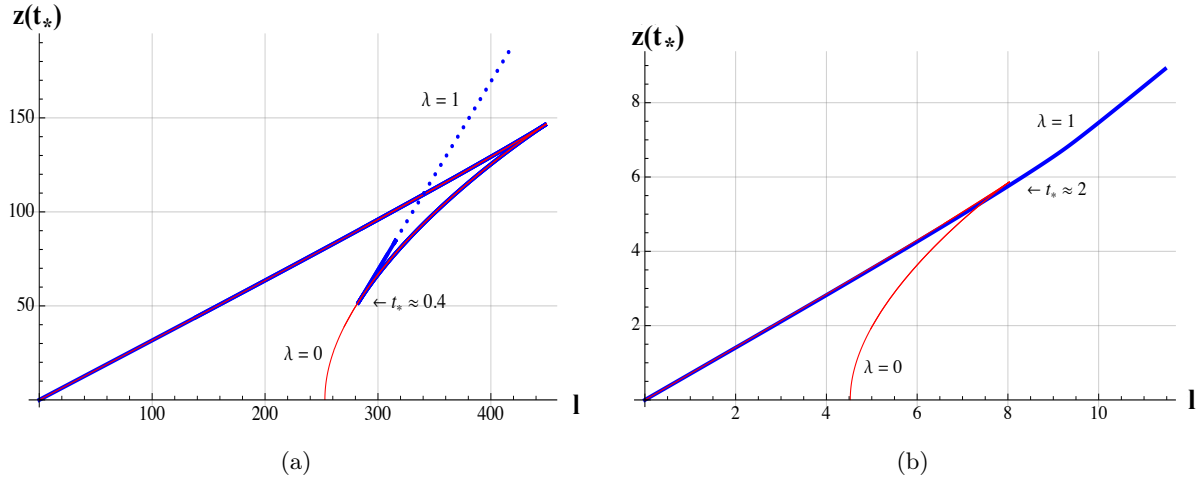

Figure 4.3: Plots of $z(t_*)$ vs. $l = x(t_0)$ for $p = -1/4$ and $a_{ext} = 1$ taken from [160, 163]. The red line represents the classical case with $\lambda = 0$, while the blue line represents the quantum corrected case with $\lambda = 1$ respectively for $t_* = t_0 = 100$ at (0,0) (a), and $t_* = t_0 = 4$ at (0,0) (b). The solid blue line was obtained from numerically evaluating the analytic solutions, while the dashed blue line is an asymptotic expansion for $t_* \to 0$ [160].

classical theory is thus resolved by quantum effects. Moreover, there are multiple $z(t_*)$ values corresponding to real geodesics with the same boundary separation (same $x(t_0)$-value), which have to be added in the correlator. The dominant contribution comes from the local minimum of $z(t_*)$ for $\lambda = 1$, which represents a clear signature of the resolved classical pole. The value that the curve takes at its local minimum approaches zero as $\lambda \to 0$, but the characteristic turnaround behaviour with corresponding resolution of the finite-distance pole persists for any $\lambda > 0$. When t_0 gets close enough to λ, the characteristic behaviour changes (Fig. 4.3 (b)), but a change of slope in the quantum corrected curve persists and $z(t_*)$ does not vanish at finite distance, i.e., the classical pole is still resolved.

4.3 Lifting Simplification 1: 4d vs. 5d Planck Scale

As anticipated in the previous section, the ansatz (4.15) for the effective quantum corrected metric was based on two key simplifications in order to allow for analytic computations.

First of all, as mentioned above, the singularity in the classical metric (4.1) comes from its 4d part. The strategy was then to incorporate quantum corrections tailored from 4d effective loop quantum cosmology (LQC) without cosmological constant to resolve the singularity in the 4d metric $\mathrm{d}s_4^2$, and consequently make the full 5d metric $\mathrm{d}s_5^2$ non-singular as well. The onset of quantum effects is then controlled by a parameter λ which is related to $\hbar$ and sets the scale at which quantum corrections become relevant at the order of the 4d Planck scale. To ensure that the approximation of the problem as one in 4d quantum cosmology remains consistent, a possible z-dependence of $\mathrm{d}s_4^2$ has to be kept small at the order of λ (we will come back to this point). From the 5d bulk point of view, however, it would be more natural that the onset of quantum effects should happen at the 5d Planck scale, and not the 4d scale.

Second, in contrast to the metric (4.15) where the Kasner exponents are fixed during the

bounce, results in anisotropic LQC [177, 179] indicates that Kasner exponents might change their values before and after the quantum bounce smoothly connecting two Kasner universes at late times. This feature is usually referred to as *Kasner transition* in the literature.

A systematic way to take into account both these features in deriving the effective quantum corrected metrics from loop quantum gravity would be to set up the full 5d quantum Einstein equations based on the higher-dimensional extension of the canonical LQG program developed in [120–122] and to extract an effective metric for the quantised symmetry-reduced model under consideration. Unfortunately, this is currently out of technical reach. Following our paper [163], in the remaining part of the chapter we will provide different examples of quantum corrected metrics progressively lifting the above simplifications and use them to study the holographic signature of the resolved singularities in the two-point correlator.

Let us start with the problem of setting the onset of quantum effects at the 5d Planck scale. The form of the quantum corrected metric for which this is achieved can be motivated by means of the following argument. As discussed in Ch. 3 for homogeneous and isotropic LQC, the phase space regularisation $b \mapsto \sin(\lambda b)/\lambda$ (polymerisation procedure) introduces a upper bound in the 4d Ricci scalar by $const./\lambda^2$. The relation

$$\mathcal{K}^{(5)} = R^{(5)}_{\mu\nu\rho\sigma} R^{(5)\,\mu\nu\rho\sigma} = z^4 \mathcal{K}^{(4)} + \dots \tag{4.17}$$

for the 5d Kretschmann scalar, together with the 4d bound $\mathcal{K}^{(4)} \sim \lambda^{-4}$, suggest us to consider then an effective 5d polymerisation scale $\lambda_{5\mathrm{d}} = z\lambda_{4\mathrm{d}} = z\lambda$ in order to obtain a upper bound on $\mathcal{K}^{(5)}$ of order $\lambda_{5\mathrm{d}}^{-4}$ and an onset of quantum effects in the bulk at the 5d Planck scale. This leads us to replace in the effective bulk metric (4.15) the following z-dependent quantum corrected scale factor

$$a(t,z) = \frac{a_{\mathrm{ext}}}{\lambda^p} \left(t^2 + z^2\lambda^2\right)^{p/2} \ , \tag{4.18}$$

where we absorbed the z-scaling of the λ appearing in the prefactor into a_{ext}. Therefore, unlike the previous case of a z-independent λ where quantum effects appear at lower and lower 5d bulk scales as one approaches the boundary, while appearing at the 4d Planck scale in the boundary theory, now quantum corrections would become negligible as one approaches the boundary at $z = 0$ so that the background spacetime of the dual CFT is effectively classical. Moreover, the classical scaling symmetry (4.3) which was broken for a constant λ is now restored in the z-dependent case (4.18).

Both of these features, a z-dependent scale for the onset of quantum effects and the inclusion of Kasner transitions, can have important qualitative effects on the results for the two-point correlator. Indeed, first as discussed in Sec. 4.1, the divergence in the two-point correlator is due to a family of bulk geodesics approaching a null geodesic lying entirely on the boundary [161,162]. Such a geodesic is still present in the quantum corrected bulk spacetime since $\lambda_{5\mathrm{d}} = z\lambda$ goes to zero at the boundary ($z = 0$) and the metric reduces to the classical Kasner solution. However, as we will discuss in the next sections, our analysis suggests that such a null geodesic is isolated and not the limit of a family of bulk geodesics as in the classical case. Second, the long distance behaviour of the correlator in the z-independent case is due to geodesics passing arbitrarily close

to t = 0 [160], where the scale factor $(t^2+\lambda^2)^p$ in (4.15) has a local maximum (for $p<0$). A Kasner transition as in [177] where a negative exponent would transition into a positive one would alter the form of the metric around $t=0$ such that no extremum could be found there. In the following, we will investigate the effect of dropping these simplifications by numerical computations and show that the finite-distance pole in the two-point correlator is still resolved.

4.3.1 Solving Geodesic Equations

In the light of the above considerations, the computation of the equal time two-point correlator in the geodesic approximation boils down to compute the (renormalised) length of geodesics obtained from a metric of the form

$$\mathrm{d}s_5^2 = \frac{1}{z^2}\left(\mathrm{d}z^2 - \mathrm{d}t^2 + a(t,z)^2\mathrm{d}x^2 + \dots\right) . \tag{4.19}$$

This is a two-point boundary value problem. Indeed, the two-point correlator is computed via space-like bulk geodesics anchored at two boundary points on a fixed time slice $t=t_0>0$ with boundary length separation $L_{\mathrm{bdy}} = 2a(t_0, z=0)x(t_0)$. In particular, due to the translation symmetry in the x-direction, we can always choose a coordinate system such that the initial and final points of the geodesics lie symmetrically around the origin. The boundary value problem that needs to be solved is then to determine all geodesics starting at $(t,x,z)=(t_0,-x(t_0),0)$ and ending at $(t_0,x(t_0),0)$, whose input data are given by the values of t_0 and $x(t_0)$. In what follows we will focus on real geodesics. As discussed in [160, 162], there are also contributions coming from conjugate pairs of complex geodesics but these lie outside of the quantum region and affect only the long distance behaviour of the correlator without adding new insights on the behaviour near the singularity.

Since the geodesics we are interested in start and end on the same time slice, there must be a turning point. In our coordinate system, this is identified by the coordinates $(t=t_*, x(t_*)=x_*=0, z=z(t_*)=z_*)$ so that the geodesics are characterised by two branches symmetric around the turning point (towards the turning point and back again). In order to parametrise both branches at the same time, it is more convenient to study geodesics in the affine parametrisation rather than a coordinate parametrisation. In such a parametrisation, the geodesic equation can be obtained from the length functional

$$S = \int \mathrm{d}s \sqrt{g_{\mu\nu}\frac{\mathrm{d}x^\mu}{\mathrm{d}s}\frac{\mathrm{d}x^\nu}{\mathrm{d}s}} = \int \mathrm{d}s \sqrt{\frac{\dot{z}^2}{z^2} - \frac{\dot{t}^2}{z^2} + a(t,z)^2\frac{\dot{x}^2}{z^2}} , \tag{4.20}$$

from which using the relation

$$1 = g_{\mu\nu}\dot{x}^\mu\dot{x}^\nu = \frac{\dot{z}^2}{z^2} - \frac{\dot{t}^2}{z^2} + a(t,z)^2\frac{\dot{x}^2}{z^2} , \tag{4.21}$$

we get

$$\ddot{t} - 2\frac{\dot{t}\dot{z}}{z} + \frac{\dot{x}^2}{2}\frac{\partial}{\partial t}\left(a(t,z)^2\right) = 0 \,, \tag{4.22}$$

$$\ddot{z} - 2\frac{\dot{z}^2}{z} - \frac{\dot{x}^2}{2}\frac{\partial}{\partial z}\left(a(t,z)^2\right) + z = 0 \,, \tag{4.23}$$

$$\frac{\mathrm{d}}{\mathrm{d}s}\left(a(t,z)^2\frac{\dot{x}}{z^2}\right) = 0 \,. \tag{4.24}$$

Eq. (4.24) encodes the conservation law associated with the translation symmetry in x-direction. Moreover, unlike the case of a z-independent scale factor, the geodesic equations do not decouple anymore as the equation (4.23) for $z(s)$ now has an additional term involving the z-derivative of $a(t,z)$. This makes the problem hard to be treated analytically and a numerical solution is required.

To this aim, it is necessary to reformulate the problem in a way that can be handled numerically. First of all, since the boundary lies at infinite proper distance form the turning point, to numerically integrate the geodesic equations it is convenient to compactify the parameter s as

$$\sigma = \tanh(s) \qquad , \qquad \sigma \in [-1,1] \,. \tag{4.25}$$

In such a parametrisation, our boundary value problem becomes

$$\begin{cases} t' = p_t \quad , \quad x' = p_x \quad , \quad z' = p_z \\ p_t' = \frac{2\sigma}{1-\sigma^2}p_t + \frac{2}{z}p_t p_z - \frac{1}{2}\,p_x^2\,\partial_t\left(a^2\right) \\ p_x' = \frac{2\sigma}{1-\sigma^2}p_x + \frac{2}{z}p_x p_z - \frac{1}{a^2}p_x\left(p_t\partial_t\left(a^2\right) + p_z\partial_z\left(a^2\right)\right) \\ p_z' = \frac{2\sigma}{1-\sigma^2}p_z + \frac{2}{z}p_z^2 - \frac{z}{(1-\sigma^2)^2} + \frac{1}{2}p_x^2\partial_z\left(a^2\right) \end{cases} \quad \text{with} \quad \begin{aligned} & t(\sigma=-1) = t(\sigma=1) = t_0 \\ & x(\sigma=-1) = -x(\sigma=1) = -l \\ & z(\sigma=-1) = z(\sigma=1) = 0 \end{aligned} \tag{4.26}$$

where primes denote derivatives w.r.t. σ, we introduced p_t, p_x, p_z to rewrite the equations as first order ODEs, and $l = x(t_0)$. The additional terms in σ are due to the Jacobian factors of derivatives under the parameter transformation (4.25), namely $\frac{\mathrm{d}\sigma}{\mathrm{d}s} = 1-\sigma^2$ and $\frac{\mathrm{d}^2\sigma}{\mathrm{d}s^2}\big/\left(\frac{\mathrm{d}s}{\mathrm{d}\sigma}\right)^2 = -\frac{2\sigma}{1-\sigma^2}$.

Second, let us note that we are only interested in those geodesics which have a turning point in t and z. Geodesics which do not come back to the boundary or come back but on a different time slice are not solutions of (4.26). The main idea to simplify the numerical integration is then to reformulate the above boundary value problem as an initial value problem at the turning point as follows. As discussed before, due to the translation symmetry in x-direction, the value $x(t_*) = x_*$ at the turning point can be set to 0 so that the behavior of the geodesics at this point is characterised only in terms of the values t_* and $z_* = z(t_*)$. Moreover, the affine parametrisation of the geodesics can be shifted in such a way that the turning point corresponds to $s = 0$ and hence $\sigma = \tanh(0) = 0$. Next, in order to express the first derivatives in terms of the turning point data, we note that the velocities in t- and z-direction should vanish at the turning point, i.e.

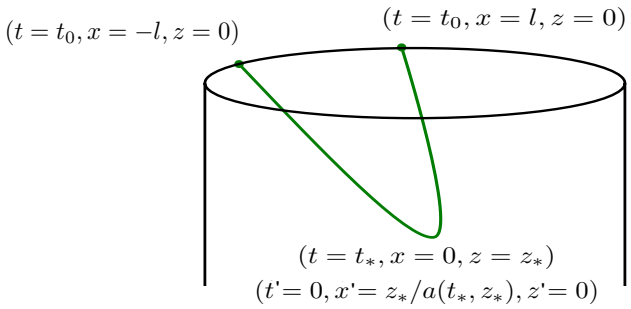

Figure 4.4: Mapping the two-point boundary value problem (4.26) into the initial value problem (4.29) at the turning point of the geodesics.

$$
\begin{aligned}
0 = \dot{t}(s=0) = t'(\sigma=0)\frac{\mathrm{d}\sigma}{\mathrm{d}s}\Big|_{\sigma=0} = t'(\sigma=0)\,, \\
0 = \dot{z}(s=0) = z'(\sigma=0)\frac{\mathrm{d}\sigma}{\mathrm{d}s}\Big|_{\sigma=0} = z'(\sigma=0)\,,
\end{aligned}
\tag{4.27}
$$

and, using again (4.21), we also have

$$
x'(\sigma=0) = x'(\sigma=0)\frac{\mathrm{d}\sigma}{\mathrm{d}s}\Big|_{\sigma=0} = \dot{x}(s=0) = \frac{z_*}{a(t_*,z_*)} = \frac{z_*\lambda^p}{a_{\rm ext}(t_*^2+\lambda^2 z_*^2)^{p/2}}\,. \tag{4.28}
$$

The boundary value problem (4.26) can be thus mapped into the following initial value problem

$$
\begin{cases}
t' = p_t \quad , \quad x' = p_x \quad , \quad z' = p_z \\
p_t' = \frac{2\sigma}{1-\sigma^2}p_t + \frac{2}{z}p_t p_z - \frac{1}{2}\,p_x^2\,\partial_t\left(a^2\right) \\
p_x' = \frac{2\sigma}{1-\sigma^2}p_x + \frac{2}{z}p_x p_z - \frac{1}{a^2}p_x\left(p_t\partial_t\left(a^2\right) + p_z\partial_z\left(a^2\right)\right) \\
p_z' = \frac{2\sigma}{1-\sigma^2}p_z + \frac{2}{z}p_z^2 - \frac{z}{(1-\sigma^2)^2} + \frac{1}{2}p_x^2\partial_z\left(a^2\right)
\end{cases}
\quad \text{with} \quad
\begin{aligned}
&(t(0),x(0),z(0)) = (t_*,0,z_*) \\
&(p_t(0),p_x(0),p_z(0)) = (0,z_*/a(t_*,z_*),0)
\end{aligned}
\tag{4.29}
$$

where, as schematically shown in Fig. 4.4, the Cauchy data are expressed only in terms of the input values t_* and z_* given at the turning point. The parameter σ runs from 0 to 1, i.e. we only cover one of the two branches, but this is not a problem since around $\sigma = 0$ the solution is symmetric in t and z and anti-symmetric in x.

The crucial point becomes then to relate the turning point values t_* and z_* with the boundary data t_0 and $x(t_0) = l$. A proper inversion of the mapping $(t_*, z_*) \mapsto (t_0(t_*, z_*), l((t_*, z_*))$ is not possible however as in general, for given values of t_0 and l, there might be multiple solutions of the boundary value problem (4.26) with different t_* and z_*. From a numerical point of view, since we are interested in those (t_*, z_*) whose corresponding solutions end at fixed t_0, such points correspond to the level lines of $t_0(t_*, z_*)$ and relate z_* with t_*. Finally, to determine the relation $z_*(l)$ for given values of t_0, we need to look at the intersection points of such level lines with the level lines of $l(t_*, z_*)$. Therefore, the solution of the original boundary value problem amounts to 1) solve an initial value problem, 2) computing two level lines, and 3) determining their

intersections. For doing so, the initial value problem needs to be solved for numerous values of (t_*, z_*). This is convenient for our purposes since we are not interested in specific values of l rather in varying it. Moreover, as we are interested in different values of t_0, we solve the initial value problem for a given grid of (t_*, z_*) and use these data to compute different t_0-level lines, thus decreasing the total numerical effort. We implemented the above method with *Matlab* and its built in library. For the solution of the ODE we used the routine `ode45`, which is based on fifth-order Runge-Kutta method with adaptive step size. For the calculation of the level lines we used the routine `contourc`. Since the coefficients of Eqs. (4.29) diverge at $\sigma = \pm 1$, we cut the integration interval such that $\sigma \in [0, 1-\epsilon]$, with $\epsilon = 0.00001$[5].

4.3.2 Renormalised Geodesic Length and Two-Point Correlator

Before presenting the results of the numerical strategy outlined in the previous section, one last point needs to be discussed. This concerns the computation of the renormalised geodesic lenght. Indeed, as discussed both in the classical and in the z-independent case, the evaluation of the equal time two-point correlator in the geodesic approximation (4.5) requires to compute the complete length of the geodesics, from boundary to boundary. In the affine parametrisation chosen in such a way that the turning point corresponds to $s = 0$, this is given by $L = 2s$. As we have already noticed, the geodesic length needs then to be renormalised in order to remove the divergence resulting from the fact that by construction the conformal boundary of spacetime lies at infinity. As discussed in Sec. 4.1 (cfr. Eq. (4.14)), this is achieved by cutting the geodesics near the boundary and evaluating the geodesic length only up to a finite but small value $z_{\rm UV}/t \to 0$. This ratio is preserved by the scaling symmetry (4.3) and, as discussed in [162], a finite constant value of the conformal factor in the metric (4.4) corresponds to a UV cutoff in pure AdS so that the removal of the logarithmically divergent contribution in the limit of zero cutoff corresponds to subtracting the length of a geodesic in pure AdS.

However, in the z-dependent case (4.19) for which the problems can only be treated numerically, this is in principle a non trivial task since no analytic expression is available and the singular part cannot be isolated. Our strategy remains nevertheless the same, that is we define the renormalised lenght as $L_{\rm ren} = L - L_0$, where L and L_0 are evaluated at finite cut-off $z_{\rm UV}$ in the z-direction and L_0 is the length of a pure AdS-geodesic. Specifically, recalling the relation (4.25) between the affine and the compactified parameter and that the initial value problem starting at the turning point ($\sigma = 0$) involves the branch of the geodesics in the range $\sigma \in [0, 1]$, we see that $s = \operatorname{arctanh}(\sigma)$ diverges as we approach the boundary ($\sigma \to 1$)[6]. To renormalise the length of the geodesics, we evaluate our numerical solutions up to the given $z_{\rm UV}$ and the corresponding value $\bar\sigma$ of the curve parameter such that $z_{\rm UV} = z(\bar\sigma)$ is read off. Correspondingly, we have $\sigma \in [0, 1-\delta]$, with $\delta = 1 - \bar\sigma \ll 1$ as long as $z_{\rm UV}/t \ll z_*/t_*$. Subtracting then the

[5] Some cross-checks on the numerics, including the reproduction of the analytical results of [160] discussed in the previous sections, which were not included in our paper [163] are reported in Appendix C.

[6] As remarked at the end of Sec. 4.3.1, a cutoff was already introduced to accommodate for the otherwise divergent coefficients in the system of differential equations (4.29) so that $\sigma = 1$ is never reached in practice. This is then chosen to be small enough to not conflict with the above analysis of the renormalised geodesic length.

divergent contribution $L_0 = -\log(|z_{\rm UV}/t(\bar{\sigma})|)$ for a single branch of a pure AdS-geodesic, we get

$$L_{\rm ren} = L - L_0 = 2\,\text{arctanh}(1-\delta) + 2\log(|z_{\rm UV}/t(\bar{\sigma})|)\ , \tag{4.30}$$

which as can be checked numerically approaches a non-zero constant for small values of $z_{\rm UV}$ as expected from the relation

$$\text{arctanh}(1-\delta) + \log(|z_{\rm UV}/t(\bar{\sigma})|) = -\frac{1}{2}\log\left(\delta\, t(\bar{\sigma})^2/z_{\rm UV}^2\right) + \frac{1}{2}\log(2) + \mathcal{O}(\delta)\ , \tag{4.31}$$

so that the $\delta \to 0$ ($z_{\rm UV}/t \to 0$) limit is finite. The final result should of course be independent of $z_{\rm UV}$ and as such coincide in the limit $z_{\rm UV}/t \to 0$ (see Appendix C). Finally, in order to conclude that the pole in the two-point correlator is resolved, we need to check whether or not its dependence from z_* is of the same kind of the one (4.14) discussed analytically in the previous sections both for the classical [161, 162] and the z-independent polymerisation scale considered in [160]. Although no analytic expression for the correlator is now available, our numerical strategy relates the turning point value z_* and the boundary separation l so that the behaviour[7]

$$L_{\rm ren} = 2\log(2z_*/t_0)\ , \tag{4.32}$$

corresponding to the z_*-dependence (4.14) in the two-point correlator can be checked by plotting z_* as a function of l. The numerical results are presented in the next section.

4.3.3 Numerical Results

Let us apply the numerical methods discussed in Sec. 4.3.1 and 4.3.2 to the case in of a 5d bulk quantum corrected metric (4.19) with z-dependent scale factor given by (4.18) for which the t- and z-derivatives entering the system of equations (4.29) yield

$$\partial_t\left(a(t,z)^2\right) = \frac{2pa_{\rm ext}^2}{\lambda^{2p}} t(t^2+\lambda^2 z^2)^{p-1} = 2pa(t,z)^2 \frac{t}{(t^2+\lambda^2 z^2)}\ , \tag{4.33}$$

$$\partial_z\left(a(t,z)^2\right) = \frac{2pa_{\rm ext}^2}{\lambda^{2p}} \lambda^2 z(t^2+\lambda^2 z^2)^{p-1} = 2pa(t,z)^2 \frac{\lambda^2 z}{(t^2+\lambda^2 z^2)}\ . \tag{4.34}$$

As discussed in Sec. 4.3, such kind of effective metric features an onset of quantum effects at the 5d Planck scale but still neglecting Kasner transitions. The latter will be included in the next section. For such a metric, quantum corrections in (4.18) are negligible for $t \gg \lambda z$ and the classical Kasner-AdS solution is recovered. Moreover, the proper classical boundary limit also exists, i.e. $a(t,z) \to t^p$ in the double scaling limit $z \to 0$ and $a_{\rm ext}/\lambda^p \to 1$. From (4.34), we see that the z-derivative of $a(t,z)$ is of order λ with finite coefficients and can thus be accounted for by quantum corrections in the z-direction, which we systematically neglect here.

The numerical solutions for the boundary data $t_0(t_*, z_*)$ and $l(t_*, z_*)$ as functions of the turning point data would describe surfaces in a 3-dimensional space respectively spanned by

[7] Unlike Eq. (4.14) which was based on the results of [160], a t_0 factor in now included in the logarithm due to the introduction of a cutoff $z_{\rm UV}/t \to 0$ instead of $z_{\rm UV} \to 0$.

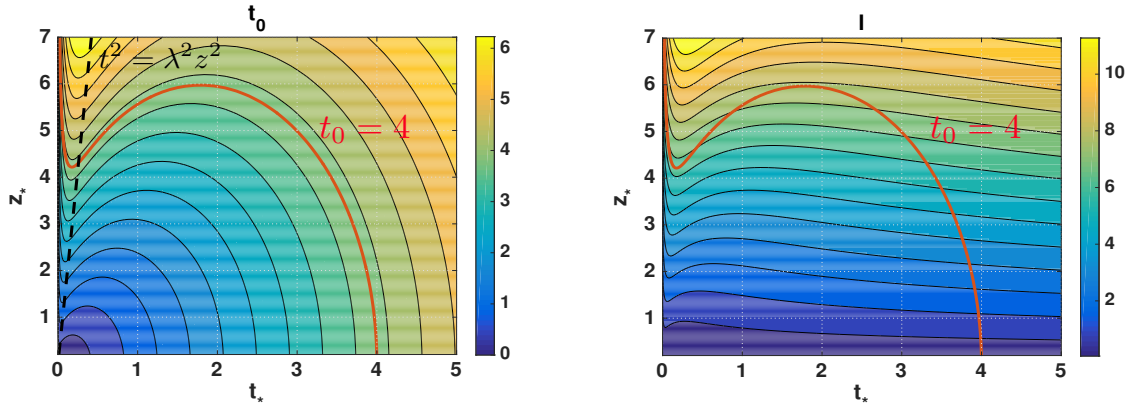

$$p = -1/4 \ , \ \lambda = 0.06 \ , \ a_{ext} = \lambda^p$$

Figure 4.5: Colour plots of $t_0(t_*, z_*)$ (left) and $l(t_*, z_*)$ (right) for $p = -1/4$, $\lambda = 0.06$, $a_{\text{ext}} = \lambda^p$. The red curve corresponds to the $t_0 = 4$ level line, while the black dashed line corresponds to $t^2 = \lambda^2 z^2$ and separates the quantum and classical regimes.

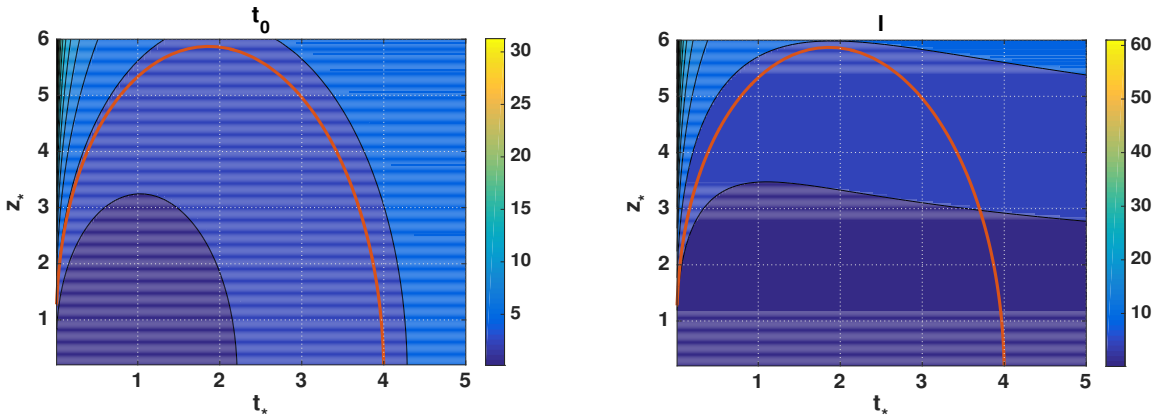

(a) (b)

Figure 4.6: Colour plot of (a) $t_0(t_*, z_*)$ and (b) $l(t_*, z_*)$ for the classical Kasner-AdS metric ($\lambda = 0$ and $a_{\text{ext}}/\lambda^p = 1$ in (4.18)) with $p = -1/4$. The red curves correspond again to the $t_0 = 4$ level line.

(t_*, z_*, t_0) and (t_*, z_*, l). To visualise them we report in Fig. 4.5 the 2-dimensional colour plots of z_* vs. t_*, where the colour scale replaces the third directions t_0 and l respectively and the range of t_* and z_* is chosen to be in the interval $[0, 10]$. The level lines in the left plot correspond to different values of t_0 (the red curve selects for instance the one for $t_0 = 4$) and relate z_* with t_* for that given constant value of t_0. The classical region corresponds to the area where $t^2 \gg \lambda^2 z^2$, but since in the plot $\lambda = 0.06$ is chosen very small the black dashed "quantum/classical dividing line" $t^2 = \lambda^2 z^2$ in Fig. 4.5 is close to the z_*-axis. Indeed, on the one hand, for large t_* ($\gtrsim 1$ here) and small z_* (< 10 here) the classical behaviour is recovered (cfr. Fig. 4.6). On the other hand, going close to the z_*-axis in the quantum regime $t^2 \ll \lambda^2 z^2$, the level lines exhibit turning points. Therefore, unlike the classical case where the finite-distance pole in the two-point correlator was due to bulk geodesics approaching a null geodesic lying entirely on the boundary, that is for which $z_* \to 0$ as $t_* \to 0$ on a constant t_0 level line, quantum corrections induce a turning point leading to z_* growing as $t_* \to 0$. Within our numerical accuracy ($t_* \gtrsim 10^{-8}$), the null-boundary solution is thus isolated and not the limit of a family of bulk space-like geodesics. Correspondingly, as we

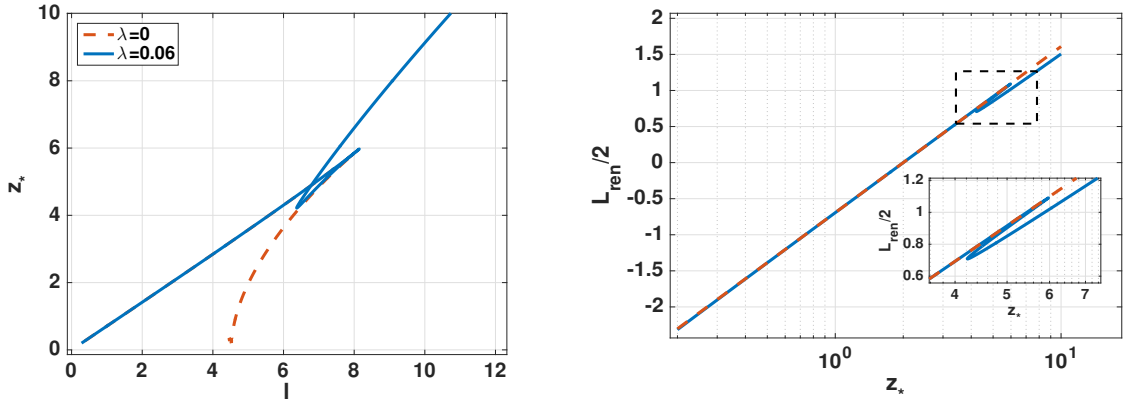

(a) (b)

Figure 4.7: (a) Plot of z_* vs. l for $t_0 = 4$ and $p = -1/4$, $\lambda = 0.06$, $a_{ext} = \lambda^p$. The blue curve corresponds to the quantum corrected metric (4.18), the red curve to the classical metric ($\lambda = 0$ in (4.18)). (b) Plot of L_{ren} vs. z_* on a logarithmic x-axis for the metric (4.18) with $t_0 = 4$, $\lambda = 0.06$, $p = -1/4$, $a_{ext} = \lambda^p$. The almost linear behaviour indicates a log-dependence of L_{ren} from z_* (cfr. Eq. (4.32)).

see in the right plot of Fig. 4.5, l increases as z_* becomes larger so that following the level line and reading off the corresponding values of l leads to the plot of Fig. 4.7 (a), where the results of $z_*(l)$ for the quantum corrected metric (blue line) and for the classical result (red line) are reported. As we might expect, the classical result agrees with the results of [161, 162] (cfr. Fig. 4.2 in Sec. 4.1). Unlike the analytical results, the classical red line now does not reach $z_* = 0$ since we introduced a numerical cutoff close to which some numerical uncertainties occur and we are not able to see the classical pole. Nevertheless, the classical curve converges towards $z_* = 0$ for finite l within numerical accuracy and hence, as argued in Sec. 4.2, this reflects into a pole in the boundary two-point correlator. In the quantum case (blue line in Fig. 4.7 (a)), instead, z_* exhibits a turning point at finite l, and then increases again as it was already visible from the right colour plot in Fig. 4.5. Therefore, it never hits 0 for finite non-zero values of l[8]. Moreover, similarly to the analytical case, there are multiple solutions corresponding to the same boundary separation, whose contribution has to be added in the two-point correlator.

Finally, the renormalised geodesic length L_{ren} can be computed by means of the procedure discussed in Sec. 4.3.2 and the log-dependence (4.32) can be checked via a log-plot like that shown in Fig. 4.7 (b), where a straight line is expected. Few comments however are in order. First of all, in agreement with the analytic results of [160], the upper region provides a purely quantum contribution to the long-distance behaviour of the two-point correlator which decays faster than the short distance (lower region) contribution. Moreover, there are turning points reflecting the above mentioned existence of multiple solutions for a given boundary separation. Indeed, the renormalised length L_{ren} is calculated for each point along the same $t_0 = 4$ level line selected before in Fig. 4.5. The shape of a straight line is nevertheless qualitatively kept[9]. Therefore, as our main interest concerns $L_{\text{ren}}(z_*)$ to be well-behaved and not diverging at finite z_*, we can

[8] Because of the cutoff in z_* both the classical and quantum curves do not start at $z_* = l = 0$.

[9] Deviations from this behaviour might occur in the lower region where z_* comes close to z_{UV}, the approximation $z_{UV}/t \ll z_*/t_*$ fails, and the error increases.

combine our numerical results to conclude that, also in the case of a quantum corrected metric with properly settled onset of quantum effects at the 5d bulk Planck scale, the resolution of the gravitational singularity in the bulk spacetime corresponds to a resolution of the finite-distance pole of the two-point correlator in the boundary theory.

4.4 Lifting Simplification 2: Inclusion of Kasner Transitions

Let us now come to the issue of including Kasner transitions in our 5d bulk effective quantum corrected metric. Following our analysis in [163], in this section we do no rigorously derive a completely satisfactory 5d metric incorporating Kasner transition from a full 5d midisuperspace loop quantisation but rather construct two proposal for a metric incorporating Kasner transitions and discuss their features and drawbacks. This is enough for the purposes of the present chapter where our main interest is to study the holographic signature of resolved cosmological singularities in the equal time two-point correlator of the putative dual boundary theory. As we will show in this section, the finite distance pole in the two-point correlator gets resolved also when Kasner transitions are included so that, even though we do not have access to a completely satisfactory 5d effective metric, we can think of the following analysis as providing further support and strengthening the results discussed in the previous sections.

4.4.1 Quantum Corrected Metric

Let us start by considering a 5d quantum corrected bulk metric of the form

$$\mathrm{d}s_5^2 = \frac{1}{z^2}\left(\mathrm{d}z^2 - \mathrm{d}t^2 + a(t,z)^2\mathrm{d}x^2 + \dots\right) , \tag{4.35}$$

with z-dependent scale factor in the 4d part of the metric given by

$$a(t,z)^2 = \frac{a_{\text{ext}}^2}{\lambda^{2p}}\left(t^2+\lambda^2 z^2\right)^p \exp\left(2\,\Delta p\,\sinh^{-1}\left(\frac{t}{\lambda z}\right)\right) \qquad , \qquad \Delta p \in \mathbb{R}\,. \tag{4.36}$$

The above form of the metric has not been derived from any specific effective quantum gravity model but, as we will now argue, it shares some of their features and can be motivated as follows.

As done for the quantum corrected metric with no Kasner transition discussed in the previous sections, let us start from the following 4d Planck scale quantum corrected bulk metric with z-independent polymerisation scale (cfr. Eq. (4.15))

$$a(t) = \frac{a_{\text{ext}}}{\lambda^p}\left(t^2+\lambda^2\right)^{p/2}\exp\left(\Delta p\,\sinh^{-1}\left(\frac{t}{\lambda}\right)\right) , \tag{4.37}$$

where, as we will discuss below, the additional exponential factor implements a smooth transition between two Kasner universes at late and early times. The above form of the four-dimensional part of the metric can be motivated from the so-called limiting curvature mimetic gravity, a modified version of General Relativity proposed by Chamseddine and Mukhanov in [176] to implement the idea of a limiting curvature ε_m responsible for high-curvature modifications which

resolve the singularities already at the classical level. In fact, the metric (4.37) can be directly related to the metric proposed in [176] by identifying the parameters as $p = 1/3$, $\lambda = 1/\sqrt{3\varepsilon_m}$, and specifying the values of a_{ext} and Δp accordingly (cfr. Eq. (40) in [176]). In what follows, however, we do not need to specify the values of a_{ext}, p, and Δp as we leave them as generic input parameters for our numerical analysis. Moreover, the model of Chamseddine and Mukhanov has been proposed as a toy model effective quantum gravity theory in [180, 181]. In particular, it has been shown that the model agrees with the effective dynamics of spatially flat, homogeneous and isotropic LQC if the limiting curvature is identified with a multiple of the Planck curvature. However, as we showed for Bianchi I cosmology in our later paper [182] which in turn complements similar results in the spherically-symmetric setting [183], the equivalence between limiting curvature mimentic gravity and LQC does not survive leaving the homogeneous and isotropic sector and the two theories show different higher curvature corrections. Nevertheless, the the solution given in [176] shows a similar transition behaviour in the high curvature regime which qualitatively agrees with the LQC numerical analysis of [178]. This is the reason why, in absence of analytic results derived from a full 5d quantum gravity model, we kept (4.37) as starting point for the construction of a 5d bulk metric implementing Kasner transitions to be used in our numerical investigation of the two-point correlator.

Following then the arguments which led us to the 5d Planck scale quantum corrected metric (4.18) considered in Sec. 4.3, we can take a 5d bulk quantum gravity point of view and replace λ with the z-dependent 5d effective scale λz in (4.37) thus yielding the bulk metric (4.36). The latter is not singular at $t = 0$. Moreover, as can be seen from the late times approximation in the past and in the future

$$\sinh^{-1}\left(\frac{t}{\lambda z}\right) \simeq \pm \log\left|\frac{2t}{\lambda z}\right| \qquad \text{for} \qquad \left|\frac{t}{\lambda z}\right| \gg 1 \tag{4.38}$$

with plus and minus signs to be taken respectively for $t \gg \lambda z$ and $t \ll \lambda z$, the scale factor (4.36) reduces to

$$a(t,z)^2 \simeq \frac{a_{\text{ext}}^2}{\lambda^{2p}}\left(\frac{2}{\lambda z}\right)^{\pm 2\Delta p} t^{2p_\pm} \qquad , \qquad p_\pm = p \pm \Delta p \,. \tag{4.39}$$

Hence at late times far in the past and in the future, as we can also see from the plot in Fig. 4.8, the scale factor (4.36) for fixed non-zero z reduces (up to the scaling factor $(2/\lambda z)^{\pm 2\Delta p}$) to that of a 4d classical Kasner metric with Kasner exponents $p_\pm = p \pm \Delta p$, respectively. Quantum effects become dominant in the regime $|t/\lambda z| \ll 1$ for which we have

$$a(t,z)^2 \simeq a_{\text{ext}}^2\, z^{2p}\left(1 + 2\Delta p \frac{t}{\lambda z}\right) \,, \tag{4.40}$$

and the metric (4.36) describes a regular bounce at $t = 0$ during which the values of the exponents characterising the classical late times Kasner universes transition from p_- to $p_+ = p_+ + 2\Delta p$. This is in agreement with the results expected from LQC [177, 179], where it has been shown that this is the only possible transition behaviour matching with the correct classical GR limit at early and late times [179]. Consistently, $p_- = p_+$ for $\Delta p = 0$ so that no Kasner transition

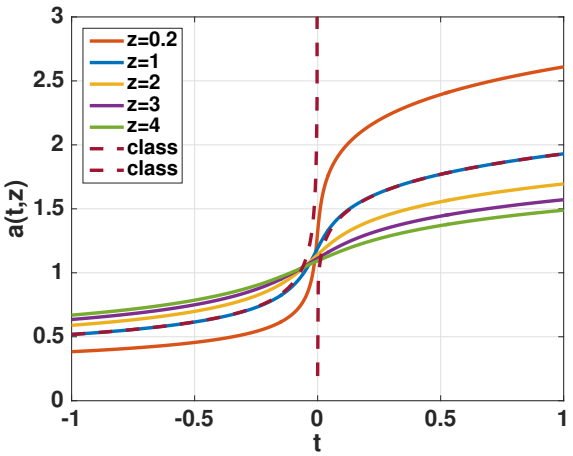

Figure 4.8: Plot of the scale factor $a(t,z)$ given in (4.36) at fixed non-zero z vs. t for $\lambda = 0.06$, $p = -1/16$, and $\Delta p = 3/16$ (i.e. $p_- = -1/4$, $p_+ = 1/8$). The different lines, which correspond to different values of z, show a smooth transition during the bounce at $t = 0$ and agree with the classical behaviour far from the bounce point. The classical behaviour is explicitly reported with the dashed lines for $z = 1$.

occurs and the metric (4.36) reduces to (4.18).

However, let us notice that even though the metric (4.36) might seem a good candidate for a 5d effective quantum metric sharing the same qualitative behaviour as expected from LQC and an onset of quantum effects at 5d Planck scale, it has the following two problems. First of all, it is not a solution of 5d Einstein's equations up to quantum corrections of order λ. The reason for this comes from the fact that, for a scale factor of the kind (4.36), the two Kasner branches with negative and positive exponents are matched in such a way that the solution is monotonously increasing or decreasing (cfr. Fig. 4.8). This is achieved by rescaling the prefactors of t^{2p_+} and t^{2p_-} relatively to each other and, as it can be seen from Eq. (4.39), the relative scaling diverges in the classical limit $\lambda \to 0$ (or equivalently $z \to 0$ for the 4d part of the metric). For finite z, such a matching during the bounce induces a z-dependence in the scale factor which persists at late times and in turn is responsible for the metric (4.35), (4.36) not solving classical Einstein's equations at large t. In particular, since (4.39) diverges for $\lambda = 0$, the 4d classical Kasner geometry cannot be recovered globally. Moreover, the analogous divergence for $z = 0$ indicates that the boundary limit is also not well-defined.

In order to circumvent the above problems, one may try to modify the scale factor (4.36) as follows

$$a(t,z)^2 = \frac{a_{\rm ext}^2}{\lambda^{2p}} \left(t^2 + \lambda^2 z^2\right)^p \exp\left(2\,\Delta p\, \sinh^{-1}\left(\frac{t}{\lambda z}\right)\right) (\lambda z)^{2\Delta p \tanh\left(\frac{t}{\lambda z}\right)} , \tag{4.41}$$

where the additional factor $(\lambda z)^{2\Delta p \tanh\left(\frac{t}{\lambda z}\right)}$ has been included so that, for $|t/\lambda z| \gg 1$, we have $\tanh(t/\lambda z) \simeq \mathrm{sgn(t)}$ with $z, \lambda \geq 0$ and, together with the late times expansion (4.38), Eq. (4.41) reduces to

$$a(t,z)^2 \simeq a(t)^2 = \frac{a_{\rm ext}^2}{\lambda^{2p}} t^{2p_\pm} , \tag{4.42}$$

thus yielding the proper z-independent boundary limit with the classical Kasner solution recovered in the double scaling limit $\lambda \to 0$, $a_{\rm ext}/\lambda^p \to 1$. Indeed, as it can be seen from the plot

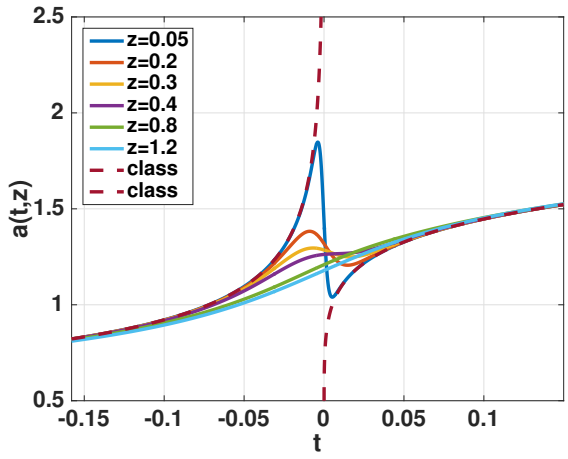

Figure 4.9: Plot of the scale factor $a(t,z)$ given in (4.41) at fixed non-zero z vs. t for $\lambda = 0.06$, $p = -1/16$, and $\Delta p = 3/16$ (i.e. $p_- = -1/4$, $p_+ = 1/8$). The different lines corresponding to different values of z show a smooth transition during the bounce at $t = 0$ and the same classical behaviour (dashed lines) for all z values is recovered far from the bounce point.

of the scale factor (4.41) in Fig. 4.9, in contrast to the previous case plotted in Fig. 4.8 now the same classical solution is approached at large t for all values of z. However, although the above modification allows us to recover the correct classical and boundary limits, the behaviour around the bouncing point at $t = 0$ differs qualitatively from the one expected from LQC. Indeed, around $t = 0$, the scale factor (4.41) can be written as

$$a(t,z)^2 \simeq a_{\rm ext}^2\, z^{2p} \left(1 + \frac{2\Delta p t}{\lambda z}\,(1 + \log(\lambda z))\right) , \tag{4.43}$$

so that, for small z, the logarithmic term is responsible for a change in the sign of the slope around $t = 0$ and we have no relative rescaling of the prefactors thus yielding a non-monotonous behaviour around the bounce (cfr. Fig. 4.9).

Moreover, in contrast to the metric (4.35), (4.36), the modified metric (4.41) does solve the 5d Einstein equations at zeroth order in λ. As already remarked in Sec. 4.3, in fact, two conditions have to be satisfied in order to have a plausible embedding of the 4d metric into the 5d bulk spacetime. First, the boundary limit needs to be well-defined and the resulting metric has to be a solution of 4d Einstein equations. Second, the z-derivative of the scale factor has to vanish at zeroth order in the quantum parameter λ. Therefore, as summarised in the table 4.1 below, a comparison between our two proposals shows that for both metrics all the proper requirements for a bulk effective 5d metric incorporating Kasner transitions are only partially satisfied as there are still some remaining unsolved issues. Specifically, on the one hand, for the metric (4.36) the proper boundary limit is not recovered and the z-derivative does not vanish in zeroth order in λ (see Eq. (4.45) below). On the other hand, both conditions are satisfied for the metric (4.36). However, as can be checked using computer algebra, the Kretschmann scalar for $t = 0$ is not constant in z and diverges as $z \to 0$ due to a blow-up of the $\mathcal{O}(\lambda)$ coefficient. Therefore, unlike (4.36), the metric (4.41) cannot be interpreted as an effective metric of a quantum gravity theory that resolves singularities by means of a limiting 5d bulk curvature.

To conclude, finding a plausible metric for which all problems are cured at once turns out to be a highly non-trivial task. As already stressed before, in principle the correct effective form of the quantum corrected metric should be derived from setting up full 5d quantum Einstein equations and extracting an effective metric, at least in a suitable midisuperspace approximation. Being aware of this, in our work [163], we decided to take the metric (4.36) as a case study and use it for our numerical investigation of the two-point correlator to check the generic absence of the finite-distance pole also when Kasner transitions are included. The reason behind this choice relies on the fact that, unlike (4.41), the metric (4.36) shows qualitatively the behaviour expected from LQC in the 4d part of metric, the Kretschmann scalar exhibits the right $\mathcal{K}^{(5)} = \mathcal{O}(\lambda_{5d}^{-4})$ behaviour, and it is also symmetric under the scaling symmetry (4.3) (cfr. Table 4.1 below). The numerical results for the metric (4.36) are presented in the next subsection. The numerical analysis has been performed also for the metric (4.36) and the main conclusions regarding the resolution of the finite-distance pole in the two-point correlator remain qualitatively unaffected by the modification of the metric.

Property	Metric (4.36)	Metric (4.41)
Boundary 4d classical Kasner	✗	✓
Solution of 5d Einstein eqs. up to $\mathcal{O}(\lambda)$	✗	✓
Kretschmann condition $\mathcal{K}^{(5)} = \mathcal{O}(\lambda_{5d}^{-4})$	✓	✗
Qualitative LQC behavior	✓	✗
Scaling symmetry (4.3)	✓	✗

Table 4.1: Comparison of the two proposals (4.36) and (4.41) for an effective quantum corrected 5d bulk metric incorporating Kasner transitions.

4.4.2 Numerical Results

Let us now apply the procedure discussed in Sec. 4.3.1 to solve numerically the geodesic equations with initial conditions given in Eq. (4.29) for the quantum corrected metric (4.35), (4.36). In this case, the t- and z-derivatives of the scale factor (4.36) read as

$$\partial_t \left(a(t,z)^2\right) = 2a(t,z)^2 \left(\frac{p\,t}{t^2+\lambda^2 z^2} + \frac{\Delta p}{\sqrt{t^2+\lambda^2 z^2}}\right) , \tag{4.44}$$

$$\partial_z \left(a(t,z)^2\right) = 2a(t,z)^2 \left(\frac{p\,\lambda^2\, z}{t^2+\lambda^2 z^2} - \frac{\Delta p\, t}{z\sqrt{t^2+\lambda^2 z^2}}\right) . \tag{4.45}$$

As we can see from the corresponding color plot of $t_0(t_*, z_*)$ reported in Fig. 4.10 below, also negative values are included now in the range of t_* and there exist geodesics passing through the resolved singularity at $t = 0$. There are solutions which exhibit a turning point in z_*, close to $t_* = 0$. Among them there are solutions that start at a negative t_0, pass through the resolved

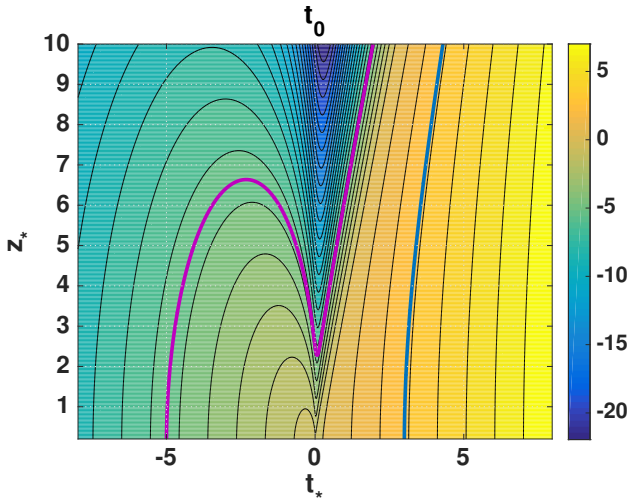

Figure 4.10: Colour plot of $t_0(t_*, z_*)$ for the metric (4.35), (4.36) with $t_0 = -5$ (purple line) and $t_0 = 3$ (blue line), $\lambda = 0.06$, $a_{\text{ext}} = \lambda^p$, $p = -1/16$, $\Delta p = 3/16$. Following the t_*-axis, we have a Kasner transition from $p_- = -1/4$ to $p_+ = 1/8$ going from negative to positive t with bouncing point at $t = 0$. There exist two kinds of solutions: positive p geodesics starting at positive t, which are bent away from the resolved singularity (blue line), and those starting at negative t with negative p which are bent towards the resolved singularity and eventually passing it (purple line).

singularity, have their turning point at positive t_* and come back to the t_0-value they started from. For example, there are points of the purple level line in Fig. 4.10 for $t_0 = 5$ that reach positive t_*. Moreover, it is possible to observe the expected behaviour of geodesics corresponding to positive and negative Kasner exponents p. In the negative t_* region, the plot looks similar to that of Fig. 4.5, just mirrored. For positive t, instead, the plot has exactly the expected behaviour of positive p solutions. Indeed, as discussed in Sec. 4.1, geodesics starting at negative t with negative p which are bent towards the resolved singularity and eventually passing it (see e.g. the purple line corresponding to $t_0 = -5$), while those starting at positive t are characterised by positive Kasner exponents and are bent away from the resolved singularity at $t = 0$ (see e.g. the blue line for $t_0 = 3$). Correspondingly, this is reflected in the behaviour of $z_*(l)$ as shown by the purple and blue curves in in Fig. 4.11 (a), respectively. In both cases, z_* never hits zero for finite values of the boundary sepration l.

Finally, the numerical evaluation of the renormalised geodesic length according to the procedure discussed in Sec. 4.3.2 leads to the plot of L_{ren} vs. z_* in logarithmic scale reported in Fig. 4.11 (b). As we can see from the plot, up to the above-mentioned errors occurring in the lower region, there is still a linear asymptotic behaviour corresponding then to a $\log(z_*)$-dependence of L_{ren}, staying away form $z_* = 0$ for finite l. Focusing then on the $t_0 < 0$ solutions (purple line), which are those relevant for probing the resolved bulk singularity, the renormalised geodesic length remains finite for $l \neq 0$, and hence the two-point correlator does not diverge. For completeness, also the positive t_0 blue line has been included in Fig. 4.11 (b). As already noticed, being bent away from the region where quantum effects become dominant, such kind of solutions behave as in the classical case and there is no pole in the two-point correlator[10].

[10] As remarked at the end of Sec. 4.4.1, we have performed our numerical analysis also for the metric (4.41) and the results exhibit the same qualitative behaviour.

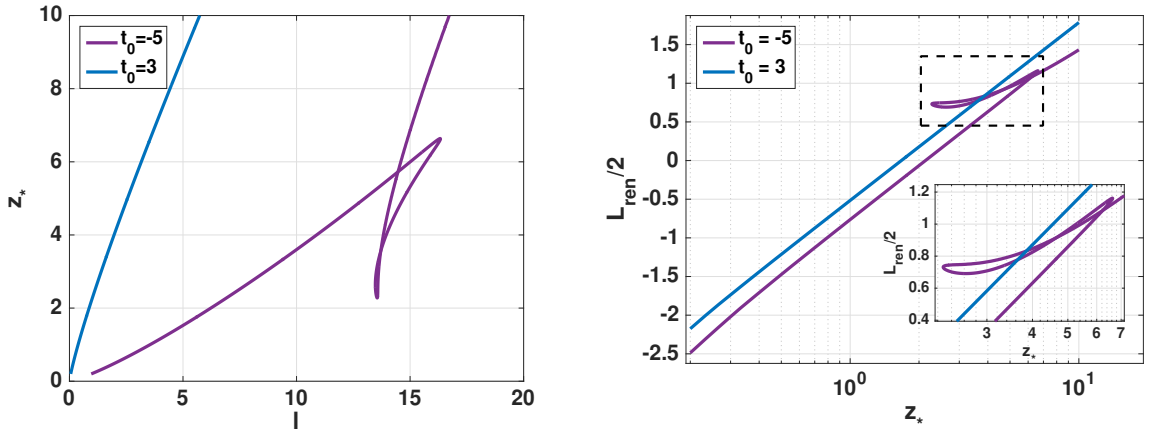

(a) (b)

Figure 4.11: Plot of z_* vs. l (a) and Log-scale plot of $L_{\rm ren}$ vs. z_* (b) for the metric (4.36) with $\lambda = 0.06$, $a_{\rm ext} = \lambda^p$, $p = -1/16$, and $\Delta p = 3/16$. The purple line corresponds to $t_0 = -5$ and the blue line to $t_0 = 3$.

4.5 Discussion

In this chapter, based on [160, 163], we have explored the holographic signature of a resolved cosmological singularity using a simple ansatz for the quantum corrected metrics inspired by loop quantum gravity. The simplifying assumptions made in [160] to treat the problem analytically (see Sec. 4.2) have been progressively lifted by treating the problem numerically in Sec. 4.3 and 4.4, where we provided improved ansatz for the bulk effective metrics featuring a proper onset of quantum effects at 5d Planck scale and finally including Kasner transitions [163]. Our analysis shows that the resolution of the bulk gravitational singularity gives sensible results for the dual field theory which can be seen as an improvement over the classical gravity approximation used in [161, 162]. Specifically, the examples of quantum corrected metrics studied in this chapter suggest that the finite distance pole in the two-point correlator, which was interpreted as a dual holographic signature of the classical bulk singularity, gets smoothed out by quantum gravity corrections resolving the gravitational singularity. From a conceptual viewpoint, the question of whether to incorporate quantum gravity effects inspired by other QG approaches into an AdS/CFT framework gives a good approximation to what would happen in string theory remains open. The answer would require to establish a precise relation between the parameters controlling the quantum effects in both theories, say e.g. finite N corrections and non-perturbative LQG corrections[11]. In this respect, however, our strategy can be motivated as follows.

First, from a string theory perspective, seen as a QG theory, no clear picture of the fate of generic gravitational singularities has emerged so far. In particular, one expects quantum effects to be strong in the high curvature regime, thus casting doubt on a straightforward application of perturbative techniques[12]. Second, even if one uses the AdS/CFT correspondence

[11] See the discussion in [54] for possible suggestions in this direction.

[12] However, some progress has been made recently on different fronts. These include for instance the study of the tensionless limit of string theory described by higher-spin theories [184–186], or O(d,d)-invariant formulations of string cosmology motivated by T-duality [187].

itself as a non-perturbative definition of string theory via its dual field theory and transfers the question to the dual side, no definite clear picture has emerged so far despite of the large effort in studying cosmological singularities [164–173]. Therefore, given recent progress in singularity resolution from other approaches to non-perturbative QG, it seems reasonable to ask the inverse question and check whether the implementation of existing techniques for including quantum gravity effects leads to sensible results or contradictions. The question becomes then whether it is possible to infer signatures of resolved singularities in the dual field theory. Our analysis can be then thought of as providing prototype examples in which the application of LQG-inspired techniques in a gauge/gravity framework is possible and leads to improvements over the dual field theory description based on a classical gravitational bulk approximation. Moreover, knowing what to look for, although it might be in general more complicated than the usual QFT setting on Minkowski spacetime due to the fact that as discussed in Sec. 4.1 the field theory is defined on a anisotropic (time-dependent) Kasner-AdS background, one may be able to confirm these signatures by a field theoretic computation, either analytic or on the lattice. This might be relevant to understand whether non-perturbative QG can be an adequate description of a subsector of string theory non-perturbatively defined via its dual theory.

The considerations presented in this chapter can be then extended in several directions. First, as we have already noticed, a more rigorous derivation of the bulk effective metric would require to set up the full 5d (loop) quantisation of the symmetry-reduced model under consideration, determine the proper effective dynamics incorporating the relevant quantum corrections, and solve the effective equations to determine the geometry of the resulting quantum corrected spacetime. Second, in the light of the above discussion, a better understanding of the field theory side would be necessary. This might include the study of the two-point correlator beyond the geodesic approximation, that is to take derivatives of the bulk on-shell action to compute the two-point functions as discussed in Ch. 2, or to consider other kinds of bulk probes such as minimal surfaces for instance to study quantum corrections to the holographic entanglement entropy and compare them with existing results obtained by using AdS/CFT [95, 98, 188–190].

Finally, it would be interesting to extend the present calculation to more general spacetimes. Of particular interest are spacetimes containing black hole singularities. In this respect, while one could simply substitute the Kasner spacetime in $\mathrm{d}s_5^2$ by a 4-dimensional black hole spacetime, a better strategy consists of using directly 5-dimensional black hole solutions, so that the boundary is Minkowski and the above-mentioned difficulties of the dual field theory being defined on a time-dependent background can be avoided. Having the latter direction in mind, in the next chapter we will focus on effective quantum corrected models of LQG-inspired polymer black holes. As we will discuss, despite of the large effort devoted to the study of such gravitational systems within the LQG community over the last years, much less is know in such a context and there is no definite consensus. In particular, undesirable features and unphysical effects may arise depending on the details of the model. Given this situation, in the next chapter we will focus on the simplest black hole scenario provided by a stationary spherically symmetric Schwarzschild spacetime and present a new effective quantum corrected model where no obvious physical inconsistencies arise. This is a necessary step to prepare the stage for studying more

complicated black holes. Of particular interest from the AdS/CFT perspective would be the case of asymptotically AdS black holes on which we will briefly comment at the end of Ch. 6.

Chapter 5

Effective Quantum Corrected Schwarzschild Black Holes

In the previous chapters, we mainly focused on cosmological singularities, their fate once quantum gravitational effects are taken into account, and their holographic signatures. In this chapter, we will focus on black holes (BHs), the other paradigmatic physical situations in which gravitational singularities occur. In the high curvature region near the central singularity the classical description of continuous spacetime geometry provided by general relativity breaks down and quantum gravitational effects become dominant. It is widely believed that gravitational singularities might be resolved in a consistent theory of quantum gravity (QG), see e.g. [191, 192] for reviews. However, despite of the continuously growing interest among different approaches, there is still no agreement on whether and how spacetime singularities get resolved in QG.

Within the framework of LQG, and more precisely LQC, the promising results obtained in the cosmological setting (cfr. Ch. 3 and references therein) have motivated the development of similar techniques also for studying BHs. In this chapter, we will consider the simplest example of a spherically symmetric Schwarzschild BH, which as such has gained considerable attention over the last years [193–208]. After briefly reviewing the general strategy underlying LQG-inspired investigations, we will present two new models of quantum corrected Schwarzschild BH based on the definition of new canonical variables [209–211]. These are motivated by physical considerations about the onset of quantum effects and, in particular, to have a unique Planckian upper bound on spacetime curvature. For both models, similarly to what happens in LQC where the Big Bang singularity is replaced by a quantum bounce smoothly connecting a contracting and an expanding branch, in the resulting effective spacetime the central singularity is replaced by a smooth transition between a trapped and an anti-trapped region, respectively interpreted as black hole (BH) and white hole (WH) interior regions. At low curvatures, quantum effects are negligible and the geometry is well approximated by the classical Schwarzschild solution.

A key aspect in our analysis relies on the observation that a gauge (i.e. coordinate) independent specification of the initial conditions for the dynamics of the system requires the construction of Dirac observables. Unlike the classical theory where there is only one physically

relevant observable interpreted as the BH mass on-shell, in the effective quantum theory there exist two Dirac observables respectively interpreted as the BH and WH masses. A careful analysis of these observables in our first model shows that physically acceptable solutions require us to select a certain subset of initial conditions, corresponding to specific relations between the masses [209]. Such a limitation is surpassed in the second model [210, 211] where the definition of a new set of canonical variables allows us to achieve all criteria for physical viability for a large class of initial conditions independently of the relation between the black and white hole masses.

Finally, as we will discuss in the next chapter, the simple form of the Hamiltonian in the new variables makes the construction of the quantum theory analytically solvable.

5.1 Strategy and Polymerisation Schemes

Forgetting for a moment about the motivations behind this thesis, the following question might spontaneously arise at first sight: Why yet another effective model of Schwarzschild BH should be needed? Before entering the details of our model, let us first try to address this question. To this aim, let us start by stating the requirements that any model of quantum corrected BHs is expected to satisfy to be considered physically reasonable. These include:

- a quantum corrected effective geometry describing both the interior and exterior regions;
- quantum effects become relevant at high curvatures and provide a unique (mass-independent) upper bound on curvature invariants which resolves the classical singularity;
- quantum effects become negligible in the low curvature regime where the classical GR description is expected to provide a good approximation. For sufficiently massive BHs, this includes already the horizon scale. Indeed, recalling for instance the expression $\mathcal{K} = 48M^2/r^6$of the Kretschmann scalar for a Schwarzschild BH, we see that at the horizon $r = 2M$ and $\mathcal{K} \sim M^{-4}$.

The starting point of LQG-inspired analyses is based on the following observations. In the interior region of a Schwarzschild BH, the radial coordinate becomes time-like. The Schwarzschild interior can be thus foliated into spatially homogeneous and anisotropic slices of topology $\mathbb{R} \times \mathbb{S}^2$ whose geometric description can be modeled as a spherically symmetric Kantowski-Sachs cosmological spacetime. This allows to import techniques from homogeneous and anisotropic LQC to construct a Hamiltonian framework for the effective quantum theory. As discussed in Ch. 3 (Sec. 3.3), at the effective level, quantum corrections are captured by a phase space regularisation procedure called polymerisation according to which the canonical momenta are replaced by combinations of their complex exponentials (point holonomies). The simplest polymerisation choice is provided by the sin function, namely the effective quantum theory is obtained by replacing $P \mapsto \sin(\lambda P)/\lambda$ in the classical Hamiltonian which acquires then corrections controlled by the parameter λ (polymerisation scale) of order of the Planck scale[1]. These are the so-called

[1] As we already mentioned in Ch. 3 for the LQC context, also in the case of black holes alternative proposals exist which include choosing different functions or polymerising only parts of the phase space or different choices

holonomy corrections and, as we already discussed in Sec. 3.2, they are the analogue of approximating the field strength by holonomies of the gauge connection in lattice gauge theory. The structure of such modifications is motivated by a weakly discontinuous polymer-like quantisation of the classical symmetry-reduced theory inspired by the quantisation techniques developed in full LQG, which in turn can be thought of as a diffeomorphism invariant extension of lattice gauge theory where the quantum properties of spacetime geometry are encoded in the dynamical lattice itself (cfr. App. B).

The classical phase space description and the resulting effective polymer quantum theory of LQG-inspired BH models are commonly based on Ashtekar-Barbero connection variables. However, although these effective models share a similar qualitative picture of the quantum-extended interior regions in which the central singularity is resolved by a BH-to-WH transition, subtle differences and undesirable physical predictions come out in the previous proposals depending on whether the polymerization scales are considered to be purely constant or phase space dependent functions. According to this methodological distinction, effective BH models inspired by LQG can be divided into the following classes:

- μ_o-*schemes*: these are the simplest cases where the polymerisation scales are chosen to be pure phase space independent constants (see e.g. [193–195, 214, 215]);
- $\bar{\mu}$-*schemes*: the polymerisation scales are allowed to be phase space functions (see e.g. [200, 201] for black holes and [216, 217] for Kantowski-Sachs cosmologies).
- *Generalised* μ_o-*schemes*: a more recent middle way between μ_o- and $\bar{\mu}$-schemes has been proposed in [197, 198, 207, 208] where the polymerisation scales are taken to be phase space dependent but only through Dirac observables and are thus constant only along the solutions of the effective EOMs.

If on the one hand, to have constant quantum parameters in μ_o-type schemes hugely simplifies the analytic treatment of the system, on the other hand these approaches turn out to be plagued by drawbacks such as the final outcome fails to be independent of the fiducial structures introduced in the construction of the classical phase space and large quantum effects may survive even in the low-curvature regime. In the $\bar{\mu}$-approaches, instead, the issue of dependence on fiducial structures is cured by selecting the quantum parameters to be functions of the classical phase space, but large quantum corrections near the horizon still survive. Finally, in the generalised μ_o-schemes both issues are resolved by introducing a mass dependence in the polymerisation scales which as such become Dirac observables. The specific form of the quantum parameters is determined by arguments based on the identification of the radius of the fiducial sphere with a physical length scale settled to be the classical Schwarzschild radius [197] or by considering holonomies along plaquettes enclosing the minimal area at the transition surface (see e.g. [198] later improved in [207, 208]). Some issues and subtleties however still survive in these models.

for the polymerisation scales [138, 195, 203, 212, 213]. Such different models can be motivated by physical inputs or full theory based results and arguments like general covariance and anomaly-free realisations of the constraint algebra at the quantum level. For simplicity we do not consider such alternative choices here thus focusing on the commonly adopted sin-polymerisation.

In [197] for instance the curvature scale at which quantum effects become dominant depends on the BH mass and the BH-to-WH transition features a huge mass amplification. A unique mass-independent curvature upper bound is achieved in [207, 208] and, as a consequences of the choice of the polymerisation scales, the BH and WH masses are selected to be equal (symmetric bounce). Despite of these remarkable features, the recursive structure of the effective Hamiltonian introduced by the mass dependence of the quantum parameters makes the derivation of the effective dynamics problematic (see [218] for details). Moreover, departures form the asymptotic Schwarzschild structure appear in the resulting effective spacetime [219, 220].

Given the above situation, in [209–211] we took a different route. Instead of directly using connection variables, we start from a metric description so that the geometric interpretation from a spacetime viewpoint is transparent and introduce new canonical variables adapted to physical considerations about the onset of quantum effects in such a way that the simplest (μ_o-type) polymerisation scheme can be used to construct an effective model with satisfactory physical outcomes. As we will discuss in the following, similarly to the case of (b, v)-variables for LQC discussed in Ch. 3 where the on-shell value of b was related to the Ricci scalar (cfr. Eq. (3.26)), the main idea is to construct canonical momenta which are directly related to spacetime curvature invariants so that the resulting polymerisation induces a natural curvature bound in the Planck regime and quantum effects become negligible in the low curvature regime. The resulting effective theory can be eventually translated in standard connection variables via a canonical transformation.

5.2 Classical Theory

Along the same line of Ch. 3, let us discuss first the classical theory which serves as a preparation for the construction of the effective quantum theory. We will start by recalling the main aspects of the Schwarzschild spacetime, move then to the Hamiltonian formulation of the system, and finally introduce our new canonical variables.

5.2.1 Hamiltonian Description of Classical Schwarzschild Black Holes

Spherically symmetric and static solutions of Einstein's equations are locally isometric to the Schwarzschild metric whose line element in 4-dimensions (with natural units $G = c = 1$) reads [159, 221][2]

$$\mathrm{d}s^2 = -\left(1 - \frac{2M}{r}\right)\mathrm{d}t^2 + \left(1 - \frac{2M}{r}\right)^{-1}\mathrm{d}r^2 + r^2\mathrm{d}\Omega_2^2\,, \tag{5.1}$$

where $\mathrm{d}\Omega_2^2 = \mathrm{d}\theta^2 + \sin^2\theta\,\mathrm{d}\phi^2$ denotes the round metric on the $r = const.$, $t = const.$ 2-sphere. Three-dimensional rotations act as isometries for the metric (5.1) and it has only one Killing vector field $\partial/\partial t$ orthogonal to the $t = const$ hypersurfaces so that spacetime is static in the region $r > 2M$. The $r \to \infty$ limit yields Minkowski metric in polar coordinates so that the spacetime is asymptotically flat. $r = const$ hypersurfaces are time-like (resp. space-like) for

[2] Higher-dimensional cases will be considered in Sec. 6.3 where we focus on possible extensions to Schwarzschild-AdS black holes.

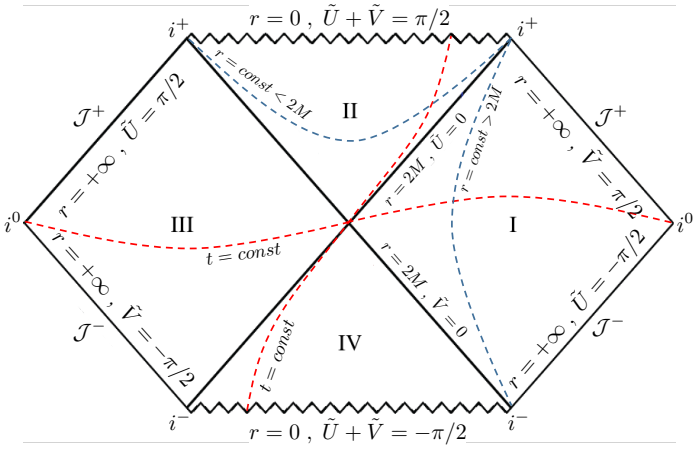

Figure 5.1: Penrose diagram for the Kruskal extension of Schwarzschild spacetime. The angular coordinates θ, ϕ are suppressed so that each point of the diagram can be thought of as representing a 2-sphere of radius r.

$r > 2M$ (resp. $r < 2M$) and the $r = 2M$ null hypersurface is called horizon as objects crossing it from $r > 2M$ can never come back. The horizon radius $r = r_s = 2M$ is called Schwarzschild radius and it is just a coordinate singularity that can be removed by changing the coordinate system. A true curvature singularity occurs instead at $r = 0$ where the Kretschmann scalar

$$\mathcal{K} = R_{\mu\nu\rho\delta}R^{\mu\nu\rho\delta} = \frac{48M^2}{r^6}\,, \tag{5.2}$$

diverges. The causal structure of the spacetime described by the metric (5.1) can be easily visualised by means of the well-known Penrose diagram for a Schwarzschild BH reported in Fig. 5.1. The latter can be constructed by introducing the so-called Kruskal-Szekeres coordinates and performing a conformal compactification of the asymptotically flat regions far from the hole. The values taken by such coordinates in the different regions together with $t = const$ and $r = const$ slices are explicitly reported in Fig. 5.1 for completeness. The main steps of the construction can be found in Appendix D, where we also report the details of the construction of the Penrose diagram for the quantum corrected effective spacetime presented in the next sections.

The Hamiltonian description of Schwarzschild spacetime can be now constructed along similar steps to the cosmology case discussed in Sec. 3.1.1, that is by considering a generic ansatz for the metric compatible with the symmetries of our spacetime, plugging it into the Einstein-Hilbert action, and Legendre transforming the resulting Lagrangian. Let us consider then a line element of the form [222, 223]

$$\mathrm{d}s^2 = -\bar{a}(r)\mathrm{d}t^2 + N(r)\mathrm{d}r^2 + 2\bar{B}(r)\mathrm{d}t\mathrm{d}r + \bar{b}^2(r)\mathrm{d}\Omega_2^2\,, \tag{5.3}$$

which describes a generic static and spherically symmetric spacetime of topology $\mathbb{R}\times\mathbb{R}\times\mathbb{S}^2$. At this stage $\bar{a}, N, \bar{B}, \bar{b}$ are unknown functions of the radius r which can be determined later by solving the EOMs. $N(r)$ plays the role of the lapse w.r.t. the foliation in r-slices. Plugging (5.3) into the Einstein-Hilbert action without cosmological constant ($G = c = 1$)

$$S_{EH} = \frac{1}{16\pi}\int \mathrm{d}^4x\sqrt{-g}\,\mathcal{R}\,, \tag{5.4}$$

and integrating by parts to get rid of the second order derivatives, yields the following first-order action (up to boundary terms)

$$S = \frac{1}{4}\int \mathrm{d}r L(\bar{a},\bar{b},\bar{n}) \qquad , \qquad L(\bar{a},\bar{b},\bar{n}) = 2L_o\sqrt{\bar{n}}\left(\frac{\bar{a}'\bar{b}'\bar{b}}{\bar{n}} + \frac{\bar{a}\bar{b}'^2}{\bar{n}} + 1\right) \tag{5.5}$$

where primes denote derivatives w.r.t. r, $\bar{n}$ is a Lagrange multiplier reflecting the gauge freedom in the definition of the coordinates r and t given by

$$\bar{n}(r) = \bar{a}(r)N(r) + \bar{B}^2(r)\,, \tag{5.6}$$

and, similarly to Sec. 3.1.1, we regularised the otherwise divergent integral in the non-compact t-directions by introducing a fiducial cell $\mathcal{C}$ of topology $[0, L_o]\times\mathbb{S}^2$ in the $r = const.$ slices with L_o playing the role of an infrared cut-off in the t-direction. Defining the integrated variables

$$\sqrt{n} = \int_0^{L_o}\mathrm{d}t\sqrt{\bar{n}} = L_o\sqrt{\bar{n}} \quad , \quad \sqrt{a} = \int_0^{L_o}\mathrm{d}t\sqrt{\bar{a}} = L_o\sqrt{\bar{a}} \quad , \quad b = \bar{b} \quad , \quad B = \int_0^{L_o}\mathrm{d}t\bar{B} = L_o\,\bar{B}\,, \tag{5.7}$$

the L_o-factor in the Lagrangian (5.5) can be absorbed and we have

$$L(a,b,n) = 2\sqrt{n}\left(\frac{a'b'b}{n} + \frac{ab'^2}{n} + 1\right)\,. \tag{5.8}$$

Note that L_o is the coordinate length of the fiducial cell in t-direction and as such it depends on the choice of the chart. The physical size of the cell at a certain reference point r_{ref} is given by

$$\mathscr{L}_o := \sqrt{a}\big|_{r=r_{\mathrm{ref}}} = L_o\sqrt{\bar{a}}\big|_{r=r_{\mathrm{ref}}}\,, \tag{5.9}$$

which has the same behaviour of L_o under fiducial cell rescaling, say $\mathscr{L}_o \mapsto \alpha\mathscr{L}_o$ as $L_o \mapsto \alpha L_o$, but in contrast to L_o it is a spacetime scalar, i.e. it does not transform under any coordinate transformation preserving the form (5.3) of the metric. Both L_o and $\mathscr{L}_o$ are fiducial structures and of course physical quantities must not depend on them.

Looking at the Lagrangian (5.8) we see that the dynamical variables of our systems are a, b, and n. The corresponding conjugate momenta are given by

$$p_a = \frac{\partial L}{\partial a'} = \frac{2bb'}{\sqrt{n}} \qquad , \qquad p_b = \frac{\partial L}{\partial b'} = \frac{4ab' + 2a'b}{\sqrt{n}} \qquad , \qquad p_n = \frac{\partial L}{\partial n'} \approx 0\,, \tag{5.10}$$

where, similarly to the canonical analysis of FLRW cosmology in Sec. 3.1.1, the Lagrangian does not depend on the derivative of n thus yielding the primary constraint $p_n \approx 0$. The Hamiltonian associated to the Lagrangian (5.8) reads

$$H_{\rm cl} = \sqrt{n}\mathcal{H}_{cl} + \gamma p_n \quad , \quad \mathcal{H}_{\rm cl} = \frac{p_a p_b}{2b} - \frac{a p_a^2}{2b^2} - 2 \, , \tag{5.11}$$

where $\gamma(r)$ is a Lagrange multiplier implementing the primary constraint $p_n \approx 0$. As expected for reparametrisation invariant systems (cfr. Appendix A), stability of p_n (i.e. $p_n' = \{p_n, H_{\rm cl}\} \approx 0$) then gives the Hamiltonian constraint $\mathcal{H}_{cl} \approx 0$. The EOM for n yields $n' = \{n, H\} = \gamma$ from which it follows that gauge-fixing n to be constant is equivalent to setting $\gamma = 0$. With this gauge choice, the EOMs for the canonical pairs (a, p_a) and (b, p_b) are given by

$$\begin{cases} a' = \sqrt{n}\left(\frac{p_b}{2b} - \frac{a p_a}{b^2}\right) \\ p_a' = \sqrt{n}\frac{p_a^2}{2b^2} \\ b' = \sqrt{n}\frac{p_a}{2b} \\ p_b' = \sqrt{n}\left(\frac{p_a p_b}{2b^2} - \frac{a p_a^2}{b^3}\right) \end{cases} \qquad \text{with} \qquad \mathcal{H}_{cl} = \frac{p_a p_b}{2b} - \frac{a p_a^2}{2b^2} - 2 \approx 0 \, . \tag{5.12}$$

Note that, under rescaling of the fiducial length $L_o \mapsto \alpha \, L_o$ by a constant α, we have

$$\sqrt{n} \mapsto \alpha\sqrt{n} \quad , \quad a \mapsto \alpha^2 \, a \quad , \quad b \mapsto b \quad , \quad p_a \mapsto \alpha^{-1} \, p_a \quad , \quad p_b \mapsto \alpha \, p_b \tag{5.13}$$

so that the above EOMs are left invariant. Moreover, according to the transformation behaviour (5.13), physical quantities can only depend on the fiducial cell independent combinations $b, a/L_o^2, L_o \, p_a, p_b/L_o$ or their coordinate-free versions $b, a/\mathscr{L}_o^2, \mathscr{L}_o \, p_a, p_b/\mathscr{L}_o$[3].

Finally, it is easy to check that solving the EOMs (5.12) for $a(r)$, $b(r)$, $p_a(r)$, $p_b(r)$ and inserting the resulting expressions into the metric (5.3), the Schwarzschild solution (5.1) is recovered by choosing the lapse to be $N(r) = \left(1 - \frac{2M}{r}\right)^{-1}$. As we will explicitly check this statement for our new variables in the next section, we do not report here the explicit computations which can be found for instance in [223].

5.2.2 New Variables: A First Model

In order to construct the effective quantum theory via polymerisation, it is convenient to introduce a new set of phase space variables defined by[4] [209]

$$v_1 = \frac{2}{3} b^3 \quad , \quad P_1 = \frac{a'}{\sqrt{n}\, b} = \left(\frac{p_b}{2b^2} - \frac{a p_a}{b^3}\right) \quad , \quad v_2 = 2ab^2 \quad , \quad P_2 = \frac{b'}{\sqrt{n}\, b} = \frac{p_a}{2b^2} \, . \tag{5.14}$$

These are related to the original variables (a, p_a, b, p_b) by a canonical transformation. Indeed, as it can be easily checked using the canonical Poisson brackets $\{a, p_a\} = \{b, p_b\} = 1$, we have

$$\{v_1, P_1\} = 1 \quad , \quad \{v_2, P_2\} = 1 \quad , \quad \{v_1, v_2\} = \{P_1, P_2\} = \{v_1, P_2\} = \{v_2, P_1\} = 0 \, . \tag{5.15}$$

[3] The presence of $\mathscr{L}_o$ may however introduce a spurious dependence on the reference point $r_{\rm ref}$ so one must check in the end that physical quantities will not depend on it.

[4] A polymerisation scheme based on the metric variables (a, p_a, b, p_b) has been discussed in [223], but the classical singularity is not resolved in the resulting effective quantum theory.

Under a fiducial cell rescaling $L_o \mapsto \alpha\, L_o$, the canonical variables (5.14) transform as

$$v_1 \mapsto v_1 \quad , \quad v_2 \mapsto \alpha^2\, v_2 \quad , \quad P_1 \mapsto \alpha\, P_1 \quad , \quad P_2 \mapsto \alpha^{-1}\, P_2\,, \tag{5.16}$$

and hence physical quantities can only depend on the combinations $v_2/L_o^2, P_1/L_o, L_o P_2$ or $v_2/\mathscr{L}_o^2$, $P_1/\mathscr{L}_o, \mathscr{L}_o P_2$ and v_1. In the new variables, the Hamiltonian constraint (5.11) and the corresponding EOMs are given by

$$\begin{aligned} &H_{cl} = \sqrt{n}\,\mathcal{H}_{cl} \\ &\mathcal{H}_{cl} = 3v_1P_1P_2 + v_2P_2^2 - 2 \approx 0 \end{aligned} \quad , \quad \begin{cases} v_1' = 3\sqrt{n}v_1P_2 \\ v_2' = 3\sqrt{n}v_1P_1 + 2\sqrt{n}v_2P_2 \\ P_1' = -3\sqrt{n}P_1P_2 \\ P_2' = -\sqrt{n}P_2^2 \end{cases} . \tag{5.17}$$

As expected, according to the scaling behaviours (5.16), the EOMs are invariant under fiducial cell rescaling. Choosing the gauge $\sqrt{n} = const. = \mathscr{L}_o$, the above EOMs can be solved straightforwardly. Indeed, integrating the equation for P_2 and replacing the result into the first and third equations of (5.17), we get the following solutions

$$P_2(r) = \frac{1}{\sqrt{n}(r+A)} \quad , \quad P_1(r) = \frac{C}{(r+A)^3} \quad , \quad v_1(r) = D\,(r+A)^3 \tag{5.18}$$

where A, C and D are integration constants. Finally, using the Hamiltonian constraint (5.17) together with the solutions (5.18), we find

$$v_2(r) = \frac{2}{P_2^2(r)} - 3v_1(r)\frac{P_1(r)}{P_2(r)} = \sqrt{n}(r+A)^2\left(2\sqrt{n} - \frac{3CD}{r+A}\right) . \tag{5.19}$$

Note that, since we used the Hamiltonian constraint to solve one of the equations, we have three integration constants instead of four. The integration constant A just reflects the gauge freedom in shifting the r coordinate and we can set $A = 0$ without loss of generality.[5] The remaining integration constants can be fixed in a gauge invariant way by means of Dirac observables. Besides of the Hamiltonian itself, which we already used, there exists only one further independent Dirac observable given by

$$\mathfrak{F} = \left(\frac{3}{2}v_1\right)^{\frac{4}{3}} P_1P_2 = \frac{b^2a'b'}{n}\,, \tag{5.20}$$

which, as can be checked by direct computation, Poisson commutes with the Hamiltonian constraint and is also invariant under fiducial cell rescaling (cfr. Eqs. (5.16)). Inserting the solutions (5.18) and (5.19) into (5.20), we have

$$F = \left(\frac{3}{2}D\right)^{\frac{4}{3}} \frac{C}{\sqrt{n}}\,, \tag{5.21}$$

[5] This can be also seen in a gauge-independent way by rephrasing the EOMs in terms of b, the latter being a scalar under t- and r-transformations. The number of equations then reduces to three so that, using the Hamiltonian constraint, only two independent integration constants are left.

where we used the notation $\mathfrak{F}$ and F for the *off-shell* (phase space) and *on-shell* (on the solutions of the EOMs) expressions, respectively. Therefore, we have only one condition for a combination of both C and D. Note that, since Dirac observables also determine the dynamics of the system, of course there exists one further independent phase space function which commutes with the Hamiltonian, say $\overline{\mathfrak{F}} = v_1 P_1$. However, this is not invariant under fiducial cell rescaling (cfr. Eqs. (5.16)) and hence cannot have physical meaning[6]. This means that it is not possible to find a second gauge invariant condition which allows to determine C and D individually.

In order to understand the physical interpretation of the Dirac observable (5.20) let us look at the expression for the spacetime metric determined by the solutions of the Hamiltonian EOMs. Inverting the definitions (5.14) to express a and b in terms of v_1 and v_2 and expressing a in terms of the physical areal radius b[7], we get the following coordinate-independent expression

$$a(b) = \frac{\mathscr{L}_o^2}{(3D/2)^{\frac{2}{3}}}\left(1 - \left(\frac{3}{2}D\right)^{\frac{4}{3}}\frac{C}{\sqrt{n}}\frac{1}{b}\right) = \frac{\mathscr{L}_o^2}{(3D/2)^{\frac{2}{3}}}\left(1 - \frac{F}{b}\right) , \tag{5.22}$$

where we used the relation $\sqrt{n} = \mathscr{L}_o$. Redefining now the coordinates as

$$t \longmapsto \tau = \mathscr{L}_o\left(\frac{3D}{2}\right)^{-\frac{1}{3}} t/L_o \qquad , \qquad r \longmapsto b = \left(\frac{3D}{2}\right)^{\frac{1}{3}} r \tag{5.23}$$

the line element (5.3) reads

$$\mathrm{d}s^2 = -\bar{a}(b)\mathrm{d}\tau^2 + N(b)\mathrm{d}b^2 + 2\bar{B}(b)\mathrm{d}\tau\mathrm{d}b + b^2\mathrm{d}\Omega_2^2 , \tag{5.24}$$

with

$$\bar{a}(b) = 1 - \frac{F}{b} \qquad , \qquad \bar{B}(b) \overset{(5.6)}{=} \left[1 - \left(1 - \frac{F}{b}\right)N(b)\right]^{1/2} . \tag{5.25}$$

The classical Schwarzschild solution (5.1) is thus recovered by choosing $F = 2M$ and $N(b) = \left(1 - \frac{2M}{b}\right)^{-1}$ and all dependencies on fiducial structures $\mathscr{L}_o$, L_o and the reference r_{ref} are removed[8]. This also allows us to give a physical interpretation to the Dirac observable (5.20) whose on-shell value is given by the Schwarzschild horizon radius and is thus related to the black hole mass M.

Remarks:

i) From the Hamiltonian perspective, we have one first class constraint for four phase space d.o.f. thus yielding two physical d.o.f. on the reduced phase space. Therefore, one might expect to have two independent Dirac observables which, together with the Hamiltonian constraint,

[6] As we will see in the next section, this will not be the case anymore in the effective quantum theory.

[7] Often in GR jargon b is referred to as the physical radius to distinguish it from the radial coordinate r. However, properly speaking, the physical distance from the center to the surface of a $t, b = const.$ sphere is given by $\int \sqrt{g_{rr}}dr$, while b appears in the surface area $A = 4\pi b^2$.

[8] We could now just rename $b \mapsto r$, to come back to the usual notation. We could also fix $D = 2/3$, i.e. $\tau = \mathscr{L}_o t/L_o$ and $b = r$, which is then the gauge choice usually chosen in the classical Schwarzschild setting. Here it was important to show that the standard Schwarzschild result can be obtained even without fixing both integration constants. Later on, we will use the identification $b = r$ for the classical solution.

completely determine our dynamical system. However, only one Dirac observable (F) appears in the final form of the metric (5.24), (5.25) and is related to the mass, the only physical quantity characterising our (classical) Schwarzschild BH. The apparent discrepancy between the phase space and spacetime perspectives can be explained as follows. As anticipated, the second Dirac observable is not physical as it is not invariant under fiducial cell rescaling and hence can not be fixed by physical inputs. Note that, contrary to what one might naively think, to just divide it by L_o or $\mathscr{L}_o$ does not solve the problem. Indeed, in the former case, a dependence on the coordinate chart is introduced as L_o is the coordinate size of the fiducial cell. In the latter case, on the other hand, even though $\mathscr{L}_o$ does not depend on the choice of coordinates, the problem is shifted to a dependence from the reference point entering its definition (5.9). This reflects into the fact that one of the integration constants (D) can be removed from the final metric by using a residual diffeomorphism (5.23) so that its specific value does not affect the physics. These features are not visible at the canonical level where only one constraint, the Hamiltonian constraint generating time evolution is left. As the quantities occurring in the Hamiltonian picture are all integrated over the fiducial cell and hence independent of the t-coordinate, the canonical transformation corresponding to the rescaling $t \mapsto \tau = \mathscr{L}_o\,(3D/2)^{-\frac{1}{3}}\,t/L_o$ in (5.23) corresponds to the identity transformation at the phase space level. Therefore, there exists no non-trivial first class constraint generating it. Its effect can only be seen by going back to the non-canonical components of the metric, which transform as usual under coordinate transformations, and this allows us to get rid of one of the Dirac observables. The fact that this is possible highly depends on the Hamiltonian and the solutions. As we will see in the next sections, for the polymer effective model, the second Dirac observable can not be removed from the final metric and acquires then a physical meaning.

ii) Substituting the expressions (5.25) for the metric components into the definitions (5.14) of P_1 and P_2, we find

$$\frac{P_1(b)}{\mathscr{L}_o} = \frac{2M}{b^3}\left(\frac{2}{3D}\right)^{\frac{1}{3}} \qquad , \qquad P_2(b)\mathscr{L}_o = \frac{1}{b}\left(\frac{3D}{2}\right)^{\frac{1}{3}} . \tag{5.26}$$

This provides us with an *on-shell* geometric interpretation for the canonical momenta. Indeed, provided that D does not depend on the mass[9], the quantity $P_1(b)/\mathscr{L}_o$ is related to the square root of the Kretschmann scalar (5.2), while $P_2(b)\mathscr{L}_o$ is related to the angular components of the extrinsic curvature (w.r.t. r) by the relation $P_2(b)\mathscr{L}_o\left(\frac{3D}{2}\right)^{-\frac{1}{3}} = 1/b = \sqrt{N(b)}K_\phi^\phi = \sqrt{N(b)}K_\theta^\theta$. Note that, consistently with the statement below Eq. (5.16), now the fiducial cell rescaling independent quantities are $P_1(b)/\mathscr{L}_o$, $P_2(b)\mathscr{L}_o$ and admits then a spacetime interpretation. As we will discuss in the following sections, this on-shell interpretation guarantees that in the polymerised effective theory quantum effects become relevant at high curvatures and small areal radii for an appropriate fixing of the integration constants. Let us also remark that polymerising P_1 with constant scale here plays the role of polymerising the spatial mean curvature (Hubble rate) in LQC with a constant scale as discussed in Ch. 3. There, the on-shell value of the spatial mean curvature was proportional to the square root of the spacetime Ricci scalar (cfr. Eq. (3.26)).

[9] We will come back on this point in Sec. 5.4.

Similarly, here, one of the canonical momenta is related to the relevant curvature invariant in the system, the Kretschmann scalar[10].

From the *off-shell* point of view, this analogy can be made more explicit by considering the relation of our variables with connection variables usually adopted in the LQG literature. In such variables, the line element for the BH interior region reads [193–202, 207, 208, 214]

$$\mathrm{d}s^2 = -N_T^2 \mathrm{d}T^2 + \frac{\left(p_b^{(\mathrm{conn})}\right)^2}{L_o^2 |p_c^{(\mathrm{conn})}|} \mathrm{d}x^2 + |p_c^{(\mathrm{conn})}| \mathrm{d}\Omega_2^2 \,, \tag{5.27}$$

which reduces to (5.3) (in the gauge $\bar{B}(r) = 0$) by identifying

$$T = r \quad , \quad x = t \quad , \quad N = -N_T^2 \quad , \quad |p_c^{(\mathrm{conn})}| = b^2 \quad , \quad (p_b^{(\mathrm{conn})})^2 = -ab^2 \,. \tag{5.28}$$

Here, $p_b^{(\mathrm{conn})}$ and $p_c^{(\mathrm{conn})}$ denote the components of the triads canonically conjugate to the two independent components $c^{(\mathrm{conn})}$ and $b^{(\mathrm{conn})}$ of the Ashtekar-Barbero connection, the latter playing the role of configuration space variables in the symmetry reduced setting. We introduced the explicit "(conn)" label to avoid confusion with the metric variables of Sec. 5.2.1. The variables $(c^{(\mathrm{conn})}, p_c^{(\mathrm{conn})}, b^{(\mathrm{conn})}, p_b^{(\mathrm{conn})})$ are related to our variables (v_1, P_1, v_2, P_2) given in Eq. (5.14) via[11]

$$\begin{aligned} \left(p_b^{(conn)}\right)^2 = -8v_2 \quad &, \quad |p_c^{(conn)}| = (24v_1)^{\frac{2}{3}} \,, \\ b^{(conn)} = \mathrm{sgn}(p_b^{(conn)}) \, \frac{\beta}{4} \sqrt{-8v_2} \, P_2 \quad &, \quad c^{(conn)} = -\mathrm{sgn}(p_c^{(conn)}) \, \frac{\beta}{8} \, (24v_1)^{\frac{1}{3}} \, P_1 \,, \end{aligned} \tag{5.29}$$

where β is the Barbero-Immirzi parameter. From Eqs. (5.29), we see that

$$P_1 = -\frac{8c^{(\mathrm{conn})}}{\beta |p_c^{(\mathrm{conn})}|^{1/2}} \qquad , \qquad v_1 = \frac{1}{24} |p_c^{(\mathrm{conn})}|^{3/2} \mathrm{sgn}(p_c^{(conn)}) \tag{5.30}$$

which is the analogue of the definition (3.18) of (b, v)-variables in LQC.

5.3 Effective Quantum Theory

With the Hamiltonian framework developed in the previous section at our disposal, we can now proceed to construct the effective quantum theory. As anticipated in Sec. 5.1, the starting point is the observation that in the BH interior $a, N < 0$ and the radial coordinate r becomes then time-like. The interior region can be thus foliated into homogeneous but anisotropic $r = const.$ space-like hypersurfaces and is isometric to the vacuum Kantowski-Sachs cosmological model. This allows to import techniques from homogeneous and anisotropic LQC and construct a Hamiltonian framework for the effective quantum theory. As discussed in Sec. 3.3, at the semi-classical level,

[10] The Schwarzschild metric is a solution of the vacuum Einstein equations so that the Ricci tensor $R_{\mu\nu}$ and the Ricci scalar $R = g^{\mu\nu} R_{\mu\nu}$ are both zero in this case.

[11] Note that in the action (5.5), we did not include the factor 1/4 into the Lagrangian, while in the LQG literature it is. Dynamically this is not a problem, but has to be taken into account in comparing the canonical structures. To this aim, we first need to rescale $v_i \to 16 v_i$, $P_i \to P_i/16$ which leads to the relations (5.29).

quantum corrections can be captured by an effective Hamiltonian obtained by polymerising the canonical momenta. This amounts to replace them by functions of their complex exponentials (point holonomies). A commonly adopted and particularly simple choice in LQC-literature is the sin function, which in our case amounts to the following polymerisation

$$P_1 \longmapsto \frac{\sin(\lambda_1 P_1)}{\lambda_1} \quad , \quad P_2 \longmapsto \frac{\sin(\lambda_2 P_2)}{\lambda_2} \tag{5.31}$$

where λ_1, λ_2 denote the polymerisation scales, which are related to the Planck length. The classical behaviour is recovered in the regime $\lambda_i P_i \ll 1$, $i = 1, 2$, where $\sin(\lambda_1 P_i)/\lambda_i = P_i + \mathcal{O}(\lambda_i^2)$. From the transformation behaviours (5.16) under fiducial cell rescaling $\mathscr{L}_o \mapsto \alpha \mathscr{L}_o$ it follows that λ_1 and λ_2 must scale accordingly as

$$\lambda_1 \longmapsto \alpha^{-1} \lambda_1 \quad , \quad \lambda_2 \longmapsto \alpha \, \lambda_2 \, . \tag{5.32}$$

Therefore, consistently with the scaling invariant expressions for the momenta $P_1/\mathscr{L}_0$ and $P_2 \mathscr{L}_o$ given in (5.26), the physical polymerisation scales are given by $\mathscr{L}_o \lambda_1$ and $\lambda_2/\mathscr{L}_o$. In particular, according to the classical on-shell interpretation for the canonical momenta discussed at the end of Sec. 5.2.2 (cfr. Eq. (5.26)), P_1 is related to the square root of the Kretschmann scalar so that the replacement (5.31) gives corrections in the Planck curvature regime. In turn, since P_2 is a measure of the angular components of the extrinsic curvature, the quantum corrections regulated by λ_2 become relevant at small areal radii of the $t, r = const.$ 2-spheres ($b^2 \sim \ell_P^2$) where these components of the extrinsic curvature become large. From a dimensional point of view, denoting with L the dimension of length, we have $[a] = [n] = L^2, [b] = L$ (in natural units) so that $[P_1] = L^{-1}$ and $[P_2] = L^{-2}$ (cfr. Eqs. (5.14)). Dimensionless of the products $\lambda_i P_i$ implies then the physical scales $\mathscr{L}_o \lambda_1$ and $\lambda_2/\mathscr{L}_o$ to have dimensions L^2 and L so that they can be interpreted as (inverse) curvature and small length quantum scales, respectively.

5.3.1 Effective Polymer Dynamics

The effective form of the polymerised Hamiltonian is obtained by replacing (5.31) in the classical expression (5.17), thus yielding

$$H_{\text{eff}} = \sqrt{n} \, \mathcal{H}_{\text{eff}} \quad , \quad \mathcal{H}_{\text{eff}} = 3 v_1 \frac{\sin(\lambda_1 P_1)}{\lambda_1} \frac{\sin(\lambda_2 P_2)}{\lambda_2} + v_2 \frac{\sin^2(\lambda_2 P_2)}{\lambda_2^2} - 2 \approx 0 \, . \tag{5.33}$$

Using the gauge $\sqrt{n} = const. = \mathscr{L}_o$ and $B = 0$ as in the classical case, the effective EOMs are

$$\begin{cases} v_1' = 3\sqrt{n} v_1 \cos(\lambda_1 P_1) \dfrac{\sin(\lambda_2 P_2)}{\lambda_2} \, , & (5.34) \\ v_2' = 3\sqrt{n} v_1 \dfrac{\sin(\lambda_1 P_1)}{\lambda_1} \cos(\lambda_2 P_2) + 2\sqrt{n} v_2 \dfrac{\sin(\lambda_2 P_2)}{\lambda_2} \cos(\lambda_2 P_2) \, , & (5.35) \\ P_1' = -3\sqrt{n} \dfrac{\sin(\lambda_1 P_1)}{\lambda_1} \dfrac{\sin(\lambda_2 P_2)}{\lambda_2} \, , & (5.36) \\ P_2' = -\sqrt{n} \dfrac{\sin^2(\lambda_2 P_2)}{\lambda_2^2} \, . & (5.37) \end{cases}$$

Noting that the coupling of the above equations is similar to the classical case (cfr. Eq. (5.17)), the same solution strategy can be applied. First, the equation (5.37) for P_2 can be integrated directly yielding

$$\cot(\lambda_2 P_2) = \frac{\sqrt{n}}{\lambda_2}(r+A) \qquad \Rightarrow \qquad P_2(r) = \frac{1}{\lambda_2}\cot^{-1}\left(\frac{\sqrt{n}\,r}{\lambda_2}\right) + \frac{\pi}{\lambda_2}\theta\left(-\frac{\sqrt{n}\,r}{\lambda_2}\right), \tag{5.38}$$

where we set the integration constant $A = 0$ as it just reflects the gauge freedom in shifting r like in the classical case, and $\theta(x)$ is the Heavyside-step-function required to ensure continuity at $r = 0$. Indeed, since r is just a coordinate which does not necessarily coincide with the areal radius $b(r) > 0$ of the 2-sphere, it can take also negative values so that the function $\cot(x)$ has different branches for positive and negative values of its argument.

Inserting the expression (5.38) into the equation (5.36) for P_1, we get

$$P_1' = -\frac{\sin(\lambda_1 P_1)}{\lambda_1}\frac{3\sqrt{n}/\lambda_2}{\sqrt{1+\left(\frac{\sqrt{n}\,r}{\lambda_2}\right)^2}} \quad \Rightarrow \quad P_1(r) = \frac{2}{\lambda_1}\cot^{-1}\left(\frac{\lambda_2^3}{4C\lambda_1\sqrt{n^3}}\left(\frac{\sqrt{n}\,r}{\lambda_2}+\sqrt{1+\frac{n\,r^2}{\lambda_2^2}}\right)^3\right), \tag{5.39}$$

where C is an integration constant and we used the relations

$$\frac{\sin(\lambda_2 P_2)}{\lambda_2} = \frac{1}{\lambda_2}\frac{1}{\sqrt{1+\left(\frac{\sqrt{n}\,r}{\lambda_2}\right)^2}} \quad , \quad \cos(\lambda_2 P_2) = \frac{1}{\lambda_2}\frac{\sqrt{n}\,r}{\sqrt{1+\left(\frac{\sqrt{n}\,r}{\lambda_2}\right)^2}}. \tag{5.40}$$

The argument of $\cot^{-1}$ in (5.39) is always positive and no continuity issues arise. Similarly, using now the relations

$$\frac{\sin(\lambda_1 P_1)}{\lambda_1} = \frac{\lambda_2^3}{2C\lambda_1^2\sqrt{n^3}}\frac{\left(\frac{\sqrt{n}r}{\lambda_2}+\sqrt{1+\frac{nr^2}{\lambda_2^2}}\right)^3}{\frac{\lambda_2^6}{16C^2\lambda_1^2n^3}\left(\frac{\sqrt{n}r}{\lambda_2}+\sqrt{1+\frac{nr^2}{\lambda_2^2}}\right)^6+1}, \tag{5.41}$$

$$\cos(\lambda_1 P_1) = \frac{\frac{\lambda_2^6}{16C^2\lambda_1^2n^3}\left(\frac{\sqrt{n}r}{\lambda_2}+\sqrt{1+\frac{nr^2}{\lambda_2^2}}\right)^6-1}{\frac{\lambda_2^6}{16C^2\lambda_1^2n^3}\left(\frac{\sqrt{n}r}{\lambda_2}+\sqrt{1+\frac{nr^2}{\lambda_2^2}}\right)^6+1}. \tag{5.42}$$

together with (5.40), equation (5.34) gives

$$\frac{v_1'}{v_1} = 3\frac{\sqrt{n}}{\lambda_2}\frac{1}{\sqrt{1+\left(\frac{nr}{\lambda_2}\right)^2}}\frac{\frac{\lambda_2^6}{16C^2\lambda_1^2n^3}\left(\frac{\sqrt{n}r}{\lambda_2}+\sqrt{1+\frac{nr^2}{\lambda_2^2}}\right)^6-1}{\frac{\lambda_2^6}{16C^2\lambda_1^2n^3}\left(\frac{\sqrt{n}r}{\lambda_2}+\sqrt{1+\frac{nr^2}{\lambda_2^2}}\right)^6+1}, \tag{5.43}$$

which can be integrated to

$$v_1(r) = \frac{2C^2\lambda_1^2\sqrt{n^3}}{\lambda_2^3}D\frac{\frac{\lambda_2^6}{16C^2\lambda_1^2n^3}\left(\frac{\sqrt{n}r}{\lambda_2}+\sqrt{1+\frac{nr^2}{\lambda_2^2}}\right)^6+1}{\left(\frac{\sqrt{n}r}{\lambda_2}+\sqrt{1+\frac{nr^2}{\lambda_2^2}}\right)^3}, \tag{5.44}$$

where D is an integration constant. Finally, using the Hamiltonian constraint (5.33) together with Eq. (5.40) and the fact that

$$v_1 \frac{\sin(\lambda_1 P_1)}{\lambda_1} = CD = const. \qquad \text{(cfr. Eqs. (5.41) and (5.44))}\,, \tag{5.45}$$

we get the following solution for $v_2(r)$

$$v_2(r) = 2n\left(\frac{\lambda_2}{\sqrt{n}}\right)^2\left(1+\frac{nr^2}{\lambda_2^2}\right)\left(1-\frac{3CD}{2\lambda_2}\frac{1}{\sqrt{1+\frac{nr^2}{\lambda_2^2}}}\right)\,. \tag{5.46}$$

As in the classical case we are left with two integration constants C and D which, according to the scaling behaviours (5.13) and (5.32), must transform under fiducial cell rescaling as

$$C \longmapsto \alpha C \qquad , \qquad D \longmapsto D \tag{5.47}$$

for the solutions (5.38), (5.39), (5.44), (5.46) to have the desired scaling properties (5.16). Moreover, taking the limit $\sqrt{n}r/\lambda_2 \gg 1$ and $2r^3/C\lambda_1 \gg 1$, we get[12]

$$P_1(r) \xrightarrow{\frac{\sqrt{n}r}{\lambda_2}\to\infty} \frac{2}{\lambda_1}\cot^{-1}\left(\frac{2r^3}{C\lambda_1}\right) \xrightarrow{\frac{2r^3}{C\lambda_1}\to\infty} \frac{C}{r^3}\,, \tag{5.48}$$

$$v_1(r) \xrightarrow{\frac{\sqrt{n}r}{\lambda_2}\to\infty} D\frac{C^2\lambda_1^2}{4r^3}\left(\frac{4r^6}{C^2\lambda_1^2}+1\right) \xrightarrow{\frac{2r^3}{C\lambda_1}\to\infty} Dr^3\,, \tag{5.49}$$

$$P_2(r) = \frac{1}{\lambda_2}\cot^{-1}\left(\frac{\sqrt{n}\,r}{\lambda_2}\right)+\frac{\pi}{\lambda_2}\theta\left(-\frac{\sqrt{n}\,r}{\lambda_2}\right) \xrightarrow{\frac{\sqrt{n}r}{\lambda_2}\to\infty} \frac{1}{\sqrt{n}\,r}\,, \tag{5.50}$$

$$v_2(r) \xrightarrow{\frac{\sqrt{n}r}{\lambda_2}\to\infty} 2nr^2\left(1-\frac{3CD}{2\sqrt{n}r}\right)\,, \tag{5.51}$$

in agreement with the classical solutions (5.18), (5.19). Given the above solutions of the effective equations, we can invert the definitions (5.14) to express the metric components a and b in terms of v_1 and v_2, thus yielding the following effective spacetime metric

$$\mathrm{d}s^2 = -\frac{a(r)}{L_o^2}\mathrm{d}t^2+\frac{\mathscr{L}_o^2}{a(r)}\mathrm{d}r^2+b(r)^2\mathrm{d}\Omega_2^2\,, \tag{5.52}$$

with

$$b = \left(\frac{3v_1}{2}\right)^{\frac{1}{3}} = \frac{\sqrt{n}}{\lambda_2}\left(3DC^2\lambda_1^2\right)^{\frac{1}{3}}\frac{\left(\frac{\lambda_2^6}{16C^2\lambda_1^2n^3}\left(\frac{\sqrt{n}r}{\lambda_2}+\sqrt{1+\frac{nr^2}{\lambda_2^2}}\right)^6+1\right)^{\frac{1}{3}}}{\left(\frac{\sqrt{n}r}{\lambda_2}+\sqrt{1+\frac{nr^2}{\lambda_2^2}}\right)}\,, \tag{5.53}$$

$$a = \frac{v_2}{2b^2} = n\left(\frac{\lambda_2}{\sqrt{n}}\right)^4\left(1+\frac{nr^2}{\lambda_2^2}\right)\left(1-\frac{3CD}{2\lambda_2}\frac{1}{\sqrt{1+\frac{nr^2}{\lambda_2^2}}}\right)\frac{\left(\frac{1}{3DC^2\lambda_1^2}\right)^{\frac{2}{3}}\left(\frac{\sqrt{n}r}{\lambda_2}+\sqrt{1+\frac{nr^2}{\lambda_2^2}}\right)^2}{\left(\frac{\lambda_2^6}{16C^2\lambda_1^2n^3}\left(\frac{\sqrt{n}r}{\lambda_2}+\sqrt{1+\frac{nr^2}{\lambda_2^2}}\right)^6+1\right)^{\frac{2}{3}}} \tag{5.54}$$

[12] As can be easily checked the two limits commute.

where we used the relation $\bar{a} = a/L_o^2$ (cfr. Eq. (5.7)) and the fact that $\sqrt{n} = \mathscr{L}_o$ as stated in the beginning of this section. Note that all the solutions (5.38), (5.39), (5.44), (5.46) and hence (5.53), (5.54) are smoothly well-defined in the whole r-domain $r \in (-\infty, \infty)$. As we will discuss in the next section, this observation plays a key role in determining the integration constants C and D by means of Dirac observables.

5.3.2 Fixing the Integration Constants: Mass Observables

As discussed in Sec. 5.2.2 for the classical case, integration constants can be fixed in a gauge (coordinate) independent way by means of Dirac observables. This turns out to be of crucial importance for the analysis of the effective theory where the integration constants can not be fixed by just demanding the classical (interior) solutions to be recovered at the horizon as this would depend on the choice of coordinates and moreover, as we will discuss in Sec. 5.5, the horizon itself differs from the classical one due to sub-leading quantum corrections. In order to construct the Dirac observables, let us look at the asymptotic behaviour of the effective metric given in Eqs. (5.52)-(5.54). As already stressed before, r is just a coordinate and has no physical meaning, hence in order to get coordinate-independent expressions we should rephrase all the quantities in terms of the areal radius b. Specifically, inverting Eq. (5.53), we get

$$r^{(\pm)}(b) = \frac{\lambda_2}{2\sqrt{n}} \frac{z_\pm^2(b) - 1}{z_\pm(b)} \quad , \quad z_\pm(b) = \left(\frac{8}{3D} \left(\frac{\sqrt{n} b}{\lambda_2} \right)^3 \pm \frac{4C\lambda_1 \sqrt{n}^3}{\lambda_2^3} \sqrt{\frac{4b^6}{9\lambda_1^2 D^2 C^2} - 1} \right)^{\frac{1}{3}} \tag{5.55}$$

which has two distinct branches in the positive and negative r range, respectively. The point $b_\mathcal{T} = (3\lambda_1 CD/2)^{\frac{1}{3}}$ such that $z_+(b_\mathcal{T}) = z_-(b_\mathcal{T})$ corresponds to the minimal value of b and the 3-dimensional space-like hypersurface where $b = b_\mathcal{T}$ will be called *transition surface*. The meaning of this name as well as its physical interpretation will become clear in Sec. 5.5 where the structure of the effective spacetime is studied.

Plugging (5.55) into the expression (5.54) of $a(r)$, allows us to express a as a function of b. The resulting expression for $a(b)$ also exhibits two branches $a_\pm(b) \equiv a(r^{(\pm)}(b))$, which in the $b \to +\infty$ limit are given by

$$a_\pm(b) \xrightarrow{b\to+\infty} \begin{cases} a_+ \simeq \frac{n}{4} \left(\frac{16}{3D}\right)^{\frac{2}{3}} \left(1 - \frac{F_Q}{b}\right) \\ a_- \simeq \frac{n}{4} \left(\frac{\lambda_2}{\sqrt{n}}\right)^4 \left(\frac{1}{3DC^2\lambda_1^2}\right)^{\frac{2}{3}} \left(1 - \frac{\overline{F}_Q}{b}\right) \end{cases} , \tag{5.56}$$

where

$$F_Q = \left(\frac{3}{2} D\right)^{\frac{4}{3}} \frac{C}{\sqrt{n}} \quad , \quad \overline{F}_Q = \frac{3CD\sqrt{n}}{\lambda_2^2} \left(3DC^2\lambda_1^2\right)^{\frac{1}{3}} . \tag{5.57}$$

and we used the limits (cfr. Eq. (5.55))

$$z_\pm(b) \xrightarrow{b\to+\infty} \begin{cases} z_+ \simeq \left(\frac{16}{3D}\right)^{\frac{1}{3}} \frac{\sqrt{n} b}{\lambda_2} \\ z_- \simeq \left(3DC^2\lambda_1^2\right)^{\frac{1}{3}} \frac{\sqrt{n}}{\lambda_2 b} \end{cases} , \tag{5.58}$$

corresponding to $r^{(\pm)} \to \pm\infty$, respectively. Finally, similarly to the classical case, rescaling $t \mapsto \tau = \mathscr{L}_o(3D/2)^{-\frac{1}{3}} t/L_o$ and accordingly $r \mapsto b = (3D/2)^{\frac{1}{3}} r$ for the positive branch, the line element (5.52) yields

$$\mathrm{d}s^2_+ \simeq -\left(1 - \frac{F_Q}{b}\right)\mathrm{d}\tau^2 + \left(1 - \frac{F_Q}{b}\right)^{-1}\mathrm{d}b^2 + b^2\mathrm{d}\Omega_2^2\,, \tag{5.59}$$

while, rescaling $t \mapsto \tau = \mathscr{L}_o(24DC^2\lambda_1^2\mathscr{L}_o^6/\lambda_2^6)^{-\frac{1}{3}} t/L_o$, $r \mapsto b = (24DC^2\lambda_1^2\mathscr{L}_o^6/\lambda_2^6)^{\frac{1}{3}}(-r)$ for the negative branch, we get

$$\mathrm{d}s^2_- \simeq -\left(1 - \frac{\overline{F}_Q}{b}\right)\mathrm{d}\tau^2 + \left(1 - \frac{\overline{F}_Q}{b}\right)^{-1}\mathrm{d}b^2 + b^2\mathrm{d}\Omega_2^2\,, \tag{5.60}$$

so that the effective spacetime asymptotically approaches two classical Schwarzschild solutions in the positive and negative r-domain respectively characterised by the masses $F_Q/2$ and $\overline{F}_Q/2$. We will refer to the positive branch as black hole exterior and the negative branch as white hole exterior and correspondingly to $M_{\rm BH} = F_Q/2$ and $M_{\rm WH} = \overline{F}_Q/2$ as black and white hole masses, respectively. These names will become more clear in Sec. 5.5 where the causal structure of the effective spacetime is studied.

Therefore, as can be seen from the expressions (5.57), the integration constants C and D can be completely fixed by specifying the independent boundary data $M_{\rm BH}$ and $M_{\rm WH}$, namely

$$M_{\rm BH} = \left(\frac{3}{2}D\right)^{\frac{4}{3}}\frac{C}{2\sqrt{n}} \qquad , \qquad M_{\rm WH} = \frac{3CD\sqrt{n}}{2\lambda_2^2}\left(3DC^2\lambda_1^2\right)^{\frac{1}{3}} \tag{5.61}$$

or equivalently

$$C = \frac{\lambda_2^3}{4\lambda_1\sqrt{n}^3}\left(\frac{M_{WH}}{M_{BH}}\right)^{\frac{3}{2}} \quad , \quad D = \left(\frac{2\sqrt{n}}{\lambda_2}\right)^3\left(\frac{2}{3}\left(\frac{\lambda_1\lambda_2}{3}\right)^3 M_{BH}^3\left(\frac{M_{BH}}{M_{WH}}\right)^{\frac{9}{2}}\right)^{\frac{1}{4}}. \tag{5.62}$$

Thus, unlike the classical theory where there was only one $\mathscr{L}_o$-independent Dirac observable for two integration constants, in the effective quantum theory there are two physically meaningful Dirac observables. In particular, using the solutions (5.38), (5.39), (5.44), (5.46) of the effective dynamics to express C and D in terms of the phase space variables, the on-shell quantities (5.57) yield the following off-shell expressions

$$\mathfrak{F}_Q = 3v_1\frac{\sin(\lambda_1 P_1)}{\lambda_1}\frac{\left(\frac{3}{2}v_1\cos^2\left(\frac{\lambda_1 P_1}{2}\right)\right)^{\frac{1}{3}}}{\lambda_2\cot\left(\frac{\lambda_2 P_2}{2}\right)}\,, \tag{5.63}$$

$$\overline{\mathfrak{F}}_Q = 3v_1\frac{\sin(\lambda_1 P_1)}{\lambda_1}\left(\frac{3}{2}v_1\sin^2\left(\frac{\lambda_1 P_1}{2}\right)\right)^{\frac{1}{3}}\frac{\cot\left(\frac{\lambda_2 P_2}{2}\right)}{\lambda_2}\,, \tag{5.64}$$

which, as can be checked by direct computation, commute with the effective Hamiltonian (5.33) and are both fiducial cell independent[13]. Note that $\mathfrak{F}_Q$ reduces to $\mathfrak{F}$ (cfr. Eq. (5.20)) in the limit

[13] As discussed in our paper [211], two fiducial cell independent Dirac observables can be found also for previous

$\lambda_1, \lambda_2 \to 0$. For $\overline{\mathfrak{F}}_Q$ this limit is not well-defined as it depends on how exactly the double limit $\lambda_1, \lambda_2 \to 0$ is performed. This is consistent with it not being present at the classical level. Indeed, it is possible to multiply $\overline{\mathfrak{F}}_Q$ by suitable powers of λ_1 and λ_2 such that the limit exists and yields a classical Dirac observable commuting with the Hamiltonian. Nevertheless, this introduces a fiducial cell dependence, as both λ_1 and λ_2 scale with $\mathscr{L}_o$ (cfr. Eq. (5.32)).

From a spacetime perspective, the above difference between the classical and effective theory can be explained as follows. In the classical case, there is only one independent non-zero curvature invariant, say the Kretschmann scalar. Consistently, as discussed in Sec. 5.2.1, there is only one Dirac observable related to the BH mass which can be used to fix the initial value of the Kretschmann scalar thus completely determining the system. In the effective quantum theory, instead, there are two independent non-zero curvature invariants, say the Kretschmann scalar and the Ricci scalar, the latter being non-zero due to quantum effects. Indeed, we have that $\mathcal{R}^2 \sim \mathcal{O}(\lambda^4)$ and the classical behaviour is recovered in the $\lambda \to 0$ limit. Therefore, in the effective quantum theory, two Dirac observables have to be specified to uniquely determine the system. As already anticipated, we will refer to them as BH and WH masses respectively for the positive and negative r branches. This nomenclature will be more clear once the Penrose diagram of our effective spacetime is studied in Sec 5.5. The names "black" and "white" hole have no definite meaning and can be completely exchanged as an observer in the WH asymptotic region would experience this region as the exterior Schwarzschild spacetime of a black hole. Further details will be discussed in Sec. 5.5. Here and in the next section, we keep however this terminology as it helps to distinguish the two branches and it will acquire more meaning by studying the causal structure of the effective spacetime. Note that, at this stage, the two masses play the role of initial value parameters and can be chosen arbitrarily. As we will discuss in the next section, studying the behaviour of the Kretschmann scalar constrains the boundary data to be related to each other if certain physical viability criteria are met.

5.4 Admissible Initial Conditions

We are now in the position to address two main important questions for the physical viability of our model: at which scale quantum effects become relevant? and do they induce a curvature upper bound? For phenomenologically viable models, we expect quantum effects to be relevant in the high curvature regime, while becoming negligible at low curvatures so that the system is well approximated by the classical GR description in such a regime. Moreover, as we have also discussed in Ch. 3 for LQC, quantum effects provide a universal upper bound on curvature invariants which remain finite at the Planck scale and in turn resolve the classical singularity. In this section we want then to investigate the above two points in details.

BH effective models based on connection variables. These can be then interpreted as BH and WH horizon radii or masses depending on whether or not a description of the exterior spacetime region is available for the specific model and classical Schwarzschild geometry is approached asymptotically.

5.4.1 Onset of Quantum Effects

Let us first study when the quantum effects controlled by the polymerisation scales λ_1 and λ_2 become relevant by asking when the classical approximation $\sin(\lambda_i P_i)/\lambda_i \simeq P_i$ holds. As discussed in the previous section, the coordinate r can take both positive and negative values and correspondingly the areal radius $b(r)$ exhibits two branches approaching the classical behaviour asymptotically as $r \to \pm\infty$. Let us then consider the two branches separately.

From the expression (5.39) for $P_1(r)$ together with the limits (5.48) it follows that the classical solution is approached in the the positive r-branch when ($\sqrt{n} = \mathscr{L}_o$)

$$\frac{\mathscr{L}_o r}{\lambda_2} \gg 1 \qquad , \qquad \frac{2r^3}{C\lambda_1} \gg 1 \ . \tag{5.65}$$

In order to get coordinate-free conditions we need to re-express r in terms of b. For the $r > 0$ branch, we have

$$b_+ := b(r \to +\infty) \simeq \left(\frac{3D}{2}\right)^{\frac{1}{3}} r \qquad \text{(cfr. Eq. (5.53))} \tag{5.66}$$

so that the conditions (5.65) can be rewritten as

$$\frac{\mathscr{L}_o}{\lambda_2}\left(\frac{2}{3D}\right)^{\frac{1}{3}} b_+ \gg 1 \qquad , \qquad \frac{1}{\mathscr{L}_o^2\lambda_1^2} \gg \frac{9C^2D^2}{16\mathscr{L}_o^2 b_+^6} \ . \tag{5.67}$$

Now, as discussed in the classical theory (cfr. Eq. (5.26)), $P_1/\mathscr{L}_o$ can be related to the classical value of Kretschmann scalar only if the integration constant D is mass independent. Looking then at the expression (5.62) of D in terms of $M_{\rm BH}$ and $M_{\rm WH}$, we see that the mass-dependence drops out if $M_{\rm WH} \sim M_{\rm BH}^{5/3}$. More precisely, the r.h.s. of the second equation of (5.67) can be related to the classical Kretschmann scalar $\mathcal{K}_{BH}^{\rm class} = 48M_{\rm BH}^2/b_+^6$ of the black hole side (cfr. Eq. (5.2)) by demanding that

$$\frac{9C^2D^2}{16\mathscr{L}_o^2} \propto M_{BH}^2 \ . \tag{5.68}$$

Assuming a simple power law of the kind

$$M_{WH} = M_{BH}\left(\frac{M_{BH}}{\bar{m}_{(\beta)}}\right)^{\beta-1} \ , \tag{5.69}$$

with $\bar{m}_{(\beta)}$ an arbitrary constant of dimension mass, the condition (5.68) is satisfied for $\beta = \frac{5}{3}$ for which Eqs. (5.62) yields

$$\frac{C}{\mathscr{L}_o} = \frac{\lambda_2^3}{4\lambda_1\mathscr{L}_o^4}\frac{M_{BH}}{\bar{m}_{(\frac{5}{3})}} = 2\frac{M_{BH}}{m_{(\frac{5}{3})}} \quad , \quad D = \frac{1}{3}\left(\frac{2\mathscr{L}_o}{\lambda_2}\right)^3\left[2(\bar{m}_{(\frac{5}{3})}\lambda_1\lambda_2)^3\right]^{\frac{1}{4}} = \frac{2}{3}\big(m_{(\frac{5}{3})}\big)^{\frac{3}{4}} \tag{5.70}$$

where we defined the dimensionless constant $m_{(\beta)} = 8\lambda_1\mathscr{L}_o^4\bar{m}_{(\beta)}/\lambda_2^3$. In particular, for such value of β, we have a mass dependent amplification of the white hole side, namely

$$M_{WH} = M_{BH}\left(\frac{M_{BH}}{\bar{m}_{(\frac{5}{3})}}\right)^{2/3} . \tag{5.71}$$

Moreover, the conditions (5.67) identifying the classical regime now read

$$b_+ \gg \left(m_{(\frac{5}{3})}\right)^{\frac{1}{4}}\frac{\lambda_2}{\mathscr{L}_o} \qquad , \qquad \frac{1}{\mathscr{L}_o^2\lambda_1^2} \gg \frac{M_{BH}^2}{\left(m_{(\frac{5}{3})}\right)^{\frac{1}{2}}b_+^6} = \frac{1}{48\left(m_{(\frac{5}{3})}\right)^{\frac{1}{2}}}\mathcal{K}_{BH}^{\text{class}} , \tag{5.72}$$

so that quantum effects get relevant at the critical length and the curvature scale

$$\ell_{crit}^{(\frac{5}{3})} = \left(m_{(\frac{5}{3})}\right)^{\frac{1}{4}}\frac{\lambda_2}{\mathscr{L}_o} \qquad , \qquad \mathcal{K}_{crit}^{(\frac{5}{3})} = \frac{48\left(m_{(\frac{5}{3})}\right)^{\frac{1}{2}}}{\mathscr{L}_o^2\lambda_1^2} . \tag{5.73}$$

Let us now look at the negative r branch. Recalling the rescaling needed in Sec. 5.3.2 to recover the asymptotic Schwarzschild solution (5.60), the classical regime is reached when

$$\frac{\mathscr{L}_o|r|}{\lambda_2} \gg 1 \qquad , \qquad \frac{32C\lambda_1\mathscr{L}_o^6|r|^3}{\lambda_2^6} \gg 1 \tag{5.74}$$

or in a coordinate-free version

$$b_- \gg \frac{\mathscr{L}_o}{\lambda_2}\left(24DC^2\lambda_1^2\right)^{\frac{1}{3}} \qquad , \qquad \frac{1}{\mathscr{L}_o^2\lambda_1^2} \gg \frac{9D^2C^2}{16\mathscr{L}_o^2b_-^6} , \tag{5.75}$$

where we expressed r in terms of b via the relation

$$b_- := b(r\to-\infty) \simeq \left(\frac{24DC^2\lambda_1^2\mathscr{L}_o^6}{\lambda_2^6}\right)^{\frac{1}{3}}|r| \qquad \text{(cfr. Eq. (5.53))} \tag{5.76}$$

Following the same logic as before, the r.h.s. of the second equation of Eq. (5.75) can be related to the classical Kretschmann scalar $\mathcal{K}_{WH}^{\text{class}} = 48M_{\text{WH}}^2/b_-^6$ on the white hole side by requiring

$$\frac{9C^2D^2}{16\mathscr{L}_o^2} \propto M_{WH}^2 , \tag{5.77}$$

which is satisfied if $\beta = \frac{3}{5}$ in (5.69) so that Eq. (5.62) yields

$$\frac{C}{\mathscr{L}_o} = \frac{\lambda_2^3}{4\lambda_1\mathscr{L}_o^4}\frac{\bar{m}_{(\frac{3}{5})}}{M_{WH}} \qquad , \qquad D = \frac{2}{3}\left[\left(\bar{m}_{(\frac{3}{5})}\right)^{-5}\left(\frac{8\mathscr{L}_o^4\lambda_1}{\lambda_2}\right)^3\right]^{\frac{1}{4}}M_{WH}^2 \tag{5.78}$$

and we have a de-amplified white hole mass

$$M_{WH} = M_{BH}\left(\frac{M_{BH}}{\bar{m}_{(\frac{3}{5})}}\right)^{-\frac{2}{5}} . \tag{5.79}$$

For such value of β, the conditions (5.75) then become

$$b_- \gg \left(m_{(\frac{3}{5})}\right)^{\frac{1}{4}} \frac{\lambda_2}{\mathscr{L}_o} \qquad , \qquad \frac{48\left(m_{(\frac{3}{5})}\right)^{\frac{1}{2}}}{\mathscr{L}_o^2\lambda_1^2} \gg \frac{48M_{WH}^2}{b_-^6} = \mathcal{K}_{WH}^{\text{class}} \, , \tag{5.80}$$

so that quantum effects become relevant at the critical scales

$$\ell_{crit}^{(\frac{3}{5})} = \left(m_{(\frac{3}{5})}\right)^{\frac{1}{4}} \frac{\lambda_2}{\mathscr{L}_o} \qquad , \qquad \mathcal{K}_{crit}^{(\frac{3}{5})} = \frac{48\left(m_{(\frac{3}{5})}\right)^{\frac{1}{2}}}{\mathscr{L}_o^2\lambda_1^2} \, . \tag{5.81}$$

where again $m_{(\beta)} = 8\lambda_1\mathscr{L}_o^4\bar{m}_{(\beta)}/\lambda_2^3$.

Remarks:

i) We have found two possible relations between the masses given by (5.69) with $\beta = \frac{5}{3}, \frac{3}{5}$ for which quantum effects get relevant at unique mass-independent scales. Compatibly with the interpretation of λ_1 and λ_2 as regulating inverse curvature and small areal radius quantum effects, these scales are given by (5.73) and (5.81) respectively coming from the BH and WH sides. This is consistent with $\sin(\lambda_1 P_1)/\mathscr{L}_o\lambda_1$ being related to the classical Kretschmann scalar in the BH exterior for one case ($\beta = 5/3$) and in the WH exterior for the other case ($\beta = 3/5$). Indeed, using the relations (5.70) for $\beta = 5/3$, we have

$$\frac{\sin\left(\lambda_1 P_1\right)}{\mathscr{L}_o\lambda_1} \overset{r\gg 1}{\simeq} \frac{C}{\mathscr{L}_o r^3} = \frac{3CD}{2\mathscr{L}_o b_+^3} = 2\left(m_{(\frac{5}{3})}\right)^{-\frac{1}{4}} \frac{M_{BH}}{b_+^3} \propto \sqrt{\mathcal{K}_{BH}^{\text{class}}} \, , \tag{5.82}$$

while, using the relations (5.78) for $\beta = 3/5$, we find

$$\frac{\sin(\lambda_1 P_1)}{\mathscr{L}_o\lambda_1} \overset{r\ll -1}{\simeq} \frac{\lambda_2^6}{16C\lambda_1^2\mathscr{L}_o^7}\frac{1}{|r|^3} = \frac{3CD}{2\mathscr{L}_o b_-^3} = 2\left(m_{(\frac{3}{5})}\right)^{-\frac{1}{4}} \frac{M_{WH}}{b_-^3} \propto \sqrt{\mathcal{K}_{WH}^{\text{class}}} \, . \tag{5.83}$$

ii) Given the relations (5.71) and (5.79) between the masses, we can then ask when quantum effects become relevant on the other side. Specifically, going from the BH to the WH side for $\beta = 5/3$, the expressions (5.70) for the integration constants C and D together with the conditions (5.75) lead to

$$b_- \gg \frac{M_{WH}}{M_{BH}}\ell_{crit}^{(\frac{5}{3})} \qquad , \qquad \frac{M_{WH}^2}{M_{BH}^2}\mathcal{K}_{crit}^{(\frac{5}{3})} \gg \mathcal{K}_{WH}^{\text{class}} \tag{5.84}$$

from which we see that, since $M_{WH} > M_{BH}$ for $\beta = \frac{5}{3}$, both scales are larger than the critical scales $\ell_{crit}^{(5/3)}$ and $\mathcal{K}_{crit}^{(5/3)}$ on the BH side. Therefore, on the WH side curvature effects become relevant only at higher curvatures while small area effects become relevant already at larger areas. Similarly, going from the WH to the BH side for $\beta = 3/5$, the insertion of (5.78) into (5.67) leads to the following conditions for the classical regime of the BH side

$$b_+ \gg \frac{M_{BH}}{M_{WH}}\ell_{crit}^{(\frac{3}{5})} \qquad , \qquad \frac{M_{BH}^2}{M_{WH}^2}\mathcal{K}_{crit}^{(\frac{3}{5})} \gg \mathcal{K}_{BH}^{\text{class}} \, , \tag{5.85}$$

which is perfectly consistent with (5.84). In particular, being now $M_{BH} > M_{WH}$ for $\beta = 3/5$, both the scales (5.85) are shifted to higher values on the BH side.

iii) Finally, we notice that the amplification (5.71) with $\beta = \frac{5}{3}$ is consistent with the de-amplification (5.79) for $\beta = \frac{3}{5}$. In fact, by inverting the relation (5.79), we get

$$M_{BH} = M_{WH}\left(\frac{M_{WH}}{\bar{m}_{(\frac{3}{5})}}\right)^{2/3} , \tag{5.86}$$

which, for $\bar{m}_{(\frac{3}{5})} = \bar{m}_{(\frac{5}{3})} =: \bar{m}$ (hence $m_{(\frac{3}{5})} = m_{(\frac{5}{3})} =: m$), is exactly (5.71) with M_{BH} and M_{WH} exchanged. Therefore, Eq. (5.86) describes exactly the inverse amplification of (5.71) and hence both values of β are consistent with each other. Moreover, the identification $m_{(\frac{3}{5})} = m_{(\frac{5}{3})} =: m$ leads to the following β-independent critical scales for quantum effects

$$\ell_{crit} = m^{\frac{1}{4}}\frac{\lambda_2}{\mathscr{L}_o} \quad , \quad \mathcal{K}_{crit} = \frac{48m^{\frac{1}{2}}}{\mathscr{L}_o^2\lambda_1^2} . \tag{5.87}$$

To sum up, the above considerations about the onset of quantum effects led us to the following:

Admissible initial conditions

Requiring the onset of quantum effects to be at a unique, mass-independent Kretschmann-curvature scale $\mathcal{K}_{crit}$ selects the following relation between M_{BH} and M_{WH}

$$M_{WH} = M_{BH}\left(\frac{M_{BH}}{\bar{m}}\right)^{\beta-1} \quad , \quad \beta = \frac{5}{3}\,,\,\frac{3}{5}\,, \tag{5.88}$$

with one value of β describing exactly the inverse relation as the other. Correspondingly, this leads us to relate in the classical regime $\sin(\lambda_1 P_1)/\mathscr{L}_o\lambda_1$ with the square-root of the Kretschmann scalar for the smaller mass (respectively M_{BH}, M_{WH} for $\beta = \frac{5}{3}, \frac{3}{5}$). On the side with lower mass (denoted by subscript 1), quantum effects become relevant when

$$b_1 \sim \ell_{crit} = m^{\frac{1}{4}}\frac{\lambda_2}{\mathscr{L}_o} \quad , \quad \mathcal{K}_1 \sim \mathcal{K}_{crit} = \frac{48m^{\frac{1}{2}}}{\mathscr{L}_o^2\lambda_1^2} , \tag{5.89}$$

where m is a dimensionless number, which is related to $\bar{m}$ (and for $\beta = 5/3$ to D) via

$$m = \frac{8\lambda_1\mathscr{L}_o^4}{\lambda_2^3}\bar{m} \overset{\beta=\frac{5}{3}}{=} \left(\frac{3}{2}D\right)^{\frac{4}{3}} . \tag{5.90}$$

Therefore, as expected from the classical interpretation of the canonical momenta (5.26), the quantities $\lambda_2/\mathscr{L}_o$ and $\mathscr{L}_o\lambda_1$ set the critical length ℓ_{crit} and the critical curvature scale $\mathcal{K}_{crit}$ thus giving corrections at small volumes and high curvatures, respectively. For an onset of quantum effects around the Planck curvature and Planck area, D needs to be chosen at the order of 1 (in Planck units) as very large or small values of D would lead to quantum effects arising too early in one of the sectors. Indeed, as alredy stressed in Sec. 5.2.1, for $D = 2/3$ we recover again the classical gauge for which $b \simeq r$ as $r \to \infty$.
On the other hand, on the amplified side (denoted by subscript 2), the critical scales are

$$b_2 \sim \frac{M_2}{M_1}\,\ell_{crit} \quad , \quad \mathcal{K}_2 \sim \left(\frac{M_2}{M_1}\right)^2 \mathcal{K}_{crit} \quad \text{with} \quad M_2 > M_1 . \tag{5.91}$$

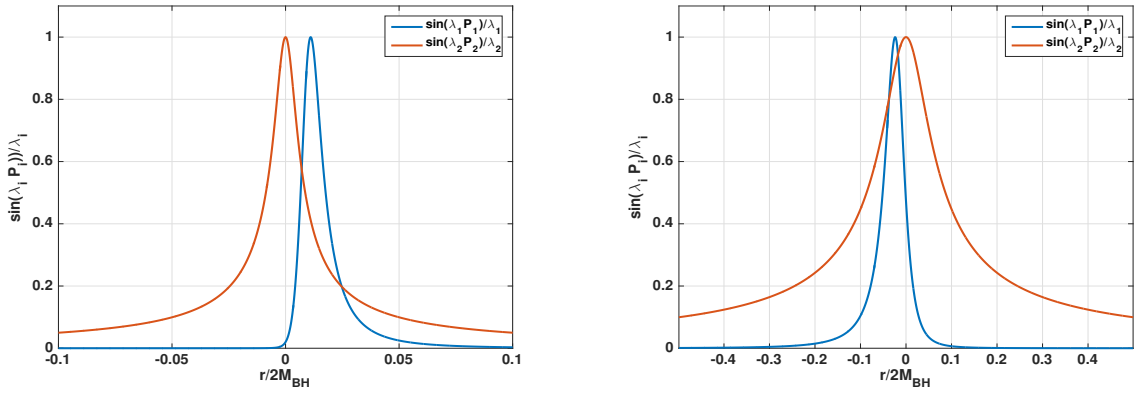

Figure 5.2: Plot of $\sin(\lambda_1 P_1)/\mathscr{L}_o\lambda_1$ and $\sin(\lambda_2 P_2)\mathscr{L}_o/\lambda_2$ for $\beta = 5/3$ in (a) and $\beta = 3/5$ in (b) for the parameters $\mathscr{L}_o = \lambda_1 = \lambda_2 = \bar{m} = 1$ and $M_{BH} = 100$. The plot shows that the order of high curvature corrections and finite volume corrections is exchanged coming from the other side or changing β.

Similar restrictions on the masses, or more precisely the horizon observables, can be found also in previous polymer models. We refer to our paper [211] for details.

Moreover we notice that, according to the change of critical scales (5.91) on the amplified side, the curvature scale is shifted to higher curvatures, such that curvature corrections become relevant closer to the transition surface, while the length scale is shifted to larger lengths, such that finite volume effects become relevant earlier. This is not a problem as they will never be relevant at the horizon scale. Indeed, as we will discuss in Sec. 5.5, $b(r_s) \sim M_2$ for large masses like those of astrophysical black holes, while $M_2/M_1 \sim M_2^{\frac{3}{5}}$ so that $b(r_s)$ grows with the mass faster than $M_2/M_1\ell_{crit}$. Moreover, the change of scales on the amplified side leads to an exchange of when curvature effects or volume effects become relevant. Indeed, as can be seen from Fig. 5.2 where we plot $\sin(\lambda_1 P_1)/\mathscr{L}_o\lambda_1$ and $\sin(\lambda_2 P_2)\mathscr{L}_o/\lambda_2$ for both values of β, exchanging the two β-values corresponds to exchange whether P_1 or P_2-corrections become relevant first. Therefore, an in-falling observer coming from the lower mass side would first experience high curvature corrections and then finite volume corrections, while an observer falling in from the other side would first see finite volume corrections and afterwards high curvature corrections.

5.4.2 Curvature Upper Bound

In the light of the above discussion for the onset of quantum effects, we can now proceed to address the second important question pointed out at the beginning of this section, that is whether curvature invariants have a unique upper bound. To this aim, let us study the Kretschmann scalar at the transition surface where quantum effects are large and it reaches almost its maximal value. In Fig. 5.3 we report as a colorplot the logarithm of the Kretschmann scalar evaluated at the transition surface as a function of the two masses M_{BH} and M_{WH}. As we can see from the plot, different mass relations yield different values of the curvature at the transition surface. Physically plausible are those relations for which the Kretschmann scalar remains non-zero and finite for all masses, especially in the large mass limit corresponding to astrophysical black holes.

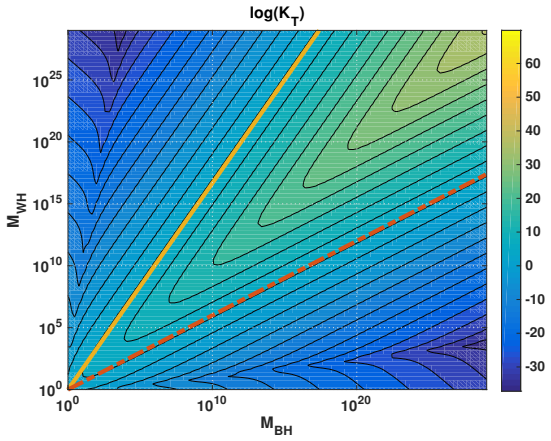

Figure 5.3: The color scale encodes the value of the logarithm of the Kretschmann scalar at the transition surface as a function of the black hole M_{BH} and white hole mass M_{WH} for $\mathscr{L}_o\lambda_1 = \lambda_2/\mathscr{L}_o = 1$. Both axis are logarithmically. Finite non-zero curvatures for large masses can only be achieved by following a level line asymptotically given by Eq. (5.69) for $\beta = \frac{5}{3}$ and $\beta = \frac{3}{5}$. Different values of $\bar{m}$ correspond to different choices of the level line. The yellow line corresponds to $\beta = \frac{5}{3}$ and the red dashed line to $\beta = \frac{3}{5}$.

This is achieved for relations between $M_{\rm BH}$ and $M_{\rm WH}$ corresponding to the level lines of the plot, at least in the large mass limit. This in turn is exactly the case for a relation of the kind $M_{WH} = M_{BH}\left(\frac{M_{BH}}{\bar{m}}\right)^{\beta-1} \sim M_{BH}^{\beta}$ for $\beta = \frac{5}{3}$ and $\beta = \frac{3}{5}$ as we also checked by considering the large mass expansion of the full expression for the Kretchmann scalar at the transition surface[14]. Different level lines correspond to different values of $\bar{m}$[15]. Therefore, the demand for a unique upper bound of curvature invariants[16] is consistent with the mass relations derived from the previous discussion of a unique curvature scale where quantum effects become relevant. Finally, in Fig. 5.4 we plot the full Kretschmann scalar as a function of the areal radius b for the two β-values and for different masses. Confirming the above discussions, quantum effects become relevant always at the same scale for both β-values, the only exception being the case $M_{BH} = 1$ which corresponds to a Planck sized black hole and quantum effects caused by the polymerisation of P_2 become relevant earlier. The horizontal dashed line indicates the critical curvature $\mathcal{K}_{crit}$ which is close to the maximal curvature. Moreover, for both cases, the classical behavior is approached before and after the bounce but with a different mass. Indeed, compatibly with the analysis of the previous subsection, a mass amplification and de-amplification are visible for $\beta = \frac{5}{3}$ and $\beta = \frac{3}{5}$, respectively. As expected from Eq. (5.88), only for $M_{BH}/m = 1$ we see a symmetric bounce but we do not consider the effective equations to be reliable in this "Planck size" regime.

[14]The computation of the Kretschmann scalar $\mathcal{K} = R_{\mu\nu\rho\delta}R^{\mu\nu\rho\delta}$ for the effective metric (5.53), (5.54) is quite involved and requires computer algebra. Therefore, we do not report the full expression here.

[15]Note that also $\beta = -1$ would be in principle a solution as analytic computations confirm and can be also seen in Fig. 5.3 close to the axes. However, since such value of β corresponds to Planck size BH and WH masses and effective models are expected to not be valid for such small masses, we exclude this solutions.

[16]As can be checked by computer algebra, other curvature invariants such as the Weyl scalar, the Ricci scalar, and the fourth-rank scalar constructed from the Ricci tensor also exhibit a unique mass independent upper bound.

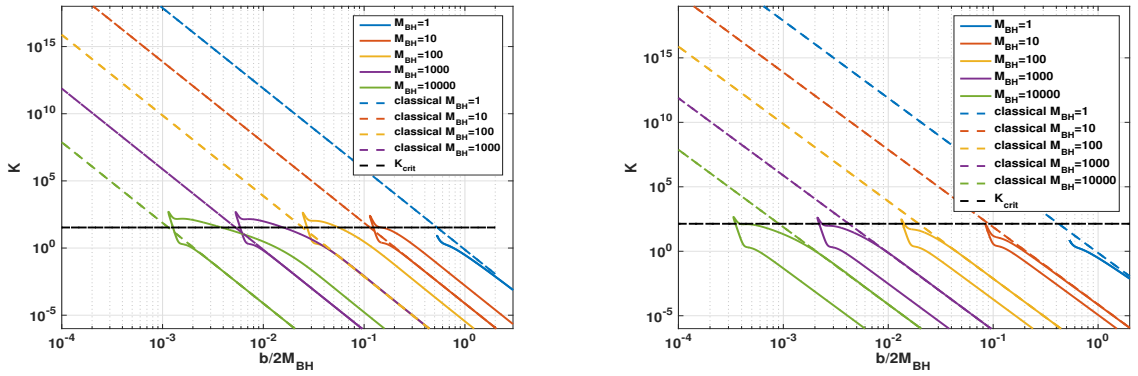

(a) (b)

Figure 5.4: Kretschmann scalar $\mathcal{K}$ against b in a log-log scale for different masses. The dashed lines correspond to the classical result. We choose the parameters $\mathscr{L}_o\lambda_1 = \lambda_2/\mathscr{L}_o = 1$, $\bar{m} = 1$ and $\beta = \frac{5}{3}$ in (a) as well as $\beta = \frac{3}{5}$ in (b). Quantum effects become relevant always at the same scale. The horizontal dashed line corresponds to $\mathcal{K}_{crit}$ given in Eq. (5.87). Differences occur only for Planck sized black holes ($M_{BH} = 1$), for which quantum effects due to the polymerisation of P_2 become relevant first.

5.5 Effective Quantum Corrected Spacetime

We are now ready to study the structure of the effective spacetime geometry described by the quantum corrected metric (5.52), (5.53), (5.54). First of all, similarly to the classical case, the effective metric is again spherically symmetric and the resulting spacetime will still be foliated by homogeneous space-like Cauchy surfaces. Moreover, as already anticipated in Sec. 5.3.2 (cfr. Eqs. (5.59), (5.60)), the quantum corrected metric approaches two classical Schwarzschild solutions asymptotically far in the positive and negative r-branches, respectively characterised by different masses $M_{\rm BH}$ and $M_{\rm WH}$. As discussed in the previous section, these are related to each other via the relations (5.88), respectively corresponding to a mass amplification and de-amplification[17]. Similarly to the classical case, the horizon is again characterised by the vanishing of $a(r)$ or equivalently the divergence of $N(r) = \mathscr{L}_o^2/a(r)$. However, unlike the classical case where there is only one horizon at $r = r_s = 2M$, the effective spacetime has now two horizons, one in the positive and one in the negative r-branch, respectively. Indeed, looking at the expression (5.54), the condition $a(r) = 0$ for the effective metric component corresponds to the vanishing of $v_2(r)$ in the phase space description. Therefore, using the solution (5.46) for $v_2(r)$, we have

$$v_2(r) = 0 \qquad \Leftrightarrow \qquad 1 - \frac{3CD}{2\lambda_2}\left(1 + \frac{nr^2}{\lambda_2^2}\right)^{-1/2} = 0\,, \tag{5.92}$$

which admits the following two solutions for the (coordinate) location of the horizon

$$r_s^{(\pm)} = \pm\frac{3CD}{2\sqrt{n}}\sqrt{1 - \left(\frac{2\lambda_2}{3CD}\right)^2}\,. \tag{5.93}$$

[17] Although the mass not being the same might sound a bit counterintuitive, we recall that in the interior region t becomes space-like. Therefore, due to the absence of a time-like Killing vector, there is no standard notion of energy conservation preventing the masses to be different.

These in turn correspond to the following values of the areal radius (5.53)

$$b(r_s^{(\pm)}) = \left[\frac{3}{2}\, v_1(r_s^{(\pm)})\right]^{1/3} = \left[\frac{3}{2}\left(\frac{\lambda_2^3 D}{8\sqrt{n}^3} f^{(\pm)}(x) + \frac{2\lambda_1^2\sqrt{n}^3 DC^2}{\lambda_2^3}\frac{1}{f^{(\pm)}(x)}\right)\right]^{1/3} , \tag{5.94}$$

where in the second equality we used the expression (5.44) for $v_1(r)$ and introduced the shorthand notation

$$f^{(\pm)}(x) = \frac{1}{x^3}\left(1 \pm \sqrt{1-x^2}\right)^3 \qquad , \qquad x = \frac{2\lambda_2}{3CD} . \tag{5.95}$$

To make a comparison with the classical situation, let us study the horizon dependence from the BH and WH masses, respectively for the two physically relevant mass relations given in Eq. (5.88). Let us start with the $\beta = 5/3$ case for which $M_{WH} = \bar{m}^{-2/3} M_{BH}^{5/3}$. By using the relations (5.62) for C and D in terms of the masses, the expression of $v_1(r_s^{(\pm)})$ given in the round brackets in the Eq. (5.94) above reads

$$v_1(r_s^{(\pm)}) = \left[\frac{2}{3}\left(\frac{\bar{m}\,\lambda_1\lambda_2}{3}\right)^3\right]^{\frac{1}{4}} \left(f^{(\pm)}(x) + \frac{M_{BH}^2}{\bar{m}^2 f^{(\pm)}(x)}\right) \quad , \quad x = \left(\frac{\bar{m}\,\lambda_1\lambda_2}{2}\right)^{1/4}\frac{1}{M_{BH}} . \tag{5.96}$$

Considering then a large mass expansion ($x \ll 1$), we have

$$v_1(r_s^{(+)}) \simeq \frac{16 M_{BH}^3}{3} - 2\sqrt{2\bar{m}\lambda_1\lambda_2}\, M_{BH} + \mathcal{O}\left(\frac{(\lambda_1\lambda_2)^{3/2}}{\bar{m}^{1/2} M_{BH}}\right) , \tag{5.97}$$

$$\begin{aligned} v_1(r_s^{(-)}) &\simeq \frac{16 M_{BH}^5}{3\bar{m}^2} - 2\sqrt{\frac{2\lambda_1\lambda_2}{\bar{m}^3}}\, M_{BH}^3 + \mathcal{O}\left(\frac{(\lambda_1\lambda_2)^{3/2}}{\bar{m}^{1/2} M_{BH}}\right) \\ &= \frac{16 M_{WH}^3}{3} - 2\sqrt{\frac{2\lambda_1\lambda_2}{\bar{m}^{3/5}}}\, M_{WH}^{9/5} + \mathcal{O}\left(\frac{(\lambda_1\lambda_2)^{3/2}}{\bar{m}^{9/10} M_{WH}^{3/5}}\right) , \end{aligned} \tag{5.98}$$

where in the second line of (5.98) we expressed everything in terms of $M_{\rm WH}$ by using the relation $M_{WH} = \bar{m}^{-2/3} M_{BH}^{5/3}$. The expansions (5.97), (5.98) correspond then to the classical result, respectively for the positive and negative r-branch, plus quantum corrections suppressed in the limit $\lambda_1, \lambda_2 \to 0$ as well as $M_{BH} \to +\infty$. Correspondingly, the large mass expansions for the areal radius (5.94) of the two horizons yield

$$b(r_s^{(+)}) \simeq 2M_{BH} - \sqrt{\frac{\bar{m}\lambda_1\lambda_2}{8}}\frac{1}{M_{BH}} + \mathcal{O}\left(\frac{\bar{m}\lambda_1\lambda_2}{M_{BH}^3}\right) , \tag{5.99}$$

$$\begin{aligned} b(r_s^{(-)}) &\simeq \frac{2M_{BH}^{5/3}}{\bar{m}^{2/3}} - \sqrt{\frac{\lambda_1\lambda_2}{8\bar{m}^{1/3}}}\frac{1}{M_{BH}^{1/3}} + \mathcal{O}\left(\frac{\bar{m}^{1/3}\lambda_1\lambda_2}{M_{BH}^{7/3}}\right) \\ &= 2M_{WH} - \sqrt{\frac{\lambda_1\lambda_2}{8\bar{m}^{3/5}}}\frac{1}{M_{WH}^{1/5}} + \mathcal{O}\left(\frac{\lambda_1\lambda_2}{\bar{m}^{3/5} M_{WH}^{7/5}}\right) , \end{aligned} \tag{5.100}$$

which, consistently with having two asymptotically classical Schwarzschild geometries for the two branches, correspond to the classical results at leading order (respectively with $M_{\rm BH}$ and $M_{\rm WH}$) plus sub-leading quantum corrections. Moreover, for large masses, the ratio $b(r_s^{(-)})/b(r_s^{(+)})$ yields

$$\frac{b(r_s^{(-)})}{b(r_s^{(+)})} \simeq \left(\frac{M_{BH}}{\bar{m}}\right)^{2/3} - \mathcal{O}\left(\frac{\bar{m}^{1/3}\lambda_1\lambda_2}{M_{BH}^{10/3}}\right) , \tag{5.101}$$

from which we see that the radius of the WH horizon grows with $M_{\rm BH}$. This may be interpreted as a quantum gravity induced mass amplification similarly to what happens in some previous models based on generalised μ_o-schemes (see e.g. [197]).

Similarly, for the $\beta = 3/5$ case, we have

$$v_1(r_s^{(\pm)}) = \left[\frac{2}{3}\left(\frac{\bar{m}\,\lambda_1\lambda_2}{3}\right)^3\right]^{\frac{1}{4}} \left(\frac{M_{WH}^2}{\bar{m}^2} f^{(\pm)}(x) + \frac{1}{f^{(\pm)}(x)}\right) \quad , \quad x = \left(\frac{\bar{m}\,\lambda_1\lambda_2}{2}\right)^{1/4} \frac{1}{M_{WH}} \tag{5.102}$$

where now we expressed everything in terms of $M_{\rm WH}$, i.e we used the relation $M_{BH} = \bar{m}^{-2/3} M_{WH}^{5/3}$ (cfr. Eq. (5.88) with $\beta = 3/5$). The corresponding large mass expansions ($x \ll 1$) now read as

$$\begin{aligned} v_1(r_s^{(+)}) &\simeq \frac{16 M_{WH}^5}{3\bar{m}^2} - 2\sqrt{\frac{2\lambda_1\lambda_2}{\bar{m}^3}}\, M_{WH}^3 + \mathcal{O}\left(\frac{(\lambda_1\lambda_2)^{3/2}}{\bar{m}^{1/2} M_{WH}}\right) \\ &= \frac{16 M_{BH}^3}{3} - 2\sqrt{\frac{2\lambda_1\lambda_2}{\bar{m}^{3/5}}}\, M_{BH}^{9/5} + \mathcal{O}\left(\frac{(\lambda_1\lambda_2)^{3/2}}{\bar{m}^{9/10} M_{BH}^{3/5}}\right) , \end{aligned} \tag{5.103}$$

$$v_1(r_s^{(-)}) \simeq \frac{16 M_{WH}^3}{3} - 2\sqrt{2\bar{m}\lambda_1\lambda_2}\, M_{WH} + \mathcal{O}\left(\frac{(\lambda_1\lambda_2)^{3/2}}{\bar{m}^{1/2} M_{WH}}\right) , \tag{5.104}$$

which are exactly the same as Eq. (5.97) and (5.98) just with M_{BH} and M_{WH} exchanged. In particular, we now get the following ratio between the BH and WH horizon areal radii

$$\frac{b(r_s^{(+)})}{b(r_s^{(-)})} \simeq \left(\frac{M_{WH}}{\bar{m}}\right)^{2/3} - \mathcal{O}\left(\frac{\bar{m}^{1/3}\lambda_1\lambda_2}{M_{WH}^{10/3}}\right) , \tag{5.105}$$

which corresponds to a mass de-amplification of the same magnitude as the amplification (5.101) for the other β-value.

Therefore, the classical Schwarzschild radius gets modified by quantum corrections and we now have two solutions respectively in the positive and negative r regions. As we can see from the large mass expansions (5.99) and (5.100), for astrophysical black holes, quantum effects become negligible already as the horizon is approached. As already anticipated in Sec. 5.3, the effective metric is smooth all over the r-domain and the geometry is well approximated by the classical description in the low curvature regimes. To visualise the situation let us consider the plot of Fig. 5.5 where we report the behaviour of metric coefficient $a(b)$ as a function of the physical areal radius b for the two cases $\beta = \frac{5}{3}$ and $\beta = \frac{3}{5}$. As we can see from the plots, the effective spacetime approaches the classical behaviour already inside the black hole, and coincides with the classical result for larger b. Moreover, the plots also show a bouncing behaviour in the areal radius b which does not shrink to zero but rather reaches a minimal value. This is similar to the situation of LQC discussed in Ch. 3. In the present case, in fact, quantum effects become relevant at high curvatures and induce a finite upper bound on curvature invariants as discussed

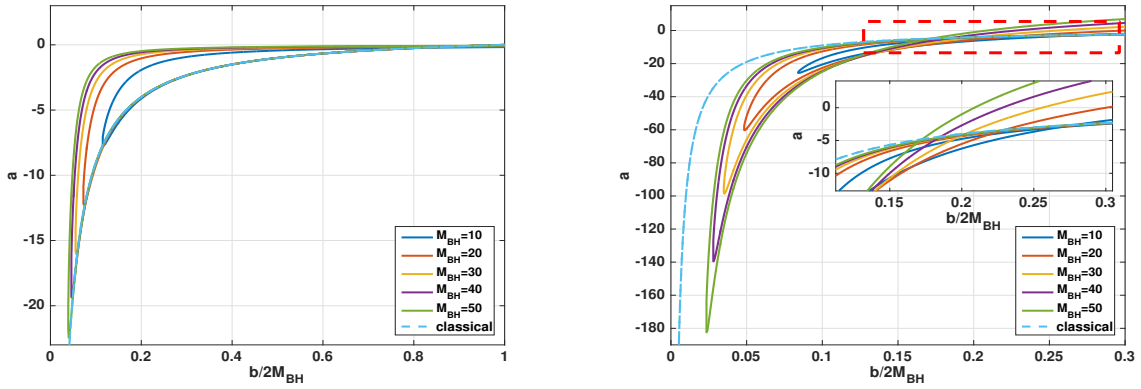

(a) (b)

Figure 5.5: Plot of a as a function of b for different BH masses and for the parameters $\mathscr{L}_o\lambda_1 = \lambda_2/\mathscr{L}_o = 1$. The two plots correspond to the mass relations (5.88) respectively with $\beta = \frac{5}{3}$ (a) and $\beta = \frac{3}{5}$ (b) where we set $m = 1$. The plots refer only to the interior of the black hole as indicated by the fact that a takes negative values. In both cases, a good agreement with the classical solution is reached already at the horizon scale where $a = 0$. Moreover, the minimal value of b is also visible.

in the previous section. This in turn reflects into the fact that the black hole reaches a minimal size and the classical singularity is resolved by a quantum bounce. To see this, let us consider the expression for the areal radius $b(r)$ given in Eq. (5.53). The minimal value is reached at the radial coordinate

$$r_{\mathcal{T}} = \frac{\lambda_2}{2\mathscr{L}_o}\left[\left(\frac{\lambda_2^3}{4C\lambda_1\mathscr{L}_o^3}\right)^{-\frac{1}{3}} - \left(\frac{\lambda_2^3}{4C\lambda_1\mathscr{L}_o^3}\right)^{\frac{1}{3}}\right] , \tag{5.106}$$

for which $b' = 0$, and the corresponding minimal areal radius is given by

$$b_{\mathcal{T}} := b(r_{\mathcal{T}}) = \left(\frac{3}{2}\lambda_1 CD\right)^{\frac{1}{3}} . \tag{5.107}$$

Using then the expressions (5.70) (resp. (5.78)) of C and D in terms of the masses for the case $\beta = \frac{5}{3}$ (resp. $\beta = \frac{3}{5}$) together with Eqs. (5.88) and (5.90), the above minimal value can be written in terms of $M_{\rm BH}$ (resp. $M_{\rm WH}$) as

$$b_{\mathcal{T}} = 2^{1/12}(\lambda_1\lambda_2)^{1/4}(M_{BH}M_{WH})^{1/8} = \left(\frac{2\lambda_1\mathscr{L}_o}{m^{\frac{1}{4}}}\right)^{\frac{1}{3}} \cdot \begin{cases} M_{BH}^{\frac{1}{3}} & \text{for } \beta = \frac{5}{3} \\ M_{WH}^{\frac{1}{3}} & \text{for } \beta = \frac{3}{5} \end{cases} \tag{5.108}$$

which goes to zero in the $\lambda_1 \to 0$ limit as expected in the classical regime. Note that the above expressions of the minimal radius for the two β-values are identical up to the exchange of the black and white hole masses. As it will be clear later in this section, the occurrence of the two β-values just reflects a certain choice of initial conditions in the BH (resp. WH) exterior region.

The minimal value $b = b_{\mathcal{T}}$ identifies a space-like 3-dimensional surface smoothly connecting a trapped and a anti-trapped region. This can be explicitly checked by computing the expansions $\theta_\pm$ of the future pointing null normals $u_\pm$ to the $t, r = const.$ metric 2-spheres in the region

$r_s^{(-)} < r < r_s^{(+)}$. These are given by [159]

$$\theta_\pm = S^{ab}\nabla_a u_b^\pm \,, \tag{5.109}$$

where $S^{ab} = g^{ab} + u_+^a u_-^b + u_-^a u_+^b$ is the projector on the metric 2-spheres, and

$$u_\pm = u_\pm^a \frac{\partial}{\partial x^a} = \frac{1}{\sqrt{-2N}}\frac{\partial}{\partial r} \pm \frac{1}{\sqrt{-2a}}\frac{\partial}{\partial t} \,, \tag{5.110}$$

with normalisation conditions $g(u_\pm, u_\pm) = 0$ and $g(u_\pm, u_\mp) = -1$. For the metric (5.52), Eq. (5.109) yields then

$$\theta_\pm = -\sqrt{-\frac{2}{N}}\frac{b'}{b} \,, \tag{5.111}$$

from which we see that, since $N(r)$ does not vanish and $b(r)$ is always positive, $\theta_\pm = 0$ if and only if $b' = 0$, i.e. at $r = r_{\mathcal{T}}$. Moreover, both expansions are negative (resp. positive) for $r_{\mathcal{T}} < r < r_s^{(+)}$ (resp. $r_s^{(-)} < r < r_{\mathcal{T}}$). The two horizons $b(r_s^{(\pm)})$ come then to be the past and future boundaries of a trapped ($b(r_s^{(+)})$) and a anti-trapped ($b(r_s^{(-)})$) region, respectively interpreted as black hole and white hole interior regions. The two regions are smoothly connected by the transition surface where $b(r)$ reaches its minimal value, which describes then a BH-to-WH transition in which the classical singularity is replaced by a quantum bounce occurring when spacetime curvature enters the Planck scale and interpolating between two asymptotically classical Schwarzschild spacetimes[18].

The causal structure of the effective spacetime described by the metric (5.52)-(5.54) can be summarised in the Penrose diagram of Fig. 5.6. As for the classical case, we refer to Appendix D for the details of the construction of the Kruskal extension for the effective spacetime. The diagram shows two asymptotic Schwarzschild spacetimes respectively in the exterior regions `I` and `III` (or equivalently `II` and `IV`) causally connected via a space-like transition surface $\mathcal{T}$ (dotted line) between a trapped BH interior and a anti-trapped WH interior region. Moreover, being the spacetime of topology $\mathbb{R}\times\mathbb{R}\times\mathbb{S}^2$, the diagram extends infinitely both in the past and in the future thus resulting into an infinite tower of BH and WH regions smoothly connected by a transition surface. Passing from one interior region to the next through a transition surface, the ADM mass characterising the corresponding asymptotic Schwarzschild exterior region changes according to the relations (5.71) and (5.79), respectively for $\beta = \frac{5}{3}$ and $\beta = \frac{3}{5}$. However, going through the Penrose diagram the mass oscillates between M_{BH} and M_{WH} so that there is no

[18] From a classical GR perspective, the resolution of the Schwarzschild singularity in effective polymer models can be understood as follow [208]. The quantum corrections to the effective spacetime can be thought of as inducing an effective stress-energy tensor $T_{\mu\nu} := G_{\mu\nu}/8\pi G$, with $G_{\mu\nu}$ the Einstein tensor constructed from the effective metric. This energy-momentum tensor can be written as that of an anisotropic fluid [224], say $T_{\mu\nu} = (\varrho + \mathfrak{p}_2)v_\mu v_\nu + (\mathfrak{p}_1 - \mathfrak{p}_2)x_\mu x_\nu + \mathfrak{p}_2 g_{\mu\nu}$ where ϱ is the energy density measured by a co-moving observer with the fluid, v^μ and x^μ are the time-like four-velocity and the space-like unit vector orthogonal to v^μ and the angular directions, $\mathfrak{p}_1$ and $\mathfrak{p}_2$ are the radial and the tangential pressure, respectively. The explicit expressions of $\varrho, \mathfrak{p}_1, \mathfrak{p}_2$ can be calculated from $G_{\mu\nu}$ and depend of course on the details of the model. In the vicinity of the transition surface $\varrho + \mathfrak{p}_1 + 2\mathfrak{p}_2 < 0$ and $\varrho + \mathfrak{p}_1 < 0$ so that the strong and the null energy conditions are violated and the classical singularity is avoided. The explicit check of this property for our model has been worked out recently in [225] where the authors also studied in detail the junction conditions for the smoothness of the effective spacetime at the transition surface as well as perturbations of our effective BH and their associated quasi-normal modes.

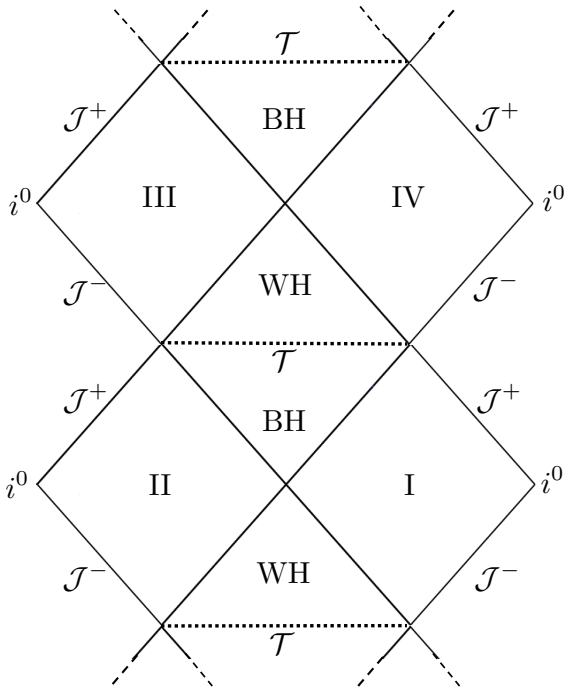

Figure 5.6: Penrose diagram for the effective quantum corrected polymer Schwarzschild spacetime. The angular coordinates θ, ϕ are again suppressed so that each point can be thought of as representing a 2-sphere of radius b.

indefinite mass amplification or de-amplification. Indeed, let assume an observer 1 starting in region `I` at a certain distance b^o to provide certain initial conditions, say v_1^o, P_1^o, P_2^o, v_2^o as well as $M_{BH}^{(1)}$ and $M_{WH}^{(1)}$. In particular, being in the black hole exterior where curvature is low, the initial data will be $P_1^o \sim 0$, $P_2^o \sim 0$. With observer 1 falling into the black hole and exiting into region `III`, the momenta will evolve from ~ 0 to $P_1 \sim \pi/\lambda_1$ and $P_2 \sim \pi/\lambda_2$ at the same distance b^o and, in the $\beta = \frac{5}{3}$ case for instance, the observer will experience a mass amplification $M_{WH}^{(1)} > M_{BH}^{(1)}$. Now, an observer 2 in region `III` will provide the initial conditions $\tilde{v}_1^o = v_1^o$, $\tilde{P}_1^o \sim 0$, $\tilde{P}_2^o \sim 0$ and some $\tilde{v}_2^o$ at the same value b^o. The values of v_1, P_1, v_2, P_2 resulting from the evolution of observer 1 from region `I` to region `III` are related to the corresponding values of observer 2 at the same b_o via the transformation

$$v_1 \longmapsto v_1 \quad , \quad P_1 \longmapsto \frac{\pi}{\lambda_1} - P_1 \quad , \quad P_2 \longmapsto \frac{\pi}{\lambda_2} - P_2 \quad , \quad v_2 \longmapsto v_2 \tag{5.112}$$

and, as can be deduced from the expressions (5.63) and (5.64) of the Dirac observables, we have $\mathfrak{F}_Q \mapsto \overline{\mathfrak{F}}_Q$, $\overline{\mathfrak{F}}_Q \mapsto \mathfrak{F}_Q$ and hence $M_{BH} \mapsto M_{WH}$, $M_{WH} \mapsto M_{BH}$. Therefore, observer 2 would fix $M_{BH}^{(2)} = M_{WH}^{(1)}$ and $M_{WH}^{(2)} = M_{BH}^{(1)}$, i.e., for observer 2 the WH side of observer 1 actually looks like a BH side. In particular, for observer 2, $M_{WH}^{(2)}$ is now smaller than $M_{BH}^{(2)}$, i.e. observer 2 would experience exactly the mass relation corresponding to the other β value. In other words, assuming region `I` and `II` to have mass M_{BH}, region `III` and `IV` admit a de-amplified (or amplified) mass M_{WH}. Crossing then the transition surface in the next future interior region we have a mass amplification (or de-amplification) such that the regions `V` and `VI` in the future of `III` and `IV` in Fig. 5.6 will be characterised by the mass M_{BH} again.

5.6 Removing Previous Restrictions: Curvature Variables

The effective model for polymer Schwarzschild BHs presented in the previous sections is still plagued by some limitations. Indeed, as discussed in Sec. 5.4, in order for the effective quantum theory to meet certain criteria for physical viability such as an onset of quantum effects at a unique mass independent scale and a universal curvature upper bound, certain relations between the BH and WH masses and hence certain initial conditions need to be selected (cfr. Eq. (5.88)). The source of such a restriction on admissible initial conditions lies in the fact that the on-shell value (5.26) of the canonical momentum P_1 is not exactly proportional to the square root of the Kretschmann scalar unless the integration constant entering the proportionality factor is selected to be independent of the mass. This is exactly the case only when we restrict to the subset of initial conditions corresponding to the two mass relations (5.88) for which the polymerised momentum $\sin(\lambda_1 P_1)/\lambda_1$ can be identified with (the square root of) the Kretschmann scalar in the classical regime of respectively the BH and WH side (cfr. Eq. (5.82) and (5.83)).

A natural way to overcome such limitations would be to introduce a new set of canonical variables in which one of the momenta is exactly the square root of the Kretschmann scalar with no integration constants of the EOMs occurring in the proportionality factor. To this aim, let us look at the phase space expression of the Kretschmann scalar. Starting from metric variables (a, p_a, b, p_b) given in Sec. 5.2.1, a systematic derivation of the phase space function yielding the Kretschmann scalar on-shell would consist of using the definition $\mathcal{K} = R_{\mu\nu\alpha\beta}R^{\mu\nu\alpha\beta}$ of the Kretschmann scalar in terms of the Riemann tensor to explicitly write it as a function $\mathcal{K}(a, a', a'', b, b', b'')$ of the metric coefficients a, b and their first and second r-derivatives. Using then the definitions (5.14) of (v_1, P_1, v_2, P_2)-variables to express a and b in terms of v_1 and v_2 and a', b' (resp. a'', b'') as functions of P_1, P_2 (resp. P_1', P_2'), together with the Hamiltonian constraint, a straightforward but lengthy calculation leads to the expression of $\mathcal{K} = \mathcal{K}(v_1, P_1, v_2, P_2)$. More easily, we can get the same result by considering the on-shell expression $48M^2/b^6$ for the Kretschmann scalar and plugging in the phase space expression (5.20) for the classical Dirac observable $F = 2M$ together with $b^3 = 3v_1/2$ (cfr. Eq. (5.14)), thus yielding

$$\mathcal{K}(v_1, P_1, v_2, P_2) = 12\left(\frac{3}{2}v_1\right)^{\frac{2}{3}} P_1^2 P_2^2 \,. \tag{5.113}$$

The idea is then to introduce new canonical variables, say (v_k, k, v_j, j), in which one of the momenta (say k) is directly related to (5.113). Specifically, taking $k = \left(\frac{3}{2}v_1\right)^{\frac{1}{3}} P_1 P_2$, which is the square root of the Kretschmann scalar (5.113) (up a numerical factor), and $j = P_2$ which clearly commutes with k, the corresponding canonical configuration variables can be determined via the generating function approach. This leads to the following variables

$$v_k = \left(\frac{3}{2}v_1\right)^{\frac{2}{3}} \frac{1}{P_2} \quad , \quad v_j = v_2 - \frac{3v_1 P_1}{2P_2} \quad , \quad k = \left(\frac{3}{2}v_1\right)^{\frac{1}{3}} P_1 P_2 \quad , \quad j = P_2 \tag{5.114}$$

which, as can be easily checked by direct computation, satisfy the canonical Poisson brackets $\{v_k, k\} = \{v_j, j\} = 1$ and $\{k, j\} = \{v_k, v_j\} = \{k, v_j\} = \{j, v_k\} = 0$.

Remarkably, in the new variables, the Hamiltonian constraint (5.17) and hence the corresponding EOMs keep exactly the same form as in the previous variables, namely

$$\begin{aligned} H_{\rm cl} &= \sqrt{n}\,\mathcal{H}_{\rm cl} \\ \mathcal{H}_{\rm cl} &= 3v_k kj + v_j j^2 - 2 \approx 0 \end{aligned} \quad , \quad \begin{cases} v_k' = 3\sqrt{n}\,v_k\,j \\ v_j' = 3\sqrt{n}\,v_k\,k + 2\sqrt{n}\,v_j\,j \\ j' = -\sqrt{n}\,j^2 \\ k' = -3\sqrt{n}\,k\,j \end{cases} \tag{5.115}$$

which can then be solved via the same steps discussed in Sec. 5.2.2, thus yielding the solutions

$$j(r) = \frac{1}{\sqrt{n}\,r} \quad , \quad k(r) = \frac{C}{r^3} \quad , \quad v_k(r) = D\,r^3 \quad , \quad v_j(r) = n\,r^2\left(2 - \frac{3CD}{\sqrt{n}\,r}\right) , \tag{5.116}$$

where again $\sqrt{n} = const. = \mathscr{L}_o$ and we are left with only two integration constants C and D. As discussed for our previous model, in the classical setting there is only one fiducial cell independent Dirac observable identified on-shell with the horizon radius and uniquely specified by the BH mass. Its expression can be obtained by simply rewriting (5.20) into the new variables (5.114), thus yielding the following off- and on-shell quantities

$$\mathfrak{F} = k\,(v_k\,j)^{\frac{3}{2}} \qquad , \qquad F = 2M_{BH} = C\left(\frac{D}{\sqrt{n}}\right)^{\frac{3}{2}} \tag{5.117}$$

which provides us with a coordinate-independent condition for a combination of both integration constants. Finally, the metric coefficients a and b can be then written as

$$b(r) = \sqrt{v_k\,j} = \sqrt{\frac{D}{\sqrt{n}}}\,r \qquad , \qquad a(r) = \frac{j\,v_j + k\,v_k}{2v_k\,j^2} = \frac{n\sqrt{n}}{D}\left(1 - \frac{CD}{\sqrt{n}\,r}\right) \tag{5.118}$$

so that, similarly to Sec. 5.2.2, one of the integration constants can be reabsorbed into a coordinate redefinition $t \mapsto \tau = \sqrt{\frac{\mathscr{L}_o^3}{D\,L_o^2}}\,t$, $r \mapsto b = \sqrt{\frac{D}{\mathscr{L}_o}}\,r$ with $\sqrt{n} = \mathscr{L}_o$, and the line element (5.24) reduces to the standard Schwarzschild form for $N(b) = \left(1 - \frac{2M_{BH}}{b}\right)^{-1}$, i.e. $B^2 = Na - n = 0$.

Remarks:

i) According to the transformation properties (5.16) of (v_1, P_1, v_2, P_2)-variables, under fiducial cell rescaling the variables (5.114) transform as

$$v_k \longmapsto \alpha v_k \qquad , \qquad k \longmapsto k \qquad , \qquad v_j \longmapsto \alpha^2 v_j \qquad , \qquad j \longmapsto \alpha^{-1} j \ , \tag{5.119}$$

i.e., as expected, the EOMs (5.115) are invariant under rescaling of the fiducial cell and physical quantities can only depend on the combinations $v_k/\mathscr{L}_o, k, v_j/\mathscr{L}_o^2, \mathscr{L}_o j$. In particular, compatibly with its intepretation as a spacetime curvature scalar, k does not depend on any fiducial structure.

ii) Consistently with remark i), by inverting Eq. (5.118) to rewrite the coordinate r in terms of the areal radius b and plugging the result into the solutions (5.116) for the momenta k and j, we get the following on-shell expressions

$$k(b) = \left(\frac{D}{\mathscr{L}_o}\right)^{\frac{3}{2}} \frac{C}{b^3} \overset{(5.117)}{=} \frac{2M_{BH}}{b^3} \qquad , \qquad \mathscr{L}_o\, j(b) = \left(\frac{D}{\mathscr{L}_o}\right)^{\frac{1}{2}} \frac{1}{b} \tag{5.120}$$

from which we see that, as anticipated above, k is related to the square root of the Kretschmann scalar (i.e. $\mathcal{K} = 12\,k^2$)[19] while, since the momentum $j = P_2$ is not modified by the canonical transformation (5.114), the on-shell interpretation for $\mathscr{L}_o\, j$ as related to the angular components of the extrinsic curvature still holds. Therefore, again in a similar spirit to the LQC variables discussed in Ch. 3, we have now a new set of canonical variables whose canonical momenta are directly related to the Kretschmann scalar and the extrinsic curvature, respectively. As we will discuss in the next sections, a polymerisation scheme based on these variables turns out to be well suited for achieving our criteria of physical viability with a unique curvature upper bound at which quantum effects become dominant without any further restriction on the initial conditions for the effective dynamics of the model. Note that one of the integration constant (D) still occurs in the on-shell value of the momentum j. As we will discuss in Sec. 5.8, this will give rise to slight differences concerning the onset of quantum effects respectively coming from the k- and j-sectors but without affecting the physical viability of the model.

iii) In principle, we could have considered a canonical transformation such that $j \neq P_2$. However, we leave it unchanged in (5.114) to keep a clear on-shell geometric interpretation for the other momentum as sensitive to small volume corrections ($\sim 1/b$ cfr. Eqs. (5.26) and (5.120))[20]. Moreover, as discussed above, the simple choice $j = P_2$ preserves the simple form of the Hamiltonian (5.115). In particular, as we will discuss in Sec. 6.2, the simple structure of the Hamiltonian makes the corresponding quantum theory analytically solvable.

5.7 Polymerisation and Effective Quantum Theory

As for the previous model, the effective quantum theory is constructed via polymerisation of the canonical momenta which in the present case amounts to

$$k \longmapsto \frac{\sin(\lambda_k\, k)}{\lambda_k} \qquad , \qquad j \longmapsto \frac{\sin(\lambda_j\, j)}{\lambda_j} \tag{5.121}$$

[19] From a off-shell point of view, the momentum k can be related to the so-called Misner-Sharp mass $M_{\text{Misner-Sharp}}(b)$ which measures the gravitational mass enclosed in a $t = const$ 2-sphere of areal radius b [65]. In fact, we have

$$k \overset{\mathcal{H}\approx 0}{\approx} R_{\mu\nu\alpha\beta}\epsilon^{\mu\nu}\epsilon^{\alpha\beta} = b\left(1 - \frac{b'^2}{N}\right) = \frac{2M_{\text{Misner-Sharp}}(b)}{b^3}\,,$$

where $\epsilon^{\mu\nu} = g^{\mu\alpha}g^{\nu\beta}\epsilon_{\alpha\beta}$ with $\epsilon_{\alpha\beta}\mathrm{d}x^\alpha \wedge \mathrm{d}x^\beta = b^2 \sin\theta \mathrm{d}\theta \wedge \mathrm{d}\phi$ is the volume two-form of the $r, t = const.$ sphere. This provides us with a off-shell interpretation for the variable k which is then related to the Riemann curvature tensor. Consistently, the above expression reduces on-shell to (5.120).

[20] In [211] we provide an example of such a situation where one of the momenta is still related to the Kretschmann scalar but the other one is modified in such a way that it does not scale with the fiducial cell. Interestingly, when both the momenta (and hence the polymerisation scales) are independent of fiducial cell rescaling, in the resulting effective theory there is no second fiducial cell independent Dirac observable which can be related with the WH mass and the relation between the masses is determined as an outcome of the effective dynamics. In particular, arguments based on time-reversal symmetry as those discussed at the end of Sec. 5.5 (cfr. Eq. (5.112)), select two possibilities, namely $M_{\text{WH}} = M_{\text{BH}}$ or $M_{\text{WH}} \sim M_{\text{BH}}^{-1}$. However, since for the specific example considered in [211] turns out that $M_{\text{WH}} \sim M_{\text{BH}}^{-1}$ so that large BH masses would correspond to Planckian regimes on the WH side and this is beyond the regime of applicability of a polymer-type effective description, we do not report it here.

where, according to the on-shell interpretations (5.120) for the momenta k and j, the constant polymerisation scales λ_k and λ_j control the high curvature and small areal radius quantum effects, respectively. Indeed, the scaling behaviours (5.119) of the new canonical variables imply λ_k and λ_j to transform under fiducial cell rescaling $\mathscr{L}_o \mapsto \alpha\mathscr{L}_o$ as

$$\lambda_k \longmapsto \lambda_k \qquad , \qquad \lambda_j \longmapsto \alpha\,\lambda_j \tag{5.122}$$

so that the scale invariant quantities λ_k and $\lambda_j/\mathscr{L}_o$ have respectively the dimensions $[\lambda_k] = [1/k] = L^2$ and $[\lambda_j/\mathscr{L}_o] = [1/\mathscr{L}_o\, j] = L$, compatibly with their interpretations as inverse curvature and small length quantum scales.

Replacing the polymerised momenta (5.121) into the classical Hamiltonian (5.115), we obtain the effective Hamiltonian

$$H_{\text{eff}} = \sqrt{n}\,\mathcal{H}_{\text{eff}} \qquad , \qquad \mathcal{H}_{\text{eff}} = 3v_k\frac{\sin(\lambda_k\,k)}{\lambda_k}\frac{\sin(\lambda_j\,j)}{\lambda_j} + v_j\frac{\sin^2(\lambda_j\,j)}{\lambda_j^2} - 2 \approx 0\,, \tag{5.123}$$

which has the same form as the one in the previous (v_1, P_1, v_2, P_2)-variables just with the replacements $v_1 \leftrightarrow v_k$, $v_2 \leftrightarrow v_j$, $P_1 \leftrightarrow k$, and $P_2 \leftrightarrow j$ (cfr. Eq. (5.33)). This means that the resulting EOMs and hence the corresponding solutions will also have the same form (cfr. Eqs. (5.38), (5.39), (5.44), (5.46)). What is now different is the form of the metric components resulting from the solutions of the effective dynamics. Indeed, the relation between the metric coefficients and the phase space variables is different in the two models already at the classical level, so that the coefficients a and b entering the effective line element

$$\mathrm{d}s^2 = -\frac{a(r)}{L_o^2}\mathrm{d}t^2 + \frac{\mathscr{L}_o^2}{a(r)}\mathrm{d}r^2 + b^2(r)\mathrm{d}\Omega_2^2\,, \tag{5.124}$$

can be now expressed as phase space functions by means of the relations (5.118) with polymerised momenta (5.121), which after plugging in the solutions of the EOMs yield

$$b^2(r) = v_k(r)\frac{\sin(\lambda_j j(r))}{\lambda_j} = \frac{2DC^2\lambda_k^2\sqrt{n}^3}{\lambda_j^4}\,\frac{1}{\sqrt{1+\frac{nr^2}{\lambda_j^2}}}\,\frac{\frac{\lambda_j^6}{16C^2\lambda_k^2n^3}\left(\frac{\sqrt{n}\,r}{\lambda_j}+\sqrt{1+\frac{nr^2}{\lambda_j^2}}\right)^6+1}{\left(\frac{\sqrt{n}\,r}{\lambda_j}+\sqrt{1+\frac{nr^2}{\lambda_j^2}}\right)^3}\,, \tag{5.125}$$

$$\begin{aligned} a(r) &= \frac{1}{2v_k(r)}\frac{\lambda_j^2}{\sin^2(\lambda_j j(r))}\left(v_j(r)\frac{\sin(\lambda_j j(r))}{\lambda_j} + v_k(r)\frac{\sin(\lambda_k k(r))}{\lambda_k}\right) \\ &= \frac{\lambda_j^6}{2DC^2\lambda_k^2\sqrt{n}^3}\left(1+\frac{nr^2}{\lambda_j^2}\right)^{\frac{3}{2}}\left(1-\frac{CD}{\lambda_j\sqrt{1+\frac{nr^2}{\lambda_j^2}}}\right)\frac{\left(\frac{\sqrt{n}\,r}{\lambda_j}+\sqrt{1+\frac{nr^2}{\lambda_j^2}}\right)^3}{\frac{\lambda_j^6}{16C^2\lambda_k^2n^3}\left(\frac{\sqrt{n}\,r}{\lambda_j}+\sqrt{1+\frac{nr^2}{\lambda_j^2}}\right)^6+1}\,, \end{aligned} \tag{5.126}$$

where we recall that $\sqrt{n} = \mathscr{L}_o$ and C, D are integration constants which, according to the scaling behaviours (5.122), scale as $C \mapsto C$ and $D \mapsto \alpha D$ under a fiducial cell rescaling. Also in this

new model the effective metric is smoothly well-defined in the whole $r \in (-\infty, +\infty)$ domain, thus describing both the interior and exterior regions.

The two remaining integration constants can be fixed by means of two fiducial cell independent Dirac observables respectively related to the BH and WH masses. These can be determined by looking at the asymptotic behaviour of the effective metric as $r \to \pm\infty$. In the $r \to +\infty$ limit, the metric coefficients (5.125), (5.126) reduce to their classical expressions (5.118) from which, expressing r in terms of b, we get

$$a(b(r \to +\infty)) = \frac{n\sqrt{n}}{D}\left(1 - \left(\frac{D}{\sqrt{n}}\right)^{\frac{3}{2}}\frac{C}{b}\right) . \tag{5.127}$$

Rescaling away the pre-factor in (5.127) via a coordinate redefinition, the classical Schwarzschild result $a(b) = 1 - \frac{2M_{\rm BH}}{b}$ is recovered with the identification

$$F_Q = 2M_{BH} = C\left(\frac{D}{\sqrt{n}}\right)^{3/2} . \tag{5.128}$$

In the limit $r \to -\infty$, instead, the metric components (5.125), (5.126) read as

$$b^2(r \to -\infty) = \frac{16DC^2\lambda_k^2}{\sqrt{n}}\left(\frac{\sqrt{n}}{\lambda_j}\right)^6 |r|^2 \quad , \quad a(r \to -\infty) = \frac{n\sqrt{n}}{16DC^2\lambda_k^2}\left(\frac{\lambda_j}{\sqrt{n}}\right)^6\left(1 - \frac{CD}{\sqrt{n}|r|}\right) \tag{5.129}$$

i.e.

$$a(b(r \to -\infty)) = \frac{n\sqrt{n}}{16DC^2\lambda_k^2}\left(\frac{\lambda_j}{\sqrt{n}}\right)^6\left(1 - \frac{4nDC^2\lambda_k}{\lambda_j^3}\sqrt{\frac{D}{\sqrt{n}}}\frac{1}{b}\right) , \tag{5.130}$$

from which, performing another coordinate redefinition to remove the pre-factor, the classical Schwarzschild form is recovered with the following on-shell expression for the WH mass Dirac observable

$$\overline{F}_Q = 2M_{WH} = \frac{4\lambda_k C^2\sqrt{n}^3}{\lambda_j^3}\left(\frac{D}{\sqrt{n}}\right)^{\frac{3}{2}} \overset{(5.128)}{=} 8C\lambda_k\left(\frac{\sqrt{n}}{\lambda_j}\right)^3 M_{BH} . \tag{5.131}$$

Thus, inverting the relations (5.128) and (5.131), the integration constants C and D are completely specified in terms of the two masses as

$$C = \frac{\lambda_j^3}{4\lambda_k\sqrt{n}^3}\frac{M_{WH}}{M_{BH}} \quad , \quad D = \sqrt{n}\left(\frac{8\lambda_k\sqrt{n}^3}{\lambda_j^3}\frac{M_{BH}^2}{M_{WH}}\right)^{\frac{2}{3}} . \tag{5.132}$$

As we also did for the previous model, the corresponding off-shell expressions for the mass observables can be determined by expressing C and D in terms of the phase space variables via the solutions of the effective dynamics and substituting the result into Eqs. (5.128) and (5.131). This gives

$$\mathfrak{F}_Q = \frac{\sin(\lambda_k k)}{\lambda_k}\cos\left(\frac{\lambda_k k}{2}\right)\left(\frac{2v_k}{\lambda_j\cot\left(\frac{\lambda_j j}{2}\right)}\right)^{\frac{3}{2}} \quad , \quad \overline{\mathfrak{F}}_Q = \frac{\sin(\lambda_k k)}{\lambda_k}\sin\left(\frac{\lambda_k k}{2}\right)\left(\frac{2v_k}{\lambda_j}\cot\left(\frac{\lambda_j j}{2}\right)\right)^{\frac{3}{2}} \tag{5.133}$$

which, as can be checked by direct computation, Poisson commute with the effective Hamiltonian (5.123), and are both fiducial cell independent (cfr. Eqs. (5.119) and (5.122)). Moreover, compatibly with the discussion of the observables for the previous model, also in this case $\mathfrak{F}_Q$ reduces to the classical observable (5.117) in the $\lambda_j, \lambda_k \to 0$ limit while $\overline{\mathfrak{F}}_Q$ is not well-defined in this limit, as it depends on how the double limit is taken, coherently with it not being present at the classical level where the system is completely characterised in terms of the BH mass only.

The effective quantum corrected spacetime described by the line element (5.124)-(5.126) has a similar structure as in the previous model. Indeed, according to the above discussion, the areal radius $b(r)$ has two monotonous branches for positive and negative values of the r-coordinate. The corresponding asymptotic regions are isometric to two classical Schwarzschild solutions with AMD masses $M_{\rm BH}$ and $M_{\rm WH}$, respectively. The metric has two horizons located at $r = r_s^{(\pm)}$ for which $a(r_s^{(\pm)}) = 0$. Indeed, looking at the second line of the expression (5.126) for $a(r)$, we see that the condition $a(r) \stackrel{!}{=} 0$ amounts to the following equation

$$1 - \frac{CD}{\lambda_j \sqrt{1 + \frac{nr^2}{\lambda_j^2}}} = 0 \,, \tag{5.134}$$

which has two solutions respectively in the positive and negative r-branch given by

$$r_s^{(\pm)} = \pm \sqrt{\frac{C^2 D^2}{\mathscr{L}_o^2} - \frac{\lambda_j^2}{\mathscr{L}_o^2}} = \pm \frac{\lambda_j}{\mathscr{L}_o} \sqrt{\left(\frac{M_{BH} M_{WH}}{\lambda_k} \right)^{\frac{2}{3}} - 1} \,, \tag{5.135}$$

where $\sqrt{n} = \mathscr{L}_o$ and, in the second equality, we expressed C and D in terms of the masses by using (5.132). The corresponding values of the horizon areal radius b then read

$$\begin{aligned} b\left(r_s^{(\pm)}\right)^2 = {} & \frac{M_{BH}}{2M_{WH}} \left((M_{BH} M_{WH})^{\frac{1}{3}} \pm \sqrt{(M_{BH} M_{WH})^{\frac{2}{3}} - \lambda_k^{\frac{2}{3}}} \right)^3 \\ & + \frac{M_{WH}}{2M_{BH}} \frac{\lambda_k^2}{\left((M_{BH} M_{WH})^{\frac{1}{3}} \pm \sqrt{(M_{BH} M_{WH})^{\frac{2}{3}} - \lambda_k^{\frac{2}{3}}} \right)^3} \,, \end{aligned} \tag{5.136}$$

which, for $M_{BH} M_{WH} \gg \lambda_k$, yield

$$b\left(r_s^{(+)}\right)^2 \simeq 4M_{BH}^2 - 3\lambda_k^{\frac{2}{3}} \frac{M_{BH}^{\frac{4}{3}}}{M_{WH}^{\frac{2}{3}}} + \mathcal{O}\left(\frac{\lambda_k^2}{M_{BH}^2}\right) + \mathcal{O}\left(\frac{\lambda_k^2}{M_{WH}^2}\right) \,, \tag{5.137}$$

$$b\left(r_s^{(-)}\right)^2 \simeq 4M_{WH}^2 - 3\lambda_k^{\frac{2}{3}} \frac{M_{WH}^{\frac{4}{3}}}{M_{BH}^{\frac{2}{3}}} + \mathcal{O}\left(\frac{\lambda_k^2}{M_{WH}^2}\right) + \mathcal{O}\left(\frac{\lambda_k^2}{M_{BH}^2}\right) \,, \tag{5.138}$$

that is the (squared) classical Schwarzschild radius plus sub-leading quantum corrections suppressed by powers of λ_k independently of how M_{BH} and M_{WH} are chosen. Therefore, for large BH and WH masses, the spacetime is well approximated by the classical description already at the horizon scales and the classical Schwarzschild result is recovered asymptotically.

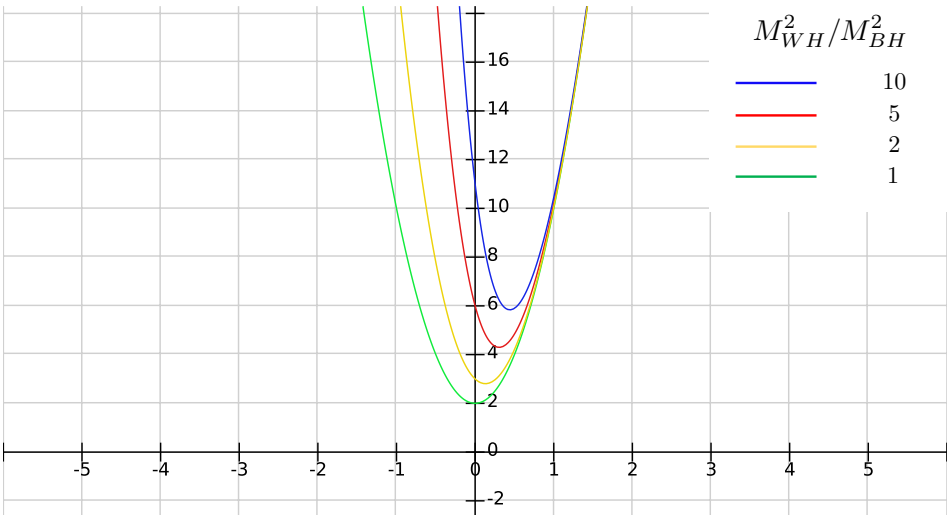

Figure 5.7: Plot of the function $f(x;\mathfrak{M})$ defined in (5.139) with $x = \mathscr{L}_o r/\lambda_j$ for different values of the parameter $\mathfrak{M}^2 = M^2_{WH}/M^2_{BH}$. The minimum corresponds to the transition surface where the areal radius b also takes its minimal value.

The two interior regions are connected via a smooth space-like transition surface where $b' = 0$ and b reaches its minimal value. The explicit form of the solution is rather involved and can be found in Sec. 5 of [211]. Here, we can convince ourselves by plotting the areal radius b. To this aim, let us first notice that using the relations (5.132) the expression (5.125) for $b(r)$ can be written in terms of the masses as

$$b^2(x) = \frac{1}{2}\left(\frac{\lambda_k M^2_{BH}}{M_{WH}}\right)^{\frac{2}{3}} f(x;\mathfrak{M}) \qquad , \qquad f(x;\mathfrak{M}) := \frac{1}{\sqrt{1+x^2}}\frac{\left(x+\sqrt{1+x^2}\right)^6 + \mathfrak{M}^2}{\left(x+\sqrt{1+x^2}\right)^3} \tag{5.139}$$

where $x = \mathscr{L}_o r/\lambda_j$ and we took out as a common factor M^2_{BH} to rewrite the x-dependent part in terms of the ratio $\mathfrak{M} = M_{WH}/M_{BH}$ between the masses. As $b \neq 0$, the condition $b' = 0$ is equivalent to $(b^2)' = 0$ so that we can just look at the behaviour of the above function $f(x;\mathfrak{M})$ parametrised by $\mathfrak{M}$. This is plotted in Fig. 5.7 where we see that for each value of the ratio $\mathfrak{M} = M_{WH}/M_{BH}$ the curve has a unique global minimum. The two horizons (5.136) come then to be respectively the past and future boundaries of a trapped and a anti-trapped region where the expansions $\theta_\pm$ given in (5.111) are respectively negative ($b' > 0$) and positive ($b' < 0$). The causal structure of the effective spacetime can be visualised by means of a Penrose diagram which, according to the general discussion of the Kruskal extension reported in Appendix D, is the same as for the previous model (cfr. Fig. 5.6). Moreover, since the functional form of the solutions of the effective dynamics is the same for both models, similar considerations on the evolution of the initial conditions from the BH to the WH asymptotic region hold. Specifically, following the spacetime evolution from the BH classical regime to the WH classical regime up to the same value of b, we have $v_j \mapsto v_j, v_k \mapsto v_k, k \mapsto \frac{\pi}{\lambda_k} - k, j \mapsto \frac{\pi}{\lambda_j} - j$ and correspondingly $\mathfrak{F}_Q \mapsto \overline{\mathfrak{F}}_Q, \overline{\mathfrak{F}}_Q \mapsto \mathfrak{F}_Q$ (cfr. Eq. (5.133)). Going through the Penrose diagram there is then an continuous transition between Schwarzschild spacetimes with oscillating masses M_{BH} and M_{WH}.

5.8 Curvature Invariants and Onset of Quantum Effects

We are now in the position to answer the original question motivating the introduction of the new variables that is whether the criteria for physical viability of a unique mass independent curvature scale for the onset of quantum effects and in turn a universal upper bound on curvature invariants are satisfied without demanding any restriction on the initial conditions. To this aim we need to repeat the analysis of Sec. 5.4 for the current model.

First, as for the onset of quantum effects, we have to check where the classical approximations $\sin(\lambda_k k) \simeq \lambda_k k$, $\sin(\lambda_j j) \simeq \lambda_j j$ hold true. Since as discussed in Sec. 5.7 the solutions of the effective dynamics have the same form as in the previous variables, we get similar conditions as (5.65) (resp. (5.74)) for large and positive (resp. negative) r just with λ_1, λ_2 replaced by λ_k, λ_j, namely

$$\frac{\mathscr{L}_o\, r}{\lambda_j} \gg 1 \quad , \quad \frac{2r^3}{C\lambda_k} \gg 1 \qquad (r \to +\infty) \tag{5.140}$$

$$\frac{\mathscr{L}_o|r|}{\lambda_j} \gg 1 \quad , \quad \frac{32C\lambda_k\mathscr{L}_o^6|r|^3}{\lambda_j^6} \gg 1 \qquad (r \to -\infty) \tag{5.141}$$

which, using the expressions (5.127) and (5.129) for the areal radius $b_\pm$ in the $r \to \pm\infty$ limit together with the on-shell expressions (5.128) and (5.131) for the mass Dirac observables, yield the coordinate-free conditions

$$b_+ \gg \left(8\lambda_k \frac{M_{BH}^2}{M_{WH}}\right)^{\frac{1}{3}} \quad , \quad \frac{M_{BH}}{b_+^3} \ll \frac{1}{\lambda_k}\,, \tag{5.142}$$

$$b_- \gg \left(8\lambda_k \frac{M_{BH}^2}{M_{WH}}\right)^{\frac{1}{3}} \frac{M_{WH}}{M_{BH}} = \left(8\lambda_k \frac{M_{WH}^2}{M_{BH}}\right)^{\frac{1}{3}} \quad , \quad \frac{M_{WH}}{b_-^3} \ll \frac{1}{\lambda_k}\,. \tag{5.143}$$

Of particular interest are the second conditions in Eqs. (5.142) and (5.143) which can be rewritten in terms of the classical Kretschmann scalar of the black and white hole sides respectively as

$$\mathcal{K}_{cl}^{BH} = \frac{48M_{BH}^2}{b_+^6} \ll \frac{48}{\lambda_k^2} \quad , \quad \mathcal{K}_{cl}^{WH} = \frac{48M_{WH}^2}{b_-^6} \ll \frac{48}{\lambda_k^2} \tag{5.144}$$

thus identifying a unique mass independent curvature scale $\mathcal{K}_{\rm crit} = 48/\lambda_k^2$ at which quantum effects become relevant compatibly with the interpretation of λ_k as related to the inverse Planck curvature given in Sec. (5.7). On the other hand, we interpret the first conditions in Eqs. (5.142) and (5.143) as small volume (small areal radius) effects and we will come back on them later in this section. In particular, we can ask whether such kind of quantum effects may overcome the large curvature effects. On the BH side, by comparing the first condition in Eq. (5.142) with (the cube root of) the second, we have that this corresponds to

$$\left(8\lambda_k \frac{M_{BH}^2}{M_{WH}}\right)^{\frac{1}{3}} > (M_{BH}\lambda_k)^{\frac{1}{3}} \quad \Rightarrow \quad \frac{M_{WH}}{M_{BH}} < 8\,. \tag{5.145}$$

Similary, from the conditions (5.143) on the WH side, we get

$$\left(8\lambda_k \frac{M_{WH}^2}{M_{BH}}\right)^{\frac{1}{3}} > (M_{WH}\lambda_k)^{\frac{1}{3}} \quad \Rightarrow \quad \frac{M_{WH}}{M_{BH}} > \frac{1}{8}\,. \tag{5.146}$$

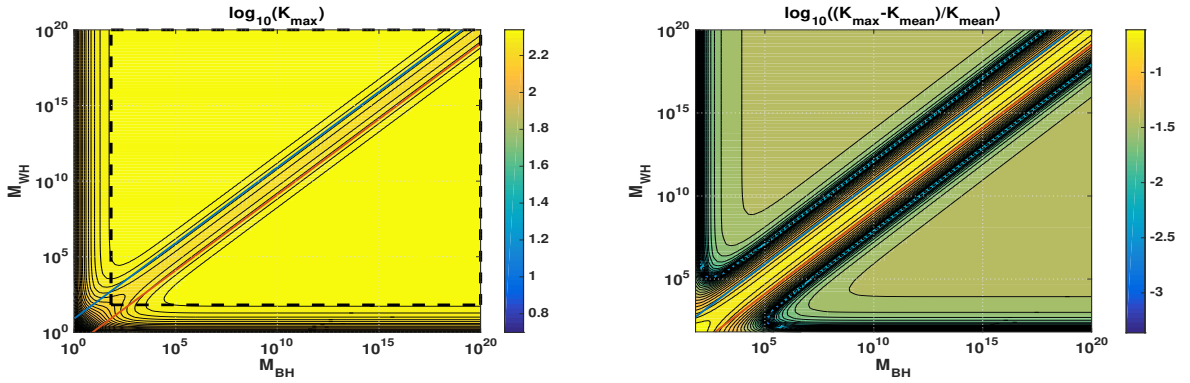

(a) (b)

Figure 5.8: Logarithm of the maximal value of the Kretschmann scalar (a) and the deviation of the Kretschmann scalar from its mean value (mean over all masses in the black dashed box) (b) as a function of M_{BH} and M_{WH} in logarithmic axis. The maximal value of the Kretschmann scalar remains largely independent of the masses. The two colour lines represent the boundaries of Eqs. (5.145) and (5.146). For the plot the maximal value of the Kretschmann scalar is computed numerically. The parameters are settled to $\lambda_j = \lambda_k = \mathscr{L}_o = 1$.

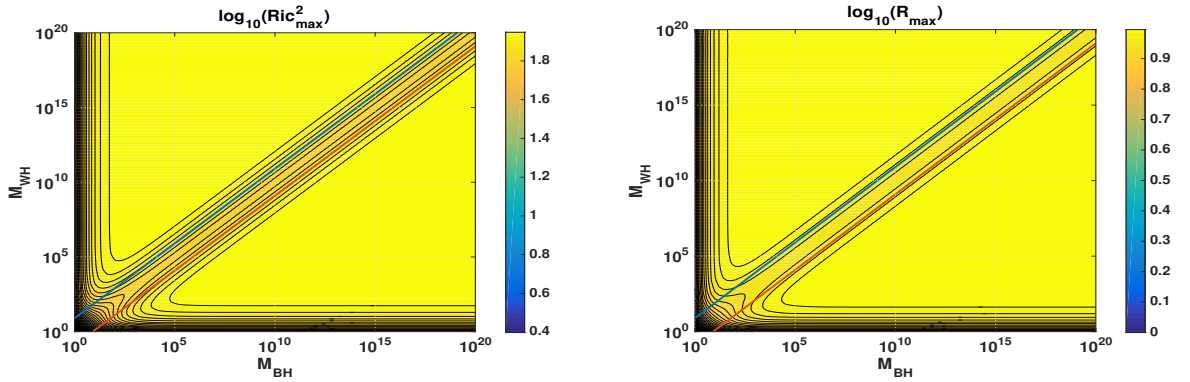

(a) (b)

Figure 5.9: Logarithm of the maximal value of the fourth-rank scalar $R_{\mu\nu}R^{\mu\nu}$ constructed from the Ricci tensor (a) and the Ricci scalar (b) as functions of M_{BH} and M_{WH}. As before, the two colour lines represent the boundaries of Eqs. (5.145) and (5.146), and the parameters are $\lambda_j = \lambda_k = \mathscr{L}_o = 1$.

Therefore, in the regime $1/8 < \frac{M_{WH}}{M_{BH}} < 8$ finite volume effects become relevant earlier than the high curvature effects.

Finally, as for the upper bound on curvature invariants, we can check what happens to them in the deep quantum regime, i.e. at the transition surface where they reach their maximal value. To this aim, in Fig. 5.8 we report the color plots of (the logarithm of) the maximal value of the Kretschmann scalar (a) and the deviation from its mean value over all masses in the black dashed box (b) as a function of $M_{\rm BH}$ and $M_{\rm WH}$. As expected from the above discussion on the mass independent curvature scale (5.144) for the onset of quantum effects and the interpretations (5.120) of the classical canonical momenta, for a very broad range of masses (with numerically stable results for $M_{\rm BH}, M_{\rm WH} < 10^{20}$), the maximum value of the Kretschmann scalar is bounded by approximately the Planck curvature for $\lambda_k \approx 1$ (in Planck units). Similar results hold also for the other curvature invariants as shown in Fig. 5.9 where the logarithm of the maximal value of

the fourth-rank scalar $R_{\mu\nu}R^{\mu\nu}$ constructed from the Ricci tensor (a) and the Ricci scalar (b) are reported. This is also confirmed by the large mass expansions of the above curvature invariants evaluated at the transition surface. Indeed, although their full expressions turn out to be quite lengthy, they can be schematically written as[21]

$$\mathcal{K} = \mathcal{K}_{cl} + \mathcal{O}(\lambda_k^2)\,, \tag{5.147}$$

$$\mathcal{R}^2 = \mathcal{O}(\lambda_k^4) + \mathcal{O}(\lambda_k^2\lambda_j^2) \qquad \text{(similar for } R_{\mu\nu}R^{\mu\nu})\,, \tag{5.148}$$

$$\mathcal{W} = C_{\mu\nu\rho\sigma}C^{\mu\nu\rho\sigma} = \mathcal{K} - 2\,R_{\mu\nu}R^{\mu\nu} + \frac{1}{3}\mathcal{R}^2 = \mathcal{K}_{cl} + \mathcal{O}(\lambda^2)\,, \tag{5.149}$$

thus yielding the classical results plus quantum corrections suppressed as $\lambda_k, \lambda_j \to 0$. Note that $\mathcal{R}$ and $R_{\mu\nu}R^{\mu\nu}$ vanish in the limit $\lambda_k, \lambda_j \to 0$ in agreement with them being both zero for the classical Schwarzschild case.

Therefore, according to the above discussions, this second effective model based on polymerisation of the (v_k, k, v_j, j)-variables satisfies the criteria for physical viability of a unique upper curvature bound and quantum effects being negligible at low curvatures with no need of specifying a relation between the BH and WH masses, i.e., with no restrictions on admissible initial conditions. A closer inspection of the quantum effects coming from the polymerisation of the j-sector shows however that some specific choices may lead to particularly interesting features. These include the following two cases:

1) Linear mass relation and symmetric bounce

Let us consider the class of relations between the masses given by

$$M_{WH} = mM_{BH}\,, \tag{5.150}$$

with m a dimensionless number. For such mass relations, both kinds of quantum effects respectively due to the polymerisation of the k- and j-sectors can be interpreted as high curvature effects. Indeed, the first conditions in Eqs. (5.142) and (5.143) due to the j-polymerisation can be in general rewritten in terms of the Kretschmann scalar as curvature scales modulated by the mass asymmetry of the two sides, namely

$$\mathcal{K}_{cl}^{BH} = \frac{48M_{BH}^2}{b_+^6} \ll \frac{3}{4\lambda_k^2}\left(\frac{M_{WH}}{M_{BH}}\right)^2 \quad , \quad \mathcal{K}_{cl}^{WH} = \frac{48M_{WH}^2}{b_-^6} \ll \frac{3}{4\lambda_k^2}\left(\frac{M_{BH}}{M_{WH}}\right)^2 . \tag{5.151}$$

In particular for the mass relations (5.150), we have

$$\mathcal{K}_{cl}^{BH} \ll \frac{3m^2}{4\lambda_k^2} \quad , \quad \mathcal{K}_{cl}^{WH} \ll \frac{3}{4\lambda_k^2 m^2} \tag{5.152}$$

from which we see that, in agreement with the range of masses given in Eqs. (5.145) and (5.146),

[21] We also included the Weyl scalar $\mathcal{W}$ which is related to the other curvature invariants via the Ricci decomposition as explicitly written in the second equality of (5.149).

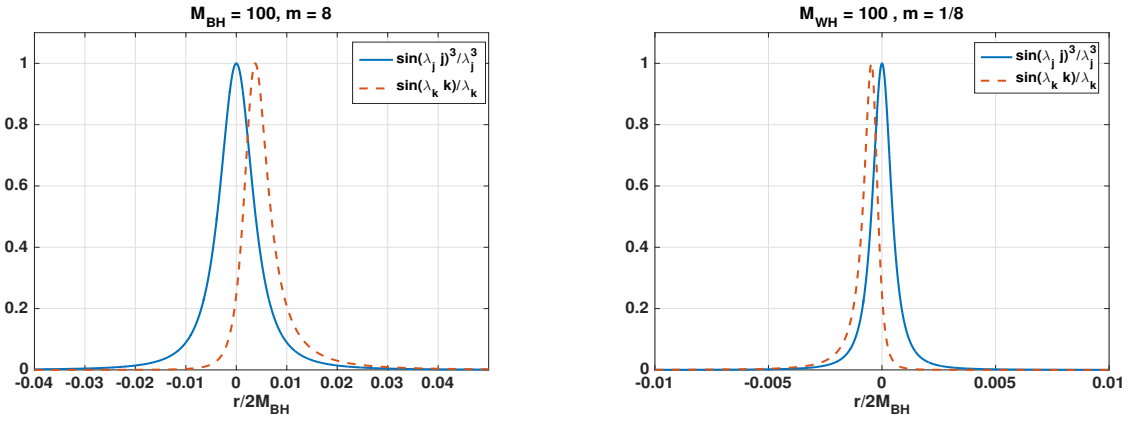

(a) (b)

Figure 5.10: $\sin(\lambda_j j)^3/\lambda_j^3$ compared to $\sin(\lambda_k k)/\lambda_k$ for $m = 8$ (a) and $m = 1/8$ (b). The parameters are $\lambda_j = \lambda_k = \mathscr{L}_o = 1$.

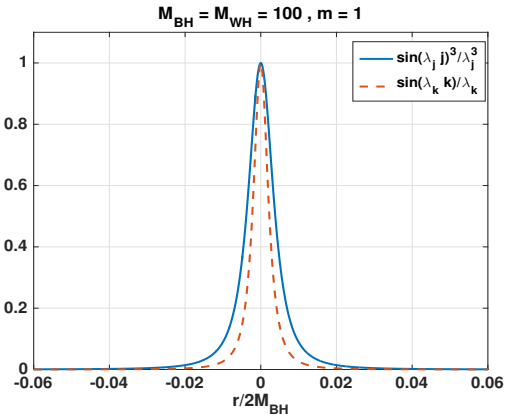

Figure 5.11: $\sin(\lambda_j j)^3/\lambda_j^3$ compared to $\sin(\lambda_k k)/\lambda_k$ for $m = 1$. The curve of j encloses completely k, i.e. the dominant contribution for quantum effects comes from j. Coming from both sides the onset of quantum effects is at the Kretschmann curvature scale $3/4\lambda_k^2$. Parameters are $\lambda_j = \lambda_k = \mathscr{L}_o = 1$

for $m = 8$ the new curvature scale on the BH side agrees with the curvature scale $\mathcal{K}_{\rm crit} = 48/\lambda_k^2$ of the k-sector (cfr. first relation in (5.144)), while the curvature scale of the j-sector on the WH side is smaller than the one of the k-sector (cfr. second relation in (5.144)) so that quantum effects of the j-sector become relevant first coming from the WH side. Similarly for $m = 1/8$, the situation on the two sides is exchanged, i.e. quantum effects of the j- and k-sectors match on the WH side while coming from the BH side j-sector quantum effects become relevant earlier. This exchange of quantum effects, graphically shown in Fig. 5.10, also explains the slightly different values of the maximal value of curvature invariants in the central strip of Fig. 5.8 and 5.9.

Of particular interest is then the case $m = 1$, which corresponds to a symmetric bounce ($M_{\rm BH} = M_{\rm WH}$). In this case, in fact, both types of quantum corrections perfectly align and appear at high curvatures. Moreover, as shown in Fig. 5.11, coming from both sides quantum effects of the j-sector become first relevant at the same Kretschmann curvature scale $3/4\lambda_k^2$ (cfr. Eqs. (5.152) with $m = 1$) followed by effects of the k-sector becoming relevant at the higher curvature scale $48/\lambda_k^2$ (cfr. Eqs. (5.144)).

2) Quadratic mass relation

Another interesting class of mass relations is given by

$$M_{WH} = \frac{M_{BH}^2}{m} \,, \tag{5.153}$$

where now m denotes a constant of dimension mass. In this case, as we can see from the expression of the integration constants (5.132) in terms of the masses, the integration constant D becomes mass independent and hence the on-shell value (5.120) of the momentum j is truly proportional to the angular components of the extrinsic curvature ($\sim 1/b$). Correspondingly, the first condition of (5.142) becomes

$$b_+ \gg (8\lambda_k m)^{\frac{1}{3}} \,, \tag{5.154}$$

thus yielding a proper length scale. Coming then from the BH side, for large masses with a quadratic mass amplification (5.153) at the bounce, quantum effects coming from the k-polymerisation become relevant at the Kretschmann curvature scale $\mathcal{K}_{\text{crit}} = 48/\lambda_k^2$ followed by finite 2-sphere area effects coming from the j-polymerisation at the length scale $\ell_{\text{crit}} = (8m\lambda_k)^{\frac{1}{3}}$. Similarly, for the corresponding mass de-amplification $M_{BH} = \frac{M_{WH}^2}{m}$, the same considerations hold true coming from the WH side as we can see from the first condition in (5.143).

To sum up, although the present model leads to physically reasonable predictions for the whole range of masses allowed by the validity of an effective polymer-like description with no specific restrictions on the initial conditions, the above two cases given by Eq. (5.150) with $m = 1$ and Eq. (5.153) seem to be physically special. The first option corresponds to a symmetric bounce with a unique onset of quantum effects on both sides. The second option, instead, leads to sensible finite 2-sphere area effects coming from the j-sector and allows for a true distinction between high curvature and small length quantum effects. Further insights on which mass relation would lead to sensible outcomes require additional inputs. These may be found by studying for instance the phenomenological implications of the effective spacetime described by the model such as the resulting quantum corrected black hole thermodynamics or going beyond the effective semiclassical description to consider the underlying quantum theory where one can try to address the question using wave packets and BH-to-WH transition amplitudes. We are currently investigating both aspects and some preliminary results in such directions are discussed in the next chapter.

Chapter 6

Some Work in Progress

Before moving at the conclusions of this work, we would like to discuss some further aspects about the models of quantum black holes presented in the previous chapter. In this last chapter we will then collect some preliminary results about ongoing research directions.

Remaining at the effective level, these concern two aspects. First of all, as anticipated at the end of Ch. 5, the effective polymer model for Schwarzschild black holes based on (v_k, k, v_j, j)-variables allows to overcome previous undesirable features without imposing any restriction on admissible initial conditions for the effective dynamics so that the black and white hole masses can be in principle freely specified. However, among all possible mass relations, the cases of a symmetric bounce and a quadratic mass relation have somehow a special role leading to sensible results about the physical interpretation of the nature of quantum effects. Given this situation, the following questions naturally arise: Can the masses be further specified by means of phenomenological considerations such as the analysis of thermodynamic quantities for our quantum corrected black hole? Do they confirm the special role of the above two cases? In the first part of the chapter, we will then study the quantum corrected thermodynamics resulting from our model. In particular, as we will discuss, the case of a quadratic mass relation turns out to be phenomenologically preferred in the sense that it leads to logarithmic corrections to the horizon entropy as expected also from other QG approaches. Second, since the classical Schwarzschild geometry gets now modified by quantum corrections, the thermodynamic analysis also gives us the opportunity to check whether our effective models are compatible with the entropy-area spherical bound discussed in Ch. 1.

In the second part of the chapter, instead, we leave the effective description and take the first steps in the construction of the quantum theory from which the polymer effective dynamics is expected to emerge. As anticipated in Ch. 5, the exceptionally simple structure of the Hamiltonian of both our models allows us to solve the resulting quantum Hamiltonian constraint and determine the solution for physical states in closed form thus suggesting that the quantum theory might be under analytic control.

Finally, coming back to our original motivations of using effective quantum corrected geometries motivated by LQG in the AdS/CFT framework, we close the chapter by discussing a possible

canonical phase space formulation for Schwarzschild-AdS black holes in generic dimensions and comment on possible subtleties that may arise when polymerising the model.

6.1 Quantum Corrected Black Hole Thermodynamics

In this section we perform the thermodynamic analysis of the effective quantum corrected models for stationary spherically symmetric Schwarzschild black holes discussed in Ch. 5 [226]. As our main interest relies on understanding whether certain relations between the black and white hole masses can be selected by studying the thermodynamic properties of our effective geometries, we will focus on the second model discussed in Secs. $5.6-5.8$ whose validity does not require to specify a priori any mass relation[1]. Specifically, in what follows, we do not aim at a full derivation of thermodynamic quantities like Hawking temperature, horizon entropy, and specific heat – which would require the study of quantum fields over a polymer black hole background or equivalently a saddle point analysis of the corresponding gravitational path integral – but rather we are interested in studying the quantum corrections to classical thermodynamics coming from the effective quantum-corrected metric (5.124)-(5.126). Our strategy is then to start with the standard definitions of thermodynamic quantities for black holes [1–4, 159, 227] and specify them for our quantum corrected metric. This can be heuristically motivated as follows. As we have discussed in Ch. 5, quantum gravity effects are negligible in the low curvature regime so that already at the horizon the geometry is well approximated by the classical description plus subleading quantum corrections, at least for large masses for which the effective description is most reliable (cfr. Eqs. (5.137) and (5.138)). Therefore, one would expect also the thermodynamic properties of the quantum corrected horizon to be well approximated by the classical results at leading order. This will also give us the opportunity to check whether the quantum corrections to the spacetime geometry are compatible with the general discussion on black hole physics given in Ch. 1. In particular, we do not assume a priori any entropy-area relation and instead compute the horizon entropy by integrating the first law of BH mechanics. Looking then at the large mass expansion of the resulting thermodynamical quantities, we can check to which extent the entropy-area law is satisfied. Moreover, being effective models of quantum black holes in general valid for macroscopic black holes, this will allow us also to compare and contrast our results with other effective models relying on different QG approaches.

6.1.1 Temperature

Assuming the no-hair theorem [159, 227] to be valid, effective quantum corrected black holes would be also characterized only by three macroscopic quantities: the mass, the angular momen-

[1] We repeated the analysis also for our first model for which the relation between the masses has been already fixed in Sec. 5.4 via physical considerations about curvature invariants and the onset of quantum effects. In this case, one could in principle check whether the selected mass relation would lead to reasonable results from the thermodynamics point of view and eventually compare with other models available in the literature. Although for brevity we do not include the explicit computations here, the qualitative behaviour of the thermodynamic quantities is the same and the classical results are reproduced at leading order in the large mass expansions. The form of the quantum corrections is however different so that a comparison with the literature would require a case by case study which goes beyond the purposes of the present section.

tum and the charge. In our case, since the geometry is a quantum modification of the static, neutral, non-rotating Schwarzschild black hole, there is no charge nor angular momentum and the only relevant quantity is the mass. The First Law of black hole mechanics then reads

$$\mathrm{d}M = T\mathrm{d}S, \tag{6.1}$$

where M is the mass, S the horizon entropy, and T the Bekenstein-Hawking temperature. As anticipated above, we will compute the entropy by integrating Eq. (6.1) as a function of the mass. The starting point for our thermodynamic analysis is then to compute the temperature as a function of the mass. To this aim, let us recall that the Bekenstein-Hawking temperature is related to the surface gravity via the relation

$$T = \frac{\kappa}{2\pi}\,, \tag{6.2}$$

where the surface gravity κ is defined by $\kappa^2 = -g^{\mu\nu}g_{\rho\sigma}\nabla_\mu\chi^\rho\nabla_\nu\chi^\sigma/2 = -g^{\mu\nu}g_{\rho\sigma}\Gamma^\rho_{\mu 0}\Gamma^\sigma_{\nu 0}/2$, with $\chi^\mu = (1,0,0,0)$ being a time-like Killing vector, and $\Gamma^\mu_{\nu\rho}$ being the Christoffel symbols associated to the connection compatible with the effective metric (5.124)-(5.126). Following previous work on effective quantum corrected black holes derived from various approaches (see e.g. [228, 229]), to compute (6.2) it is convenient to bring our static spherically symmetric metric in the general form

$$\mathrm{d}s^2 = -f(r)\mathrm{d}v^2 + 2h(r)\mathrm{d}v\mathrm{d}r + b^2(r)\mathrm{d}\Omega_2^2\,, \tag{6.3}$$

for which the surface gravity at the horizon reads as

$$\kappa^2 = \left(\frac{f(r)'}{2h(r)}\right)^2\Bigg|_{r=r_s}\,, \tag{6.4}$$

where primes denote derivatives w.r.t. r and r_s denote the radial coordinate of the horizon. As we have discussed in Ch. 5, our effective spacetime is characterised by two horizons respectively corresponding to the black and white hole sides. The computation of the thermodynamic quantities can be then specified for both horizons. In what follows we focus on the black hole side for which the horizon is located at $r = r_s^{(+)}$ given in Eq. (5.135)[2]. Moreover, as we are interested in studying the mass dependence of T and the other thermodynamic quantities, let us first rewrite the metric (5.124)-(5.126) in terms of the masses. This can be done by plugging the expressions (5.132) for the integration constants C, D in terms of $M_{\rm BH}$ and $M_{\rm WH}$ into the metric coefficients (5.125), (5.126) so that the line element (5.124) becomes

$$\mathrm{d}s^2 = -\frac{a(x)}{\lambda_j^2}\mathrm{d}\bar{t}^2 + \frac{\lambda_j^2}{a(x)}\mathrm{d}x^2 + b(x)^2\mathrm{d}\Omega_2^2\,, \tag{6.5}$$

where $x = \mathscr{L}_o r/\lambda_j$, $\bar{t} = \lambda_j t/L_o$, and

[2]By the symmetry arguments on the evolution through the Penrose diagram given at the end of Sec. 5.5 and 5.7, we expect the corresponding analysis of the WH side to be the same with the role of black and white hole masses exchanged. In particular, for any given mass amplification or de-amplification, the WH thermodynamics should match the results of the BH side for the corresponding inverse mass de-amplification or amplification.

$$b^2(x) = \frac{1}{2}\left(\frac{\lambda_k}{M_{BH}M_{WH}}\right)^{\frac{2}{3}} \frac{1}{\sqrt{1+x^2}} \frac{M_{BH}^2\left(x+\sqrt{1+x^2}\right)^6 + M_{WH}^2}{\left(x+\sqrt{1+x^2}\right)^3}\,, \tag{6.6}$$

$$\frac{a(x)}{\lambda_j^2} = 2\left(\frac{M_{BH}M_{WH}}{\lambda_k}\right)^{\frac{2}{3}}\left(1-\left(\frac{M_{BH}M_{WH}}{\lambda_k}\right)^{\frac{1}{3}}\frac{1}{\sqrt{1+x^2}}\right)\frac{\left(1+x^2\right)^{\frac{3}{2}}\left(x+\sqrt{1+x^2}\right)^3}{M_{BH}^2\left(x+\sqrt{1+x^2}\right)^6+M_{WH}^2}\,. \tag{6.7}$$

Note that λ_j appears in the line element just as a rescaling of the coordinates. Hence, its precise value can not have any physical meaning and consistently in our later computations it will not appear in any physical quantity.

Recalling now from Sec. 5.7 the coordinate rescaling necessary to recover the classical Schwarzschild solution in the asymptotic $r \to +\infty$ limit (cfr. Eq. (5.127)), i.e.

$$\tilde{r} = \sqrt{\frac{D\lambda_j^2}{\mathscr{L}_0^3}}x \qquad , \qquad \tau = \sqrt{\frac{\mathscr{L}_0^3}{D\lambda_j^2}}\bar{t} \tag{6.8}$$

the resulting line element

$$ds^2 = -\frac{a(\tilde{r})}{\mathscr{L}_0^3}Dd\tau^2 + \frac{\mathscr{L}_0^3}{Da(\tilde{r})}d\tilde{r}^2 + b^2(\tilde{r})d\Omega_2^2, \tag{6.9}$$

can be brought into the form (6.3) by using the null coordinate

$$v = \tau + r^* \qquad \text{with} \qquad r^* = \int^{\tilde{r}} \frac{\mathrm{d}\tilde{r}}{\mathfrak{a}(\tilde{r})} \quad , \quad \mathfrak{a}(\tilde{r}) := \frac{a(\tilde{r})D}{\mathscr{L}_0^3} \tag{6.10}$$

such that $\mathrm{d}v = \mathrm{d}\tau + \mathrm{d}\tilde{r}/\mathfrak{a}(\tilde{r})$ and we find

$$f(\tilde{r}) = \frac{D}{\mathscr{L}_o^3}a(\tilde{r}) \qquad , \qquad h(\tilde{r}) = 1\,. \tag{6.11}$$

Eq. (6.4) then becomes

$$\kappa = \frac{D}{2\mathscr{L}_o^3}|a'(\tilde{r})|\Big|_{r=r_s^{(+)}}\,, \tag{6.12}$$

where primes here denote derivatives w.r.t. r. Using now the chain rule and the expression (6.8) for $\tilde{r}$, we have

$$\frac{D}{\mathscr{L}_0^3}\frac{\mathrm{d}a(\tilde{r})}{\mathrm{d}r} = \frac{D}{\mathscr{L}_0^3}\frac{\mathrm{d}a}{\mathrm{d}x}\frac{\mathrm{d}x}{\mathrm{d}\tilde{r}} = \frac{1}{\lambda_j}\sqrt{\frac{D}{\mathscr{L}_0^3}}\frac{\mathrm{d}a}{\mathrm{d}x} = \frac{2}{\lambda_j^2}\left(\frac{\lambda_k M_{BH}^2}{M_{WH}}\right)^{\frac{1}{3}}\frac{\mathrm{d}a}{\mathrm{d}x}\,, \tag{6.13}$$

where in the last equality we used the expression (5.132) of D in terms of the masses. Finally, using the horizon condition

$$a(x_+) = a(x(r_s^{(+)})) = 0 \qquad \overset{(6.7)}{\Longrightarrow} \qquad x_+ = \sqrt{\left(\frac{M_{BH}M_{WH}}{\lambda_k}\right)^{\frac{2}{3}} - 1}\,, \tag{6.14}$$

the derivative of $a(x)$ given in (6.7) evaluated at the BH horizon yields

$$\left.\frac{da}{dx}\right|_{x_+} = \lambda_j^2(1+x^2)\left(\frac{M_{BH}M_{WH}}{\lambda_k}\right)^{\frac{1}{3}}\frac{x}{(1+x^2)^{3/2}}\frac{1}{b^2(x)}\bigg|_{x_+} = \lambda_j^2\frac{x_+}{b^2(x_+)}\,, \tag{6.15}$$

so that, inserting the result together with (6.13) into (6.12), we get

$$\kappa = \left(\frac{\lambda_k M_{BH}^2}{M_{WH}}\right)^{\frac{1}{3}}\frac{x_+}{b^2(x_+)} \qquad \overset{(6.2)}{\Longrightarrow} \qquad T = \frac{1}{2\pi}\left(\frac{\lambda_k M_{BH}^2}{M_{WH}}\right)^{\frac{1}{3}}\frac{x_+}{b^2(x_+)}\,. \tag{6.16}$$

As shown in Fig. 6.1, for $\lambda_k \to 0$ or more precisely for large masses $M_{BH}M_{WH} \gg \lambda_k$, $x_+ \sim (M_{BH}M_{WH}/\lambda_k)^{1/3}$ (cfr. Eq. (6.14)) and $b(x_+) \sim 2M_{BH}$ (cfr. Eq. (5.137)) so that the classical result $T \sim \frac{1}{8\pi M_{BH}}$ is recovered. On the other hand, unlike the classical result which diverges for the horizon radius approaching the Planck regime, the quantum corrected temperature reaches a maximum value where quantum effects get relevant and, continuing to smaller sizes, cools down and vanishes when M_{BH} reaches the critical value $M_c = \frac{\lambda_k}{M_{WH}}$ ($x_+ = 0$ cfr. Eq. (6.14)) for which the horizon reaches its minimal size at the transition surface. As discussed also in other models [228–230], such a critical configuration corresponds to an extremal non-radiating small objects of genuine quantum gravitational character which in our case case can be though of as a white hole remnant of mass $M_{WH} = \frac{\lambda_k}{M_c}$ in a similar spirit to previous LQG proposals [199].

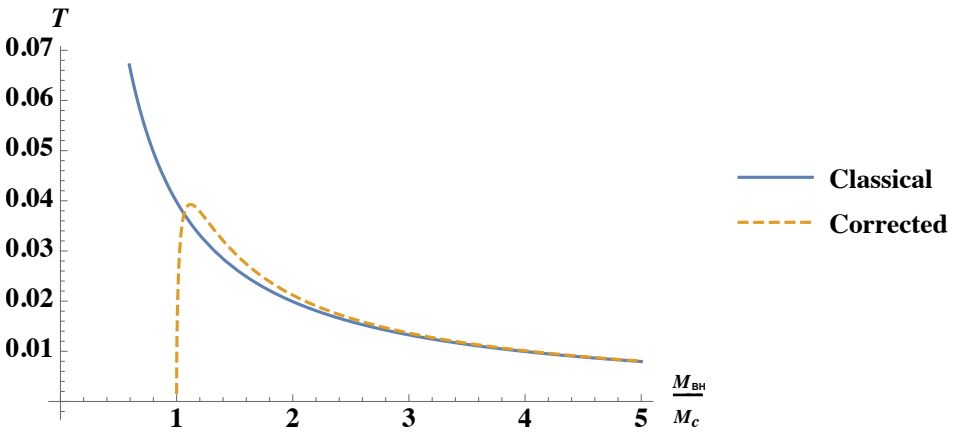

Figure 6.1: Plot of the temperature as a function of the BH mass. The solid line represents the quantum corrected result (6.16), while the dashed line is the classical result $T = 1/8\pi M_{BH}$. As it will be relevant later, the plot for the quantum corrected case refers to the mass relation $M_{WH} = M_{BH}^2/m$, with $[m] = M$, and we set the parameters to $\lambda_k = m = 1$.

To make the comparison with the classical case and the role of quantum corrections more transparent, let us consider the large mass expansion of the temperature. To this aim, recalling the full expression (5.136) for the horizon areal radius, Eq. (6.16) can be written more explicitly as

$$T = \frac{M_{BH}}{\pi}\frac{\sqrt{1-y^2}}{\left(M_{BH}^2 f(y)^3 + \frac{\lambda_k}{M_{BH}^2}\frac{1}{f(y)^3}\right)}\,, \tag{6.17}$$

where we introduced the shorthand notations

$$y := \left(\frac{\lambda_k}{M_{BH}M_{WH}}\right)^{\frac{1}{3}} = \left(\frac{M_c}{M_{BH}}\right)^{\frac{1}{3}} \qquad , \qquad f(y) := 1 + \sqrt{1-y^2}\,. \tag{6.18}$$

Expanding then (6.17) around $y = 0$, which corresponds to a large $M_{BH}M_{WH}$ expansion (say $M_{BH}M_{WH} \gg \lambda_k$ i.e. $M_{BH} \gg M_c$), we get

$$T = \frac{1}{8\pi M_{BH}}\left(1 + \frac{y^2}{4} + \mathcal{O}(y^4)\right) , \tag{6.19}$$

from which we see that the classical result is reproduced at leading order and quantum corrections go to zero for large masses or equivalently as $\lambda_k \to 0$.

6.1.2 Specific Heat

To compute the specific heat $C = \frac{\mathrm{d}M_{BH}}{\mathrm{d}T}$, we can differentiate the expression for the quantum corrected temperature w.r.t. to M_{BH} and then reverse the result. To this aim, we need to take into account the fact that the mass dependence occurs in the expression (6.16) both explicitly via M_{BH} and implicitly into y via M_{WH}, the latter being thought of as a generic function $M_{WH}(M_{BH})$. Keeping then the relation between M_{WH} and M_{BH} unspecified, we have

$$\frac{1}{C} = \frac{\mathrm{d}}{\mathrm{d}M_{BH}}T\Big(M_{BH}, y(M_{BH})\Big) = \frac{\partial T}{\partial M_{BH}} + \frac{\partial T}{\partial y}\frac{\partial y}{\partial M_{BH}} , \tag{6.20}$$

with

$$\frac{\partial y}{\partial M_{BH}} = \frac{\partial}{\partial M_{BH}}\left(\frac{\lambda_k}{M_{BH}M_{WH}}\right)^{\frac{1}{3}} = -\frac{1}{3}\frac{\lambda_k^{1/3}}{(M_{BH}M_{WH})^{4/3}}\left(M_{WH} + M_{BH}\frac{\partial M_{WH}}{\partial M_{BH}}\right) . \tag{6.21}$$

Thus, using the expression (6.16) of T to explicitly compute the derivatives in (6.20), we get

$$\frac{1}{C} = \frac{T}{M_{BH}}\left[1 - 2\frac{G^-(y)}{G^+(y)} + \frac{1-\sqrt{1-y^2}}{1-y^2}\left(\frac{f(y)}{3} - \sqrt{1-y^2}\frac{G^-(y)}{G^+(y)}\right)\left(1 + \frac{M_{BH}}{M_{WH}}\frac{\partial M_{WH}}{\partial M_{BH}}\right)\right] \tag{6.22}$$

where

$$G^{\pm}(y) := M_{BH}^2 f(y)^3 \pm \frac{\lambda_k}{M_{BH}^2 f(y)^3} . \tag{6.23}$$

The behaviour of C as a function of M_{BH} is shown in Fig. 6.2. As we can see from the plot, for small masses, the quantum corrected curve significantly deviates from the classical one. Indeed, a divergence occurs when the temperature reaches its maximum ($\mathrm{d}T/\mathrm{d}M_{BH} = 0$ and hence $1/C$ in (6.20) also vanishes). Such a discontinuity in the specific heat separates a regime in which $C < 0$ from a regime in which $C \geq 0$ with $C = 0$ for $M_{BH} = M_c$ and can be interpreted as signaling a phase transition from large thermodynamically unstable black holes to small stable quantum black holes [3, 228–230]. For large masses, although this is not explicitly visible from the plot 6.2 where we focused on masses close to the critical value to zoom on the quantum corrected behaviour, the classical behaviour is approached. This can also be seen by expanding (6.22) around $y = 0$ (or equivalently $M_{BH}M_{WH} \gg \lambda_k$ i.e. $M_{BH} \gg M_c$) thus yielding

$$C \simeq -8\pi M_{BH}^2\left[1 - \frac{1}{6}\left(\frac{5}{2} + \frac{M_{BH}}{M_{WH}}\frac{\partial M_{WH}}{\partial M_{BH}}\right)y^2 + \dots\right] , \tag{6.24}$$

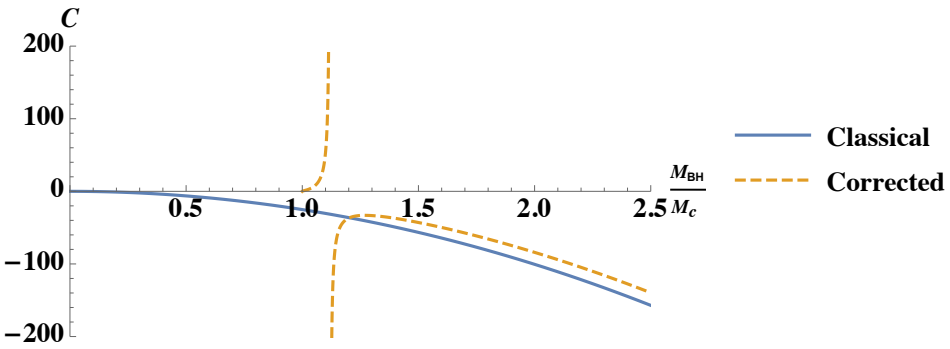

Figure 6.2: Plot of the specific heat as a function of the BH mass. The solid line represents the quantum corrected result, while the dashed line is the classical result $C = -8\pi M_{BH}^2$. As before, the quantum corrected plot refers to the mass relation $M_{WH} = M_{BH}^2/m$ and we set $\lambda_k = m = 1$.

which is again the classical result plus quantum corrections going to zero as $\lambda_k \to 0$.

6.1.3 Entropy, Mass Relation, and Logarithmic Corrections

We can finally proceed to compute the entropy of our quantum corrected black hole by integrating the first law (6.1). This provides us with the expression of the BH entropy in terms of the ADM energy which in the case under consideration amounts to

$$S = \int_{M_c}^{M_{BH}} \frac{\mathrm{d}M_{BH}}{T} \,. \tag{6.25}$$

The evaluation of the integral (6.25) with $T(M_{BH})$ given in (6.16) requires the help of computer algebra. The behaviour of the result obtained by using `Mathematica` is reported in Fig. 6.3. As we can see from the plot (b), there classical behaviour is approached for large masses, while by construction the entropy of the quantum corrected black hole becomes zero for $M_{BH} = M_c$ (cfr. Fig. 6.3 (a)). The critical configuration is then characterised by vanishing temperature and vanishing entropy, thus confirming its interpretation as a thermodynamically stable extremal remnant of the black hole life cycle shared also by other approaches to quantum BHs [228–230]. Moreover, the quantum corrected entropy is smaller than the classical result thus suggesting that the spherical entropy bound (1.4) is not violated by quantum corrections. To see this more explicitly, let us consider again a large mass expansion of the integral (6.25). Specifically, recalling the expansion (6.19), we have

$$\begin{aligned} S &\simeq \int_{M_c}^{M_{BH}} \mathrm{d}M_{BH}\, 8\pi M_{BH} \left(1 - \frac{y^2}{4} + \frac{y^6}{64} + \dots\right) \\ &= 4\pi(M_{BH}^2 - M_c^2) - 2\pi \int_{M_c}^{M_{BH}} \mathrm{d}M_{BH} \left(\frac{\lambda_k^2 M_{BH}}{M_{WH}^2}\right)^{\frac{1}{3}} + \frac{\pi}{8} \int_{M_c}^{M_{BH}} \mathrm{d}M_{BH} \left(\frac{\lambda_k^2}{M_{BH} M_{WH}^2}\right) + \cdots \end{aligned} \tag{6.26}$$

from which we see that as expected the classical result is obtained at leading order, with $4\pi r_s^2 = 16\pi M_{BH}^2$ (resp. $4\pi r_c^2 = 16\pi M_c^2$) being the classical horizon area of a black hole of

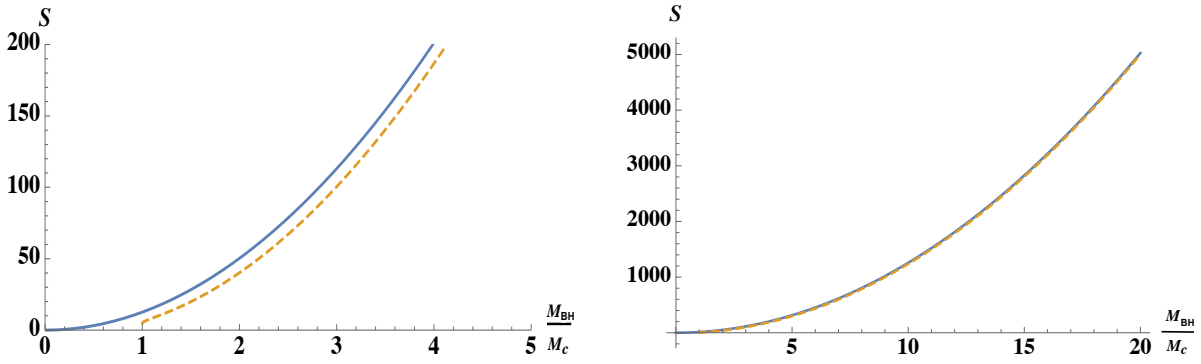

(a) (b)

Figure 6.3: Plot of the horizon entropy as a function of the BH mass. The quantum corrected entropy (dashed orange line) vanishes for $M_{BH} = M_c$ (a), while it approaches the classical result (solid blue line) for large masses (b). For the quantum corrected plot we choose $M_{WH} = M_{BH}^2/m$ and the parameters $\lambda_k = m = 1$.

mass M_{BH} (resp. M_c which goes to zero in the classical limit $\lambda_k \to 0$). Higher order terms yield quantum corrections which goes to zero in the classical limit and the relative errors w.r.t. the leading order get smaller as the mass increases[3]. In particular, we note that for a quadratic mass relation of the kind $M_{WH} = M_{BH}^2/m$ with $[m] = M$, Eq. (6.26) gives

$$S = 4\pi(M_{BH}^2 - M_c^2) - 2\pi\,(m\lambda_k)^{\frac{2}{3}} \log\left(\frac{M_{BH}}{M_c}\right) - \mathcal{O}\left(\frac{m^2\lambda_k^2}{M_{BH}^4}\right) , \tag{6.27}$$

or written in terms of the horizon area

$$S \simeq \frac{1}{4}(A - A_c) - \pi\,(m\lambda_k)^{\frac{2}{3}} \log\left(\frac{A}{A_c}\right) . \tag{6.28}$$

Therefore, for such a quadratic mass relation, the quantum corrections are in agreement with the expectations of a logarithmic term as a next to leading order correction to the classical Bekenstein-Hawking area law from all the major approaches to quantum gravity, both at the effective and full theory level [231–243]. It is quite remarkable that for our model this is the case exactly for the special kind of mass relation discussed at the end of Ch. 5 (cfr. Eq. (5.153)) for which there is a strict distinction between high curvature and small length quantum effects originating from the k- and the j-polymerisation, respectively. Whether something more fundamental may be hidden behind this result is not yet clear to us and further investigations are necessary. In this respect, a better understanding of the deep quantum regime as well as to strengthen the connections with similar results obtained from other approaches may shed some light on their physical interpretation. In [230], for instance, the extremal critical configuration has been interpreted as a Planckian holographic screen which in turn provides the fundamental quantum of area entering the expression of a discretised mass spectrum. It would be interesting to check whether such a viewpoint can be implemented in our setting and if the outcome would

[3]This is also compatible with the generalised second law discussed in Sec. 1.1.1. In fact, interpreting the quantum corrections as due to effective matter as discussed in Sec. 5.5 (see footnote p. 108), the difference between the entropies of our BH of mass M_{BH} and of its final critical stage yields $0 \leq S(M_{BH}) - S(M_c) \leq S_{BH}^{(\text{classical})} - S_{\text{eff.matter}}$.

be compatible with the spectrum of the mass observable resulting from the quantisation of our model. To this aim a full understanding of the quantum theory underlying our effective model would be necessary. The first steps of its construction will be sketched in the next section.

6.2 Polymer Schwarzschild Black Holes: Quantum Theory

Let us now discuss a possible polymer quantisation of our BH models from which the effective equations discussed in Ch. 5 are expected to emerge. As we will see in this section, the quantum theory can be constructed via similar steps as those of LQC [118, 155, 244] and presented in Ch. 3 (cfr. Sec. 3.2). In particular, the kernel of the Hamiltonian constraint operator can be found in closed form, which suggests that a complete analytic control of the quantum theory may be possible. Following our paper [209], here we will mainly focus on the first model based on the variables (v_1, P_1, v_2, P_2) for which the configuration variables v_1 and v_2 have a simpler interpretation in terms of the metric coefficients. However, since the Hamiltonian takes the same form in both our models, the main steps of the construction can be applied to both of them and the corresponding quantum theory for the second model can be formally obtained by replacing $P_1 \leftrightarrow k, v_1 \leftrightarrow v_k, P_2 \leftrightarrow j, v_2 \leftrightarrow v_j$. As we will briefly mention in the following, some considerations based on the geometric interpretations of the canonical variables are of course different for the two models.

As discussed in Ch. 3, the first steps for building up the quantum theory can be summarised as follows: 1) Construct the kinematical Hilbert space carrying a representation of the canonical variables as elementary operators, the latter being weakly discontinuous in the momenta; 2) Promote the effective Hamiltonian to a quantum operator by choosing a suitable factor ordering; 3) Solve the kernel of the Hamiltonian constraint operator to determine the physical states.

Let us discuss them more explicitly. As for the first step, similarly to the discussion of the LQC kinematics of Sec. 3.2.1, the kinematical Hilbert space is spanned by the volume eigenstates $|v_1, v_2\rangle$ on which the operators corresponding to v_1, v_2 and $\exp(-inP_1), \exp(-inP_2)$, $n \in \mathbb{Z}$, act respectively as multiplication and displacement operators, say[4]

$$\begin{aligned} \hat{v}_1 |v_1, v_2\rangle &= v_1 |v_1, v_2\rangle \quad , \quad \widehat{e^{-inP_1}} |v_1, v_2\rangle = |v_1 + n, v_2\rangle \ , \\ \hat{v}_2 |v_1, v_2\rangle &= v_2 |v_1, v_2\rangle \quad , \quad \widehat{e^{-inP_2}} |v_1, v_2\rangle = |v_1, v_2 + n\rangle \ . \end{aligned} \tag{6.29}$$

A generic state can be then decomposed as

$$|\chi\rangle = \sum_{v_1, v_2 \in \mathbb{Z}} \tilde{\chi}(v_1, v_2) |v_1, v_2\rangle \ , \tag{6.30}$$

and the elements of the Hilbert space can be realised as square integrable functions $\tilde{\chi}(v_1, v_2)$, $v_1, v_2 \in \mathbb{Z}$, w.r.t. to the scalar product

[4] As for the case of LQC, also here a generalisation to the Bohr compactification of the real line can be done by standard techniques [110], thus allowing for arbitrary real non-zero values of the representation labels.

$$\langle\chi_1|\chi_2\rangle = \sum_{v_1,v_2\in\mathbb{Z}} \overline{\tilde{\chi}_1(v_1,v_2)}\tilde{\chi}_2(v_1,v_2)\ . \tag{6.31}$$

Recalling now the effective Hamiltonian (5.33) given by

$$H_{\text{eff}} = \sqrt{n}\,\mathcal{H}_{\text{eff}} \quad , \quad \mathcal{H}_{\text{eff}} = 3v_1\frac{\sin(\lambda_1 P_1)}{\lambda_1}\frac{\sin(\lambda_2 P_2)}{\lambda_2} + v_2\frac{\sin(\lambda_2 P_2)^2}{\lambda_2^2} - 2 \approx 0\ , \tag{6.32}$$

we note that H_{eff} is at most quadratic in the polymerised momenta and there are no inverse powers involved. This implies that it can be easily promoted to an operator on the kinematical Hilbert space, up to factor ordering issues. In particular, a comparison with the techniques developed in the context of LQC [113,153,154] suggests us to work with a lapse such that $\sqrt{n} = v_2$, corresponding to a density weight 2 Hamiltonian[5], and to choose the following symmetric ordering

$$\begin{aligned} H_{\text{eff}} = 3\sqrt{v_1}&\left(\frac{\sin(\lambda_1 P_1)}{2\lambda_1}\text{sgn}(v_1) + \text{sgn}(v_1)\frac{\sin(\lambda_1 P_1)}{2\lambda_1}\right)\sqrt{v_1} \\ &\times\sqrt{v_2}\left(\frac{\sin(\lambda_2 P_2)}{2\lambda_2}\text{sgn}(v_2) + \text{sgn}(v_2)\frac{\sin(\lambda_2 P_2)}{2\lambda_2}\right)\sqrt{v_2} + \\ +\left(\sqrt{v_2}\right.&\left.\left(\frac{\sin(\lambda_2 P_2)}{2\lambda_2}\text{sgn}(v_2) + \text{sgn}(v_2)\frac{\sin(\lambda_2 P_2)}{2\lambda_2}\right)\sqrt{v_2}\right)^2 - 2v_2 \approx 0\ , \end{aligned} \tag{6.33}$$

where we omitted for simplicity the operator hat notation. The action of the operator (6.33) on the basis states $|v_1,v_2\rangle$ can be computed by using the spectral decomposition for the square root operators and decomposing the sin functions in terms of exponentials so that, using the action (6.29) of the elementary operators, we have

$$\begin{aligned} \widehat{\frac{\sin(\lambda_2 P_2)}{\lambda_2}}\widehat{\sqrt{v_2}}\,|v_1,v_2\rangle &= \frac{\sqrt{v_2}}{2i\lambda_2}\left(\widehat{e^{i\lambda_2 P_2}} - \widehat{e^{-i\lambda_2 P_2}}\right)|v_1,v_2\rangle \\ &= \frac{\sqrt{v_2}}{2i\lambda_2}\Big(|v_1,v_2-\lambda_2\rangle - |v_1,v_2+\lambda_2\rangle\Big)\ , \end{aligned} \tag{6.34}$$

and similarly for the analogous term involving $\sin(\lambda_1 P_1)/\lambda_1$ and v_1. A lengthy but straightforward calculation leads then to the following difference equation

$$\begin{aligned} H_{\text{eff}}\,|v_1,v_2\rangle = -\frac{3}{\lambda_1\lambda_2}\Big(&\sqrt{|v_1(v_1-\lambda_1)|}\sqrt{|v_2(v_2-\lambda_2)|}\,|v_1-\lambda_1,v_2-\lambda_2\rangle + \\ &-\sqrt{|v_1(v_1+\lambda_1)|}\sqrt{|v_2(v_2-\lambda_2)|}\,|v_1+\lambda_1,v_2-\lambda_2\rangle + \\ &-\sqrt{|v_1(v_1-\lambda_1)|}\sqrt{|v_2(v_2+\lambda_2)|}\,|v_1-\lambda_1,v_2+\lambda_2\rangle + \\ &-\sqrt{|v_1(v_1+\lambda_1)|}\sqrt{|v_2(v_2+\lambda_2)|}\,|v_1+\lambda_1,v_2+\lambda_2\rangle\Big) + \\ -\frac{|v_2-\lambda_2|}{\lambda_2^2}&\sqrt{|v_2(v_2-2\lambda_2)|}\,|v_1,v_2-2\lambda_2\rangle + \\ -\frac{|v_2+\lambda_2|}{\lambda_2^2}&\sqrt{|v_2(v_2+2\lambda_2)|}\,|v_1,v_2+2\lambda_2\rangle + 2v_2\left(\frac{v_2}{\lambda_2^2}-1\right)|v_1,v_2\rangle\ , \end{aligned} \tag{6.35}$$

[5]Recalling the transformation behaviour (5.16) of the canonical variables under fiducial cell rescaling $\mathscr{L}_0 \mapsto \alpha\mathscr{L}_0$, v_2 scales with α^2 so that its density weight in t-direction is 2.

which is the analogue of Eq. (3.53) for LQC, but with a more complicated structure due to the more involved form of the Hamiltonian. The above difference equation (6.35) shows that the factor ordered Hamiltonian (6.33) preserves the lattice with support on $c_i + \lambda_i n$, $n \in \mathbb{Z}$, $c_i \in \{0, 1\}$, $i = 1, 2$. In particular, since all the coefficients in Eq. (6.35) vanish for $v_2 = 0$, the ordering (6.33) ensures that states $|v_1, 0\rangle$ and in particular the zero volume state $|0, 0\rangle$ are annihilated by the Hamiltonian constraint operator. Note that $|0, v_2\rangle$ states are in general not annihilated. To get some intuition on what is going on, let us recall the classical geometric expressions of v_1 and v_2 in terms of the metric coefficients a and b, i.e. $v_1 = 2b^3/3$ and $v_2 = 2ab^2$ (cfr. Eq. (5.14)). The condition $v_1 = 0$ implies that $b = 0$ and consequently also v_2 vanishes so that the state $|0, 0\rangle$ would correspond to the singularity and there is no contradiction with $|0, v_2\rangle$ not being annihilated by the Hamiltonian. On the other hand, v_2 also vanishes at the horizon where $a = 0$ (but b and hence v_1 are not zero). Therefore, $|v_1, 0\rangle$ states would be naively interpreted as horizon states with different masses[6]. As we will discuss below, reality of our phase space variables restrict us to either the interior or the exterior of the black hole so that $a = 0$ is avoided.

Moreover, coming back to Eq. (6.35), non-zero volume states are not mapped to zero volumes thus leading to a dynamical decoupling of the zero volume sector. Also, positive and negative volume sectors are not mapped into each other. In particular, as it will turn useful in a while to perform a Fourier transform into the (P_1, P_2)-representation, the choice $\lambda_1 = \lambda_2 = 2$ leads to four dynamically selected subsectors $v_i \in 2\mathbb{Z} + c_i$, $c_i \in \{0, 1\}$, $i = 1, 2$. We choose the subsector containing $|0, 0\rangle$.

As discussed in Sec. 3.2.2 for the case of LQC, in order to determine the kernel of the Hamiltonian constraint operator, we need to translate the above finite difference equation into an analytically treatable equation. Following again standard LQC techniques [113, 154], this can be done by rescaling the wave functions and performing a Fourier transform on the lattice to the P_i-representation. Specifically, let us rescale our wave functions as (cfr. Eq. (3.55))

$$\tilde{\chi}(v_1, v_2) = \sqrt{|v_1 v_2|}\tilde{\psi}(v_1, v_2) \quad \text{for} \quad v_1, v_2 \neq 0, \tag{6.36}$$

so that the scalar product (6.31) becomes

$$\langle \psi_1 | \psi_2 \rangle = \sum_{v_1, v_2 \in \mathbb{Z}} \overline{\tilde{\psi}(v_1, v_2)} |v_1 v_2| \tilde{\psi}(v_1, v_2). \tag{6.37}$$

The Fourier transform

$$\psi(P_1, P_2) = \sum_{v_1, v_2 \in 2\mathbb{Z}} \tilde{\psi}(v_1, v_2) e^{-i(P_1 v_1 + P_2 v_2)}, \quad \tilde{\psi}(v_1, v_2) = \frac{1}{\pi^2} \int_0^\pi dP_1 \int_0^\pi dP_2 \, e^{i(v_1 P_1 + v_2 P_2)} \psi(P_1, P_2) \tag{6.38}$$

[6] In the case of v_k, v_j variables, instead, the interpretation seems a bit less clear. Indeed, combining the definitions (5.114) and (5.14) to express (v_k, k, v_j, j) in terms of metric variables, we have $v_k = \sqrt{n}\frac{b^3}{b'}$ and $v_j = b^2(2a - \frac{ba'}{b'})$. Therefore, $v_k = v_j = 0$ would again correspond to the singularity ($b = 0$). However, using the classical expressions $b = r$ and $a = 1 - \frac{2M}{r}$, we have that $v_j = 0$ also at $r = 3M$ which is the radius (in natural units) of the *photon sphere* for a Schwarzschild black hole of mass M.

for $P_1, P_2 \in [0, \pi]$ yields then the Hamiltonian constraint operator

$$\hat{H} = -3\frac{\sin(2P_1)}{2}\partial_{P_1}\frac{\sin(2P_2)}{2}\partial_{P_2} - \left(\frac{\sin(2P_2)}{2}\partial_{P_2}\right)^2 + 2i\partial_{P_2}. \tag{6.39}$$

Finally, by performing the variable transformation $x_i = \log(\tan(P_i/2))$ [113]

$$\hat{H} = -3\tanh(x_1)\partial_{x_1}\tanh(x_2)\partial_{x_2} - (\tanh(x_2)\partial_{x_2})^2 + 2i\cosh(x_2)\partial_{x_2}\ , \tag{6.40}$$

for which it was important that the dynamically selected sub-lattice has support only on even v_1, v_2 (as it was the case for $\lambda_1 = \lambda_2 = 2$), leading to $P_1, P_2 \in [0, \pi]$ in Eq. (6.38), the Hamiltonian constraint operator can be written as the following differential operator

$$\hat{H} = \Big(-3\partial_{y_1} - \partial_{y_2} + 4i\cosh(y_2)\Big)\partial_{y_2} \qquad \text{with} \qquad y_i = \log(\sinh(x_i))\ . \tag{6.41}$$

For the standard choice of branch cut of the logarithm, y_i is real only for $x_i > 0$. One may then restrict to having volume-symmetric states, see e.g. [113], leading to symmetric functions in x_i so that we can restrict to $x_i > 0$ and avoid complex y_i. This would restrict us to a either the interior ($a > 0$) or exterior ($a < 0$) of the black hole. Otherwise, one may consider both interior and exterior at the same time at the cost of having to complexify the phase space.

The general form of the solutions to the equation $\hat{H}\,|\psi\rangle = 0$ with $\hat{H}$ given in (6.41) can be written as

$$\psi_{\text{phys}}(y_1, y_2) = g(y_1) + \int^{y_2} dy_2'\, e^{4i\sinh(y_2')} f\left(y_2' - \frac{1}{3}y_1\right), \tag{6.42}$$

where f, g are arbitrary functions. This shows that the Hamiltonian constraint operator for the quantum theory of our BH model can be analytically solved. A complete construction of the quantum theory still requires the physical inner product, observables, and preferably semiclassical states peaked on classical phase space points. Although we do not have yet definite results in this respect, let us close this section with few comments. As for the physical scalar product, since we have only one constraint involved in the theory, we expect it to be possible to equip the kernel of the Hamiltonian constraint with a Hilbert space structure by means of standard group averaging techniques [245–247].

Concerning the observables, looking at the phase space expressions (5.63) and (5.64) for the effective classical observables, the main issues to construct operators corresponding to the BH and WH masses would be to deal with the trigonometric functions appearing in the denominator and to find suitable factor orderings to ensure hermiticity of the corresponding operators. However, specific combinations of both of them can be constructed. An example of an observable would be for instance the operator version of

$$O_1 = \frac{\sqrt{2}}{3}\left(\lambda_1^2\lambda_2^2\mathfrak{F}_Q\overline{\mathfrak{F}}_Q\right)^{3/8} = |\sqrt{v_1}\sin(\lambda_1 P_1)\sqrt{v_1}| = \frac{2}{3}\left(2\lambda_1^3\lambda_2^3\right)^{\frac{1}{4}}\left(M_{\text{BH}}M_{\text{WH}}\right)^{\frac{3}{8}}\ , \tag{6.43}$$

which, in the ordering indicated in the second equality, is symmetric and commutes with the Hamiltonian constraint operator. For the mass amplification choice $\beta = 5/3$, (6.43) measures

the black hole mass. Another candidate observable is given by the ratio of the masses, i.e.

$$O_2 = \frac{\mathfrak{F}_Q}{\overline{\mathfrak{F}}_Q} = \cot\left(\frac{\lambda_1 P_1}{2}\right)^{\frac{2}{3}} \tan\left(\frac{\lambda_2 P_2}{2}\right)^2 = \frac{M_{\rm BH}}{M_{\rm WH}} \,. \tag{6.44}$$

Note that, $\mathfrak{F}_Q$ and $\overline{\mathfrak{F}}_Q$ (and hence O_1 and O_2) do not commute, as can already be seen classically. Therefore, due to the Heisenberg uncertainty relations, both masses cannot be specified with arbitrary precision at the same time in the quantum theory. This might have interesting consequences for the physical interpretation. Indeed, once the two observables for the masses are properly constructed, the simultaneous eigenstates of one of them and the Hamiltonian operator can be in principle useful to distinguish between BH and WH states. In particular, the mass eigenvalues might be used for instance as quantum numbers labelling semiclassical states peaked on large masses. The latter may eventually provide useful insights for the derivation of the effective semiclassical dynamics by means of expectation values of the Hamiltonian operator as well as for computing BH-to-WH transition amplitudes. Further work is of course needed to explicitly implement these ideas and check the above statements in detail, which we leave for future investigations.

6.3 Towards Polymer Schwarzschild-AdS Black Holes

Let us now come back to the classical setting and in particular to our original interest in considering asymptotically AdS spacetimes to apply the machinery of effective polymer models and study possible holographic consequences of singularity resolution. In this last section, we will then outline a first attempt for a canonical phase space formulation of Schwarzschild-AdS (SAdS) black holes in generic $D = d+1$ dimensions and comment on possible subtleties that may arise in the effective quantum theory obtained via polymerisation of the canonical momenta as discussed in Ch. 5.

Similarly to the discussion of the Schwarzschild case in Sec. 5.2, the starting point is now to consider a generic line element of the form

$$\mathrm{d}s^2 = -\bar{a}(r)\mathrm{d}t^2 + N(r)\mathrm{d}r^2 + 2\bar{B}(r)\mathrm{d}t\mathrm{d}r + \bar{b}^2(r)\mathrm{d}\Omega^2_{D-2} \,, \tag{6.45}$$

which describes a static and spherically symmetric D-dimensional spacetime of topology $\mathbb{R}\times\mathbb{R}\times\mathbb{S}^{D-2}$. Here $\mathrm{d}\Omega^2_{D-2}$ denotes the round metric on the $t, r = const.$ $(D-2)$-sphere, and $N(r)$ plays the role of the lapse w.r.t. the foliation in $r = const.$ slices. Plugging the metric ansatz (6.45) into the Einstein-Hilbert action with negative cosmological constant $\Lambda < 0$, we get $(G, c = 1)$

$$S_{EH} = \frac{1}{16\pi}\int \mathrm{d}^D x\,\sqrt{-g}\,\left(\mathcal{R}^{(D)} - 2\Lambda\right) = \frac{\mathrm{Vol}(\mathbb{S}^{D-2})}{16\pi} L_o \int \mathrm{d}r\,\sqrt{\bar{n}}\,\bar{b}^{D-2}\left(\mathcal{R}^{(D)} - 2\Lambda\right) \,, \tag{6.46}$$

where we recall that L_o denotes the coordinate length of a fiducial cell introduced to regularise the otherwise divergent integral in the non-compact t-direction, and $\bar{n}(r) = \bar{a}(r)N(r) + \bar{B}^2(r)$ is a Lagrange multiplier reflecting the gauge freedom in the definition of the coordinates r and t.

The explicit computation of the Ricci scalar $\mathcal{R}^{(D)}$ for the metric (6.45) followed by integrations by parts of the second derivative terms, leads then to the first-order Lagrangian (up to boundary terms)

$$L(a,b,n) = \sqrt{n}\, b^{D-4}\left[(D-2)\left(D-3+(D-3)\frac{ab'^2}{n}+\frac{a'b'b}{n}\right)-2\Lambda b^2\right] , \tag{6.47}$$

where we absorbed the L_o-factors by defining the integrated variables $n = L_o^2\bar{n}$, $a = L_o^2\bar{a}$ and $b = \bar{b}$ as in (5.7). Note that the Lagrangian (6.47) reduces to (5.8) for $D = 4$ and $\Lambda = 0$. The canonically conjugate momenta are thus given by

$$p_a = \frac{\partial L}{\partial a'} = \frac{(D-2)}{\sqrt{n}} b^{D-3} b' \qquad , \qquad p_b = \frac{\partial L}{\partial b'} = \frac{(D-2)}{\sqrt{n}} b^{D-4}\Big(2(D-3)ab' + a'b\Big) \tag{6.48}$$

and again, since the Lagrangian does not depend on n', we have a primary constraint $p_n \approx 0$. Expressing a' and b' in terms of the canonical pairs (a, p_a) and (b, p_b), the total Hamiltonian reads

$$\begin{aligned} H_{\rm cl} &= p_a a' + p_b b' - L + \gamma p_n \\ &= \sqrt{n}\left[\frac{p_a p_b}{(D-2)b^{D-3}} - \frac{(D-3)}{(D-2)}\frac{a p_a^2}{b^{D-2}} - (D-2)(D-3)b^{D-4} + 2\Lambda b^{D-2}\right] + \gamma p_n \, , \end{aligned} \tag{6.49}$$

where $\gamma(r)$ is a Lagrange multiplier implementing the constraint $p_n \approx 0$. Finally, setting $n = const.$ and equivalently $\gamma = 0$ according to the EOM $n' = \{n, H_{\rm cl}\} = \gamma$, the stability requirement $p_n' = \{p_n, H_{\rm cl}\} \approx 0$ of the primary constraint yields the Hamiltonian constraint

$$H_{\rm cl} = \sqrt{n}\,\mathcal{H}_{\rm cl} \quad , \quad \mathcal{H}_{\rm cl} = \frac{p_a p_b}{(D-2)b^{D-3}} - \frac{(D-3)}{(D-2)}\frac{a p_a^2}{b^{D-2}} - (D-2)(D-3)b^{D-4} + 2\Lambda b^{D-2} \approx 0 \, , \tag{6.50}$$

which for $D = 4$ and $\Lambda = 0$ consistently reduces to the result (5.12) for the Schwarzschild case.

We can now proceed to define new canonical variables as those used in Ch. 5 for our effective models of quantum corrected Schwarzschild BHs. A first more or less straightforward attempt consists in defining the higher-dimensional analogues of the (v_1, P_1, v_2, P_2)-variables used in our first model, namely (cfr. Eq. (5.14))

$$\begin{aligned} P_1 = \frac{a'}{\sqrt{n}b} = \frac{1}{(D-2)b^{D-2}}\left(p_b - (D-3)\frac{2ap_a}{b}\right) \quad &, \quad v_1 = \frac{(D-2)}{(D-1)}b^{D-1} \\ P_2 = \frac{b'}{\sqrt{n}b^{D-3}} = \frac{p_a}{(D-2)b^{2(D-3)}} \quad &, \quad v_2 = (D-2)ab^{2(D-3)} \end{aligned} \tag{6.51}$$

which, as it can be checked by direct calculation, satisfy the canonical Poisson bracket relations $\{v_1, P_1\} = 1 = \{v_2, P_2\}$ and $\{v_1, P_2\} = \{v_1, v_2\} = \{v_2, P_1\} = \{v_2, P_1\} = 0$. In the new variables, the Hamiltonian (6.50) reads as

$$H_{\rm cl} = \sqrt{n}\left(\frac{D-1}{D-2}v_1\right)^{\frac{D-4}{D-1}}\left((D-1)v_1v_2P_2 + (D-3)v_2P_2^2 - (D-2)(D-3) + 2\Lambda\left(\frac{D-1}{D-2}v_1\right)^{\frac{2}{D-1}}\right) , \tag{6.52}$$

and reduces to (5.17) for $D = 4$ and $\Lambda = 0$.

In order to understand what kind of consequences the polymerisation of the above canonical momenta might have, we need to seek for their on-shell interpretation. To this aim, let us solve the EOMs obtained from the Hamiltonian (6.52) which are given by

$$\begin{cases} v_1' = \sqrt{n}\left(\dfrac{D-1}{D-2}v_1\right)^{\frac{D-4}{D-1}}(D-1)v_1P_2 & (6.53)\\ v_2' = \sqrt{n}\left(\dfrac{D-1}{D-2}v_1\right)^{\frac{D-4}{D-1}}\Big((D-1)v_1P_1+2(D-3)v_2P_2\Big) & (6.54)\\ P_1' \approx -\sqrt{n}\left(\dfrac{D-1}{D-2}v_1\right)^{\frac{D-4}{D-1}}\left((D-1)P_1P_2+\dfrac{4\Lambda}{D-1}\left(\dfrac{D-1}{D-2}v_1\right)^{\frac{2}{D-1}}v_1^{\frac{3D}{D-1}}\right) & (6.55)\\ P_2' = -\sqrt{n}\left(\dfrac{D-1}{D-2}v_1\right)^{\frac{D-4}{D-1}}(D-3)P_2^2 & (6.56) \end{cases}$$

Note that, unlike the $D=4$ case considered in Sec. 5.2.2 for which the EOM for P_2 decouples and can be directly integrated (cfr. Eq. (5.17)), now it contains also a term involving v_1[7]. This problem can be circumvented by recalling the definition (6.51) of P_2 and v_1 from which it follows that $b' = \sqrt{n}b^{D-3}P_2$ with $b = \left(\frac{D-1}{D-2}v_1\right)^{\frac{1}{D-1}}$, and hence we have

$$b'' = \sqrt{n}(D-3)b^{D-4}b'P_2 + \sqrt{n}b^{D-3}P_2' \overset{(6.56)}{=} 0\,, \tag{6.57}$$

whose solution is given by

$$b(r) = Br + A\,, \tag{6.58}$$

where A, B are integration constants and we can set $A=0$ with no loss of generality as it just corresponds to shift the r-coordinate. Inserting (6.58) back into the expressions (6.51) of v_1 and P_2 in terms of b and b', we get

$$v_1(r) = \frac{D-2}{D-1}\,B^{D-1}\,r^{D-1} \qquad , \qquad P_2(r) = \frac{1}{\sqrt{n}\,B^{D-4}\,r^{D-3}} \tag{6.59}$$

which can then be plugged into (6.55) yielding

$$P_1' + (D-1)\frac{P_1}{r} = -\frac{4\Lambda\sqrt{n}}{D-2}\frac{1}{Br} \qquad \Rightarrow \qquad (r^{D-1}P_1)' = -\frac{4\Lambda\sqrt{n}}{D-2}\frac{r^{D-2}}{B}\,. \tag{6.60}$$

Eq. (6.60) can be now integrated and we get the solution

$$P_1(r) = \frac{C}{r^{D-1}} - \frac{4\Lambda\sqrt{n}}{(D-1)(D-2)B}\,, \tag{6.61}$$

where C is an integration constant. Finally, using the Hamiltonian constraint $\mathcal{H}_{\rm cl}\approx 0$ together with the solutions (6.59) for v_1, P_2 and (6.61) for P_1, the solution for v_2 reads as (cfr. Eq. (6.52))

[7] We recall that $\sqrt{n} = const.$ and in the following we set it to be $\sqrt{n} = \mathscr{L}_o$ with $\mathscr{L}_o$ the physical size of the fiducial cell as done in Ch. 5.

$$v_2(r) = n\left(\frac{D-2}{D-3}\right) B^{2(D-4)}\, r^{2(D-3)} \left(D-3-\frac{B^3 C}{\sqrt{n} r^{D-3}} - \frac{2\Lambda(D-3)}{(D-1)(D-2)} B^2 r^2\right) . \tag{6.62}$$

With the solutions of the Hamiltonian EOMs at our disposal, we can then reconstruct also the metric coefficients. Indeed, inverting the definition (6.51) of v_2 and recalling that $b = Br$, we can express the metric coefficient a in terms of the areal radius b as

$$\begin{aligned} a(b) &= \frac{v_2}{(D-2)b^{2(D-3)}} \\ &\overset{(6.62)}{=} \frac{n}{(D-3)B^2}\left((D-3) - \frac{B^D C}{\sqrt{n}\, b^{D-3}} - (D-3)\frac{2\Lambda}{(D-1)(D-2)} b^2\right) \\ &= \frac{\mathscr{L}_o^2}{B^2}\left(1 + \frac{b^2}{L_{AdS}^2} - \frac{C B^D}{\mathscr{L}_o (D-3)}\frac{1}{b^{D-3}}\right) , \end{aligned} \tag{6.63}$$

where in the third line we used $\sqrt{n} = \mathscr{L}_o$ and the relation (2.19) between the cosmological constant Λ and the AdS radius L_{AdS}, which in our current notation with $D = d+1$ reads as

$$\Lambda = -\frac{(D-1)(D-2)}{2L_{AdS}^2} . \tag{6.64}$$

Therefore, performing the coordinate rescalings $r \mapsto Br = b$ and $t \mapsto \mathscr{L}_o t/BL_o = \tau$, we recover the standard form of the $D = (d+1)$-dimensional SAdS solution [39, 248, 249]

$$a(b) = 1 + \frac{b^2}{L_{AdS}^2} - \frac{2\mu}{b^{D-3}} \qquad \text{with} \qquad \mu = \frac{C\, B^D}{2\mathscr{L}_o (D-3)} \tag{6.65}$$

which has a regular horizon for any $\mu > 0$, i.e. $D \geq 4$, and μ is related to the mass M of the SAdS black hole relative to the AdS ground state via the relation ($G = 1$) [39, 250, 251]

$$M = \frac{(D-2)\mathrm{Vol}(\mathbb{S}^{D-2})}{8\pi}\mu . \tag{6.66}$$

Note that, as it was the case also for the canonical analysis of classical Schwarzschild black holes discussed in Sec. 5.2.2, now we also have one observable given by the mass whose value gives a condition for both the integration constants C and B. Here B is playing the role of the integration constant D of Sec. 5.2.2, but we denoted it by B instead of D to avoid confusion with the spacetime dimension. Moreover, expressing C in terms of μ via (6.65) and inserting the result into the solution (6.61) for P_1, the on-shell expression for the fiducial cell independent combination $P_1(b)/\mathscr{L}_o$ reads as

$$\frac{P_1(b)}{\mathscr{L}_o} = \frac{D-3}{B}\left(\frac{2\mu}{b^{D-1}}\right) + \frac{2}{BL_{AdS}^2} , \tag{6.67}$$

where in the second term we used again (6.64) to rewrite Λ in terms of L_{AdS}. Eq. (6.67) shows that, unlike the case of zero cosmological constant, now P_1^2 is not related to the Kretschmann

scalar (up to integration constants) as it will now contain an additional mixed term involving both μ and L_{AdS}. Specifically, we have

$$\frac{P_1(b)^2}{\mathscr{L}_o^2} = \frac{(D-3)^2}{B^2}\left(\frac{4\mu^2}{b^{2(D-1)}}\right) + \frac{4}{B^2 L_{AdS}^4} + \frac{8(D-3)}{B^2}\frac{\mu}{L_{AdS}^2 b^{D-1}} \not\propto \mathcal{K}\,, \tag{6.68}$$

where the first two terms are those expected from the Kretschmann scalar for a SAdS black hole, up to proportionality factors involving the integration constant B, and the last term depends on the ratio μ/L_{AdS}^2. Now, as discussed in Ch. 5, the presence of the integration constant in the proportionality factors would eventually result into the selection of a certain subset of initial conditions for the effective quantum theory which ensure B to not depend on the mass. The main issues may however come from the additional term. Indeed, since it grows with the mass, for sufficiently large masses it might affect the analysis of the onset of quantum effects and in particular of a unique mass independent curvature upper bound. The naive thought of seeking for initial conditions for which B would compensate the mass dependence in the third term will on the other hand spoil the proportionality with the Kretschmann scalar of the first two terms. However, let us notice that the last term in (6.68) becomes negligible if the BH mass is within the range $\ell_P \ll M \ll L_{AdS}$ so that the onset of quantum effects resulting from the polymerisation of P_1 would still be in the Planck curvature regime. Therefore, the variables considered here might still produce sensible results after polymerisation with further restrictions on the admissible initial conditions for the model that limit the mass range. In this sense, on the one hand, it would be still worth in principle to work out the effective quantum corrected theory with the current variables and study the above arguments for the viability of the resulting model in more details. On the other hand, learning from our discussion of Schwarzschild BHs in Ch. 5, a more efficient strategy would be to construct new canonical variables in which one of the momenta is directly related to the (square root of the) Kretschmann scalar or other combinations of curvature invariants thus avoiding restrictions on the initial conditions. We hope to be able to explore both possibilities in the near future.

Part IV

CONCLUSION

Chapter 7

Summary and Further Research

In this thesis we studied effective models for quantum corrected cosmological and black hole spacetimes motivated by loop quantum gravity (LQG), the resolution of their singularities and their possible holographic aspects. For the cosmology side, our main interest was to investigate whether it is possible to use recent advances in resolving gravitational singularities via LQG within the framework of the AdS/CFT correspondence. To this aim, we focused on Kasner-AdS spacetimes for which previous work in AdS/CFT has shown that the presence of the bulk singularity causes a finite distance pole in the equal time two-point correlators of the dual field theory. Taking inspiration from results in homogeneous and isotropic loop quantum cosmology, we discussed then different examples of quantum corrected Kasner-AdS metrics and argued via analytic and numerical methods that the resolution of the bulk singularity corresponds to a resolution of the pole in the dual theory thus suggesting that the combination of ideas from different QG approaches can give sensible improvements with respect to the classical description.

Motivated by these results, the next logical step was to try to repeat similar analyses also for other kinds of gravitational singularities such as black holes for which a lot of work has been done over the last years within different QG approaches. However, the lack of definite results on effective LQG models already for the simplest case of a Schwarzschild black hole prevented us from a direct application to asymptotically AdS black holes. Therefore, we first focused on the asymptotically flat case and developed two new models for quantum corrected spherically symmetric Schwarzschild black holes. These are based on new canonical phase space variables motivated by physical considerations on the onset of quantum effects and curvature invariants. More precisely, we constructed new sets of conjugate variables in which the on-shell values of the canonical momenta are respectively related to the Kretschmann scalar and the extrinsic curvature so that their polymerisation produces physically reasonable large curvature and small volume quantum corrections. In the resulting effective spacetime, quantum effects become relevant in the high curvature regime and the classical singularity is replaced by a smooth transition surface connecting a trapped and an anti-trapped region. The latter can be respectively interpreted as the interior regions of a black and a white hole. At low curvatures quantum effects rapidly decay so that for macroscopic black holes the geometry is well approximated by classical general relativity already at the horizon scale and the Schwarzschild solution is recovered far in the

exterior region. Another main result of our analysis is the discovery of a second previously unnoticed Dirac observable for the effective quantum theory which, similarly to the already-known black hole mass observable, can be interpreted as the ADM mass for the asymptotically Schwarzschild solution on the white hole side. Moreover, the relatively simple structure of the model allowed us also to analyse the correction to thermodynamic quantities and have a promising analytic control in taking the first steps of the construction of the quantum theory from which the effective models might be eventually derived. Finally, we sketched some preliminary attempt to construct similar variables for Schwarzschild-AdS black holes in $D \geq 4$ dimensions.

Lying at the intersection of different topics, the results presented in this thesis are expected to be of interest from both the LQG and AdS/CFT perspective and hopefully provide fruitful starting points for a more systematic merging of ideas and results developed in both theories. In this respect, the research initiated here can be continued in several directions. Let us close then this work by giving an outlook on some of the possible future directions.

First of all, from a more LQG-based perspective, as we have already noticed in Ch. 4, the cosmological Kasner-AdS metrics used in our analysis are only motivated by LQG (or better LQC) and not derived from them. Moreover, a fully satisfactory quantum corrected metric incorporating Kasner transitions is still missing. A rigorous derivation of the bulk effective metric would then require to set up the full 5-dimensional loop quantisation of the symmetry-reduced model under consideration, determine the proper effective dynamics incorporating the relevant quantum corrections, and solve the effective equations to determine the geometry of the resulting quantum corrected spacetime.

Concerning instead our work on black holes, the quantum theory needs to be completed. As anticipated in the previous chapter, this requires the definition of a physical scalar product and the construction of suitable coherent states to derive the effective dynamics. Due to the similarity of our variables to those successful in loop quantum cosmology, we expect standard LQC techniques [156, 157, 247] such as the construction of a rigging map for the physical scalar product via group averaging to be applicable. A key point would be in particular to understand the role of the mass Dirac observables at the quantum level. On a more formal level, the requirement of the latter to be self-adjoint for instance may fix some operator-ordering ambiguities. Of physical relevance would be then to understand how to construct semiclassical states which allow to distinguish the black and white hole side. Useful insights in this respect may be provided by relating our observables with the canonically conjugate observables for asymptotically flat spacetimes studied by Thiemann and Kastrup [252, 253] and by Kuchař [254]. Computing then black-to-white hole transition amplitudes would allow a direct comparison between the canonical Hamiltonian framework and results obtained from covariant spin foam path integral computations (see e.g. [255, 256]). A better understanding of the mass observables and the study of their spectrum and eigenstates may also be useful to get further insights on the thermodynamic analysis initiated in Ch. 6 and in particular on the occurrence of logarithmic corrections to the horizon entropy for a quadratic power relation between the black and white hole masses.

A further interesting aspect, which might also shed light on the previous points, concerns the relation of our model with full LQG. Given the similarity of our canonical variables with

the (b, v)-variables used in LQC, a useful starting point might be provided by [132] where some preliminary steps for the case of spherical symmetry have been also discussed.

From the holography perspective, instead, the following directions might be pursued. The first step would be of course to complete the construction of a polymer effective model for Schwarzschild-AdS black holes in D dimensions and extend then our previous analysis on holographic signatures of resolved singularities to this setting for which a similar pole in the boundary dual correlator has been studied in [257]. A comparison with the expectations from AdS/CFT may also shed light on the fate of gravitational singularities in holography where due to the so-called *no transmission principle* it was argued that not all singularities may be resolved by QG effects [258, 259]. Moreover, unlike the anisotropic cosmological examples already considered for which computations in the dual field theory side would be difficult due to the anisotropic time dependent background, an explicit proposal for a CFT state dual to a bulk Schwarzschild-AdS geometry is known in the AdS/CFT literature [92]. Knowing what to look for on the field theory side, one can then confirm the results via analytical or lattice computations. In this respect, the main point would be to understand how quantum corrections in the bulk modify the CFT state.

This can be studied in two ways. The first one is based on the observation that the dual state to an AdS black hole is a thermal state so that the thermodynamic properties of AdS black holes can be studied via the thermodynamics of the dual field theory. As such one may try to repeat the analysis of the bulk black hole quantum corrected thermodynamics and compare the results with the quantum corrections derived from CFT arguments [39, 238, 260–265].

The second aspect concerns instead the study of bulk fields propagating on a quantum corrected spacetime and their boundary values via holographic renormalisation [94, 266, 267]. The derivation of a renormalised action and asymptotic boundary charges from the renormalisation of the symplectic potential seems in fact to be well-suited for the canonical setting on which polymer models are based. As discussed in [266, 267], such a procedure is in principle applicable for generic Hamiltonian systems with or without a holographic dual. In particular, it amounts to compute ground state wavefunctionals for the quantum path integral and reproduces the holographic bulk/boundary dictionary in the asymptotically AdS case [266]. It would be interesting then to connect it with LQG modifications to path integral already discussed e.g. in cosmology [268, 269]. This may enable us to relate bulk QG effects with finite N corrections in known boundary theories.

Finally, another interesting question which concerns the inclusion of matter is the fate of the holographic entropy bound in quantum corrected black hole spacetimes. More precisely, taking as starting point recent results in modeling collapsing matter shells in presence of polymer QG corrections [270–273], one can then study null geodesics emanating from a space-like surface enclosing the matter shell and construct the associated future pointing light sheets. Given an equation of state specifying the kind of matter, the entropy flux through the lightsheet can be computed thus allowing us to ask whether the Bousso entropy bound is satisfied. In a similar spirit to the discussion for LQC in Ch. 3, of particular interest would be the point in which the shell gets close to the resolved singularity and the role of the energy conditions in the vicinity of the transition surface.

Part V

APPENDICES

Appendix A

Constrained Hamiltonian Systems

Many interesting physical systems which admit a Lagrangian description are characterised by so-called *degenerate Lagrangians*, i.e. the Hessian matrix of the Lagrangian w.r.t. the velocities is degenerate. This is in fact the case of all fundamental interactions, including gravity. For such systems, the Legendre transformation is not invertible and, passing at the Hamiltonian description, this implies the existence of constraints providing functional relations between the canonical variables. A canonical formulation of the dynamics would then require to appropriately take into account the constraints. This can be done by following the so-called Dirac algorithm for constrained systems [126, 127], which we will briefly review in this appendix. Other references for the topic including excellent reviews are [128, 274–276] (as well as [277, 278] for a modern geometric description including a Lagrangian counterpart of the constraint algorithm). We refer to them for those technical details that will be omitted here for brevity. In order to illustrate the main steps of the procedure in the simplest way possible we will focus on the case of a system with finite number of degrees of freedom, although the procedure can be generalised to the infinite dimensional case of field theories. Finally, to make contact with the content presented in the main text of the thesis, we will consider some paradigmatic examples to show how the procedure works in the case of generally covariant systems.

A.1 Dirac's Algorithm

Let us consider a dynamical system described by a N-dimensional configuration manifold $\mathcal{Q}$ and whose dynamics is governed by the first-order Lagrangian[1] $\mathscr{L} = \mathscr{L}(q^i, \dot{q}^i)$, with q^i, $\dot{q}^i$, $i = 1, \dots, N$, respectively denoting the positions and velocities of the systems[2] and playing the role of local coordinates on the tangent bundle $T\mathcal{Q}$ of $\mathcal{Q}$. Recalling then the Lagrangian EOMs

$$\frac{\partial^2 \mathscr{L}}{\partial \dot{q}^i \partial \dot{q}^j} \ddot{q}^j = \frac{\partial \mathscr{L}}{\partial q^i} - \frac{\partial^2 \mathscr{L}}{\partial \dot{q}^i \partial q^j} \dot{q}^j \,, \tag{A.1}$$

[1] We refer to [279] and references therein for the analysis of higher-order theories.

[2] Here dots denote derivatives w.r.t. "time", the latter being the parameter of the evolution which enters the action functional $S = \int \mathrm{d}t \mathscr{L}$ and it is not necessarily a coordinate time.

in the case of a regular Lagrangian (i.e. $\det\left(\frac{\partial^2\mathscr{L}}{\partial\dot{q}^i\partial\dot{q}^j}\right)\neq 0$) the evolution is unique and $\ddot{q}^i$ can be completely determined as functions of q^i and $\dot{q}^i$. In this case, the Legendre transformation

$$F\mathscr{L}: T\mathcal{Q}\ni(q^i,\dot{q}^i)\longmapsto\left(q^i,p_i=\frac{\partial\mathscr{L}}{\partial\dot{q}^i}\right)\in T^*\mathcal{Q} \tag{A.2}$$

provides us with a one-to-one correspondence between the Lagrangian and the Hamiltonian descriptions as we are able to invert this map and express all the velocities $\dot{q}$ in terms of the canonical momenta p and generalized coordinates q.

Let us consider now the case of a degenerate Lagrangian, i.e. $\det\left(\frac{\partial^2\mathscr{L}}{\partial\dot{q}^i\partial\dot{q}^j}\right)=0$. In other words, now the Hessian matrix has less than maximum rank, namely

$$\operatorname{rank}\left(\frac{\partial^2\mathscr{L}}{\partial\dot{q}^i\partial\dot{q}^j}\right)=K<N\,. \tag{A.3}$$

At the Lagrangian level, this means that the Euler-Lagrange equations are unable to uniquely determine the accelerations $\ddot{q}$ as functions of q and $\dot{q}$. At the canonical level, this implies that the q's and p's are not all independent as locally only K of the N momenta $p_i=\frac{\partial\mathscr{L}}{\partial\dot{q}^i}$ can be inverted to express the velocities $\dot{q}^i$ in terms of q and p. Therefore, in this case, there are only $N+K$ independent phase space variables and the Legendre transformation identifies a $(N+K)$-dimensional subspace Σ_0 of the $2N$-dimensional phase space defined by $(N-K)$ functionally independent relations

$$\varphi_\alpha(q,p)=0\qquad,\qquad\alpha=1,\dots,N-K\,, \tag{A.4}$$

called *primary constraints*. Note that the Legendre transform still has the property that

$$\delta(p_i\dot{q}^i-\mathscr{L})=\dot{q}^i\delta p_i+p_i\delta\dot{q}^i-\frac{\partial\mathscr{L}}{\partial q^i}\delta q^i-\frac{\partial\mathscr{L}}{\partial\dot{q}^i}\delta\dot{q}^i=\dot{q}^i\delta p_i-\frac{\partial\mathscr{L}}{\partial q^i}\delta q^i\,, \tag{A.5}$$

i.e., q^i and p_i are the dynamical variables of the Hamiltonian formulation. However, the Hamiltonian now is not unique due to the presence of the constraints (A.4). Indeed, even if the canonical Hamiltonian defined as the Legendre transform of the Lagrangian restricted to the region Σ_0 identified by the primary constraints

$$H_c=p_i\dot{q}^i-\mathscr{L}\big|_{\Sigma_0} \tag{A.6}$$

does not depend on the (unsolved) velocities and so it can be considered a function only of the q's and p's, any *total Hamiltonian* obtained by adding to it a linear combination of the primary constraints

$$H_T=H_c+u^\alpha\varphi_\alpha\,, \tag{A.7}$$

would be on the same footing. The coefficients u^α are to be treated as Lagrange multipliers and are arbitrary functions of time (as well as of q and p). The inclusion of the primary constraints in the Hamiltonian makes the Legendre transformation invertible. The Hamiltonian EOMs obtained from (A.7) reads as

$$\dot{q}^i = \frac{\partial H_c}{\partial p_i} + u^\alpha \frac{\partial \varphi_\alpha}{\partial p_i} \qquad , \qquad \dot{p}_i = -\frac{\partial H_c}{\partial q^i} - u^\alpha \frac{\partial \varphi_\alpha}{\partial q^i} \tag{A.8}$$

so that the time derivative of a generic phase space function $f(q,p)$ is given by its Poisson bracket with the Hamiltonian (A.7)

$$\dot{f} = \{t, H_T\} = \{f, H_c\} + u^\alpha \{f, \varphi_\alpha\} + \{f, u^\alpha\}\varphi_\alpha = \{f, H_c\} + u^\alpha \{f, \varphi_\alpha\} \ . \tag{A.9}$$

Note that the constraints must be imposed only after Poisson brackets are computed. Following Dirac [127, 128], we have the following definition

Definition (Weak equality): A *weak equality* denoted by $\approx$ is an equality modulo the constraints, i.e. equality on the constraint hypersurface, and can be used only after all Poisson brackets have been evaluated.

In this sense, the constraint equations are understood as $\varphi_\alpha(q,p) \approx 0$, but $\{\varphi_\alpha, f\} \not\approx 0$ in general. It should be stressed that (A.8) is the initial form of the Hamiltonian phase-space EOMs. To arrive at their final form, the theory proceeds with a step-by-step consistency analysis of constraints. Indeed, consistency of the constraints with Hamiltonian evolution implies the following stability conditions

$$0 \overset{!}{\approx} \dot{\varphi}_\alpha = \{\varphi_\alpha, H_T\} \approx \{\varphi_\alpha, H_c\} + u^\beta \{\varphi_\alpha, \varphi_\beta\} \ , \tag{A.10}$$

which geometrically amount to the requirement of dynamics not carrying out of the primary constraints surface that as such remains stable under time evolution. Such consistency conditions can lead to the following four possibilities: 1) They are trivially satisfied (e.g. $0 = 0$), in which case the procedure ends here and Eqs. (A.8) are the final form of the EOMs; 2) They are never satisfied and the theory is inconsistent; 3) The conditions (A.10) impose restrictions on the u's; 4) The conditions (A.10) lead to relations that are independent of the u's thus yielding new constraints, say $\chi_m(q,p) \approx 0$. The new constraints generated in this way are called *secondary constraints*[3] and will in turn lead to new consistency conditions. The consistency algorithm outlined above must then be iterated until new secondary constraints or restrictions on the u's can no longer be generated (or the theory is inconsistent). Assuming that in the end we get M new constraints

$$\chi_m(q,p) \approx 0 \qquad , \qquad m = 1, \dots, M \tag{A.11}$$

we will denote the set of all constraints (primary, secondary, and so on) $\{\phi_1, \dots, \phi_{N-K+M}\} = \{\varphi_1, \dots, \varphi_{N-K}, \chi_1, \dots, \chi_M\}$ with a uniform notation

$$\phi_j \approx 0 \qquad , \qquad j = 1, \dots, J = N - K + M \ . \tag{A.12}$$

[3]Note that for secondary constraints, one uses the EOMs, as opposed to primary constraints which instead are kinematical relations arising from the definition of the canonical momenta.

The consistency conditions between them lead to restrictions on the Lagrange multipliers u. In fact, we have the following inhomogeneous linear system

$$\dot{\phi}_j \approx \{\phi_j, H_c\} + u^k \{\phi_j, \phi_k\} \approx 0 \tag{A.13}$$

of J equations for the $K \leq J$ unknowns u_k. Provided the system is compatible (otherwise the dynamics would be inconsistent), the solution is given by $u^k = U^k + V^k$, where U^k is a particular solution of the inhomogeneous system and V^k represents the general solution to the associated homogeneous system $V^k\{\phi_j, \phi_k\} \approx 0$. This is expressed as a linear combination of linearly independent solutions $V^k = v^a V_a^k$, $a = 1, \ldots, A = J - r$, where r is the rank of the homogeneous system assumed to be constant all over the constraint hypersurface. Thus, the general solution of (A.13) reads as

$$u^k \approx U^k + v^a V_a^k \ , \tag{A.14}$$

which can be inserted into (A.7) yielding the total Hamiltonian

$$H_T = H' + v^a \phi_a \qquad \text{with} \qquad H' = H_c + U^k \phi_k \quad , \quad \phi_a = V_a^k \phi_k \tag{A.15}$$

whose two terms respectively include the contributions to u^k coming from the consistency conditions and those that instead remain arbitrary (we are left with A arbitrary functions v^a).

Another classification of constraints, that is physically more important than the one in primary and secondary, is that of *first* and *second class* constraints according to the following:

Definition (First and second class function): A phase space function f is said to be *first class* if it has (at least weakly) vanishing Poisson bracket with all constraints, i.e. $\{f, \phi_j\} \approx 0 \ \forall j$. Otherwise, the function is called *second class*.

All the ϕ_a above are primary first class constraints by their definition. H_T is first class by the consistency requirement of all constraints to be preserved in time, hence by linearity H' is first class as well. The Poisson bracket of two first class constraints is also first class and it is thus *strongly* equal to a linear combination of first class constraints, say

$$\{\phi_i, \phi_j\} = C_{ij}^k \phi_k \ . \tag{A.16}$$

This shows that first class constraints close an algebra. The latter is not necessarily a Lie algebra since the coefficients C_{ij}^k might a priori be phase space functions and not necessarily constants. This is for instance the case of canonical general relativity discussed in Appendix B.

The importance of first class constraints lies in the fact that first class primary constraints can be identified with generators of infinitesimal gauge transformations, i.e. they change the canonical variables q, p but do not change the physical state of the system[4]. To show this, let us

[4]Second class constraints deserve a separate discussion and require the introduction of a new mathematical object, known as the Dirac bracket. However, since in this work we will be dealing only with first class constraints, we will not discuss this topic here and refer the interested reader to the references given above.

consider a dynamical variable f and its variation Δf along the infinitesimal evolution generated by H_T from t to $t+\delta t$ given by (neglecting $\mathcal{O}(\delta^2)$)

$$\Delta f = \delta t \Delta v^a \{f, \phi_a\} =: \epsilon^a \{f, \phi_a\} \, . \tag{A.17}$$

Since the coefficients ϵ^a are entirely arbitrary, states related by such transformation correspond to the same physical state. Dirac conjectured that all first class constraints (not only primary ones) are generators of gauge transformations. The status of such a conjecture is still disputed. A proof exists under simplifying regularity conditions that are generically satisfied. It is however possible to construct counterexample, but these are pathological (see e.g. [128]). The conjecture holds true for all physically relevant systems that have been studied so far. Moreover, as discussed later in this appendix, in the quantisation of constrained systems all first class constraints are treated on equal footing. It is thus possible to define an *extended Hamiltonian* H_E given by H' plus an arbitrary combination of all first class constraints

$$H_E = H' + \lambda^a \gamma_a \, , \tag{A.18}$$

with the index a running over a complete set of first class constraints, collectively denoted by γ_a. Strictly speaking, only the total Hamiltonian H_T follows directly from the Lagrangian. The extended Hamiltonian H_E introduces more arbitrary functions of time, but its definition is more natural from the canonical point of view, since it allows to treat all of the gauge generators on the same footing. The dynamics generated by the three Hamiltonian functions H', H_T and H_E are are the same up to gauge transformations and as such are physically equivalent. Finally, only those phase space functions which Poisson-commute (at least weakly) with all first class constraints have a gauge invariant physical meaning according to the following:

Definition (Dirac observables): A phase space function F is called a *Dirac observable* if it Poisson-commutes weakly with all first class constraints, i.e. $\{F, \gamma_a\} \approx 0$.

Notice that pairs of canonically conjugate d.o.f. are removed by each first class constraint: one via the algebraic restriction imposed by the equation $\gamma_a \approx 0$, and another one by the gauge-invariance requirement for Dirac observables.

A.2 Examples

Following [280], let us show how the Dirac's algorithm works for two basic examples which share important features with gravity, that is reparametrisation invariance. An important consequence is that for such systems the Hamiltonian theory turns out to be fully constrained. The canonical analysis of general relativity is instead briefly discussed in Appendix B. Other examples provided by symmetry-reduced gravitational systems such as cosmology and Schwarzschild black holes have been considered in Ch. 3 and 5, respectively.

Example 1 – Relativistic particle: Let us consider the action for a free relativistic particle

$$S = -m \int \mathrm{d}\tau \, \sqrt{-\dot{x}_\mu \dot{x}^\mu} \, , \tag{A.19}$$

where m is the mass, the integral is over the world-line of the particle, $\dot{x}^\mu = \mathrm{d}x^\mu/\mathrm{d}\tau$, and τ is an arbitrary parameter and shall not be confused with the coordinate or proper time. The action (A.19) is in fact invariant under reparametrisation $\tau \mapsto f(\tau)$ (the Lagrangian density is homogeneous of degree one in the velocities). The canonical momenta are given by

$$p_\mu = \frac{m\dot{x}_\mu}{\sqrt{-\dot{x}_\mu \dot{x}^\mu}} \, , \tag{A.20}$$

from which it follows that the momenta obey the mass-shell condition

$$p_\mu p^\mu + m^2 = 0 \, . \tag{A.21}$$

This should be understood as a constraint in phase space $p_\mu p^\mu + m^2 \approx 0$. Moreover, reparametrisation invariance implies that the canonical Hamiltonian identically vanishes

$$H_c = p_\mu \dot{x}^\mu - \mathscr{L} \approx 0 \, . \tag{A.22}$$

The total Hamiltonian is given by

$$H_T = N(p_\mu p^\mu + m^2) \, , \tag{A.23}$$

which is then a primary first class constraint. The evolution in the parameter τ is actually a gauge transformation and, as can be seen from the corresponding Hamiltonian EOMs, the Lagrange multiplier N is proportional to the rate of change of proper time w.r.t. the time parameter τ.

Example 2 – Bosonic string: Let us consider the motion of a one-dimensional object (string) in a higher-dimensional Minkowski spacetime described by the so-called Nambu-Goto action

$$S = -\frac{1}{2\pi\alpha'} \int \mathrm{d}^2\sigma \, \sqrt{-\det G_{\alpha\beta}} \, , \tag{A.24}$$

where α' is the string constant, and $G_{\alpha\beta}$ is the induced metric on the world-sheet surface spanned by the string in its motion and parametrised by σ^α, $\alpha = 0, 1$, i.e.

$$G_{\alpha\beta} = \eta_{\mu\nu} \frac{\partial X^\mu}{\partial \sigma^\alpha} \frac{\partial X^\nu}{\partial \sigma^\beta} \, , \tag{A.25}$$

with $X^\mu(\sigma^0, \sigma^1)$ denoting the embeddings of the world-sheet in the ambient spacetime which play the role of dynamical configuration variables. The canonical momenta conjugated to them are given by

$$P_\mu = \frac{\partial_{\sigma^0} X_\mu \partial_{\sigma^1} X^\mu - (\partial_{\sigma^0} X_\mu \partial_{\sigma^0} X^\mu)(\partial_{\sigma^1} X_\nu \partial_{\sigma^1} X^\nu)}{2\pi\alpha' \sqrt{-\det G_{\alpha\beta}}} \tag{A.26}$$

and the total Hamiltonian reads as

$$H[N, N^1] = H_0[N] + H_1[N^1] = \int \mathrm{d}\sigma^1 \left(N\mathcal{H}_0 + N^1\mathcal{H}_1 \right) , \tag{A.27}$$

where the functions N, N^1 are Lagrange multipliers implementing the constraint densities

$$\mathcal{H}_0 = \frac{1}{2}\left(P_\mu P^\mu + \frac{\partial_{\sigma^1} X^\mu \partial_{\sigma^1} X_\mu}{(2\pi\alpha')^2} \right) \approx 0 \qquad , \qquad \mathcal{H}_1 = P_\mu \partial_{\sigma^1} X^\mu \approx 0 \tag{A.28}$$

which reflect the invariance of the action (A.24) under reparametrisations $\sigma^\alpha \mapsto \tilde{\sigma}^\alpha(\sigma^0, \sigma^1)$ of the world-sheet. The constraints are in fact first class as they close the following algebra of world-sheet deformations [281–283]

$$\{H_0[N], H_0[M]\} = H_1[N\partial_{\sigma^1} M - M\partial_{\sigma^1} N] ,$$
$$\{H_1[N^1], H_1[M^1]\} = H_1[N^1\partial_{\sigma^1} M^1 - M^1\partial_{\sigma^1} N^1] , \tag{A.29}$$
$$\{H_0[N], H_1[M^1]\} = H_0[N\partial_{\sigma^1} M^1 - M^1\partial_{\sigma^1} N] . \tag{A.30}$$

A.3 Brief Excursus on Quantisation

Let us close this appendix with few comments on quantisation of constrained systems. Since in this work we only deal with first class constraints, we do not consider second class constraints and discuss the so-called *Dirac quantisation* for first class systems [127, 128]. The main idea can be summarised as follows: *first quantise the system and then impose constraints at the quantum level*. This is the strategy usually adopted in LQG (and LQC) as well as the path we follow in Ch. 6 to construct the quantum theory of our non-singular polymer black hole model[5].

The starting point is a kinematical unconstrained Hilbert space $\mathcal{H}_{\text{kin}}$. Considering then a set of classical first class constraints $\phi_i(q,p) \approx 0$ and a quantisation map associating linear operators on $\mathcal{H}_{\text{kin}}$ with a (point-separating) set of phase space functions, the constraints are imposed as operator equations

$$\hat{\phi}_i \left|\psi\right\rangle \stackrel{!}{=} 0 . \tag{A.31}$$

Physical states are thus elements of the kernel of the constraint operators and define the physical Hilbert space $\mathcal{H}_{\text{phys}}$. Note that by definition physical states are in fact not modified by the unitary flow generated by the constraints, i.e. $e^{i\lambda^j \hat{\phi}_j} \left|\psi\right\rangle_{\text{phys}} = \left|\psi\right\rangle_{\text{phys}}$. Moreover, we also have that $\hat{\phi}_i\hat{\phi}_j \left|\psi\right\rangle_{\text{phys}}=0$ and hence $\widehat{\{\phi_i, \phi_j\}} \left|\psi\right\rangle_{\text{phys}} = 0$ (up to ordering problems). This is consistent with the classical Poisson brackets (A.16) of first class constraints, the latter yielding up to ordering $\widehat{C^k_{ij}\phi_k} \left|\psi\right\rangle_{\text{phys}} = 0$ at the quantum level. Therefore, consistency of the quantisation procedure demands all first class constraints (both primary and secondary) to be treated on the same footing.

[5] Note however that also to solve the constraints classically and then quantise is a equally valid strategy, although not necessarily equivalent. There is in fact no general rule for which path is the best to follow. Solving constraints classically can be very hard in practice. Quantising constraints on the other hand may give rise to ambiguities. Therefore, both options should be explored.

Appendix B

Elements of Loop Quantum Gravity

In this Appendix we briefly review the core ideas and concepts underlying the quantum kinematics of loop quantum gravity (LQG). We will focus on those aspects which are useful for understanding the quantisation procedure adopted in the symmetry-reduced models discussed in the main part of the thesis to which this appendix should be thought of as a complement. Original literature on the subject includes [247, 284–289]. Textbook references are [129] for an advanced detailed discussion, [130, 131] for an intermediate level, and [290, 291] for an introductory level. Useful reviews include [117, 292–298]. We refer to them for those aspects and technical details that will not be covered here.

B.1 Canonical General Relativity

As we will discuss later in this Appendix, LQG is a candidate theory for a background-independent canonical quantisation of general relativity. Let us start then by recalling the classical foundations of the LQG program. This includes the so-called Arnowitt-Deser-Misner (ADM) formulation [299] of general relativity and its reformulation in terms of Ashtekar connection variables [300]. The latter resemble the variables usually employed in gauge theories thus providing the starting point to build up a canonical quantisation program based on Dirac procedure.

B.1.1 The ADM Formulation

The first step to construct a canonical formulation of a dynamical theory of the gravitational field is the introduction of a foliation of the four-dimensional spacetime manifold $\mathcal{M}$ into codimension one "equal time" spatial slices Σ_t, $t \in \mathbb{R}$. Hence, in order to have a well-defined initial value problem, global hyperbolicity is assumed for the class of spacetimes under consideration, i.e. $\mathcal{M}$ has topology $\mathbb{R} \times \Sigma$ where Σ is a model Cauchy surface [159, 301]. In what follows we further assume Σ to be compact so that boundary terms can be neglected. This 3+1 splitting induces a split also in the spacetime metric tensor $g_{\mu\nu}$ as

$$\mathrm{d}s^2 = g_{\mu\nu}\mathrm{d}x^\mu \mathrm{d}x^\nu = (-N^2 + N^a N_a)\mathrm{d}t^2 + 2N_a \mathrm{d}t\mathrm{d}x^a + q_{ab}\mathrm{d}x^a\mathrm{d}x^b \,, \tag{B.1}$$

where $a, b, \ldots$ denote spatial tensor indices on Σ, q_{ab} is the Euclidean metric induced on Σ, N and N^a are respectively called the lapse function and the shift vector of the foliation which, as schematically represented in Fig. B.1, result from the decomposition into orthogonal and tangential components of the time evolution vector field $T^\mu = Nn^\mu + N^\mu$, with $n_\mu N^\mu = 0$ and n^μ being the unit time-like normal on Σ, i.e. $n_\mu n^\mu = -1$. The physical location of a neighbouring slice (i.e. how the slices are embedded in a given spacetime) is thus determined by N and N^μ.

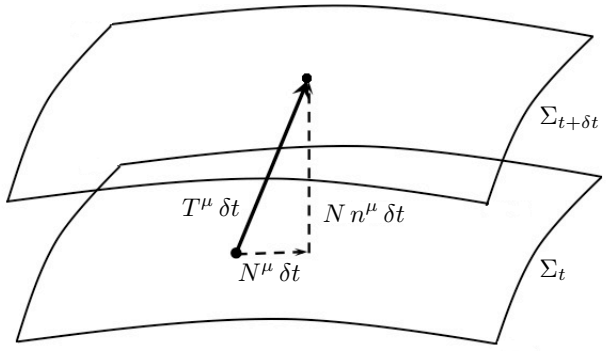

Figure B.1: Infinitesimal time evolution between two neighbouring Cauchy slices and corresponding decomposition of the evolution vector field T^μ into lapse and shift components, respectively orthogonal and tangential to Σ.

The canonical variables are given by the six independent components of the spatial metric q_{ab} and their conjugate momenta

$$P^{ab} = \frac{\sqrt{q}}{2\kappa}\left(K^{ab} - q^{ab}K\right) , \tag{B.2}$$

where q is the determinant of q_{ab}, K_{ab} is the extrinsic curvature written as an object on Σ[1], and K denotes its trace. The non-vanishing canonical Poisson brackets between them are given by

$$\{q_{ab}(x), P^{cd}(y)\} = \delta^c_{(a}\delta^d_{b)}\delta^{(3)}(x,y) . \tag{B.3}$$

In complete analogy with the reparametrisation invariant examples discussed in Appendix A, GR is also a fully constrained system, i.e. its Hamiltonian is a linear combination of first class constraints. This is the canonical counterpart of diffeomorphism invariance of the Einstein-Hilbert action. Indeed, the ADM form of the Hamiltonian reads as

$$H_{\mathrm{ADM}}[N, N^a] = H[N] + H_a[N^a] , \tag{B.4}$$

with

$$H[N] = \int_\Sigma \mathrm{d}^3x\, N\left(\frac{2\kappa}{\sqrt{q}}\left(P^{ab}P_{ab} - \frac{1}{2}P^2\right) - \frac{\sqrt{q}}{2\kappa}{}^{(3)}\mathcal{R}\right) \approx 0 , \tag{B.5}$$

$$H_a[N^a] = -2\int_\Sigma \mathrm{d}^3x\, N^a \nabla_b P^b_a \approx 0 , \tag{B.6}$$

respectively denoting the so-called Hamiltonian constraint and spatial diffeomorphism constraint.

[1] We recall the definition of the extrinsic curvature $K_{\mu\nu} = \frac{1}{2}\mathcal{L}_n g_{\mu\nu}$ in terms of the Lie derivative $\mathcal{L}_n$ w.r.t. the vector field n^μ. Since $K_{\mu\nu}n^\nu = 0$, this can be written as a tensorial object K_{ab} on Σ.

They form the following algebra known as *Dirac hypersurface deformation algebra* [302, 303]

$$\{H[M], H[N]\} = H_a\big[q^{ab}(M\partial_b N - N\partial_b M)\big] \,, \tag{B.7}$$

$$\{H[M], H_a[N^a]\} = -H[\mathcal{L}_{\vec{N}} M] \,, \tag{B.8}$$

$$\{H_a[M^a], H_b[N^b]\} = -H_a[\mathcal{L}_{\vec{N}} M^a] \,. \tag{B.9}$$

Note that a phase space dependence occurs at the r.h.s. of (B.7) via the inverse metric q^{ab} so that the constraint algebra is not a genuine Lie algebra as it features structure functions rather than structure constants[2]. This is to be contrasted with the fact that spatial diffeomorphisms do form a Lie algebra. In fact, while the the infinitesimal transformations

$$\{q_{ab}, H_c[N^c]\} = \mathcal{L}_{\vec{N}}\, q_{ab} \qquad , \qquad \{P^{ab}, H_c[N^c]\} = \mathcal{L}_{\vec{N}}\, P^{ab} \tag{B.10}$$

show that $H_a[N^a]$ generates infinitesimal spatial diffeomorphisms along the vector field $\vec{N}$, the action of H is more involved as it also encodes the dynamics of the theory. As discussed for instance in [129], these agree with the action of diffeomorphisms orthogonal to Σ only *on-shell* when Einstein equations are satisfied. The group of transformations generated by H and H_a is actually the so-called Bergmann-Komar group $\mathsf{BK}(\mathcal{M})$ and not $\mathsf{Diff}(\mathcal{M})$ [305–307]. The difference between the two groups is a physical one (see e.g. Sec. 1.4 in [129]): $\mathsf{Diff}(\mathcal{M})$ is a kinematical symmetry and it is shared by any generally covariant theory, $\mathsf{BK}(\mathcal{M})$ is instead a dynamical symmetry group for GR and it depends on the particular theory one considers (although the algebra (B.7)-(B.9) does not).

The geometrical interpretation of the infinitesimal transformations generated by the constraints is that of infinitesimal deformations of a hypersurface embedded in spacetime [280], which form a larger class of transformations than $\mathsf{Diff}(\mathcal{M})$. Lapse and shift thus appear in the ADM formulation only as arbitrary Lagrange multipliers in the Hamiltonian and correspond to a choice of gauge. Their choice determines the relative positions of neighbouring Cauchy surfaces as shown in Fig. B.1, i.e., it tells us where in the spacetime we end up after an infinitesimal time evolution generated by the Hamiltonian H. Only Dirac observables, i.e. those phase space functions $\mathcal{O}$ such that $\{\mathcal{O}, H\} \approx 0 \approx \{\mathcal{O}, H_a\}$, have some invariant physical meaning (e.g. are independent of the choice of coordinates). Therefore, in agreement with the general discussion of Appendix A, the constraints eliminate 4+4 phase space d.o.f.: 4 via the algebraic restriction imposed by the equations $H_a \approx 0$ and $H \approx 0$, and other 4 by selecting Dirac observables. We are thus left in total with 2+2 phase space d.o.f. per point.

B.1.2 Connection Variables

As already anticipated, the basic strategy underlying LQG is to recast the phase space of GR in a form that is close to gauge theories so that a non-perturbative Dirac quantisation procedure can be applied. This is achieved in two steps as follows. First, we introduce new phase space variables (E^a_i, K^i_a) defined as

[2] From a mathematical viewpoint, the Poisson brackets (B.7)-(B.9) define a Lie algebroid structure [304].

$$q\,q^{ab} = E^{ai}E^b_i \qquad , \qquad \sqrt{q}\,K^b_a = K_{ai}E^{bi} \qquad , \qquad \{K^i_a(x), E^b_j(y)\} = \kappa\,\delta^b_a\delta^i_j\delta^{(3)}(x,y) \tag{B.11}$$

with E^a_i interpreted as a densitised triad (*dreibein*) $\sqrt{q}e^a_i$, with $q^{ab} = e^a_i e^{bi}$, and K^i_a is related to the extrinsic curvature via $K_{ab} = K_{ai}e^i_b$, with e^i_b the dual co-triad[3]. Here the indices $i, j = 1, 2, 3$ label components in an internal $\mathfrak{su}(2)$ algebra and are raised and lowered by the Kronecker delta δ_{ij}. In fact, a local SU(2) symmetry is introduced in the formalism and it corresponds to the invariance under local rotations of the orthonormal frames identified by the triads. The phase space is thus enlarged by introducing new gauge d.o.f. and in turn an additional first class constraint arises. This is the so-called *Gauß law* also familiar from ordinary Yang-Mills theories

$$G_{ij}[\Lambda^{ij}] = \frac{1}{\kappa}\int_\Sigma \mathrm{d}^3x\,\Lambda^{ij}K_{a[i}E^a_{j]} \approx 0\,, \tag{B.12}$$

and it generates internal SU(2) gauge transformations

$$\{K^i_a, G_{jk}[\Lambda^{jk}]\} = \Lambda^i_\ell K^\ell_a \qquad , \qquad \{E^a_i, G_{jk}[\Lambda^{jk}]\} = \Lambda^\ell_i E^a_\ell\,. \tag{B.13}$$

Observables must be also invariant under these SU(2) transformations in addition to the gauge transformations generated by the Hamiltonian and spatial diffeomorphism constraints so that the dynamics generated by such extended formulation is equivalent to that of the ADM formulation.

However, as can be seen from (B.13), none of the new canonical variables transform as a Yang-Mills gauge connection. The second step is then to perform a further canonical transformation by introducing the so-called Ashtekar-Barbero variables

$${}^{(\beta)}A^i_a := \Gamma^i_a + \beta K^i_a \qquad , \qquad {}^{(\beta)}E^a_i := E^a_i/\beta \tag{B.14}$$

where Γ^i_a is the spin connection related to e^a_i as $\Gamma^i_a = \frac{1}{2}\epsilon^{ijk}e^b_k(2\partial_{[b}e_{a]j} + e^c_j e^\ell_a \partial_b e_{c\ell})$, and β is a free real parameter of the theory called Barbero-Immirzi parameter which will obtain a physical meaning only later at the quantum level[4]. It is in fact possible to show that the constraint (B.12) reads in the new variables as

$$G_k[\Lambda^k] := G_{ij}[-\epsilon^{ijk}\Lambda_k] = -\frac{1}{\kappa}\int_\Sigma \mathrm{d}^3x\,\Lambda_k\epsilon^{ijk}E^a_{[i}K_{a|j]} = \frac{1}{\kappa}\int_\Sigma \mathrm{d}^3x\,\Lambda^k D_a\,{}^{(\beta)}E^a_k\,, \tag{B.15}$$

where $D_a = \partial_a + \epsilon^{ijk}\,{}^{(\beta)}A^j_a$ acts only on internal indices, and we have

$$\{{}^{(\beta)}A^i_a, G_k[\Lambda^k]\} = -D_a\Lambda^i \qquad , \qquad \{{}^{(\beta)}E^a_i, G_k[\Lambda^k]\} = \epsilon^{ijk}\Lambda^{(\beta)}_j E^a_k \tag{B.16}$$

from which we see that ${}^{(\beta)}A^i_a$ transforms as a non-abelian SU(2) connection. Moreover, the transformation (B.14) is canonical and we still have the non-vanishing Poisson brackets

[3] We restrict ourselves to positive orientation to avoid additional sign factors.

[4] Although it turns out that the form of the constraints simplifies for $\beta = \pm i$ (see Eq. (B.18) below), it is not known how to formulate the quantum theory in the case of non-real β due to complicated reality conditions.

$$\{{}^{(\beta)}A^i_a(x), {}^{(\beta)}E^b_j\} = \kappa\,\delta^b_a\delta^i_j\delta^{(3)}(x,y)\ . \tag{B.17}$$

To simplify the notation, in the following we will drop the superscript $^{(\beta)}$ in the canonical variables. Finally, the Hamiltonian and spatial diffeomorphism constraints can be expressed in the new variables yielding (up to terms proportional to G which can be equivalently absorbed by linear combinations of the constraints)

$$H[N] = \frac{1}{\kappa}\int_\Sigma \mathrm{d}^3x\, N\left(\frac{\beta^2}{2\sqrt{q}}E^a_iE^b_j\epsilon^{ij}_k F^k_{ab} - \frac{1+\beta^2}{\sqrt{q}}K^i_{[a}K^j_{b]}E^a_iE^b_j\right)\ , \tag{B.18}$$

$$H_a[N^a] = \frac{1}{\kappa}\int_\Sigma \mathrm{d}^3x\, E^a_i\mathcal{L}_{\vec{N}}A^i_a\ , \tag{B.19}$$

where $F^k_{ab} = 2\partial_{[a}A^k_{b]} + \epsilon^k_{ij}A^i_aA^j_b$ is the curvature (field strength) of the Ashtekar connection, $K^i_a = \frac{1}{\beta}(A^i_a - \Gamma^i_a)$, and $\sqrt{q} = \sqrt{\epsilon_{abc}\epsilon^{ijk}E^a_iE^j_bE^k_c/6}$.

B.2 Quantum Theory: Kinematics

The key new aspect of the phase space reformulation discussed in the previous section is that the structure of the space of Ashtekar connections playing the role of configuration space is much better understood than that of a space of metrics. Moreover, such a formulation sets the stage to perform a background-independent quantization. To this aim, a suitable subalgebra of phase space functions has to be chosen to get a well-defined representation as elementary operators in the quantum theory. Such functions need to be point-separating so that other phase space functions can be reconstructed with arbitrary precision. The input for such a choice in LQG comes from lattice gauge theory and consists of:

- Holonomies $h^{(j)}_\gamma(A)$ of the gauge connection A^i_a along curves $\gamma : [0,1] \to \Sigma$, given by the path-ordered exponential

$$h^{(j)}_\gamma(A) = \mathcal{P}\exp\left(\int_\gamma A(\gamma(s))\right) \qquad \text{with} \qquad A(\gamma(s)) = A^i_a(\gamma(s))\dot\gamma^a(s)\tau^{(j)}_i\ , \tag{B.20}$$

  where s denotes the parameter along the curve γ in Σ, $\dot\gamma^a$ its tangent vector, and $\tau^{(j)}$'s the (anti-hermitian) $\mathsf{SU(2)}$ generators in a certain representation j.

- Fluxes $E_n(S)$ constructed by integrating E^a_i, contracted with a smearing function n^i, over surfaces S in Σ as

$$E_n(S) = \int_S E^a_in^i\mathrm{d}S_a = \int_S E^a_in^i\epsilon_{abc}\,\mathrm{d}x^b\wedge\mathrm{d}x^c\ . \tag{B.21}$$

Unlike lattice gauge theories, where a choice of lattice is usually specified, here we consider all possible holonomies and fluxes obtained by choosing arbitrary curves and surfaces. The information about A^i_a and E^a_i can be recovered from their holonomies and fluxes by respectively taking the limit of infinitesimally short paths and infinitesimally small surfaces (and suitable

n^i). Holonomies and fluxes identify a well-defined Poisson bracket algebra known as *holonomy-flux algebra*. The details of its computation are not relevant for our present purposes and we refer to [129] for a complete discussion. This provides the starting point to apply the Dirac quantisation procedure to our theory. For this, we need to find a kinematical unconstrained Hilbert space $\mathcal{H}_{\text{kin}}$ on which operators corresponding to holonomies and fluxes can be defined, and then impose the constraints at the operator level, namely

$$\mathcal{H}_{\text{kin}} \xrightarrow{\hat{G}_i=0} \mathcal{H}^0_{\text{kin}} \xrightarrow{\hat{H}_a=0} \mathcal{H}_{\text{Diff}} \xrightarrow{\hat{H}=0} \mathcal{H}_{\text{Phys}} \tag{B.22}$$

Note that the above sequence of Hilbert spaces has to be thought of only as a sketch summarising the main idea behind the construction of the physical Hilbert space and not as a strict sequence of subspaces. Indeed, as we will discuss in the next section, unlike the case of the Gauß constraint for which $\mathcal{H}^0_{\text{kin}}$ is actually the $\mathsf{SU(2)}$-invariant subspace of $\mathcal{H}_{\text{kin}}$, the constraint algebra forbids a straightforward implementation of $\hat{H}_a = 0$ which requires instead the dual space. Moreover, for the purposes of this thesis, we will restrict ourselves to the kinematical structure of LQG. The discussion of the Hamiltonian constraint is much more delicate and will not be covered here (see [129] for details).

B.2.1 Hilbert Space and Spin Network States

As starting point in the construction of the kinematical Hilbert space, we consider the so-called *cylindrical functions* associated with a graph Γ with $L \in \mathbb{N}_0$ edges embedded in Σ. These are complex-valued wave functionals $\Psi_\Gamma[A]$ depending on the connection through a finite number of holonomies along the edges of the graph, i.e.

$$\Psi_\Gamma[A] := \Psi(h^{(j_1)}_{\gamma_1}(A)), \dots, h^{(j_L)}_{\gamma_L}(A)) : \mathsf{SU(2)}^L \longrightarrow \mathbb{C} \,. \tag{B.23}$$

These can be equipped with a scalar product by exploiting the group elements nature of holonomies and integrating against the natural invariant Haar measure on $\mathsf{SU(2)}$, with no references to any background metric. Specifically, the scalar product between two cylindrical functions Ψ_{Γ_1} and Φ_{Γ_2} with underlying graphs Γ_1 and Γ_2 is defined as

$$\langle \Psi_{\Gamma_1} | \Phi_{\Gamma_2} \rangle_{\text{kin}} = \int \mathrm{d}\mu_{\text{AL}} \, \overline{\Psi_{\Gamma_1}[A]} \, \Phi_{\Gamma_2}[A] := \int_{\mathsf{SU(2)}^L} \prod_i \mathrm{d}h_i \, \overline{\Psi_\Gamma(h_{\gamma_1}, \dots, h_{\gamma_L})} \, \Phi_\Gamma(h_{\gamma_1}, \dots, h_{\gamma_L}) \,, \tag{B.24}$$

where μ_{AL} is called the Ashtekar-Lewandowski measure [285–288], Γ is a common refinement of the graphs Γ_1, Γ_2 containing all their edges, and Ψ, Φ are expressed as functions on Γ by adding trivial holonomies corresponding to edges labeled by the $j = 0$ representation[5]. Two cylindrical functions are orthogonal if they depend non-trivially on holonomies defined on different edges.

Elementary operators corresponding to holonomies and fluxes act on cylindrical functions

[5] Naturally, the theory should be invariant under the addition of trivial dependencies, as well as under orientation flips. This is achieved by imposing consistency conditions on cylindrincal functions and taking equivalence classes w.r.t. them [129].

respectively as multiplications and derivations, i.e.

$$\hat{h}^{(j)}_\gamma \,|\Psi\rangle = h^{(j)}_\gamma(A)\Psi[A] \qquad , \qquad \hat{E}_n(S)\,|\Psi\rangle = -i\hbar\kappa \int_S n^i \frac{\delta}{\delta A^i_a} \mathrm{d}S_a \,|\Psi\rangle \ . \tag{B.25}$$

The Hilbert space $\mathcal{H}_{\rm kin}$ is then obtained as the completion of the space spanned by cylindrical functions w.r.t. the above scalar product [129]. Remarkably, as proven by the so called LOST-F theorem [144,145], the above construction provides a unique representation of the holonomy-flux algebra under the assumptions of spatial diffeomorphism invariance and irreducibility.

The next step consists of promoting the Gauß constraint to an operator on our Hilbert space and compute its kernel. This can be done systematically as discussed in [129]. Here, to understand what are the SU(2)-invariant states, it is just sufficient to consider the transformation properties of holonomies according to which SU(2) gauge transformations only act at the endpoints, i.e.

$$h^{(j)}_\gamma(A) \longmapsto U(\gamma(0))h^{(j)}_\gamma(A)U^{-1}(\gamma(1)) \ , \tag{B.26}$$

so that gauge invariant states are given by those cylindrical functions for which the transformations at the endpoints of holonomies cancel each other. Specifically, by using the Peter-Weyl decomposition of cylindrical functions in terms of Wigner matrices

$$\Psi[A] = \sum_{j_i=0,\frac{1}{2},\dots}^{\infty} \sum_{m_i,n_i=-j_i}^{j_i} \left(\prod_{i=1}^{L} \sqrt{d_{j_i}} (\mathscr{D}^{(j_i)})^{m_i}_{n_i}(h_i) \right) (f_{j_1\dots j_L})^{n_1\dots n_L}_{m_1\dots m_L} \ , \tag{B.27}$$

the gauge invariance requirement amounts to decompose $(f_{j_1\dots j_L})^{n_1\dots n_L}_{m_1\dots m_L}$ into SU(2)-invariant tensors (intertwiners) and contract all holonomies ending or starting at a given vertex with them, with no free indices left. Such kind of cylindrical functions spanning the SU(2)-invariant subspace $\mathcal{H}^0_{\rm kin} = {\rm Inv}_{\mathsf{SU(2)}}(\mathcal{H}_{\rm kin})$ are called *spin networks*. Roughly speaking, a spin network $T_{\Gamma,\vec{j},\vec{\iota}}$ is then a (oriented) graph Γ whose edges carry SU(2) representations labeled by the spins $\vec{j} = \{j_i\}_{i=1,\dots,L}$, and whose vertices $\{v_k\}_{k=1,\dots,V}$ are coloured with SU(2)-invariant tensors $\vec{\iota} = \{\iota_k\}_{k=1,\dots,V}$ in the tensor product of the edge representations incident at v_k. Considering the same underlying graph Γ and an orthonormal basis in the SU(2) intertwiner space, we have

$$\langle T_{\Gamma,\vec{j},\vec{\iota}} | T_{\Gamma,\vec{j}',\vec{\iota}'} \rangle_{\rm kin} = \delta_{\vec{j},\vec{j}'}\delta_{\vec{\iota},\vec{\iota}'} \ , \tag{B.28}$$

i.e., spin network states form an orthonormal basis of the kinematical Hilbert space restricted to Γ. The simplest example of such gauge-invariant states is given by a Wilson loop, which is just the trace of the holonomy along a closed curve, and correspond to a single link graph whose group indices are contracted with a Kronecker delta (2-valent SU(2)-intertwiner)[6].

Since only holonomies and not the connection itself can be implemented as operators on the LQG Hilbert space, spatial diffeomorphisms generated by (B.19) are imposed as finite transformations at the quantum level (exponentiated action). Solving the constraint $\hat{H}_a = 0$ then amounts to demand invariance under finite diffeomorphisms in Σ which move spin network graphs. The

[6] The use of Wilson loops lies at the origin of LQG and its name [284].

invariant states are thus independent from the embedding in a continuum space and only their combinatorial structure becomes physically relevant. This can be rigorously done via a group averaging procedure [245,246] according to which one starts with a given spin network and average it over the action of the spatial diffeomorphism group. The resulting solutions however are not elements of the kinematical Hilbert space, but rather of its dual space. The details can be found in [129,247] and are not relevant for this thesis where we only consider symmetry-reduced models in which the constraint is automatically satisfied at the classical level.

B.2.2 Composite Operators and Quantum Geometry

Starting from the basic operators (B.25) more complicated ones can be constructed, although plagued in general by ambiguities due for instance to factor ordering choices. The strategy consists of taking the classical quantities and regularise them in terms of holonomies and fluxes. The resulting expressions can be thus implemented as operators on the kinematical Hilbert space and their action can be computed in the limit of infinitely small holonomies and fluxes, where the exact classical expression is approached. Remarkably, relatively simple expressions can be found for operators corresponding to geometric quantities such as area and volume [287,308–311], which involve only the fluxes and no factor ordering issues with holonomies arise.

Specifically, at the classical level, the area $A(S)$ of a surface S embedded in Σ is given by

$$A(S) = \int_{\mathcal{U}} \mathrm{d}^2u \, \sqrt{\det\left(X^*q\right)(u)} = \sum_i \int_{\mathcal{U}_i} \mathrm{d}^2u \, \sqrt{\det\left(X^*q\right)(u)} \,, \tag{B.29}$$

where $\mathcal{U} = \bigcup_i \mathcal{U}_i$ denotes a coordinate chart partitioned into disjoint subsets $\mathcal{U}_i$, and X^*q is the induced metric on S along the embedding $X : \mathcal{U} \to S$ of $\mathcal{U}$ into S. In the limit of small $\mathcal{U}_i$, we have

$$\int_{\mathcal{U}_i} \mathrm{d}^2u \, \sqrt{\det\left(X^*q\right)(u)} = \int_{X(\mathcal{U}_i)} \sqrt{q\, q^{ab}\, \mathrm{d}s_a \mathrm{d}s_b} \approx \beta \sqrt{E^k(\mathcal{U}_i) E_k(\mathcal{U}_i)} \,, \tag{B.30}$$

where $\mathrm{d}s_a = \epsilon_{abc}\mathrm{d}x^b \wedge \mathrm{d}x^c = \frac{1}{2}\epsilon_{abc}\epsilon^{bc}\mathrm{d}^2x$ with $\epsilon^{12} = 1$, $E_k(\mathcal{U}_i) = \int_{\mathcal{U}_i} E^a_k \mathrm{d}\mathcal{U}_a$, and the β-dependence of the E's has been made explicit (cfr. Eq. (B.14)). The continuum expression (B.29) can then be written as the limit

$$A(S) = \lim_{\mathcal{U}_i \to 0} \sum_i \beta \sqrt{E^k(\mathcal{U}_i) E_k(\mathcal{U}_i)} \,, \tag{B.31}$$

which can be promoted to an operator by replacing the classical flux with the corresponding elementary operator (B.25). The action of the resulting operator on spin network states can be computed by defining the square root via spectral theorem and considering the partition of $\mathcal{U}$ to be fine enough so that there is at most one intersection between each $\mathcal{U}_i$ and the graph. Two kinds of intersections are then possible: with interior edges or at vertices of the graph. In the first case, it turns out that the action of $\hat{E}^k(\mathcal{U}_i)\hat{E}_k(\mathcal{U}_i)$ is diagonal and each intersection contributes to the area spectrum via the Casimir of the spin j representation labeling the edge, i.e.

$$\hat{A}(S)\,|\Psi\rangle = \kappa\,\beta\,\hbar \sum_i \sqrt{j_i(j_i+1)}\,|\Psi\rangle \,. \tag{B.32}$$

In the case of a vertex intersection, the resulting formula is more complicated and a detailed analysis can be found in [129]. Eq. (B.32) shows that the area operator has discrete spectrum and the smallest eigenvalue obtained for a single edge with $j = 1/2$ is given by $4\sqrt{3}\,\pi\beta G\hbar = 4\sqrt{3}\,\pi\beta\ell_P^2$. This is called the *area gap* and we see that the parameter β sets the scale of the quantum geometry w.r.t. the Planck scale.

An operator for the volume $V(R)$ of a spatial region R can be constructed in a similar way by regularising the classical expression

$$V(R) = \int_R \mathrm{d}^3x\,\sqrt{q} = \beta^{3/2}\int_R \mathrm{d}^3x\,\sqrt{|\epsilon_{abc}\epsilon^{ijk}E^a_i E^b_j E^c_k/6|}\,. \tag{B.33}$$

The process of regularisation is however more involved than for the area operator and in particular the final expression is a lot more complicated (see [129, 295, 309, 311, 312] for details). The corresponding operator acts non-trivially on the vertices of spin networks and more precisely on the invariant intertwiners. In particular, it vanishes for three-valent intertwiners so that the first non-trivial case consists of a 4-valent vertex. It is in principle possible to choose a basis in intertwiner space such that the volume operator is diagonal. Just as fluxes, also the volume operator admits discrete spectrum[7]. However the computation of the full spectrum is generally impossible analytically, as this would require to diagonalise matrices of arbitrary dimension. Nevertheless, some closed formulas and numerical techniques exist [313–317].

The geometry of space is thus quantised in LQG. By this we mean that geometric quantities such as area and volume correspond to quantum operators which are diagonalised by spin network states and admit a discrete spectrum. This provides us with an interpretation for spin networks as quantum geometries: a spin network corresponds to a quantum state where the geometry is excited in such a way that there are quanta of volume at the vertices of the graph, as well as quanta of area on surfaces intersected by it. The edges of the graph thus define a notion of connectedness for two neighbouring quanta of volume, associated with the magnitude of a surface separating them. This is of course a qualitative picture and the above geometric operators are a priori defined only on $\mathcal{H}^0_{\text{kin}}$. The notion of quantum geometry underlying spin networks has been formalised as "twisted geometries" (see e.g. [318, 319] and references within). The definition of spatially diffeomorphism invariant operators requires for instance a relational definition of areas and volumes w.r.t. other fields, e.g. by localising them w.r.t. additional matter fields, or to consider invariant quantities such as the total volume of the universe or the area of a spatial boundary surface.

[7] While it is known that the spectrum of the volume operator is discrete, it is not known whether it has a *gap*. It may for instance be the case that the eigenvalues lie dense in $\mathbb{R}^+$ as one could add vertices with such almost vanishing volume to any spin network (see e.g. [129] for further details).

Appendix C

Addendum to Chapter 4: Numerical Checks

In this Appendix we want to check the numerics discussed in Ch. 4. In general, as we are only interested in the qualitative behaviour of the system, we did not focus on optimising the accuracy of our numerical code and just focus on some direct numerical checks. This includes on the one hand to check if our results are stable and have significance, and on the other hand the consistency of our numerical strategy to solve geodesics equations with the analytic results. Of course further numerical checks are possible as well as the accuracy could be increased.

C.1 t_0-Accuracy and Cut-Off Independence

First, we can check the accuracy of our Matlab-algorithm for computing the level lines by calculating the corresponding t_0-values along the level lines and check whether t_0 is actually constant along the level line within the numerical fluctuations. As an example, Fig. C.1 shows the t_0-value along the level line corresponding to $t_0 = 4$ for the metric (4.18) featuring no Kasner transitions, the same considered as a reference in the plots of Sec. 4.3.3, and $t_0 = -5$ for the case of Kasner transitions (metric (4.36)). For both cases the accuracy remains within the third and fourth digits. Close to $t_* = 0$ the error increases and we loose accuracy. This explains the numerical uncertainties at the end region of the line in fig. 4.7 that we also discussed in Sec. 4.3.3. Nevertheless, the turning point takes place at t_*-values where the accuracy is good (deviation of $\approx 0.05\%$ for $t_* \approx 0.2$ cfr. Fig. 4.5 in Sec. 4.3.3).

Second, we can also check how good the renormalisation procedure discussed in Sec. 4.3.2 works. To this aim, we compute the renormalised geodesic length (4.32) and hence the two-point correlator (4.14) for geodesics with a given l, that corresponds to fixed turning point values of t_* and z_*. The renormalised length is calculated for different values of the cutoff z_{UV} in order to check the result to be independent of z_{UV}. We did this for two different geodesics both in the case of no Kasner transitions (metric (4.18)) and when Kasner transitions are included (metric (4.36)). In tables C.1, C.2 we report the results for $z_{\rm UV} \in [0.05, 0.1]$ which turn out to be nicely

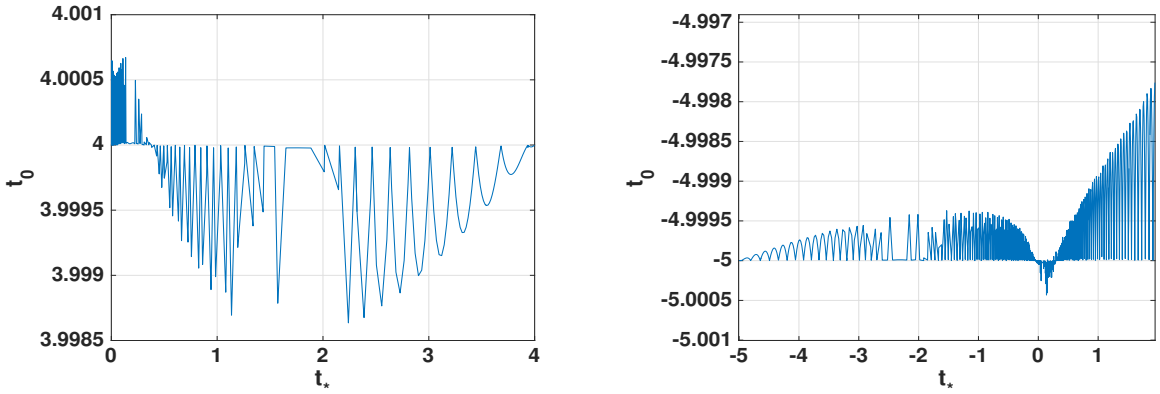

(a) (b)

Figure C.1: t_0-value along the (a) $t_0 = 4$ level line for metric (4.18) with $p = -1/4$, $\lambda = 0.06$, $a_{\text{ext}} = \lambda^p$, and (b) $t_0 = -5$ for the metric (4.36) with $p = -1/16$, $\Delta p = 3/16$, $\lambda = 0.06$, $a_{\text{ext}} = \lambda^p$. For (a) the accuracy is up to the fourth digit (maximal deviation $\lesssim 0.15\%$). The error around $t_* \to 0$ gets large, and the algorithm looses accuracy. For larger values of t_* ($t_* \gtrsim 0.2$), the accuracy is quite good. This is also the t_*-region where the turning point happens. In the case (b), the accuracy is still within the fourth digit (maximal deviation $\lesssim 0.065\%$) for negative t_*, and it decreases for positive t_* (maximal deviation $\lesssim 0.25\%$).

independent of z_{UV} within 0.1%. This is good enough for our qualitative analysis.

No Kasner Transitions:

For $\lambda = 0.06$ and $p = -\frac{1}{4}$

z_{UV}	$\exp(-L_{\text{ren}})$	$\exp(-L_{\text{ren}})$
0.05	0.761810	0.917559
0.06	0.761841	0.917597
0.07	0.761860	0.917661
0.08	0.761896	0.917716
0.09	0.761943	0.917783
0.1	0.761972	0.917897

Table C.1: $\exp(-L_{\text{ren}})$ vs. z_{UV} for $t_0 = 4$, $t_* = 3.8559$, $z_* = 2.1799$ (second column) and $t_0 = 4$, $t_* = 2.8439$, $z_* = 5.4963$ (third column).

Kasner Transitions:

For $\lambda = 0.06$ and $p = -\frac{1}{16}$, $\Delta p = \frac{3}{16}$ ($p_\pm = p \pm \Delta p$)

z_{UV}	$\exp(-L_{\text{ren}})$	$\exp(-L_{\text{ren}})$
0.05	0.367113	0.308506
0.06	0.367149	0.308554
0.07	0.367185	0.308602
0.08	0.367229	0.308661
0.09	0.367267	0.308714
0.1	0.367314	0.308774

Table C.2: $\exp(-L_{\text{ren}})$ vs. z_{UV} for $t_0 = -5$, $t_* = -0.7709$, $z_* = 5.2803$ (second column) and $t_0 = -5$, $t_* = 1.2333$, $z_* = 7.1157$ (third column).

C.2 Comparison with the z-Inpedendend Case

As a further consistency check for our numerics we can also consider the case of a z-independent λ (metric (4.15)) for which analytical results are available (see fig. 4.3 in Sec. 4.2 and [160]). A reasonable check for our numerics consists then in applying it to this metric and compare the numerical and the analytical results. As shown in fig. C.2, the behaviour of the numerical results

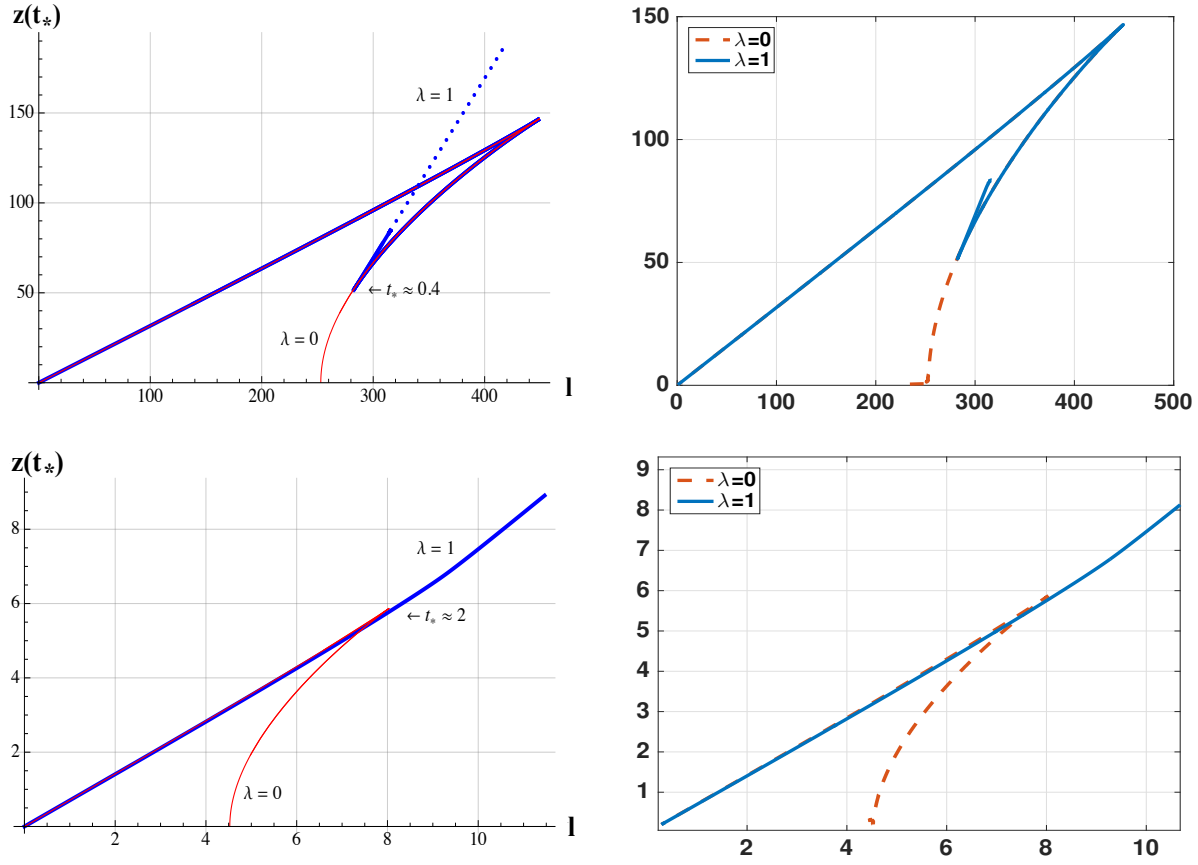

Figure C.2: Plots of $z(t_*)$ vs. $l = x(t_0)$ for $p = -1/4$ and $a_{ext} = 1$. The two plots on the left refer to the analytic results of [160] also reported in Sec. 4.2, while the two plots on the right refer to the numerical results. In both kind of plots, the red line represents the classical case with $\lambda = 0$, while the blue line represents the quantum corrected case with $\lambda = 1$ respectively for $t_0 = 100$ (upper plots), and $t_0 = 4$ (lower plots).

(plots on the right) agrees with the one expected from the analytic treatment (left).

In the case of $t_0 = 4$ (lower plots), the results actually coincide both in behaviour and scales. A very good agreement is reached also in the case of $t_0 = 100$ for almost all the range of t_* values (upper plots). However, the dashed blue line which was obtained in [160] by means of an asymptotic expansion for $t_* \to 0$ of the analytic solutions is missing in the numerical results which stop at that point. This is due to the above-mentioned loss of numerical accuracy in the vicinity of $t_* = 0$. In fact, for the metric (4.15), the classical regime is at $t^2 \gg \lambda^2$ so that, for $\lambda = 1$ and $t_0 = 100$, the geodesic is mainly following the classical solution and deviations from the classical behaviour due to quantum effects arise only for small values of t_*, where the turning point of the geodesics enters the high-curvature region near the resolved singularity. Nevertheless, the local minimum and turn around behaviour of the curve responsible for the resolution of the finite distance pole in the correlator are still clearly visible and the numerical results agree with the continuous blue curve obtained from plotting the analytic results without expanding for small values of t_*. Moreover, as already discussed in the main part of Ch. 4, numerical uncertainties also occur in the region close to $z_* = 0$ where the introduction of a cutoff is needed.

The turning point is visible also in the colour plots of t_0 reported in Fig. C.3, where the

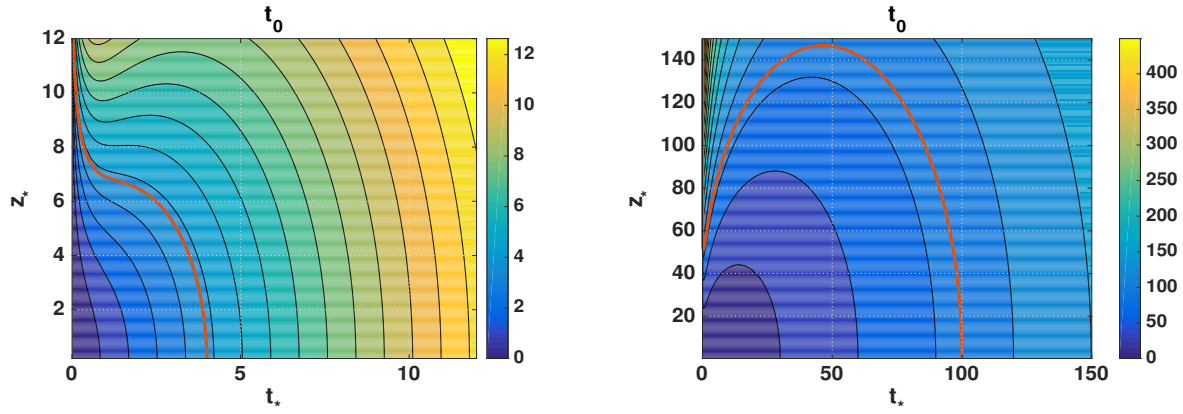

(a) (b)

Figure C.3: Colour plot of t_0 for the metric (4.15) with $p = -1/4$, $\lambda = 1$, $a_{ext} = 1$ and (a) $t_0 = 4$, (b) $t_0 = 100$.

behaviour of different t_0-level lines is visible at once. In particular, we can easily verify the statement of [160] concerning the disappearance of the turning point around $t_0 \approx 5$ due to a new long-distance subleading quantum contribution responsible for the behaviour also reported in the lower plots of Fig. C.2. Indeed, looking at the behaviour of the different t_0-level lines in Fig. C.3 (a), we see that for $t_0 \approx 5$ the turning point becomes a saddle point and finally disappears for smaller values of t_0.

Finally, Fig. C.4 shows the numerical and analytical results of L_{ren} vs. $\log(z_*)$ for $t_0 = 4$ (a) and $t_0 = 100$ (b). In both cases the numerical and analytical results coincide up to the already discussed uncertainties occurring at the lower region of evaluation in z_*.

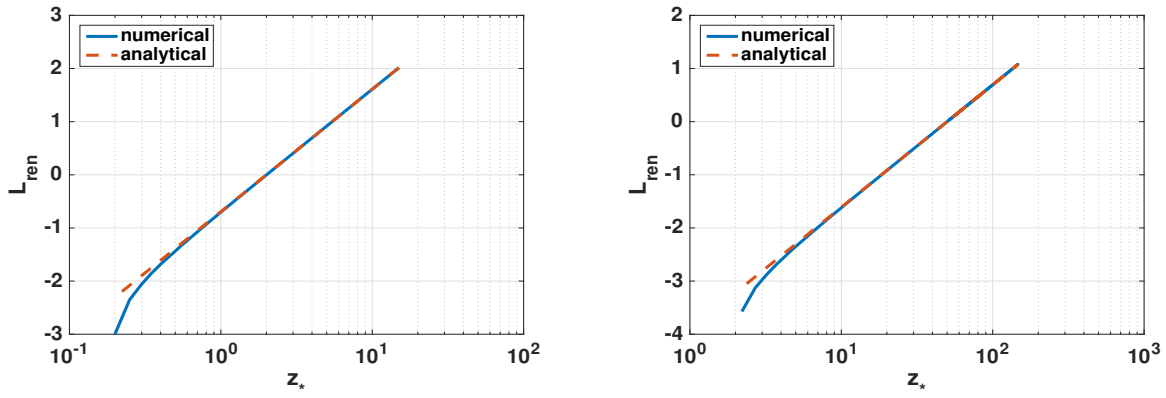

(a) (b)

Figure C.4: Plot of L_{ren} vs. z_* in log-scale for the metric (4.15) with $p = -1/4$, $\lambda = 1$, $a_{ext} = 1$ and (a) $t_0 = 4$, (b) $t_0 = 100$.

Appendix D

Penrose Diagrams for Classical and Quantum Schwarzschild BH

In this appendix we report the details of the construction of the Penrose diagram and the analysis of the corresponding causal structure for both the classical Schwarzschild solution and the quantum corrected effective models presented in Ch. 5.

D.1 Classical Case: Kruskal Extension and Causal Structure

The maximal analytic extension of the classical Schwarzschild metric (5.1) is obtained by introducing the so-called Kruskal-Szekeres coordinates as follows [320, 321]. First, we change coordinates from (t, r, θ, ϕ) to (u, v, θ, ϕ) with

$$u = t - r_* \qquad , \qquad v = t + r_* \tag{D.1}$$

where r_* is the so-called tortoise coordinate defined by

$$r_* = r + 2M \log\left(\frac{r - 2M}{2M}\right) . \tag{D.2}$$

Lines of constant v and u respectively correspond to ingoing and outgoing null geodesics. In such a coordinate system the metric takes the form

$$\mathrm{d}s^2 = -\left(1 - \frac{2M}{r}\right) \mathrm{d}u\mathrm{d}v + r^2 \mathrm{d}\Omega_2^2 \, , \tag{D.3}$$

where r is determined by $(v - u)/2 = r + 2M \log\left(\frac{r-2M}{2M}\right)$. Kruskal coordinates in the exterior region $r > 2M$ are then defined by

$$T = \frac{1}{2}(V + U) \qquad , \qquad X = \frac{1}{2}(V - U) \tag{D.4}$$

with $T \in (-\infty, \infty)$, $X > 0$ and $T^2 - X^2 < 0$, and $r(X,T)$ defined by the implicit equation $T^2 - X^2 = UV = -\left(\frac{r-2M}{2M}\right)\exp(r/2M)$ with

$$U = -\exp\left(-\frac{u}{4M}\right) \qquad , \qquad V = \exp\left(\frac{v}{4M}\right) \tag{D.5}$$

$U < 0$ and $V > 0$ for all values of r. The metric (D.3) then takes the form

$$\mathrm{d}s^2 = \frac{32M^3}{r}\exp\left(-\frac{r}{2M}\right)(-\mathrm{d}T^2 + \mathrm{d}X^2) + r^2\mathrm{d}\Omega_2^2 \,. \tag{D.6}$$

The metric (D.6) is well-defined and non-singular for the whole range $T \in \mathbb{R}$ and $X \in \mathbb{R}$. In particular, the metric is non-singular at the horizon ($r = 2M$) which in these coordinates is located at $T = \pm X$. The curvature singularity ($r = 0$) is located at $T^2 - X^2 = UV = 1$. The maximally extended Schwarzschild geometry can be thus divided into four regions separated by event horizons:

- `I`) the BH exterior region $-X < T < +X$ which is isometric to the exterior Schwarzschild solution ($r > 2M$);
- `II`) the BH interior region $|X| < T < \sqrt{1+X^2}$ which corresponds to $0 < r < 2M$ in Schwarzschild coordinates;
- `III`) the WH exterior region $+X < T < -X$ which is again isometric to the exterior Schwarzschild solution and can be regarded as another asymptotically flat universe on the other side of the Schwarzschild throat;
- `IV`) the WH interior region $-\sqrt{1+X^2} < T < -|X|$ corresponding to the region $0 < r < 2M$ on the other side.

Light-like geodesics moving in a radial direction look like straight lines at a 45-degree angle in the (X,T)-plane. Therefore, any event inside the black hole interior region will have a future light cone that remains in this region, while any event inside the white hole interior region will have a past light cone that remains in this region. This means that there are no time-like or null curves which go from region `I` to region `III`. Curves of constant r look like hyperbolas bounded by a pair of event horizons at 45 degrees, while lines of constant t-coordinate look like straight lines at various angles passing through the center $T = X = 0$.

Finally, performing the compactification

$$\tilde{U} = \arctan U \,, \quad \tilde{V} = \arctan V \qquad (-\pi/2 < \tilde{U}, \tilde{V} < \pi/2) \tag{D.7}$$

followed by a conformal transformation of the metric such that the resulting line element reads

$$\mathrm{d}\tilde{s}^2 = 4\cos^2\tilde{U}\cos^2\tilde{V}\mathrm{d}s^2 = -\frac{128M^3}{r}\exp\left(-\frac{r}{2M}\right)\mathrm{d}\tilde{U}\mathrm{d}\tilde{V} + 4r^2\cos^2\tilde{U}\cos^2\tilde{V}\mathrm{d}\Omega_2^2 \,, \tag{D.8}$$

the curvature singularity $UV = 1$ corresponds now to $\tilde{U} + \tilde{V} = \pm\frac{\pi}{2}$, and the infinitely extended spacetime can be represented with the 2-dimensional Penrose diagram of finite size given in Fig.

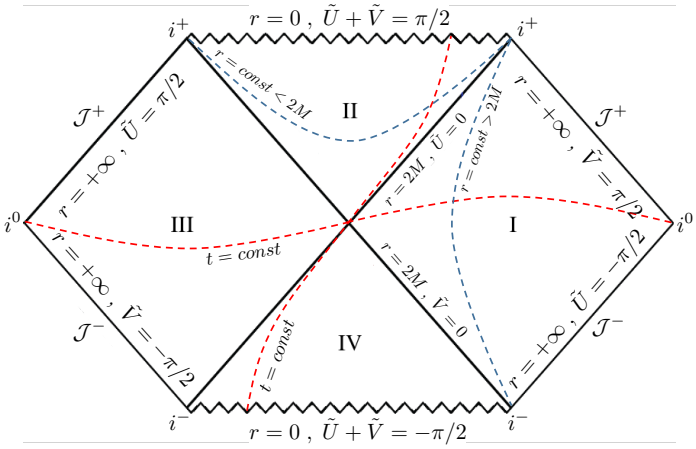

5.1, also reported here for completeness, where the angular coordinates are suppressed so that each point can be thought of as representing a 2-sphere of radius r.

D.2 Effective Quantum Corrected Case

Let us now consider the case of the quantum corrected spacetime described by the line element (5.52)-(5.54) for our first polymer model and (5.124)-(5.126) for the second model, respectively. The construction of the Penrose diagram for both models proceeds along the same steps. In particular, since the specific form of the metric is not needed in the following discussion and the only relevant aspects turn out to be the asymptotic Schwarzschild behaviour and the property $a'(r_s^{(\pm)}) \neq 0$, $\mathrm{sgn}(a'(r_s^{(\pm)})) = \pm 1$ at the horizon, we can keep the notation generic so that the considerations reported in this appendix can be applied to both our models. As for the classical case discussed in the previous section, the starting point to construct the Kruskal extension for our polymer Schwarzschild geometry is to define Kruskal-Szekeres coordinates (X, T) by (cfr. [322])

$$T^2 - X^2 = \exp\left[\left(\frac{\mathrm{d}\bar{a}}{\mathrm{d}r}\Big|_{r=r_s^{(\pm)}}\right) r_*(b)\right] \quad , \quad \frac{T}{X} = \begin{cases} \tanh\left(\frac{t}{2}\left(\frac{\mathrm{d}\bar{a}}{\mathrm{d}r}|_{r=r_s^{(\pm)}}\right)\right) & -1 < \frac{T}{X} < 1 \\ \coth\left(\frac{t}{2}\left(\frac{\mathrm{d}\bar{a}}{\mathrm{d}r}|_{r=r_s^{(\pm)}}\right)\right) & -1 < \frac{X}{T} < 1 \end{cases} , \tag{D.9}$$

where the definition now refers to the physical radius b instead of the radial coordinate r (which unlike the classical case do not coincide in the effective quantum theory), $r_s^{(\pm)}$ is the radial coordinate of the horizon respectively in the positive and negative r-ranges given in Eqs. (5.93) (resp. Eq. (5.135)) for the first (resp. second) model, and r_* is the so-called tortoise coordinate defined by

$$r_*(b) = \int_{b_0}^{b} \mathrm{d}b \, \frac{\frac{\mathrm{d}r^{(\pm)}}{\mathrm{d}b}}{\bar{a}(b)} = \int_{r_{\mathcal{T}}}^{r^{(\pm)}(b)} \mathrm{d}r \, \frac{L_o^2}{a(r)} \, . \tag{D.10}$$

where we set the reference value b_0 to be at the transition surface, i.e., $b_0 = b_{\mathcal{T}} \equiv b(r_{\mathcal{T}})$, where $b(r)$ takes its minimal value and the bounce occurs. By construction, $r_*(b_{\mathcal{T}}) = 0$ at the transition surface so that Eq. (D.9) yields $T^2 - X^2 = 1$ there. Note that we fixed the reference point to be at the transition surface for both the interior and exterior regions. As discussed below, by

performing the integrals in the complex domain, the sign switch in the definition (D.9) going from the interior to the exterior region is provided by the imaginary part of the integral (D.10) which corresponds to the residue at the pole occurring at the horizon. Moreover, the definition (D.9) implies that we need two (X,T)-coordinate charts to cover the whole range $r \in (-\infty, +\infty)$. Indeed, as discussed in Ch. 5 for both models, $b(r)$ as a function of r exhibits two branches for $r > r_{\mathcal{T}}$ and $r < r_{\mathcal{T}}$ where respectively it increases and decreases monotonously. This means that we have to split the construction of the Penrose diagram in these two regions where $b(r)$ is invertible and show that they can be smoothly glued afterwards.

The explicit evaluation of the integral (D.10) is quite involved. However, to construct the maximal extension of the polymer Schwarzschild spacetime we need to understand the behaviour of r_* for some specific values of $b(r)$, e.g., at the horizons and asymptotically far at infinity. Let us then start by considering the $r > r_{\mathcal{T}}$ region. At the horizon $b(r_s^{(+)})$, we have

$$r_*(b(r_s^{(+)})) = \int_{b_{\mathcal{T}}}^{b(r_s^{(+)})} \mathrm{d}b \, \frac{\frac{\mathrm{d}r^{(+)}}{\mathrm{d}b}}{\bar{a}(b)} = \int_{r_{\mathcal{T}}}^{r_s^{(+)}} \mathrm{d}r \, \frac{1}{\bar{a}(r)} \, . \tag{D.11}$$

In analogy to the classical case, we expect r_* to be divergent for $r \to r_s^{(+)}$. In particular, being $\bar{a}(r) < 0$ for $r_{\mathcal{T}} \leq r \leq r_s^{(+)}$, we expect the integral (D.11) to yield $-\infty$. To see this, let us rewrite the integral as follows

$$r_*(b(r_s^{(+)})) = \int_{r_{\mathcal{T}}}^{r_s^{(+)}-\epsilon} \mathrm{d}r \, \frac{1}{\bar{a}(r)} + \int_{r_s^{(+)}-\epsilon}^{r_s^{(+)}} \mathrm{d}r \, \frac{1}{\bar{a}(r)} \, . \tag{D.12}$$

for some $\epsilon > 0$. The first integral in Eq. (D.12) is finite while, for ϵ small enough, the function in the second integral can be approximated with its series expansion around $r_s^{(+)}$ thus yielding

$$\begin{aligned} r_*(b(r_s^{(+)})) &\simeq \text{finite terms} + \int_{r_s^{(+)}-\epsilon}^{r_s^{(+)}} \mathrm{d}r \, \left(\frac{1}{\bar{a}'(r_s^{(+)})(r - r_s^{(+)})} + \mathcal{O}(r - r_s^{(+)}) \right) \\ &= \text{finite terms} + \frac{1}{\bar{a}'(r_s^{(+)})} \log\left(|r - r_s^{(+)}| \right) \Big|_{r=r_s^{(+)}-\epsilon}^{r=r_s^{(+)}} \, , \end{aligned} \tag{D.13}$$

from which we see that the (finite) pre-factor in front of the logarithm cancels the derivative in the exponential of Eq.(D.9), $r_*(r_s^{(+)}) \to -\infty$ logarithmically, and hence $T^2 - X^2 = 0$ (i.e., $T = \pm X$) at $b = b(r_s^{(+)})$. For the exterior region $b(r_s^{(+)}) < b(r) < +\infty$ instead we have that

$$r_*(b(r)) = \int_{r_{\mathcal{T}}}^{r} \mathrm{d}r \, \frac{1}{\bar{a}(r)} \qquad , \qquad r > r_s^{(+)} \tag{D.14}$$

which can be split as

$$r_*(b(r)) = \int_{r_{\mathcal{T}}}^{r_s^{(+)}-\epsilon} \mathrm{d}r \, \frac{1}{\bar{a}(r)} + \int_{r_s^{(+)}-\epsilon}^{r_s^{(+)}+\epsilon} \mathrm{d}r \, \frac{1}{\bar{a}(r)} + \int_{r_s^{(+)}+\epsilon}^{r} \mathrm{d}r \, \frac{1}{\bar{a}(r)} \, , \tag{D.15}$$

with $\epsilon > 0$. Let consider the first two integrals separately. The first one is finite. Concerning the

second integral, for ϵ arbitrarily small (say $\epsilon \to 0$), we can approximate it again by expanding the integrand function around $r_s^{(+)}$ thus yielding

$$\begin{aligned}\int_{r_s^{(+)}-\epsilon}^{r_s^{(+)}+\epsilon} \mathrm{d}r\, \frac{1}{\bar{a}(r)} &\underset{\epsilon\to 0}{\simeq} \int_{r_s^{(+)}-\epsilon}^{r_s^{(+)}+\epsilon} \mathrm{d}r \left(\frac{1}{\bar{a}'(r_s^{(+)})(r-r_s^{(+)})} + \mathcal{O}(r-r_s^{(+)}) \right) \\ &= \frac{1}{\bar{a}'(r_s^{(+)})} \left(\frac{1}{2} \oint_{\mathcal{C}} \frac{\mathrm{d}r}{r-r_s^{(+)}} \right) + \text{finite terms} \\ &= -\frac{i\pi}{\bar{a}'(r_s^{(+)})} + \text{finite terms}\,, \end{aligned} \tag{D.16}$$

where in the second line $\mathcal{C}$ denotes an infinitesimally small contour in the complex plane encircling $r = r_s^{(+)}$ where the integrand function has a first order pole, and in the third line we used Cauchy's residue theorem with the minus sign coming from the clockwise orientation of the integration contour. Substituting the above result into (D.15), we get

$$r_*(b(r)) = -\frac{i\pi}{\bar{a}'(r_s^{(+)})} + \int_{r_s^{(+)}+\epsilon}^{r} \mathrm{d}r\, \frac{1}{\bar{a}(r)} + \text{finite terms}\,, \tag{D.17}$$

from which, recalling the definition (D.9), it follows that

$$T^2 - X^2 = -\exp\left(\frac{\mathrm{d}\bar{a}}{\mathrm{d}r}\bigg|_{r=r_s^{(+)}} \int_{r_s^{(+)}+\epsilon}^{r} \mathrm{d}r\, \frac{1}{\bar{a}(r)} + \text{finite terms} \right)\,, \tag{D.18}$$

where, as already anticipated in the beginning of this section, the minus sign for the $r > r_s^{(+)}$ region comes from the imaginary term in Eq. (D.17) which, after cancellation of the $\mathrm{d}\bar{a}/\mathrm{d}r$ factors, gives $e^{-i\pi} = -1$. In particular, for $r \to +\infty$, the integral in (D.18) can be written as

$$\int_{r_s^{(+)}+\epsilon}^{+\infty} \mathrm{d}r\, \frac{1}{\bar{a}(r)} = \int_{r_s^{(+)}+\epsilon}^{\tilde{r}} \mathrm{d}r\, \frac{1}{\bar{a}(r)} + \int_{\tilde{r}}^{+\infty} \mathrm{d}r\, \frac{1}{\bar{a}(r)} = \text{finite terms} + \int_{\tilde{r}}^{+\infty} \mathrm{d}r\, \frac{1}{\bar{a}(r)}\,, \tag{D.19}$$

for some finite $\tilde{r}$ large enough, the integrand in the second term of (D.19) is well approximated by its classical expression thus yielding

$$\begin{aligned}\int_{r_s^{(+)}+\epsilon}^{+\infty} \mathrm{d}r\, \frac{1}{\bar{a}(r)} &\simeq \text{finite terms} + \int_{\tilde{r}}^{+\infty} \mathrm{d}r \left(1 - \frac{2M}{r}\right)^{-1} \\ &= \text{finite terms} + \Big[2M \log(r-2M) + r \Big]\Big|_{r=\tilde{r}}^{r=+\infty} \longrightarrow +\infty\,. \end{aligned} \tag{D.20}$$

where we omitted constant pre-factors multiplying r which can be absorbed by rescaling the integration variable accordingly as they do not affect the divergent logarithmic behaviour. Therefore, since $\frac{\mathrm{d}\bar{a}}{\mathrm{d}r}\big|_{r=r_s^{(+)}}$ is finite and positive, from Eq. (D.18) we see that $T^2 - X^2 \to -\infty$ as $r \to +\infty$. Analogous computations can be repeated for the region $r < r_{\mathcal{T}}$ where, taking into account that $b'(r) < 0$ as $b(r)$ monotonously decreases for $r < r_{\mathcal{T}}$, we find that $r_*(b(r_s^{(-)})) \to -\infty$ and hence $T^2 - X^2 = 0$ at $r = r_s^{(-)}$, while $r_* \to +\infty$ as $r \to -\infty$ and consequently $T^2 - X^2 \to -\infty$ asymptotically far in the negative r range.

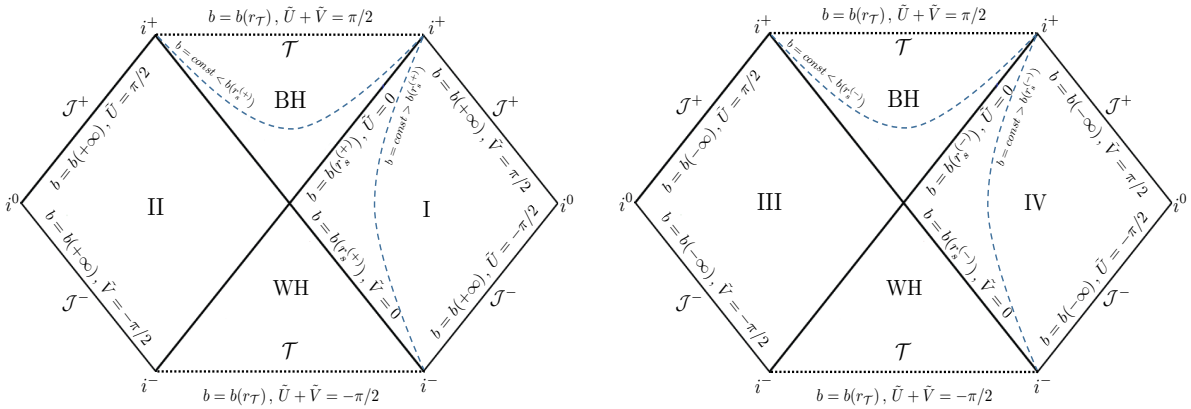

Figure D.1: Penrose diagrams for the $r > r_{\mathcal{T}}$ (a) and $r < r_{\mathcal{T}}$ (b) regions. We recall again that, although we use the same notation for both regions, they are covered by different $(\tilde{U}, \tilde{V})$-coordinate charts. As usual, the angular coordinates are suppressed so that each point of the diagram can be thought of as representing a 2-sphere of radius b.

Finally, by introducing the null coordinates $(\tilde{U}, \tilde{V})$ defined by

$$\tilde{U} = \arctan\left(T - X\right) \quad , \quad \tilde{V} = \arctan\left(T + X\right) \qquad (-\pi/2 < \tilde{U}, \tilde{V} < \pi/2) \tag{D.21}$$

we have that[1]

- $b = b_{\mathcal{T}}$ corresponds to $T^2 - X^2 = 1$ in (T, X)-coordinates which in turn corresponds to $\tilde{U} + \tilde{V} = \pm\frac{\pi}{2}$ in the $(\tilde{U}, \tilde{V})$-coordinates;
- $b = b(r_s^{(\pm)})$ corresponds to $T^2 - X^2 = 0$ and hence to $\tilde{U} \cdot \tilde{V} = 0$;
- $b \to \pm\infty$ corresponds to $T^2 - X^2 \to -\infty$ and hence to $\tilde{U} = \mp\frac{\pi}{2}$, $\tilde{V} = \pm\frac{\pi}{2}$.

Therefore, as summarized in the Penrose diagrams of Fig. D.1 (a), the $r > r(r_{\mathcal{T}})$ side of the effective quantum corrected Schwarzschild spacetime is divided in the following regions separated by event horizons located at $b = b(r_s^{(+)})$: the black hole exterior region (`I`) $-X < T < +X$ (i.e., $b > b(r_s^{(+)})$) which reduces to the classical asymptotically flat solution at infinity, the black hole interior region (BH) for which $|X| < T < \sqrt{1 + X^2}$ (i.e., $b_{\mathcal{T}} < b < b(r_s^{(+)})$), the white hole exterior region (`II`) $+X < T < -X$ which is again asymptotically flat, and the white hole interior region (WH) $-\sqrt{1 + X^2} < T < -|X|$. Similarly, for the $r < r_{\mathcal{T}}$ side we have two asymptotically flat regions `III` and `IV` where $b > b(r_s^{(-)})$ respectively corresponding to the white hole and black hole exterior regions, and the two interior regions BH and WH for which $b_{\mathcal{T}} < b < b(r_s^{(-)})$. Light-like geodesics moving in a radial direction correspond to straight lines at a 45-degree angle in the (X, T)-plane. Therefore, according to the direction of the future-pointing unit normal, any event inside the BH region will have a future light cone that remains in that region, while any event inside the WH region will have a past light cone that remains in that region until

[1] With a slight abuse of notation we use $(\tilde{U}, \tilde{V})$-coordinates for both the $r > r_{\mathcal{T}}$ and $r < r_{\mathcal{T}}$ regions. However, as already noticed, it should be kept in mind that these two regions are covered by different (T, X)-coordinate charts and hence also the corresponding $(\tilde{U}, \tilde{V})$ charts are different.

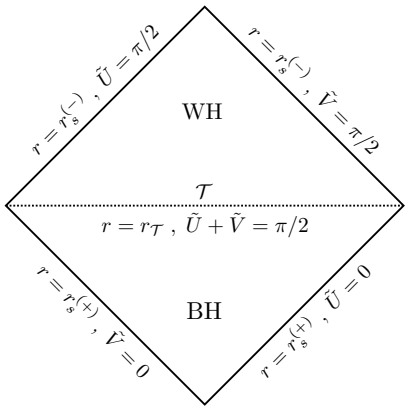

Figure D.2: Penrose diagram for the interior region $BH \cup WH$ ($r_s^{(-)} < r < r_s^{(+)}$) given by the union of the trapped and anti-trapped regions BH and WH separated by a transition surface $\mathcal{T}$ (dotted line). The past boundary is a black hole type horizon while the future boundary is a white hole type horizon.

hitting $r = r_{\mathcal{T}}$. This means that there are no time-like or null curves which go from region I to region II or from region III to IV. Moreover, the BH and WH regions correspond to a trapped and anti-trapped region and we can interpret the event horizons $b = b(r_s^{(\pm)})$ as a black hole and a white hole type horizons, respectively. The BH interior region $b_{\mathcal{T}} < b < b(r_s^{(+)})$ and the WH interior region $b_{\mathcal{T}} < b < b(r_s^{(-)})$ are causally connected through the transition surface $\mathcal{T}$ which replaces the classical singularity. Indeed, it is possible to introduce a local (T, X)-chart defined by

$$T^2 - X^2 = \exp\left[\bar{a}'(r_s^{(+)}) r_*(r)\right] \qquad , \qquad r_*(r) = \int_{r_{\mathcal{T}}}^{r} \mathrm{d}r\, \frac{1}{\bar{a}(r)} \tag{D.22}$$

which covers both interior regions[2] as schematically shown in the portion of the Penrose diagram of Fig. D.2 where we report also the corresponding values of $\tilde{U}$ and $\tilde{V}$.

The two diagrams of Fig. D.1 can be then glued together at the transition surface so that a light ray originating at the past boundary of region I will reach the future asymptotic boundary of region III passing trough the black hole and white hole interiors which are smoothly connected via the singularity resolution induced by quantum geometry effects. Similarly, region II is causally connected to region IV. Therefore, the Kruskal extension of the quantum corrected spacetime spans the whole range $r \in (-\infty, +\infty)$ corresponding to the entire region $\mathtt{I} \cup BH \cup WH \cup \mathtt{III}$ over which the metric coefficients are such that the effective 4-metric is smooth and well-defined. Moreover, since the spacetime topology is $\mathbb{R} \times \mathbb{R} \times \mathbb{S}^2$, the above considerations can be repeated over the whole non compact T-direction thus yielding the Penrose diagram for the Kruskal extension of the full quantum corrected effective Schwarzschild spacetimes discussed in Ch. 5 (cfr. Fig. 5.6) with an infinite tower of alternating trapped/anti-trapped and asymptotic regions to the past and future.

[2]Since $b(r)$ is smooth in the two branches $r > r_{\mathcal{T}}$ and $r < r_{\mathcal{T}}$, the overlapping map between the chart (D.22) and the corresponding chart (D.9) in one of the two interior regions (BH or WH) is smooth for any two intersecting open neighborhoods in that region. It is then possible to show that the chart (D.22) covers the entire $BH \cup WH$ region.

List of Figures

List of Tables

Acknowledgements

It is a pleasure for me to thank all the people who supported me during my doctoral studies and made it possible for me to complete this further step in my personal and career development.

First of all, I would like to thank my parents Pasquale and Rosaria for their unconditional support from the very beginning of my studies and for teaching me that everything in life can be faced with head held high, no matter how scaring it might seem. A very special thought goes to my mother to whom this thesis is dedicated...I know you will always be with me!

I would also like to thank the rest of my family for their support. A special thank goes to my uncle Gaspare for his precious advices through all these years.

The whole PhD experience would not have been the same without the amazing people I met here in Regensburg and I worked with. Therefore, I am very grateful to my supervisor Norbert Bodendorfer for his valuable guidance, patience and extraordinary willingness far beyond work-related questions. I learnt a lot from our discussions and I am really glad to have had the opportunity to see how research can be performed with critical open mind and honesty over the last three years. A very special thank must be reserved to my PhD colleagues Johannes Münch and Stratos Pateloudis for creating a very nice and stimulating group atmosphere which definitely contributed substantially in making the infinitely many hours spent in the office a pleasure every day. In particular, I would like to thank Johannes for sharing with me the path in this crazy journey of our PhD studies from the very first project on which this thesis is based and many more with unbelievable patience in reacting to my stupid questions and my being often late in the morning. I really enjoyed our discussions on the most random topics in math and physics which significantly improved my understanding and maybe more importantly my never-ending confusion. Even though he will never admit how a proper iced coffee must be prepared, an equally important acknowledgment goes to Stratos for all the discussions on "strings vs. loops", the meaning of general covariance, and how many dimensions we do really experience. I am really glad to have found two new valuable collaborators and friends. I'm sure that we will continue to work, discuss and have fun together in the coming years struggling in the attempt of decoding our badly written notes and totally chaotic blackboard pictures.

I would also like to thank Goffredo Chirco and Marco Laudato for their advices and for keeping active our collaboration and friendship since my master studies continuously sharing new ideas with each other. Moreover, I am very grateful to Daniele Oriti, Patrizia Vitale and Andreas Schäfer for supporting me during my postdoctoral applications. In this respect, a special thank goes again to Norbert Bodendorfer for his advices, support and for sharing with us his experience. The financial support of the Elite Network of Bavaria over my doctoral studies is also gratefully acknowledged.

Last but not least, I cannot close these acknowledgments without a word for my *brothers* Checco, Domenico, Peppe and Ciro. Although we are now far away from each other, you are like a "second family" for me and all the experiences we shared together over the years will always accompany me with a big smile...ovunque andremo e qualunque cosa faremo, saremo sempre DGS!!!

Bibliography

[1] J. M. Bardeen, B. Carter, and S. W. Hawking, "The four laws of black hole mechanics," *Commun. Math. Phys.* **31** (1973) 161–170.

[2] R. M. Wald, "The Thermodynamics of Black Holes," *Living Rev. Relativ.* **4** (1999) 6, gr-qc/9912119.

[3] S. Carlip, "Black hole thermodynamics," *Int. J. Mod. Phys. D* **23** (2014) 1430023, gr-qc/1410.1486.

[4] P. K. Townsend, "Black Holes," gr-qc/9707012.

[5] J. D. Bekenstein, "Black holes and the second law," *Lett. Al Nuovo Cim. Ser. 2* **4** (1972) 737–740.

[6] J. D. Bekenstein, "Black Holes and Entropy," *Phys. Rev. D* **7** (1973) 2333–2346.

[7] J. D. Bekenstein, "Generalized second law of thermodynamics in black-hole physics," *Phys. Rev. D* **9** (1974) 3292–3300.

[8] R. Bousso, "The holographic principle," *Rev. Mod. Phys.* **74** (2002) 825–874, hep-th/0203101.

[9] S. W. Hawking, "Particle creation by black holes," *Commun. Math. Phys.* **43** (1975) 199–220.

[10] S. W. Hawking, "Breakdown of predictability in gravitational collapse," *Phys. Rev. D* **14** (1976) 2460–2473.

[11] S. W. Hawking, "The unpredictability of quantum gravity," *Commun. Math. Phys.* **87** (1982) 395–415.

[12] G. t. Hooft, "Dimensional Reduction in Quantum Gravity," *Conf. Proc.* **C930308** (1993) 284–296, gr-qc/9310026.

[13] L. Susskind, "The World as a Hologram," *J. Math. Phys.* **36** (1994) 6377–6396, hep-th/9409089.

[14] G. t. Hooft, "The Holographic Principle," in *Basics Highlights Fundam. Phys.*, pp. 72–100, WORLD SCIENTIFIC2001.

[15] L. Smolin, "The strong and weak holographic principles," *Nucl. Phys. B* **601** (2001) 209–247, `hep-th/0003056`.

[16] S. W. HAWKING, "Black hole explosions?," *Nature* **248** (1974) 30–31.

[17] S. W. Hawking, "Black holes in general relativity," *Commun. Math. Phys.* **25** (1972) 152–166.

[18] L. Smolin, "The Bekenstein Bound, Topological Quantum Field Theory and Pluralistic Quantum Field Theory," `gr-qc/9508064`.

[19] S. D. Mathur, "The information paradox: A pedagogical introduction," *Class. Quantum Gravity* **26** (2009) 224001, `0909.1038`.

[20] D. Marolf, "The Black Hole information problem: past, present, and future," *Reports Prog. Phys.* **80** (2017) 092001, `1703.02143`.

[21] S. B. Giddings, "Black hole information, unitarity, and nonlocality," *Phys. Rev. D* **74** (2006) 106005, `hep-th/0605196`.

[22] J. Polchinski, "The Black Hole Information Problem," in *New Front. Fields Strings*, pp. 353–397, WORLD SCIENTIFIC2017.

[23] A. Ashtekar, V. Taveras, and M. Varadarajan, "Information is Not Lost in the Evaporation of 2-dimensional Black Holes," *Phys. Rev. Lett.* **100** (2008) 211302, `0801.1811`.

[24] A. Ashtekar, F. Pretorius, and F. M. Ramazano*ğ*lu, "Evaporation of 2-Dimensional Black Holes," *Phys. Rev. D* **83** (2010) 044040, `1012.0077`.

[25] Y. Nomura, J. Varela, and S. J. Weinberg, "Black Holes, Information, and Hilbert Space for Quantum Gravity," *Phys. Rev. D* **87** (2012) 084050, `1210.6348`.

[26] A. Perez, "No firewalls in quantum gravity: the role of discreteness of quantum geometry in resolving the information loss paradox," *Class. Quantum Gravity* **32** (2014) 084001, `1410.7062`.

[27] L. Amadei and A. Perez, "Hawking's information puzzle: a solution realized in loop quantum cosmology," `1911.00306`.

[28] L. Susskind, L. Thorlacius, and J. Uglum, "The Stretched Horizon and Black Hole Complementarity," *Phys. Rev. D* **48** (1993) 3743–3761, `hep-th/9306069`.

[29] L. Susskind and L. Thorlacius, "Gedanken Experiments involving Black Holes," *Phys. Rev. D* **49** (1993) 966–974, `hep-th/9308100`.

[30] J. D. Bekenstein, "Universal upper bound on the entropy-to-energy ratio for bounded systems," *Phys. Rev. D* **23** (1981) 287–298.

[31] W. Fischler and L. Susskind, "Holography and Cosmology," `hep-th/9806039`.

[32] R. Bousso, "A Covariant Entropy Conjecture," *J. High Energy Phys.* **1999** (1999) 004–004, `hep-th/9905177`.

[33] R. Bousso, "Holography in General Space-times," *J. High Energy Phys.* **1999** (1999) 028–028, `hep-th/9906022`.

[34] E. E. Flanagan, D. Marolf, and R. M. Wald, "Proof of Classical Versions of the Bousso Entropy Bound and of the Generalized Second Law," *Phys. Rev. D* **62** (1999) 084035, `hep-th/9908070`.

[35] R. Bousso, "The Holographic Principle for General Backgrounds," *Class. Quantum Gravity* **17** (1999) 997–1005, `hep-th/9911002`.

[36] J. M. Maldacena, "The Large N Limit of Superconformal Field Theories and Supergravity," *Adv.Theor.Math.Phys.* **2** (1998) 231–252, `hep-th/9711200`.

[37] J. M. Maldacena, "Wilson loops in large N field theories," *Phys. Rev. Lett.* **80** (1998) 4859–4862, `hep-th/9803002`.

[38] E. Witten, "Anti De Sitter Space And Holography," *Adv. Theor. Math. Phys.* **2** (1998) 253–291, `hep-th/9802150`.

[39] E. Witten, "Anti-de Sitter Space, Thermal Phase Transition, And Confinement In Gauge Theories," *Adv. Theor. Math. Phys.* **2** (1998) 505–532, `hep-th/9803131`.

[40] S. S. Gubser, I. R. Klebanov, and A. M. Polyakov, "Gauge Theory Correlators from Non-Critical String Theory," *Phys. Lett. B* **428** (1998) 105–114, `hep-th/9802109`.

[41] O. Aharony, S. S. Gubser, J. Maldacena, H. Ooguri, and Y. Oz, "Large N Field Theories, String Theory and Gravity," *Phys. Rep.* **323** (1999) 183–386, `hep-th/9905111`.

[42] F. Markopoulou and L. Smolin, "Holography in a quantum spacetime," `hep-th/9910146`.

[43] A. Sen, "An Introduction to Non-perturbative String Theory," `hep-th/9802051`.

[44] M. Mariño, "Lectures on non-perturbative effects in large N gauge theories, matrix models and strings," *Fortschritte der Phys.* **62** (2014) 455–540, `1206.6272`.

[45] M. Mariño, "Non-perturbative effects in string theory and AdS/CFT," *Spring Sch. Superstring Theory Relat. Top.* (2015).

[46] R. d. M. Koch, E. Gandote, and J.-H. Huang, "Non-Perturbative String Theory from AdS/CFT," *J. High Energy Phys.* **2019** (2019) 169, `1901.02591`.

[47] T. Thiemann, "The LQG – String: Loop Quantum Gravity Quantization of String Theory I. Flat Target Space," *Class. Quantum Gravity* **23** (2004) 1923–1970, hep-th/0401172.

[48] F. Markopoulou and L. Smolin, "Quantum geometry with intrinsic local causality," *Phys. Rev. D* **58** (1997) 084032, gr-qc/9712067.

[49] F. Markopoulou and L. Smolin, "Nonperturbative dynamics for abstract (p,q) string networks," *Phys. Rev. D* **58** (1997) 084033, hep-th/9712148.

[50] L. Smolin, "A candidate for a background independent formulation of M theory," *Phys. Rev. D* **62** (1999) 086001, hep-th/9903166.

[51] N. Bodendorfer, T. Thiemann, and A. Thurn, "Towards Loop Quantum Supergravity (LQSG) I. Rarita-Schwinger Sector," *Class. Quantum Gravity* **30** (2011) 045006, 1105.3709.

[52] N. Bodendorfer, T. Thiemann, and A. Thurn, "Towards Loop Quantum Supergravity (LQSG) II. p-Form Sector," *Class. Quantum Gravity* **30** (2011) 045007, 1105.3710.

[53] N. Bodendorfer, T. Thiemann, and A. Thurn, "Towards Loop Quantum Supergravity (LQSG)," *Phys. Lett. B* **711** (2011) 205–211, 1106.1103.

[54] N. Bodendorfer, "A note on quantum supergravity and AdS/CFT," 1509.02036.

[55] N. Bodendorfer, "A note on conformally compactified connection dynamics tailored for anti-de Sitter space," *Class. Quantum Gravity* **33** (2015) 237002, 1512.00605.

[56] M. Han and L.-Y. Hung, "Loop Quantum Gravity, Exact Holographic Mapping, and Holographic Entanglement Entropy," *Phys. Rev. D* **95** (2016) 024011, 1610.02134.

[57] M. Han and S. Huang, "Discrete Gravity on Random Tensor Network and Holographic R\'enyi Entropy," *J. High Energy Phys.* **2017** (2017) 148, 1705.01964.

[58] G. Chirco, D. Oriti, and M. Zhang, "Group Field theory and Tensor Networks: towards a Ryu-Takayanagi formula in full quantum gravity," *Class. Quantum Gravity* **35** (2017) 115011, 1701.01383.

[59] G. Chirco, A. Goeßmann, D. Oriti, and M. Zhang, "Group Field Theory and Holographic Tensor Networks: Dynamical Corrections to the Ryu-Takayanagi formula," *Class. Quantum Gravity* **37** (2019) 095011, 1903.07344.

[60] B. Swingle, "Constructing holographic spacetimes using entanglement renormalization," 1209.3304.

[61] F. Pastawski, B. Yoshida, D. Harlow, and J. Preskill, "Holographic quantum error-correcting codes: Toy models for the bulk/boundary correspondence," *J. High Energy Phys.* **2015** (2015) 149, 1503.06237.

[62] N. Bao, G. Penington, J. Sorce, and A. C. Wall, "Beyond Toy Models: Distilling Tensor Networks in Full AdS/CFT," *J. High Energy Phys.* **2019** (2018) 69, 1812.01171.

[63] N. Bao, G. Penington, J. Sorce, and A. C. Wall, "Holographic Tensor Networks in Full AdS/CFT," 1902.10157.

[64] S. A. Hayward, "Quasi-Local Gravitational Energy," *Phys. Rev. D* **49** (1993) 831–839, gr-qc/9303030.

[65] L. B. Szabados, "Quasi-Local Energy-Momentum and Angular Momentum in General Relativity," *Living Rev. Relativ.* **12** (2009) 4.

[66] B. Dittrich, C. Goeller, E. Livine, and A. Riello, "Quasi-local holographic dualities in non-perturbative 3d quantum gravity I - Convergence of multiple approaches and examples of Ponzano-Regge statistical duals," *Nucl. Phys. B* **938** (2017) 807–877, 1710.04202.

[67] B. Dittrich, C. Goeller, E. Livine, and A. Riello, "Quasi-local holographic dualities in non-perturbative 3d quantum gravity II - From coherent quantum boundaries to BMS3 characters," *Nucl. Phys. B* **938** (2017) 878–934, 1710.04237.

[68] C. Goeller, E. R. Livine, and A. Riello, "Non-Perturbative 3D Quantum Gravity: Quantum Boundary States and Exact Partition Function," *Gen. Relativ. Gravit.* **52** (2019) 24, 1912.01968.

[69] S. K. Asante, B. Dittrich, and H. M. Haggard, "Holographic description of boundary gravitons in (3+1) dimensions," *J. High Energy Phys.* **2019** (2018) 144, 1811.11744.

[70] S. K. Asante, B. Dittrich, F. Girelli, A. Riello, and P. Tsimiklis, "Quantum geometry from higher gauge theory," 1908.05970.

[71] M. Ammon and J. Erdmenger, *Gauge/Gravity Duality*. Cambridge University Press, Cambridge, 2015.

[72] H. Nastase, *Introduction to the AdS/CFT Correspondence*. Cambridge University Press, Cambridge, 2015.

[73] M. Natsuume, *AdS/CFT Duality User Guide*, vol. 903 of *Lecture Notes in Physics*. Springer Japan, Tokyo, 2015.

[74] J. M. Maldacena, "TASI 2003 Lectures on AdS/CFT," in *Prog. string theory. Proceedings, Summer Sch. TASI 2003, Boulder, USA*, pp. 155–203. 2003. hep-th/0309246.

[75] E. D'Hoker and D. Z. Freedman, "Supersymmetric Gauge Theories and the AdS/CFT Correspondence," in *Strings, Branes Extra Dimens. TASI 2001 Proc.*, pp. 3–1582002. hep-th/0201253.

[76] A. V. Ramallo, "Introduction to the AdS/CFT correspondence," *Springer Proc.Phys.* **161** (2013) 411–474, hep-th/1310.4319.

[77] P. Ginsparg, "Applied Conformal Field Theory," in *Les Houches Summer Sch. Theor. Phys. Fields, Strings, Crit. Phenom.*, pp. 1–1681988. `hep-th/9108028`.

[78] P. Di Francesco, P. Mathieu, and D. Sénéchal, *Conformal Field Theory*. Graduate Texts in Contemporary Physics. Springer New York, New York, NY, 1997.

[79] R. Blumenhagen and E. Plauschinn, *Introduction to Conformal Field Theory*, vol. 779 of *Lecture Notes in Physics*. Springer Berlin Heidelberg, Berlin, Heidelberg, 2009.

[80] G. Hooft, "A planar diagram theory for strong interactions," *Nucl. Phys. B* **72** (1974) 461–473.

[81] S. Coleman, *Aspects of Symmetry*. Cambridge University Press1985.

[82] G. T. Horowitz and J. Polchinski, "Gauge/gravity duality," `gr-qc/0602037`.

[83] V. E. Hubeny, "The AdS/CFT correspondence," *Class. Quantum Gravity* **32** (2015) 124010, `gr-qc/1501.00007`.

[84] D. Marolf, "Unitarity and holography in gravitational physics," *Phys. Rev. D* **79** (2009) 044010, `gr-qc/0808.2842`.

[85] K. H. Rehren, "Algebraic Holography," *Ann. Henri Poincaré* **1** (1999) 607–623, `hep-th/9905179`.

[86] G. T. Horowitz and A. Strominger, "Black strings and p-branes," *Nucl. Phys. B* **360** (1991) 197–209.

[87] I. R. Klebanov, "World Volume Approach to Absorption by Non-dilatonic Branes," *Nucl. Phys. B* **496** (1997) 231–242, `hep-th/9702076`.

[88] H. J. Kim, L. J. Romans, and P. van Nieuwenhuizen, "Mass spectrum of chiral ten-dimensional N=2 supergravity on S^5," *Phys. Rev. D* **32** (1985) 389–399.

[89] P. Breitenlohner and D. Z. Freedman, "Positive energy in anti-de Sitter backgrounds and gauged extended supergravity," *Phys. Lett. B* **115** (1982) 197–201.

[90] P. Breitenlohner and D. Z. Freedman, "Stability in gauged extended supergravity," *Ann. Phys. (N. Y).* **144** (1982) 249–281.

[91] G. T. Horowitz and N. Itzhaki, "Black Holes, Shock Waves, and Causality in the AdS/CFT Correspondence," *J. High Energy Phys.* **1999** (1999) 010–010, `hep-th/9901012`.

[92] J. M. Maldacena, "Eternal Black Holes in AdS," *J. High Energy Phys.* **2003** (2001) 021–021, `hep-th/0106112`.

[93] S. de Haro, K. Skenderis, and S. N. Solodukhin, "Holographic Reconstruction of Spacetime and Renormalization in the AdS/CFT Correspondence," *Commun. Math. Phys.* **217** (2000) 595–622, `hep-th/0002230`.

[94] K. Skenderis, "Lecture Notes on Holographic Renormalization," *Class. Quantum Gravity* **19** (2002) 5849–5876, hep-th/0209067.

[95] S. Ryu and T. Takayanagi, "Holographic Derivation of Entanglement Entropy from AdS/CFT," *Phys. Rev. Lett.* **96** (2006) 181602, hep-th/0603001.

[96] S. Ryu and T. Takayanagi, "Aspects of Holographic Entanglement Entropy," *J. High Energy Phys.* **2006** (2006) 045–045, hep-th/0605073.

[97] D. V. Fursaev, "Proof of the Holographic Formula for Entanglement Entropy," *J. High Energy Phys.* **2006** (2006) 018–018, hep-th/0606184.

[98] V. E. Hubeny, M. Rangamani, and T. Takayanagi, "A covariant holographic entanglement entropy proposal," *J. High Energy Phys.* **2007** (2007) 062–062, hep-th/0705.0016.

[99] M. Van Raamsdonk, "Building up spacetime with quantum entanglement," *Gen. Relativ. Gravit.* **42** (2010) 2323–2329, hep-th/1005.3035.

[100] M. Van Raamsdonk, "Lectures on Gravity and Entanglement," in *New Front. Fields Strings*, pp. 297–351, WORLD SCIENTIFIC2017.

[101] M. Rangamani and T. Takayanagi, *Holographic Entanglement Entropy*, vol. 931 of *Lecture Notes in Physics*. Springer International Publishing, Cham, 2017.

[102] D. Harlow, "Jerusalem lectures on black holes and quantum information," *Rev. Mod. Phys.* **88** (2016) 015002, hep-th/1409.1231.

[103] T. Banks, M. R. Douglas, G. T. Horowitz, and E. Martinec, "AdS Dynamics from Conformal Field Theory," hep-th/9808016.

[104] D. Harlow, Daniel and Stanford, "Operator Dictionaries and Wave Functions in AdS/CFT and dS/CFT," hep-th/1104.2621.

[105] V. Balasubramanian and S. F. Ross, "Holographic Particle Detection," *Phys. Rev. D* **61** (1999) 044007, hep-th/9906226.

[106] E. Susskind, Leonard and Witten, "The Holographic bound in anti-de Sitter space," hep-th/9805114.

[107] V. Balasubramanian and P. Kraus, "Spacetime and the Holographic Renormalization Group," *Phys. Rev. Lett.* **83** (1999) 3605–3608, hep-th/9903190.

[108] A. W. Peet and J. Polchinski, "UV/IR Relations in AdS Dynamics," *Phys. Rev. D* **59** (1998) 065011, hep-th/9809022.

[109] M. Bojowald, "Absence of Singularity in Loop Quantum Cosmology," *Phys. Rev. Lett.* **86** (2001) 5227–5230, gr-qc/0102069.

[110] A. Ashtekar, M. Bojowald, and J. Lewandowski, "Mathematical structure of loop quantum cosmology," *Adv. Theor. Math. Phys.* **7** (2003) 233–268, gr-qc/0304074.

[111] A. Ashtekar, T. Pawlowski, and P. Singh, "Quantum Nature of the Big Bang: Improved dynamics," *Phys. Rev. D* **74** (2006) 084003, gr-qc/0607039.

[112] M. Bojowald, "Large scale effective theory for cosmological bounces," *Phys. Rev. D* **75** (2006) 081301, gr-qc/0608100.

[113] A. Ashtekar, A. Corichi, and P. Singh, "Robustness of key features of loop quantum cosmology," *Phys. Rev. D* **77** (2008) 024046, gr-qc/0710.3565.

[114] J. Mielczarek, T. Stachowiak, and M. Szydłowski, "Exact solutions for a big bounce in loop quantum cosmology," *Phys. Rev. D* **77** (2008) 123506, gr-qc/0801.0502.

[115] D. A. Craig, "Dynamical eigenfunctions and critical density in loop quantum cosmology," *Class. Quantum Gravity* **30** (2012) 035010, 1207.5601.

[116] M. Bojowald, "Loop Quantum Cosmology," *Living Rev. Relativ.* **8** (2006) 11, gr-qc/0601085.

[117] A. Ashtekar, "An Introduction to Loop Quantum Gravity Through Cosmology," *Nuovo Cim.B* **122** (2007) 135–155, gr-qc/0702030.

[118] A. Ashtekar and P. Singh, "Loop Quantum Cosmology: A Status Report," *Class. Quantum Gravity* **28** (2011) 213001, 1108.0893.

[119] A. Barrau and B. Bolliet, "Some conceptual issues in loop quantum cosmology," *Int. J. Mod. Phys. D* **25** (2016) 1642008, 1602.04452.

[120] N. Bodendorfer, T. Thiemann, and A. Thurn, "New Variables for Classical and Quantum Gravity in all Dimensions I. Hamiltonian Analysis," *Class. Quantum Gravity* **30** (2011) 045001, 1105.3703.

[121] N. Bodendorfer, T. Thiemann, and A. Thurn, "New Variables for Classical and Quantum Gravity in all Dimensions II. Lagrangian Analysis," *Class. Quantum Gravity* **30** (2011) 045002, 1105.3704.

[122] N. Bodendorfer, T. Thiemann, and A. Thurn, "New Variables for Classical and Quantum Gravity in all Dimensions III. Quantum Theory," *Class. Quantum Gravity* **30** (2011) 045003, 1105.3705.

[123] N. Bodendorfer, T. Thiemann, and A. Thurn, "New Variables for Classical and Quantum Gravity in all Dimensions IV. Matter Coupling," *Class. Quantum Gravity* **30** (2011) 045004, 1105.3706.

[124] X. Zhang, "Higher dimensional Loop Quantum Cosmology," *Eur. Phys. J. C* **76** (2015) 395, 1506.05597.

[125] A. Ashtekar and J. Samuel, "Bianchi cosmologies: the role of spatial topology," *Class. Quantum Gravity* **8** (1991) 2191–2215.

[126] P. A. M. Dirac, "Generalized Hamiltonian Dynamics," *Can. J. Math.* **2** (1950) 129–148.

[127] P. A. M. Dirac, *Lectures on quantum mechanics*. Belfer graduate school of Science, Yeshiva University, New York, NY, 1964.

[128] M. Henneaux and C. Teitelboim, *Quantization of gauge systems*. Princeton University Press, 1992.

[129] T. Thiemann, *Modern Canonical Quantum General Relativity*. Cambridge University Press, Cambridge, 2007.

[130] C. Rovelli, *Quantum Gravity*. Cambridge University Press2004.

[131] C. Rovelli and F. Vidotto, *Covariant Loop Quantum Gravity*. Cambridge University Press, Cambridge, 2014.

[132] N. Bodendorfer, "An embedding of loop quantum cosmology in (b, v) variables into a full theory context," *Class. Quantum Gravity* **33** (2015) 125014, 1512.00713.

[133] N. Bodendorfer, "A quantum reduction to Bianchi I models in loop quantum gravity," *Phys. Rev. D* **91** (2014) 081502, 1410.5608.

[134] E. Alesci and F. Cianfrani, "A new perspective on cosmology in Loop Quantum Gravity," *EPL (Europhysics Lett.* **104** (2012) 10001, 1210.4504.

[135] E. Alesci and F. Cianfrani, "Quantum reduced loop gravity: Universe on a lattice," *Phys. Rev. D* **92** (2015) 084065.

[136] E. Alesci and F. Cianfrani, "Quantum Reduced Loop Gravity and the foundation of Loop Quantum Cosmology," *Int. J. Mod. Phys. D* **25** (2016) 1642005, 1602.05475.

[137] E. Alesci, F. Cianfrani, and C. Rovelli, "Quantum-Reduced Loop-Gravity: Relation with the Full Theory," *Phys. Rev. D* **88** (2013) 104001, 1309.6304.

[138] A. Dapor and K. Liegener, "Cosmological Effective Hamiltonian from full Loop Quantum Gravity Dynamics," *Phys. Lett. B* **785** (2017) 506–510, 1706.09833.

[139] A. Dapor and K. Liegener, "Cosmological Coherent State Expectation Values in LQG I. Isotropic Kinematics," *Class. Quantum Gravity* **35** (2017) 135011, 1710.04015.

[140] M. Han and H. Liu, "Effective Dynamics from Coherent State Path Integral of Full Loop Quantum Gravity," *Phys. Rev. D* **101** (2019) 046003, 1910.03763.

[141] M. A. Šubin, "Differential and Pseudodifferential Operators in Spaces of almost Periodic Functions," *Math. USSR-Sbornik* **24** (1974) 547–573.

[142] A. Ashtekar, S. Fairhurst, and J. L. Willis, "Quantum gravity, shadow states, and quantum mechanics," *Class. Quantum Gravity* **20** (2002) 1031–1061, gr-qc/0207106.

[143] A. Corichi, T. Vukasinac, and J. A. Zapata, "Polymer Quantum Mechanics and its Continuum Limit," *Phys. Rev. D* **76** (2007) 044016, 0704.0007.

[144] J. Lewandowski, A. Okolow, H. Sahlmann, and T. Thiemann, "Uniqueness of diffeomorphism invariant states on holonomy-flux algebras," *Commun. Math. Phys.* **267** (2005) 703–733, gr-qc/0504147.

[145] C. Fleischhack, "Representations of the Weyl Algebra in Quantum Geometry," *Commun. Math. Phys.* **285** (2004) 67–140, math-ph/0407006.

[146] A. Ashtekar and M. Campiglia, "On the Uniqueness of Kinematics of Loop Quantum Cosmology," *Class. Quantum Gravity* **29** (2012) 242001, 1209.4374.

[147] J. Engle, M. Hanusch, and T. Thiemann, "Uniqueness of the Representation in Homogeneous Isotropic LQC," *Commun. Math. Phys.* **354** (2016) 231–246, 1609.03548.

[148] R. C. Helling, "Higher curvature counter terms cause the bounce in loop cosmology," 0912.3011.

[149] J. B. Achour, S. Brahma, and M. Geiller, "New Hamiltonians for loop quantum cosmology with arbitrary spin representations," *Phys. Rev. D* **95** (2016) 086015, 1612.07615.

[150] M. Assanioussi, A. Dapor, K. Liegener, and T. Pawłowski, "Emergent de Sitter epoch of the quantum Cosmos," *Phys. Rev. Lett.* **121** (2018) 081303, 1801.00768.

[151] M. Assanioussi, A. Dapor, K. Liegener, and T. Pawlowski, "Emergent de Sitter epoch of the Loop Quantum Cosmos: a detailed analysis," 1906.05315.

[152] M. Bojowald, "Critical evaluation of common claims in loop quantum cosmology," *Universe* **6** (2020) 36, 2002.05703.

[153] M. Martin-Benito, G. A. M. Marugan, and J. Olmedo, "Further Improvements in the Understanding of Isotropic Loop Quantum Cosmology," *Phys. Rev. D* **80** (2009) 104015, 0909.2829.

[154] N. Bodendorfer, "A note on the scalar products in sLQC," *Class. Quantum Gravity* **36** (2018) 087003, 1810.12087.

[155] P. Diener, A. Joe, M. Megevand, and P. Singh, "Numerical simulations of loop quantum Bianchi-I spacetimes," *Class. Quantum Gravity* **34** (2017) 094004, 1701.05824.

[156] V. Taveras, "Corrections to the Friedmann Equations from LQG for a Universe with a Free Scalar Field," *Phys. Rev. D* **78** (2008) 064072, 0807.3325.

[157] C. Rovelli and E. Wilson-Ewing, "Why are the effective equations of loop quantum cosmology so accurate?," *Phys. Rev. D* **90** (2013) 023538, 1310.8654.

[158] A. Ashtekar and E. Wilson-Ewing, "The covariant entropy bound and loop quantum cosmology," *Phys. Rev. D* **78** (2008) 064047, 0805.3511.

[159] S. W. Hawking and G. F. R. Ellis, *The Large Scale Structure of Space-Time*. Cambridge University Press1973.

[160] N. Bodendorfer, A. Schäfer, and J. Schliemann, "Holographic signatures of resolved cosmological singularities," *J. High Energy Phys.* **2019** (2016) 43, 1612.06679.

[161] N. Engelhardt, T. Hertog, and G. T. Horowitz, "Holographic Signatures of Cosmological Singularities," *Phys. Rev. Lett.* **113** (2014) 121602, 1404.2309.

[162] N. Engelhardt, T. Hertog, and G. T. Horowitz, "Further Holographic Investigations of Big Bang Singularities," *J. High Energy Phys.* **2015** (2015) 44, 1503.08838.

[163] N. Bodendorfer, F. M. Mele, and J. Münch, "Holographic Signatures of Resolved Cosmological Singularities II: Numerical Investigations," *Class. Quantum Gravity* **36** (2018) 245013, 1804.01387.

[164] S. R. Das, J. Michelson, K. Narayan, and S. P. Trivedi, "Time Dependent Cosmologies and Their Duals," *Phys. Rev. D* **74** (2006) 026002, hep-th/0602107.

[165] T. Hertog and G. T. Horowitz, "Towards a Big Crunch Dual," *J. High Energy Phys.* **2004** (2004) 073–073, hep-th/0406134.

[166] T. Hertog and G. T. Horowitz, "Holographic Description of AdS Cosmologies," *J. High Energy Phys.* **2005** (2005) 005–005, hep-th/0503071.

[167] N. Turok, B. Craps, and T. Hertog, "From Big Crunch to Big Bang with AdS/CFT," 0711.1824 [hep-th].

[168] B. Craps, T. Hertog, and N. Turok, "On the Quantum Resolution of Cosmological Singularities using AdS/CFT," *Phys. Rev. D* **86** (2007) 043513, 0712.4180.

[169] S. R. Das, J. Michelson, K. Narayan, and S. P. Trivedi, "Cosmologies with Null Singularities and their Gauge Theory Duals," *Phys. Rev. D* **75** (2006) 026002, hep-th/0610053.

[170] A. Awad, S. R. Das, K. Narayan, and S. P. Trivedi, "Gauge Theory Duals of Cosmological Backgrounds and their Energy Momentum Tensors," *Phys. Rev. D* **77** (2007) 046008, 0711.2994.

[171] A. Awad, S. R. Das, S. Nampuri, K. Narayan, and S. P. Trivedi, "Gauge Theories with Time Dependent Couplings and their Cosmological Duals," *Phys. Rev. D* **79** (2008) 046004, 0807.1517.

[172] J. L. F. Barbon and E. Rabinovici, "AdS Crunches, CFT Falls And Cosmological Complementarity," *J. High Energy Phys.* **2011** (2011) 44, 1102.3015.

[173] M. Smolkin and N. Turok, "Dual description of a 4d cosmology," 1211.1322 [hep-th].

[174] D. Oriti, L. Sindoni, and E. Wilson-Ewing, "Emergent Friedmann dynamics with a quantum bounce from quantum gravity condensates," *Class. Quantum Gravity* **33** (2016) 224001, 1602.05881.

[175] E. Alesci and F. Cianfrani, "Improved regularization from Quantum Reduced Loop Gravity," 1604.02375 [gr-qc].

[176] A. H. Chamseddine and V. Mukhanov, "Resolving Cosmological Singularities," *J. Cosmol. Astropart. Phys.* **9** (2017) 1612.05860.

[177] B. Gupt and P. Singh, "Quantum gravitational Kasner transitions in Bianchi-I spacetime," *Phys. Rev. D* **86** (2012) 024034, 1205.6763.

[178] A. Ashtekar and E. Wilson-Ewing, "Loop quantum cosmology of Bianchi I models," *Phys. Rev. D* **79** (2009) 083535, 0903.3397.

[179] E. Wilson-Ewing, "The loop quantum cosmology bounce as a Kasner transition," *Class. Quantum Gravity* **35** (2017) 065005, 1711.10943.

[180] N. Bodendorfer, A. Schäfer, and J. Schliemann, "On the canonical structure of general relativity with a limiting curvature and its relation to loop quantum gravity," *Phys. Rev. D* **97** (2017) 084057, 1703.10670.

[181] D. Langlois, H. Liu, K. Noui, and E. Wilson-Ewing, "Effective loop quantum cosmology as a higher-derivative scalar-tensor theory," *Class. Quantum Gravity* **34** (2017) 225004, 1703.10812.

[182] N. Bodendorfer, F. M. Mele, and J. Münch, "Is limiting curvature mimetic gravity an effective polymer quantum gravity?," *Class. Quantum Gravity* **35** (2018) 225001, 1806.02052.

[183] J. B. Achour, F. Lamy, H. Liu, and K. Noui, "Non-singular black holes and the Limiting Curvature Mechanism: A Hamiltonian perspective," *J. Cosmol. Astropart. Phys.* **2018** (2017) 072–072, 1712.03876.

[184] M. Ammon, M. Gutperle, P. Kraus, and E. Perlmutter, "Spacetime Geometry in Higher Spin Gravity," *J. High Energy Phys.* **2011** (2011) 53, 1106.4788.

[185] C. Krishnan and S. Roy, "Desingularization of the Milne Universe," *Phys. Lett. B* **734** (2013) 92–95, 1311.7315.

[186] B. Craps, C. Krishnan, and A. Saurabh, "Low Tension Strings on a Cosmological Singularity," *J. High Energy Phys.* **2014** (2014) 65, 1405.3935.

[187] O. Hohm and B. Zwiebach, "Duality Invariant Cosmology to all Orders in α'," *Phys. Rev. D* **100** (2019) 126011, 1905.06963.

[188] T. Faulkner, A. Lewkowycz, and J. Maldacena, "Quantum corrections to holographic entanglement entropy," *J. High Energy Phys.* **2013** (2013) 74, 1307.2892.

[189] N. Engelhardt and G. T. Horowitz, "Entanglement Entropy Near Cosmological Singularities," *J. High Energy Phys.* **2013** (2013) 41, 1303.4442.

[190] N. Engelhardt and A. C. Wall, "Quantum Extremal Surfaces: Holographic Entanglement Entropy beyond the Classical Regime," *J. High Energy Phys.* **2015** (2014) 73, 1408.3203.

[191] M. Bojowald, "Singularities and Quantum Gravity," in *AIP Conf. Proc.*, vol. 910, pp. 294–333, AIP, 2007.

[192] M. Natsuume, "The singularity problem in string theory," in *Meet. Front. Cosmol. Gravit.* 2001. gr-qc/0108059.

[193] A. Ashtekar and M. Bojowald, "Quantum geometry and the Schwarzschild singularity," *Class. Quantum Gravity* **23** (2005) 391–411, gr-qc/0509075.

[194] L. Modesto, "Loop quantum black hole," *Class. Quantum Gravity* **23** (2005) 5587–5601, gr-qc/0509078.

[195] L. Modesto, "Space-Time Structure of Loop Quantum Black Hole," *Int. J. Theor. Phys.* **49** (2008) 1649–1683, 0811.2196.

[196] R. Gambini, J. Olmedo, and J. Pullin, "Quantum black holes in Loop Quantum Gravity," *Class. Quantum Gravity* **31** (2013) 095009, 1310.5996.

[197] A. Corichi and P. Singh, "Loop quantization of the Schwarzschild interior revisited," *Class. Quantum Gravity* **33** (2015) 055006, 1506.08015.

[198] J. Olmedo, S. Saini, and P. Singh, "From black holes to white holes: a quantum gravitational, symmetric bounce," *Class. Quantum Gravity* **34** (2017) 225011, 1707.07333.

[199] E. Bianchi, M. Christodoulou, F. D'Ambrosio, H. M. Haggard, and C. Rovelli, "White Holes as Remnants: A Surprising Scenario for the End of a Black Hole," *Class. Quantum Gravity* **35** (2018) 225003, 1802.04264.

[200] C. G. Boehmer and K. Vandersloot, "Loop Quantum Dynamics of the Schwarzschild Interior," *Phys. Rev. D* **76** (2007) 104030, 0709.2129.

[201] D.-W. Chiou, "Phenomenological loop quantum geometry of the Schwarzschild black hole," *Phys. Rev. D* **78** (2008) 064040, 0807.0665.

[202] D. Oriti, D. Pranzetti, and L. Sindoni, "Black Holes as Quantum Gravity Condensates," *Phys. Rev. D* **97** (2018) 066017, 1801.01479.

[203] J. B. Achour, F. Lamy, H. Liu, and K. Noui, "Polymer Schwarzschild black hole: An effective metric," *EPL (Europhysics Lett.* **123** (2018) 20006, 1803.01152.

[204] M. Bojowald, S. Brahma, and D.-h. Yeom, "Effective line elements and black-hole models in canonical (loop) quantum gravity," *Phys. Rev. D* **98** (2018) 046015, 1803.01119.

[205] I. P. Lobo and M. Ronco, "Rainbow-like Black Hole metric from Loop Quantum Gravity," *Universe* **4** (2018) 139, 1812.02136.

[206] H. A. Morales-Técotl, S. Rastgoo, and J. C. Ruelas, "Effective dynamics of the Schwarzschild black hole interior with inverse triad corrections," 1806.05795.

[207] A. Ashtekar, J. Olmedo, and P. Singh, "Quantum Transfiguration of Kruskal Black Holes," *Phys. Rev. Lett.* **121** (2018) 241301, 1806.00648.

[208] A. Ashtekar, J. Olmedo, and P. Singh, "Quantum Extension of the Kruskal Space-time," *Phys. Rev. D* **98** (2018) 126003, 1806.02406.

[209] N. Bodendorfer, F. M. Mele, and J. Münch, "Effective Quantum Extended Spacetime of Polymer Schwarzschild Black Hole," *Class. Quantum Gravity* **36** (2019) 195015, 1902.04542.

[210] N. Bodendorfer, F. M. Mele, and J. Münch, "(b,v)-type variables for black to white hole transitions in effective loop quantum gravity," 1911.12646.

[211] N. Bodendorfer, F. M. Mele, and J. Münch, "Mass and Horizon Dirac Observables in Effective Models of Quantum Black-to-White Hole Transition," 1912.00774.

[212] M. Assanioussi, A. Dapor, and K. Liegener, "Perspectives on the dynamics in a loop quantum gravity effective description of black hole interiors," *Phys. Rev. D* **101** (2019) 026002, 1908.05756.

[213] M. Bojowald, S. Brahma, and J. D. Reyes, "Covariance in models of loop quantum gravity: Spherical symmetry," *Phys. Rev. D* **92** (2015) 045043, 1507.00329.

[214] M. Campiglia, R. Gambini, and J. Pullin, "Loop quantization of spherically symmetric midi-superspaces," *Class. Quantum Gravity* **24** (2007) 3649–3672, gr-qc/0703135.

[215] L. Modesto, "Black hole interior from loop quantum gravity," *Adv. High Energy Phys.* **2008** (2006) 1–12, gr-qc/0611043.

[216] D.-W. Chiou, "Phenomenological dynamics of loop quantum cosmology in Kantowski-Sachs spacetime," *Phys. Rev. D* **78** (2008) 044019, 0803.3659.

[217] A. Joe and P. Singh, "Kantowski-Sachs spacetime in loop quantum cosmology: bounds on expansion and shear scalars and the viability of quantization," *Class. Quantum Gravity* **32** (2014) 015009, 1407.2428.

[218] N. Bodendorfer, F. M. Mele, and J. Münch, "A note on the Hamiltonian as a polymerisation parameter," *Class. Quantum Gravity* **36** (2019) 187001, 1902.04032.

[219] M. Bouhmadi-López, S. Brahma, C.-Y. Chen, P. Chen, and D.-h. Yeom, "Asymptotic non-flatness of an effective black hole model based on loop quantum gravity," 1902.07874.

[220] V. Faraoni and A. Giusti, "Unsettling physics in the quantum-corrected Schwarzschild black hole," 2006.12577.

[221] C. W. Misner, K. S. Thorne, and J. A. Wheeler, *Gravitation*. San Francisco, 1973.

[222] M. Cavaglia', V. de Alfaro, and A. T. Filippov, "Hamiltonian Formalism for Black Holes and Quantization," *Int. J. Mod. Phys. D* **04** (1994) 661–672, gr-qc/9411070.

[223] B. Vakili, "Classical polymerization of the Schwarzschild metric," *Adv. High Energy Phys.* **2018** (2018) 1–10, 1806.01837.

[224] L. Herrera and N. O. Santos, "Local anisotropy in self-gravitating systems," *Phys. Rep.* **286** (1997) 53–130.

[225] M. Bouhmadi-López, S. Brahma, C.-Y. Chen, P. Chen, and D.-h. Yeom, "A consistent model of non-singular Schwarzschild black hole in loop quantum gravity and its quasinormal modes," 2004.13061.

[226] N. Bodendorfer, F. M. Mele, J. Münch, and S. Pateloudis, "Quantum Corrected Polymer Black Hole Thermodynamics: Mass Relations and Logarithmic Entropy Corrections," *to Appear*.

[227] R. M. Wald, *General Relativity*. University of Chicago Press, 1984.

[228] L. Modesto and I. Prémont-Schwarz, "Self-dual Black Holes in LQG: Theory and Phenomenology," *Phys. Rev. D* **80** (2009) 064041, 0905.3170.

[229] P. Nicolini, E. Spallucci, and M. F. Wondrak, "Quantum Corrected Black Holes from String T-Duality," *Phys. Lett. B* **797** (2019) 134888, 1902.11242.

[230] P. Nicolini and E. Spallucci, "Holographic screens in ultraviolet self-complete quantum gravity," *Adv. High Energy Phys.* **2014** (2012) 1–9, 1210.0015.

[231] A. Strominger and C. Vafa, "Microscopic Origin of the Bekenstein-Hawking Entropy," *Phys. Lett. B* **379** (1996) 99–104, hep-th/9601029.

[232] R. B. Mann and S. N. Solodukhin, "Universality of quantum entropy for extreme black holes," *Nucl. Phys. B* **523** (1998) 293–307, hep-th/9709064.

[233] C. Rovelli, "Black Hole Entropy from Loop Quantum Gravity," *Phys. Rev. Lett.* **77** (1996) 3288–3291, gr-qc/9603063.

[234] A. Ashtekar, J. Baez, A. Corichi, and K. Krasnov, "Quantum Geometry and Black Hole Entropy," *Phys. Rev. Lett.* **80** (1997) 904–907, gr-qc/9710007.

[235] A. Ashtekar, J. Baez, and K. Krasnov, "Quantum Geometry of Isolated Horizons and Black Hole Entropy," *Adv. Theor. Math. Phys.* **4** (2000) 1–94, gr-qc/0005126.

[236] R. K. Kaul and P. Majumdar, "Quantum Black Hole Entropy," *Phys. Lett. B* **439** (1998) 267–270, gr-qc/9801080.

[237] R. K. Kaul and P. Majumdar, "Logarithmic correction to the Bekenstein-Hawking entropy," *Phys. Rev. Lett.* **84** (2000) 5255–5257, gr-qc/0002040.

[238] S. Carlip, "Logarithmic Corrections to Black Hole Entropy from the Cardy Formula," *Class. Quantum Gravity* **17** (2000) 4175–4186, gr-qc/0005017.

[239] F. Barbero, J. Lewandowski, and E. J. S. Villasenor, "Quantum isolated horizons and black hole entropy," in *Proc. 3rd Quantum Gravity Quantum Geom. Sch. ,Äî PoS(QGQGS 2011)*, (Trieste, Italy), p. 023, Sissa Medialab2013.

[240] K. A. Meissner, "Black hole entropy in Loop Quantum Gravity," *Class. Quantum Gravity* **21** (2004) 5245–5251, gr-qc/0407052.

[241] E. R. Livine and D. R. Terno, "Quantum Black Holes: Entropy and Entanglement on the Horizon," *Nucl. Phys. B* **741** (2005) 131–161, gr-qc/0508085.

[242] A. Sen, "Black hole entropy function, attractors and precision counting of microstates," *Gen. Relativ. Gravit.* **40** (2008) 2249–2431.

[243] F. Caravelli and L. Modesto, "Holographic actions from black hole entropy," *Phys. Lett. B* **702** (2010) 307–311, 1001.4364.

[244] A. Ashtekar, T. Pawlowski, and P. Singh, "Quantum Nature of the Big Bang: An Analytical and Numerical Investigation," *Phys. Rev. D* **73** (2006) 124038, gr-qc/0604013.

[245] D. Giulini and D. Marolf, "On the Generality of Refined Algebraic Quantization," *Class. Quantum Gravity* **16** (1998) 2479–2488, gr-qc/9812024.

[246] D. Giulini, "Group Averaging and Refined Algebraic Quantization," *Nucl. Phys. B - Proc. Suppl.* **88** (2000) 385–388, gr-qc/0003040.

[247] A. Ashtekar, J. Lewandowski, D. Marolf, J. Mourao, and T. Thiemann, "Quantization of diffeomorphism invariant theories of connections with local degrees of freedom," *J. Math. Phys.* **36** (1995) 6456–6493, gr-qc/9504018.

[248] F. Kottler, "The physical basis of Einstein's theory of gravitation," *Ann. Phys.* **56** (1918) 401.

[249] R. Emparan and H. S. Reall, "Black Holes in Higher Dimensions," *Living Rev. Relativ.* **11** (2008) 6, 0801.3471.

[250] A. Ashtekar and A. Magnon, "Asymptotically anti-de Sitter space-times," *Class. Quantum Gravity* **1** (1984) L39–L44.

[251] A. Ashtekar and S. Das, "Asymptotically Anti-de Sitter Space-times: Conserved Quantities," *Class. Quantum Gravity* **17** (1999) L17–L30, hep-th/9911230.

[252] T. Thiemann and H. Kastrup, "Canonical quantization of spherically symmetric gravity in Ashtekar's self-dual representation," *Nucl. Phys. B* **399** (1993) 211–258.

[253] H. A. Kastrup and T. Thiemann, "Spherically Symmetric Gravity as a Completely Integrable System," *Nucl. Phys. B* **425** (1994) 665–686, gr-qc/9401032.

[254] K. V. Kuchařô, "Geometrodynamics of Schwarzschild Black Holes," *Phys. Rev. D* **50** (1994) 3961–3981, gr-qc/9403003.

[255] M. Christodoulou and F. D'Ambrosio, "Characteristic Time Scales for the Geometry Transition of a Black Hole to a White Hole from Spinfoams," 1801.03027.

[256] M. Christodoulou, C. Rovelli, S. Speziale, and I. Vilensky, "Planck star tunneling time: An astrophysically relevant observable from background-free quantum gravity," *Phys. Rev. D* **94** (2016) 084035.

[257] L. Fidkowski, V. Hubeny, M. Kleban, and S. Shenker, "The Black Hole Singularity in AdS/CFT," *J. High Energy Phys.* **2004** (2003) 014–014, hep-th/0306170.

[258] N. Engelhardt and G. T. Horowitz, "Holographic Consequences of a No Transmission Principle," *Phys. Rev. D* **93** (2015) 026005, 1509.07509.

[259] N. Engelhardt and G. T. Horowitz, "New Insights into Quantum Gravity from Gauge/gravity Duality," *Int. J. Mod. Phys. D* **25** (2016) 1643002, 1605.04335.

[260] S. Mukherji and S. S. Pal, "Logarithmic Corrections to Black Hole Entropy and AdS/CFT Correspondence," *J. High Energy Phys.* **2002** (2002) 026–026.

[261] M. Hanada, Y. Hyakutake, G. Ishiki, and J. Nishimura, "Holographic description of quantum black hole on a computer," *Science (80-.).* **344** (2013) 882–885, 1311.5607.

[262] M. Hanada, Y. Hyakutake, J. Nishimura, and S. Takeuchi, "Higher derivative corrections to black hole thermodynamics from supersymmetric matrix quantum mechanics," *Phys. Rev. Lett.* **102** (2008) 191602, 0811.3102.

[263] K. Hashimoto, S. Kinoshita, and K. Murata, "Imaging black holes through AdS/CFT," *Phys. Rev. D* **101** (2018) 066018, 1811.12617.

[264] F. Benini and P. Milan, "Black holes in 4d $\mathcal{N} = 4$ Super-Yang-Mills," *Phys. Rev. X* **10** (2018) 021037, 1812.09613.

[265] M. David, J. Nian, and L. A. P. Zayas, "Gravitational Cardy Limit and AdS Black Hole Entropy," 2005.10251.

[266] I. Papadimitriou, "Holographic renormalization as a canonical transformation," *J. High Energy Phys.* **2010** (2010) 14, 1007.4592.

[267] L. Freidel, F. Hopfmüller, and A. Riello, "Asymptotic Renormalization in Flat Space: Symplectic Potential and Charges of Electromagnetism," *J. High Energy Phys.* **2019** (2019) 126, 1904.04384.

[268] A. Ashtekar, M. Campiglia, and A. Henderson, "Path Integrals and the WKB approximation in Loop Quantum Cosmology," *Phys. Rev. D* **82** (2010) 124043, 1011.1024.

[269] S. Brahma and D.-h. Yeom, "The no-boundary wave function for loop quantum cosmology," *Phys. Rev. D* **98** (2018) 083537, 1808.01744.

[270] J. B. Achour, S. Brahma, and J.-P. Uzan, "Bouncing compact objects I: Quantum extension of the Oppenheimer-Snyder collapse," *J. Cosmol. Astropart. Phys.* **2020** (2020) 041–041, 2001.06148.

[271] J. B. Achour and J.-P. Uzan, "Bouncing compact objects II: Effective theory of a pulsating Planck star," 2001.06153.

[272] J. B. Achour, S. Brahma, S. Mukohyama, and J.-P. Uzan, "Consistent black-to-white hole bounces from matter collapse," 2004.12977.

[273] N. Bodendorfer and J. Münch, "Quantum Dust Collapse via Surface Matching," *to Appear*.

[274] A. Hanson, T. Regge, and C. Teitelboim, *Constrained hamiltonian systems*. Accademia Nazionale dei Lincei, Roma, 1976.

[275] K. Sundermeyer, *Constrained Dynamics*, vol. 169 of *Lecture Notes in Physics*. Springer-Verlag, Berlin/Heidelberg, 1982.

[276] A. Wipf, "Hamilton's formalism for systems with constraints," in *Canonical Gravity From Class. to Quantum*, pp. 22–58. Springer Berlin Heidelberg, Berlin, Heidelberg, , 1994.

[277] G. Marmo, N. Mukunda, and J. Samuel, "Dynamics and symmetry for constrained systems: a geometrical analysis," *La Riv. del Nuovo Cim.* **6** (1983) 1–62.

[278] G. Marmo, G. Mendella, and W. M. Tulczyjew, "Constrained Hamiltonian systems as implicit differential equations," *J. Phys. A. Math. Gen.* **30** (1997) 277–293.

[279] K. Andrzejewski, J. Gonera, P. Machalski, and P. Maslanka, "Modified Hamiltonian formalism for higher-derivative theories," *Phys. Rev. D* **82** (2010) 045008, hep-th/1005.3941.

[280] C. Kiefer, *Quantum GravityThird Edition*. Oxford University Press2012.

[281] J. Govaerts, "The Nambu-goto String: Its Phase Space Path Integral," *Int. J. Mod. Phys. A* **04** (1989) 173–216.

[282] R. Marnelius, "Canonical quantization of polyakov's string in arbitrary dimensions," *Nucl. Phys. B* **211** (1983) 14–28.

[283] C. Teitelboim, "The Hamiltonian Structure of Two-Dimensional Space- Time and its Relation with the Conformal Anomaly," in *Quantum Theory Gravity. Essays Honor 60th Birthd. Bryce S. DeWitt* (S. M. Christensen, ed.), pp. 327–344. Adam Hilger Ltd., Bristol, England, , 1984.

[284] C. Rovelli and L. Smolin, "Loop space representation of quantum general relativity," *Nucl. Phys. B* **331** (1990) 80–152.

[285] A. Ashtekar and C. J. Isham, "Representations of the holonomy algebras of gravity and non-Abelian gauge theories," *Class.Quant.Grav.* **9** (1992) 1433–1468, `hep-th/9202053`.

[286] A. Ashtekar and J. Lewandowski, "Representation theory of analytic holonomy C* algebras," in *Knots and Quantum Gravity* (J. Baez, ed.). Oxford University Press, Oxford, , 1994. `gr-qc/9311010.`

[287] A. Ashtekar and J. Lewandowski, "Differential Geometry on the Space of Connections via Graphs and Projective Limits," *J. Geom. Phys.* **17** (1994) 191–230, `hep-th/9412073`.

[288] A. Ashtekar and J. Lewandowski, "Projective Techniques and Functional Integration," *J. Math. Phys.* **36** (1994) 2170–2191, `gr-qc/9411046`.

[289] D. Marolf and J. M. Mourao, "On the support of the Ashtekar-Lewandowski measure," *Commun. Math. Phys.* **170** (1994) 583–605, `hep-th/9403112`.

[290] R. Gambini and J. Pullin, *A First Course in Loop Quantum Gravity.* Oxford University Press2011.

[291] R. Gambini and J. Pullin, *Loop Quantum Gravity for Everyone.* WORLD SCIENTIFIC2020.

[292] T. Thiemann, "Lectures on Loop Quantum Gravity," in *Lect. Notes Phys. 631*, pp. 41–135. , 2003.

[293] A. Perez, "Introduction to Loop Quantum Gravity and Spin Foams," `gr-qc/0409061`.

[294] S. Mercuri, "Introduction to Loop Quantum Gravity," in *Proc. 5th Int. Sch. F. Theory Gravit. ,Äî PoS(ISFTG)*, vol. 016, (Trieste, Italy), Sissa Medialab2009. `gr-qc/1001.1330`.

[295] P. Doná and S. Speziale, "Introductory lectures to loop quantum gravity," `gr-qc/1007.0402`.

[296] K. Giesel and H. Sahlmann, "Loop Quantum Gravity," in *Proc. 3rd Quantum Gravity Quantum Geom. Sch. ,Äî PoS(QGQGS 2011)*, (Trieste, Italy), p. 002, Sissa Medialab2013.

[297] N. Bodendorfer, "An elementary introduction to loop quantum gravity," `gr-qc/1607.05129`.

[298] D. Vaid and S. Bilson-Thompson, *LQG for the Bewildered*. Springer International Publishing, Cham, 2017.

[299] R. Arnowitt, S. Deser, and C. W. Misner, "The Dynamics of General Relativity," *Gen. Relativ. Gravit.* **40** (2004) 1997–2027, gr-qc/0405109.

[300] A. Ashtekar, "New Variables for Classical and Quantum Gravity," *Phys. Rev. Lett.* **57** (1986) 2244–2247.

[301] R. Geroch, "Domain of Dependence," *J. Math. Phys.* **11** (1970) 437–449.

[302] P. A. M. Dirac, "The Hamiltonian Form of Field Dynamics," *Can. J. Math.* **3** (1951) 1–23.

[303] P. A. M. Dirac, "The theory of gravitation in Hamiltonian form," *Proc. R. Soc. London. Ser. A. Math. Phys. Sci.* **246** (1958) 333–343.

[304] M. Bojowald, U. Büyükçam, S. Brahma, and F. D'Ambrosio, "Hypersurface-deformation algebroids and effective spacetime models," *Phys. Rev. D* **94** (2016) 104032, gr-qc/1610.08355.

[305] P. G. Bergmann and A. Komar, "The coordinate group symmetries of general relativity," *Int. J. Theor. Phys.* **5** (1972), no. 1 15–28.

[306] P. G. Bergmann and A. Komar, "The Phase Space Formulation of General Relativity and Approaches Toward its Canonical Quantization," in *Gen. Relativ. Gravitation, vol. 1, One Hundred Years after Birth Albert Einstein* (A. Held, ed.). Plenum, , 1981.

[307] A. Komar, "Generalized constraint structure for gravitation theory," *Phys. Rev. D* **27** (1983) 2277–2281.

[308] L. Smolin, "Recent Developments in Non-Perturbative Quantum Gravity," in *Proc. XXIIth Gift Int. Semin. Theor. Phys.*, pp. 3–84, World Scientific1992. hep-th/9202022.

[309] C. Rovelli and L. Smolin, "Discreteness of area and volume in quantum gravity," *Nucl. Phys. B* **442** (1994) 593–619, gr-qc/9411005.

[310] A. Ashtekar and J. Lewandowski, "Quantum Theory of Gravity I: Area Operators," *Class. Quantum Gravity* **14** (1996) A55–A81, gr-qc/9602046.

[311] A. Ashtekar and J. Lewandowski, "Quantum Theory of Geometry II: Volume operators," *Adv. Theor. Math. Phys.* **1** (1997) 388–429, gr-qc/9711031.

[312] R. Loll, "Spectrum of the Volume Operator in Quantum Gravity," *Nucl. Phys. B* **460** (1995) 143–154, gr-qc/9511030.

[313] J. Brunnemann and T. Thiemann, "Simplification of the Spectral Analysis of the Volume Operator in Loop Quantum Gravity," *Class. Quantum Gravity* **23** (2004) 1289–1346, gr-qc/0405060.

[314] R. De Pietri, "Spin Networks and Recoupling in Loop Quantum Gravity," *Nucl. Phys. B - Proc. Suppl.* **57** (1997) 251–254, gr-qc/9701041.

[315] R. De Pietri and C. Rovelli, "Geometry eigenvalues and the scalar product from recoupling theory in loop quantum gravity," *Phys. Rev. D* **54** (1996) 2664–2690.

[316] R. Loll, "Simplifying the spectral analysis of the volume operator," *Nucl. Phys. B* **500** (1997) 405–420, gr-qc/9706038.

[317] K. A. Meissner, "Eigenvalues of the volume operator in loop quantum gravity," *Class. Quantum Gravity* **23** (2005) 617–625, gr-qc/0509049.

[318] L. Freidel and S. Speziale, "Twisted geometries: A geometric parametrization of SU(2) phase space," *Phys. Rev. D* **82** (2010) 084040, gr-qc/1001.2748.

[319] E. Bianchi, P. Doná, and S. Speziale, "Polyhedra in loop quantum gravity," *Phys. Rev. D* **83** (2011) 044035, gr-qc/1009.3402.

[320] M. D. Kruskal, "Maximal Extension of Schwarzschild Metric," *Phys. Rev.* **119** (1960) 1743–1745.

[321] G. Szekeres, "On the singularities of a Riemannian manifold," *Math. Debrecen* **7** (1960) 285–301.

[322] T. Kloesch and T. Strobl, "Classical and Quantum Gravity in 1+1 Dimensions, Part II: The Universal Coverings," *Class. Quantum Gravity* **13** (1995) 2395–2421, gr-qc/9511081.